

**University of Vigo**  
Department of Signal Theory and Communications



**UNIVERSIDADE  
DE VIGO**

**DOCTORAL DISSERTATION  
INTERNATIONAL MENTION**

---

**Estimation, Detection, and Learning  
for Dynamic Spectrum Access**

Author:  
Daniel Romero González

Directed by:  
Roberto López Valcarce

2015



Roberto López Valcarce  
Profesor Titular  
Universidade de Vigo

Esc. de Enxeñaría  
de Telecomunicación  
Campus Universitario  
36310 Vigo

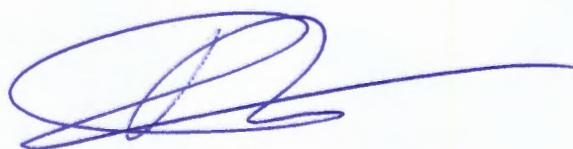
Tel. +34 986 818659  
valcarce@gtis.uvigo.es

En Vigo, a 1 de Abril de 2015

Por la presente, y como Director de la misma, autorizo la presentación y defensa de la tesis doctoral titulada "Estimation, Detection, and Learning for Dynamic Spectrum Access", por parte de su autor, Daniel Romero González.

Igualmente autorizo la solicitud de la Mención Internacional para la misma.

Atentamente,



Roberto López Valcarce



*To my parents.*



# Acknowledgements

I would like to express my sincere gratitude to a number of people that contributed to my scientific and personal development during the years that I spent working on this thesis. What follows is a list of those people, which I provide with the intention of immortalizing this gratitude and giving them proper recognition. I will try my best not to skip anyone but, if I do, please accept my apologies.

First of all, I would like to thank my advisor, Prof. Roberto López-Valcarce, for his guidance and support during my years as a PhD student at the University of Vigo, and especially for the entire afternoons we spent over the whiteboard doing math. There, he transmitted me his taste for mathematical elegance and taught me that even a difficult problem may have a simple and intuitive solution. His support also allowed me to collaborate with some of the greatest researchers in the realm of signal processing, whom I will thank below following an approximate chronological order of publication.

During my visits to the University of Cantabria, I had the opportunity to work with Prof. Javier Vía and Prof. Ignacio Santamaría. Although I learned many things with them, I will especially remember that they showed me the true power of intuition. Prof. Vía, with whom I worked more closely, taught me not to ever fear a problem, no matter how difficult it is, and helped me conciliate my engineer and mathematician sides.

In the meantime, I moved to Delft, which was undoubtedly one of the best decisions of my life. There, I had the privilege of starting to work with Prof. Geert Leus, whose enthusiasm and creativity soon spurred me on to start thinking as a researcher. I am deeply thankful to Prof. Leus not only for having accepted me as a visiting scholar but also for the vast amount of things I have learned with him. It was also a pleasure to me to work with Dr. Dyonisius Dony Ariananda, who taught me the importance of careful thinking.

After one year back in Vigo, I moved to Minneapolis, which was one of the experiences that helped me most to mature as a person and as a researcher. There, I had the honor of working with Prof. Seung-Jun Kim and Prof. Georgios B. Giannakis. I am very grateful to Prof. Kim because conducting research with him is an immensely enriching experience, mainly because of

his rigorous thinking and ability to envision new solutions by establishing connections to related problems. I am profoundly thankful to Prof. Giannakis both for having accepted me as a visiting scholar and for giving me self-confidence as a researcher. He soon attracted my interest when I noticed his energy and capacity, when I found that he would take every opportunity to teach something, and, especially, when I learned that the door of his office was open everyday for discussion with no time nor coffee limits. While I was at the University of Minnesota, I also had the opportunity to start collaborating with Prof. Zhi Tian, who made me appreciate the actual value of thinking clearly.

During my time in Vigo, I also worked with Dr. Jorge F. Schmidt, who showed me the benefits of bridging theory and practice. It was also a pleasure to have initiated some collaborations with Prof. Carlos Mosquera, Prof. Nuria González-Prelcic, and Prof. M. Elena Domínguez-Jiménez. Although I learned many things from them, such as the importance of practical and critical thinking, I do regret the brevity of our collaborations, which owes to lack of time. I sincerely wish to keep on working with these researchers in the future.

I have also to thank my colleagues and friends of the *Signal Processing for Communications Group* (GTSC) from the University of Vigo for the nice working atmosphere that they contributed to generate. I am especially thankful to those who shared with me lots of hours in the office: Dr. Alberto Rico-Alvariño, Dr. Jesus Arnau, Dr. Bamrung Tau Sieskul, Dr. Massimo Vecchio, David Pérez Cabo, Alberto Espiña Barros, Dr. Roi Méndez-Rial, and Dr. Cristian Rusu. Due thanks also to my colleagues and friends of the *Circuits and Systems Group* (CAS) from TU Delft, especially to Dr. Sina Maleki, Dr. Shahzad Gishkori, Hadi Jamali Rad, Seyran Khademi, Hamid Ramezani, Raj Thilak Rajan, and Dr. Rocío Arroyo-Valles. Last but not least, I have to thank my colleagues and friends of the *Signal Processing in Networking and Communications Group* (SPiNCOM) from the University of Minnesota: Dr. Vassilis Kekatos, Luis M. Lopez-Ramos, Morteza Mardani, Donghoon Lee, Wang Gang, Yu Zhang, Prof. Gonzalo Mateos, Dr. Emiliano Dall’Anese, Fatemeh Sheikholeslami, Brian Baingana, Panagiotis Traganitis, Dimitris Berberidis, Tianyi Chen, Liang Zhang, Yanning Shen, Georgios V. Karanikolas, Nasim Yahya Soltani, and Eric Blake.

On the personal side, I would like to thank my family and friends for making these years unforgettable for me. In particular, my deepest gratitude goes to my parents. Not only do their patience and support know no limits, their effort in stimulating my mind during my childhood is the very reason why I am writing these lines. Finally, I would like to thank my *little darling*, Julia, for all her patience and support, and for making my life wonderful.

*Daniel Romero*  
*Lobeira; April 5, 2015*







# Abstract

The incessant demand for enhanced communication services has rendered current RF spectrum allocation policies obsolete. The astronomic price of licensed channels stands in sharp contradiction with their heavy underutilization and propels the adoption of novel spectrum management paradigms where spectral resources are assigned in a dynamic fashion, possibly respecting hierarchical relations among multiple classes of users. In those scenarios, it is expected that emerging communication systems will leverage spectrum awareness information to drastically improve spectrum usage efficiency.

*Spectrum sensing* comprises a collection of signal processing procedures intended to characterize spectrum occupation along time, frequency and space based on the observations of the RF environment reported by one or more sensors. It is the purpose of the present thesis to contribute to this field by putting forward a number of statistical methods that capitalize on the special features of different communication scenarios to reliably obtain detailed occupancy information at low implementation costs.

We first propose a family of techniques aimed to detect, relying on the noisy observations of a sensor with one or multiple antennas, the presence of constant magnitude and/or bandlimited transmissions in a frequency band of interest, as motivated by the new regulations of the Federal Communications Commission. Next, we address the problem of detecting constant-magnitude and Gaussian-distributed waveforms in time-varying channels, relevant in this context since spectrum sensing algorithms typically require long observation windows to meet the stringent performance requirements enforced by spectrum regulations in low-SNR conditions.

We then apply sub-Nyquist acquisition techniques to characterize the occupancy state of a wide frequency band via inexpensive sensing architectures with minimal computational resources, where spectral prior information typically available in practice — e.g. spectral masks, roll-off factors, etc. —, is exploited to enable compression. To minimize the sampling rate, we extensively analyze the general problem of recovering second-order statistical information of wide-sense stationary processes from compressed measurements. Our results in this direction are of application well beyond spectrum sensing contexts.

Finally, we look at the problem of *spectrum cartography*, where the goal is to construct power spectrum maps characterizing the spectrum utilization not only along frequency and time, but also across space. We propose several methods capable of *learning* those maps based on the highly compressed observations reported by a collection of inexpensive sensors.



# Resumo (Galician)

A presente tese de doutoramento enmárcase no contexto de sistemas de sensado espectral con especial atención a esquemas de acceso dinámico ao espectro. Baixo este último termo englóbanse aqueles sistemas que pretenden incrementar a eficiencia de uso dos recursos espectrais existentes mediante unha flexibilización das políticas empregadas para a súa asignación. Nos esquemas empregados na actualidade, a autoridade reguladora do espectro electromagnético asigna bandas de frecuencia a grandes operadores, tipicamente mediante un sistema de poxas multimillonarias. Paradoxalmente, recentes campañas de medidas puxeron de manifesto o elevado grado de infrautilización que impera nestas bandas con licenza. Na vista destes resultados, varias comunidades de expertos suxiren considerar a opción de que usuarios sen licenza exploten estes *baleiros espectrais* para as súas actividades de comunicación a condición de que non degraden a calidade da comunicación do usuario con licenza cando este último accede ao canal. Por esta e outras razóns, tórnase necesario investigar mecanismos que permitan aos chamados *usuarios secundarios* coñecer, en cada momento, o estado do canal.

O problema principal radica en empregar un conxunto de observacións do canal, proporcionadas por un sensor espectral, para dar resposta a unha ou máis preguntas do tipo: hai algún *usuario primario* a operar na banda  $b$ ? se é así, con que potencia se recibe? Para proporcionar tal resposta, un riguroso conxunto de ferramentas estatísticas ponse en funcionamento para crear funcións dos sinais observados que devolven decisións que satisfacen certos requirimentos, tamén formulados en termos estatísticos. O noso abano inclúe metodoloxías importadas da teoría da detección, como o *cociente xeneralizado de verosimilitudes* ou a procura de *tests invariantes*, da teoría da estimación, como os estimadores de *máxima verosimilitude*, ou da teoría de aprendizaxe estatístico, como a *máquina de vectores soporte*.

## FORMULACIÓN DO SENSADO ESPECTRAL

O sensado espectral comprende unha colección de procedementos destinados a determinar o estado de ocupación de un canal de comunicacións — tipicamente sen fíos — a partir das

observacións obtidas por un ou máis sensores espectrais [Axell et al., 2012]. Por simplicidade, ao longo de toda a tese asumiremos que ningún usuario secundario está a transmitir durante a ventá de observación, de modo que o sensor espectral só recibirá un ou máis sinais primarios xunto con ruído/interferencia. Nótese a distinción terminolóxica entre estas dúas entidades mencionadas: a pesares de que un mesmo dispositivo poida actuar de sensor espectral e de usuario secundario, o primeiro engloba as funcións de sensado espectral mentres que o segundo encárgase das funcións de transmisión e recepción de comunicacións sen licenza.

Ao longo da tese, consideraremos dúas clases de procedementos de sensado espectral: aqueles destinados a determinar a potencia coa que se recibe o sinal primario e aqueles que simplemente tratan de establecer se algún usuario primario está a transmitir ou non.

- **Estimación de Potencia:** No escenario máis sinxelo, o sinal recibido por un sensor espectral pode ser expresado como

$$y = r + w, \quad (1)$$

onde  $r$  representa o termo de sinal, que contén o sinal primario despois de sufrir os efectos de propagación do canal, e  $w$  é ruído. No instante  $t$ , os sinais  $y$ ,  $r$  e  $w$  toman valores  $y(t)$ ,  $r(t)$  e  $w(t)$  respectivamente. Se non existise ambigüidade, a primeira notación será usada para se referir aos sinais en si mesmos, vistos como funcións ou procesos estocásticos, mentres que a segunda será usada para se referir ao resultado de avaliar tales sinais, vistos como escalares ou vectores. Se non se menciona o contrario, os sinais aleatorios serán modelados como procesos estocásticos estacionarios en sentido amplo de media cero, resultado de filtrar e converter a banda de interese a banda base.

O noso obxectivo é proporcionar unha estima da potencia do termo de sinal, definido como  $\eta_0^2 \triangleq E \{|r(t)|^2\}$ , que pode ser directamente enviada ao usuario secundario ou usada como paso intermedio para detección de actividade (ver máis abaixo). Estas estimas son obtidas a partir de caracterizacións estatísticas parciais do sinal recibido e mediante o emprego de metodoloxías como a de máxima verosimilitude [Kay, 1993].

- **Detección de Actividade:** Nalgunhas ocasións, a potencia do sinal primario non é relevante e o usuario secundario soamente está interesado en coñecer se un usuario primario está a transmitir ou non. No escenario máis sinxelo, deberemos decidir se as observacións conteñen o termo de sinal correspondente ao sinal primario despois de pasar polo canal ou se conteñen exclusivamente ruído. Formalmente, o problema consiste en decidir entre as

dúas hipóteses seguintes:

$$\mathcal{H}_0 : y = w, \quad \mathcal{H}_1 : y = r + w. \quad (2)$$

Problemas de este tipo son o obxecto de estudo da *teoría da detección* e da, máis xeral, *teoría de tests de hipóteses estatísticas* [Lehmann and Romano, 2005]. Da mesma forma que en estimación de potencia, a decisión baséase nunha caracterización estatística parcial das observacións. Tipicamente, avalíase unha función escalar das observacións, coñecida coma o estatístico do test, e decídese  $\mathcal{H}_1$  se este estatístico excede un umbral  $\nu$  e  $\mathcal{H}_0$  en caso contrario:

$$\mathcal{T}(y) \underset{\mathcal{H}_0}{\overset{\mathcal{H}_1}{\geq}} \nu. \quad (3)$$

O comportamento dun test, tamén coñecido neste contexto coma *detector*, caracterízase habitualmente mediante dúas métricas: a *probabilidade de falsa alarma* ( $P_{FA}$ ) e a *probabilidade de detección* ( $P_D$ ) [Kay, 1998]. Habitualmente en teoría da detección, o obxectivo é maximizar a  $P_D$  suxeito a unha cota superior sobre  $P_{FA}$ . Sen embargo isto non é posible en moitas circunstancias debido a que non existe un test que se comporte mellor que calquera outro test en calquera condición. Por esta razón, empregaremos basicamente dous métodos diferentes para construír  $\mathcal{T}$ : o primeiro é o coñecido *cociente xeneralizado de verosimilitudes* [Kay, 1998], mentres que o segundo consiste na busca de tests (localmente) óptimos en familias de tests que satisfacen certas propiedades de invarianza [Lehmann and Romano, 2005].

## O PAPEL DA INFORMACIÓN A PRIORI

Na ausencia de información *a priori*, non é posible distinguir o sinal primario do ruído e, en consecuencia, ningún estimador ou detector pode ser deseñado con garantías razoables de comportamento. É necesario, por tanto, explotar algunha característica que diferencie o sinal do ruído. Nesta tese, as características consideradas serán:

- **Información de Amplitude:** Nalgúns casos, é sabido que o sinal transmitido presenta unha amplitude constante, como acontece en moitos escenarios prácticos onde esta propiedade relaxa os requirimentos impostos sobre os amplificadores de potencia. Entre os exemplos deste tipo de sinais destacamos modulacións como FSK, CPM ou GMSK (ver Capítulo 1). No contexto de sistemas de acceso dinámico ao espectro, esta propiedade é especialmente relevante dado que os micrófonos sen fíos, que son considerados usuarios primarios nalgúns casos, empregan a modulación analóxica de frecuencia (FM), que produce

formas de onda con magnitude constante.

Noutros casos, é posible asumir que a amplitude do sinal primario segue unha distribución normal. Esta suposición está altamente motivada en escenarios de comunicacións por varias razóns: primeiramente, moitos sistemas de transmisión empregan modulacións con amplitude aproximadamente normal dado que esta distribución acada a capacidade do canal aditivo Gaussiano. Segundo, a amplitude de sinais multiportadora é aproximadamente Gaussiana. Terceiro, é unha hipótese de traballo moi habitual en procesado do sinal e estatística dado que conduce a modelos tratables e dado que moitos métodos que asumen Gaussianidade presentan un comportamento aceptable incluso en condicións afastadas desta suposición [Anderson, 2003, p. 3].

- **Estrutura Espectral:** En moitos escenarios prácticos, o coñecemento da estrutura espectral do sinal transmitido é altamente detallado debido a que moitos sistemas de transmisión actuais seguen estándares e regulacións coñecidos publicamente. Por exemplo, as características das formas de onda de WiFi, Bluetooth, telefonía celular, televisión dixital, etc son ditadas polo correspondente estándar, que especifica factores de *roll-off*, modulacións, número de portadoras, posición das portadoras piloto, etc. Outras características coma máscaras espectrais, frecuencias de portadora e anchos de banda están ditados polas regulacións do espectro. Por iso, é razoable asumir que a densidade espectral de potencia do sinal transmitido é aproximadamente coñecido excepto por un factor de escala.
- **Estrutura do Canal:** Espérase que os usuarios secundarios/sensores espectrais estean dotados de múltiples antenas debido ás súas vantaxes para comunicación e sensado espectral [Taherpour et al., 2010, Cabric, 2008]. Nalgúns casos, por exemplo, sábese que o ruído en diferentes antenas está incorrelacionado, mentres que o sinal primario pode estar altamente correlacionado. Outras formas de estrutura que explotaremos inclúen variacións temporais: debido ás longas ventás de observación necesarias para garantir un certo comportamento do método de sensado espectral, a suposición de que o canal permanece invariante no tempo podería estar moi afastada da realidade.

## SINOPSE

Mediante o emprego desta información *a priori*, esta tese presenta métodos de sensado espectral, tanto para estimación de potencia como para detección de actividade, encamiñados a resolver unha colección de problemas prácticos. De acordo co detallada que é a súa descrición dos *baleiros espectrais* [Zhao and Sadler, 2007], estes métodos poden ser clasificados en tres categorías:

- Sensado espectral nun só canal,



- Sensado espectral en múltiples canais,
- Cartografía espectral en múltiples canais.

Inda que o noso traballo é principalmente teórico, levamos a cabo un esforzo especial para garantir que os métodos propostos satisfagan certas propiedades necesarias en aplicacións prácticas. En concreto, ningún dos nosos métodos requiren o coñecemento da potencia de ruído. Ademais, todos os nosos métodos son invariantes a escalados, o cal minimiza os problemas asociados á calibración dos sensores. Ademais, ningún dos procedementos propostos precisa do coñecemento dos coeficientes do canal, o cal se motiva polo feito de que a relación sinal a ruído pode ser considerablemente baixa e polo feito de que os usuarios primarios non cooperan cos usuarios secundarios.

A continuación resumimos os problemas considerados e as nosas contribucións nas tres categorías anteriormente mencionadas.

## **SENSADO ESPECTRAL NUN SÓ CANAL**

Se concentramos a nosa atención no estado de ocupación dun canal de frecuencia en particular e nunha localización espacial en particular, o baleiro espectral é, polo tanto, unha colección unidimensional de intervalos temporais onde ningún usuario primario está a transmitir. Neste contexto consideraremos dúas clases de problemas:

### **Detección de Actividade de Micrófonos sen Fíos**

A organización reguladora do espectro electromagnético nos Estados Unidos de América, a *Federal Communications Commission* (FCC), permitirá a usuarios sen licenza transmitir nunha banda de televisión en localizacións onde esta non estea a ser usada polos usuarios primarios, que neste caso serían, entre outros, as estacións de televisión e os micrófonos sen fíos. Polo tanto, é de importancia crítica desenvolver esquemas capaces de detectar fiablemente a actividade deste tipo de dispositivos.

A literatura contén numerosos métodos especialmente deseñados para detectar a presenza de micrófonos sen fíos mediante o uso de sensores cunha soa antena. Entre estes destacamos [Xu et al., 2008, Hassan and Nasr, 2011, Chen and Gao, 2011, Chen et al., 2008, ElRamly et al., 2011, Gautier et al., 2010]. Por outra banda, existe unha ampla variedade de métodos para a detección de sinais primarios que empregan sensores multiantena, por exemplo [Alamgir et al., 2008, Besson et al., 2006, Taherpour et al., 2010, Wang et al., 2010, Ramírez et al., 2011, Sala-Álvarez et al., 2012, Vázquez-Vilar et al., 2011b, Zeng and Liang, 2009a]. Sen embargo, estas técnicas non están

enfocadas á detección de micrófonos sen fíos, e polo tanto o seu funcionamento é mellorable. Ao noso entender, na literatura non existe ningún detector destinado especificamente a detectar micrófonos sen fíos mediante sensores multiantena. Un dos nosos cometidos nesta tese será encher este baleiro, para o cal proporemos esquemas que explotan a información espacial xunto coas características propias das formas de onda dos micrófonos sen fíos. En particular, explotaremos o feito de que estes sinais ocupan un ancho de banda espectral considerablemente inferior ao do canal de televisión, e o feito de que estes micrófonos empregan habitualmente a modulación analóxica en frecuencia, a cal produce formas de onda con magnitude constante. Seguindo as directrices de simulación do grupo de traballo IEEE 802.22, concluímos que os esquemas propostos melloran notablemente os existentes.

## **Detección de Actividade en Canais Variantes no Tempo**

Consideremos un detector deseñado baixo a hipótese de que o canal é invariante no tempo. Cando este detector sexa usado na práctica, onde os canais satisfacen esta suposición só de forma aproximada, o seu rendemento incorrerá nunha certa degradación. En efecto, existe un amplo abano de situacións nas que as variacións do canal dentro da ventá de observación deben ser tidas en conta. Este é o caso, por exemplo, dos sistemas de comunicación de banda estreita, onde o tempo de coherencia do canal pode ser comparable ao período de símbolo. Outro exemplo radica nos sistemas de comunicación subacuática, onde as características de propagación dan lugar a rápidas variacións no canal [Marage and Mori, 2010]. No contexto de sistemas de acceso dinámico ao espectro, as regulacións imponen duros requisitos en canto ao comportamento dos detectores en condicións de baixa relación sinal a ruído, o que obriga a empregar longas ventás de observación [Cabric, 2008], nas que o canal pode variar significativamente, especialmente en entornos afectados por mobilidade.

A investigación previa relacionada con canais variantes no tempo considerou modelado, estimación, predición, ecualización, codificación, deseño de formas de onda, etc (ver [Hlawatsch and Matz, 2011] e as súas referencias). Sen embargo, ao noso entender, poucos esforzos foron destinados a resolver problemas de sensado espectral. Entre estes, só temos coñecemento de [Wang et al., 2010, Chen et al., 2007], obtidos coma implementacións adaptativas de esquemas para sensado en canais invariantes, co cal cabe esperar grandes degradacións en presenza de variacións rápidas. Ademais, no noso coñecemento, non existe ningún esquema na literatura capaz de aproveitar as variacións do canal no seu favor. É un dos labores desta tese o de propoñer métodos de detección de actividade en canais variantes no tempo que exploten no seu beneficio as variacións deste ao longo do tempo.

Primeiramente consideramos o problema de detectar sinais con magnitude constante ob-

servados con ruído de potencia descoñecida despois de atravesar un canal de propagación con resposta plana en frecuencia e con variacións no tempo aleatorias. Usando unha parametrización lineal con coordenadas aleatorias para modelar as variacións no tempo [Tsatsanis and Giannakis, 1996a, Giannakis and Tepedelenlioglu, 1998], derivamos o cociente xeneralizado de verosimilitudes. Se o sinal de módulo constante transmitido é coñecido, o esquema resultante xeneraliza o detector de filtro adaptado [Kay, 1998]; en caso contrario requírese a solución dun difícil problema non convexo, para o cal propoñemos diferentes aproximacións con baixos requirimentos computacionais e un eficiente algoritmo iterativo de punto fixo.

A continuación, consideramos o problema de detectar sinais Gaussianos observados con ruído de potencia descoñecida despois de atravesar un canal de propagación con resposta plana en frecuencia e con variacións no tempo. Baixo diferentes modelos para o canal, derivamos varios detectores para sensores cunha soa antena e un detector para sensores con múltiples antenas. Este último resulta de derivar o cociente xeneralizado de verosimilitudes e de empregar un algoritmo de estimación-maximización (EM) para o seu cómputo. Sen embargo, as limitacións do modelo impiden a este detector operar en condicións de variación moi rápidas, o cal motiva o uso de tests para a homoxeneidade de covarianzas. Inda que non nos internamos neste ámbito, sí proporcionamos un dos primeiros pasos nesta liña de investigación ao obter de forma teórica os tests invariantes localmente óptimos. Estes tests estarían indicados para casos de baixa relación sinal a ruído, coma pode acontecer en sistemas de acceso dinámico ao espectro. Para realizar este traballo de natureza fundamental restrinximos a nosa atención aos tests invariantes baixo un grupo de transformacións nas que incluímos transformacións afíns invertibles e permutacións. O resultado tamén é particularizado ao test de escala (ver Apéndice).

## SENSADO ESPECTRAL EN MÚLTIPLES CANAIS

Se o noso obxectivo é caracterizar a ocupación espectral do conxunto de canais contidos nunha banda ancha de frecuencias nun lugar determinado, o baleiro espectral é, por tanto, o conxunto bidimensional de puntos no plano tempo-frecuencia no que ningún usuario primario está a operar. Considerar múltiples canais simultaneamente presenta numerosas vantaxes xa que permite incrementar a probabilidade de que os usuarios secundarios atopen un canal vacante ou, incluso, transmitir en múltiples canais ao mesmo tempo.

Un dos maiores retos do sensado espectral de bandas anchas é a problemática asociada á limitación práctica na elección da frecuencia de mostreo: o mostreo a taxa de Nyquist pode ser prohibitivo en termos de custo do hardware e en termos de consumo de potencia. Para afrontar esta dificultade, é habitual introducir compresión na etapa de adquisición. Neste contexto, consideramos dous problemas:

## Sensado Espectral

O obxectivo é determinar o estado de ocupación dunha banda de frecuencias a partir de mostras comprimidas. Unha posible aproximación ao problema é primeiramente reconstruír o sinal non comprimido, por exemplo usando *compressed sensing* [Donoho, 2006, Candès and Wakin, 2008], e a continuación aplicar unha técnica convencional de sensado espectral sobre o resultado (ver [Sun et al., 2013] e as súas referencias). Para poder introducir compresión, é necesario que exista certa estrutura no sinal, por exemplo *sparsity*. Outra opción é tratar de obter directamente a información de interese a partir das mostras obtidas, evitando o paso intermedio de reconstrución [Ariananda and Leus, 2012, Lexa et al., 2011]. Claramente, esta aproximación permite acadar unha maior compresión e reducir significativamente o custo computacional. A compresión é posible dado que soamente os estatísticos de segunda orde son necesarios para obter a información de ocupación, e estes estatísticos están altamente estruturados en procesos estacionarios en sentido amplo. Nesta tese propoñemos métodos de sensado espectral capaces de operar directamente sobre as mostras comprimidas de acordo con esta segunda filosofía.

O noso cometido é superar as limitacións dos esquemas existentes para sensado de banda ancha [Quan et al., 2009, Taherpour et al., 2008, Vázquez-Vilar and López-Valcarce, 2011, Ariananda and Leus, 2012] (ver Capítulo 1). Para iso presentamos unha colección de métodos paramétricos para a estimación do espectro de potencia a partir de medidas comprimidas. A información *a priori* captúrase empregando unha parametrización lineal dos estatísticos de segunda orde, motivados pola observación anteriormente mencionada de que a densidade espectral de potencia dos sinais primarios é habitualmente coñecida de forma aproximada. Inda que o problema se poida formular en termos de estimación de covarianza estruturada [Burg et al., 1982], os algoritmos existentes para esta disciplina son excesivamente complexos. Por esta razón desenvolvemos unha colección de métodos que permiten obter a información de interese con un baixo custo computacional.

## Deseño da Etapa de Compresión

O uso de algoritmos de sensado espectral capaces de operar sobre mostras comprimidas require o deseño do propio sistema de adquisición. Nesta tese consideramos este problema, que resulta ser unha cuestión fundamental extensible a múltiples ámbitos de procesado do sinal máis alá do sensado espectral.

Os traballos existentes na literatura só consideran casos particulares deste problema [Moffet, 1968, Hooft and Kassam, 1990, Pillai et al., 1985, Pal and Vaidyanathan, 2010, Pal and Vaidyanathan, 2011, Rédei and Rényi, 1949, Leech, 1956, Wichmann, 1963, Wild, 1987, Pearson

et al., 1990, Linebarger et al., 1993, Pillai et al., 1985, Wichmann, 1963, Pearson et al., 1990, Linebarger et al., 1993, Pumphrey, 1993, Pal and Vaidyanathan, 2010, Pal and Vaidyanathan, 2012] ou proporcionan deseños baseados nas necesidades de determinados algoritmos [Ariananda and Leus, 2012, Domínguez-Jiménez and González-Prelcic, 2013, Yen et al., 2013]. Ao noso entendemento, a máxima taxa de compresión posible permanece como un problema aberto en moitos casos de interese, e poucos esforzos foron destinados a proporcionar resultados con validez universal. É o noso obxectivo nesta tese presentar un marco de traballo xeral e formal, non baseado en ningún algoritmo en concreto, que permita deseñar os sistemas de compresión a partir de criterios abstractos. Proporcionamos ferramentas sinxelas que permiten establecer a admisibilidade dun sistema de compresión para tódolos casos onde os estatísticos de segunda orde obedecen a unha parametrización lineal e para algúns dos casos nos que esta parametrización non é lineal. Derivamos as máximas taxas de compresión acadables usando demostracións construtivas, polo que tamén obtemos deseños óptimos.

## CARTOGRAFÍA ESPECTRAL EN MÚLTIPLES CANAIS

A noción máis xeral de baleiro espectral que consideraremos nesta tese resulta de incorporar a dimensión espacial ao sensado de múltiples canais. Nese caso, o noso obxectivo consiste en monitorizar o uso do espectro ao longo do espazo, tempo e frecuencia. Esta información represéntase en *mapas espectrais*, que poden ser empregados por usuarios secundarios para identificar *zonas reusables* [Nishimori et al., 2007]. Os métodos de cartografía espectral tipicamente obteñen estes mapas a partir das observacións proporcionadas por unha colección de sensores espectrais distribuídos pola zona de interese.

Entre os esquemas de cartografía propostos na literatura, unha parte significativa están destinados á elaboración de *mapas de potencia*, os cales representan a distribución espacial da potencia dun sinal [Alaya-Feki et al., 2008, Jayawickrama et al., 2013, Huang et al., 2015, Kim et al., 2011b, Kim and Giannakis, 2013]. A principal desvantaxe destes métodos radica en que non distinguen sinal de ruído, polo que as tarefas de sensado espectral non poden levarse a cabo sen coñecer a potencia de ruído. Outra parte está composta polos esquemas que incorporan a dimensión frecuencial, considerando múltiples canais simultaneamente e distinguindo, posiblemente, sinal de ruído [Bazerque and Giannakis, 2010, Dall’Anese et al., 2012, Bazerque et al., 2011]. Desafortunadamente estes métodos requiren que os sensores intercambien co centro de fusión ou con outros sensores unha elevada cantidade de datos, e requiren de complexas arquitecturas de hardware.

Para solventar as limitacións destes métodos, propoñemos unha familia de técnicas de cartografía espectral onde os sensores poden ser implementados en dispositivos de baixo custo e

onde as necesidades de comunicación son mínimas. Mediante ferramentas de regresión en *espazos de Hilbert con núcleo reprodutor* para funcións vectoriais [Micchelli and Pontil, 2005], propoñemos un método non paramétrico e un método semiparamétrico para estimar os mapas espectrais a partir de medidas altamente comprimidas. Os problemas de optimización resultante son idénticos aos empregados en aprendizaxe estatístico polas *máquinas de vectores soporte* [Schölkopf and Smola, 2001, Cherkassky and Mulier, 2007, Smola and Schölkopf, 2004, Smola et al., 1998], o cal reporta múltiples vantaxes en termos teóricos e prácticos. Finalmente propoñemos unha implementación *en liña* para o método non paramétrico mediante descenso por gradiente no espacio de funcións [Kivinen et al., 2004, Audiffren and Kadri, 2013]. Neste contexto, propoñemos unha nova representación para o campo vectorial que pode ser de aplicación en calquera problema de estimación non paramétrica con redes de sensores.

## **ESTRUTURA DA TESE**

O contido principal desta tese estrutúrase en 8 capítulos, agrupados en 3 partes, e un apéndice. A primeira parte, que inclúe os Capítulos 2, 3 e 4, considera problemas de sensado espectral nun só canal. A segunda parte, que comprende os Capítulos 5 e 6, contén a nosa contribución ao sensado espectral en múltiples canais. A terceira parte, que inclúe o Capítulo 7, trata o problema da cartografía espectral en múltiples canais. Finalmente, o Capítulo 8 presenta as conclusións e as liñas futuras. O Apéndice considera un problema de natureza fundamental, con implicacións máis alá do sensado espectral.

# Publications

The following is a list of journal and conference publications that have been produced as a result of the work on this thesis.

## Journal publications

1. **D. Romero**, J. Vía, R. López-Valcarce, and I. Santamaría, *On the existence of locally optimal invariant tests for homogeneity of covariance matrices*, In preparation.
2. **D. Romero**, S.-J. Kim, G. B. Giannakis, and R. López-Valcarce, *Learning spectrum maps from quantized observations*, IEEE Trans. Sig. Process., *Submitted Mar. 2015*.
3. **D. Romero**, D. D. Ariananda, Z. Tian, and G. Leus, *Compressive Covariance Sensing: A new look at estimation from compressed observations*, IEEE Sig. Process. Mag., *Submitted. Feb. 2015*.
4. D. D. Ariananda, **D. Romero**, and G. Leus, *Compressive Periodogram Reconstruction Using Uniform Binning*, IEEE Trans. Sig. Process. (Accepted), 2015, Online: <http://arxiv.org/abs/1407.4017>.
5. **D. Romero**, R. López-Valcarce, and G. Leus, *Compression limits for random vectors with linearly parameterized second-order statistics*, IEEE Trans. Inf. Theory, vol. 61, pp. 1410-1425, Mar. 2015.
6. J. Schmidt, **D. Romero**, and R. López-Valcarce, *Active interference cancellation for OFDM spectrum sculpting: Linear processing is optimal*, IEEE Commun. Lett., vol. 18, pp. 1543–1546, Sep. 2014.
7. **D. Romero** and R. López-Valcarce, *Spectrum sensing for wireless microphone signals using multiple antennas*, IEEE Trans. Veh. Technol., vol. 63, pp. 4395–4407, Nov. 2014.

8. **D. Romero** and G. Leus, *Wideband spectrum sensing from compressed measurements using spectral prior information*, IEEE Trans. Sig. Process., vol. 61, no. 24, pp. 6232–6246, 2013.

## Conference publications

1. **D. Romero**, S.-J. Kim, R. López-Valcarce, and G. B. Giannakis, *Spectrum Cartography using Quantized Observations*, in Proc. IEEE Int. Conf. Acoust., Speech, Sig. Process., (Brisbane, Australia), 2015.
2. **D. Romero**, S.-J. Kim, and G. B. Giannakis, *Online Spectrum Cartography via Quantized Measurements*, in Proc. Conf. Inf. Sci. Syst., (Baltimore, MD), Mar. 2015.
3. J. F. Schmidt, **D. Romero**, and R. López-Valcarce, *Low-power active interference cancellation for OFDM spectrum sculpting*, in Proc. European Sig. Process. Conf. (Lisbon, Portugal), pp. 581–585, Sep. 2014.
4. **D. Romero** and R. López-Valcarce, *Nearly-optimal compression matrices for signal power estimation*, in Proc. IEEE Int. Workshop Sig. Proc. Advances Wireless Commun., (Toronto, Canada), pp. 434–438, Jun. 2014.
5. D. D. Ariananda, **D. Romero**, and G. Leus, *Cooperative compressive power spectrum estimation*, in Proc. IEEE Sensor Array Multichannel Sig. Proc. Workshop, (A Corunha, Spain), pp. 97–100, Jun. 2014.
6. D. D. Ariananda, **D. Romero**, and G. Leus, *Compressive angular and frequency periodogram reconstruction for multiband signals*, in Proc. IEEE Int. Workshop Comput. Advances Multi-Sensor Adaptive Process., (San Martin, France), pp. 440–443, Dec. 2013.
7. **D. Romero**, R. López-Valcarce, and G. Leus, *Compressive wideband spectrum sensing with spectral prior information*, in Proc. IEEE Int. Conf. Acoust., Speech, Sig. Process., (Vancouver, Canada), pp. 4469–4473, May. 2013.
8. **D. Romero** and R. López-Valcarce, *Spectrum sensing in time-varying channels using multiple antennas*, in Proc. IEEE Int. Workshop Sig. Process. Advances Wireless Commun., (Darmstadt, Germany), pp. 135–139, Jun. 2013.
9. **D. Romero** and G. Leus, *Compressive covariance sampling*, in Inform. Theory Appl. Workshop, (San Diego, CA), pp. 1–8, Feb. 2013.



10. **D. Romero**, J. Via, R. López-Valcarce, and I. Santamaria, *Detection of Gaussian signals in unknown time-varying channels*, in Proc. IEEE Statistical Sig. Process. Workshop, (Ann Arbor, MI), pp. 916–919, Aug. 2012.
11. **D. Romero** and R. López-Valcarce, *Detection of unknown constant magnitude signals in time-varying channels*, in Cognitive Inform. Process., (Baiona, Spain), pp. 1-6, May 2012.
12. **D. Romero**, R. López-Valcarce, and G. Leus, *Generalized matched filter detector for fast fading channels*, in Proc. IEEE Int. Conf. Acoust., Speech, Sig. Process., (Kyoto, Japan), pp. 3165–3168, Mar. 2012.
13. **D. Romero** and R. López-Valcarce, *Bandlimited or constant envelope? exploiting wave-form properties in wireless microphone detection*, in Proc. IEEE Int. Workshop Comput. Advances Multi-Sensor Adaptive Process., (San Juan, Puerto Rico), pp. 321–324, Dec. 2011.
14. **D. Romero** and R. López-Valcarce, *Multiantenna detection of constant-envelope signals in noise of unknown variance*, in Proc. IEEE Int. Workshop Sig. Process. Advances Wireless Commun., (San Francisco, CA), pp. 446–450, Jun. 2011.
15. **D. Romero** and R. López-Valcarce, *Distributed spectrum sensing with multiantenna sensors under calibration errors*, in Proc. IEEE Int. Workshop Sig. Process. Advances Wireless Commun., (San Francisco, CA), pp. 441–445, Jun. 2011.



# Contents

<b>Acknowledgements</b>	<b>iii</b>
<b>Abstract</b>	<b>vii</b>
<b>Resumo (Galician)</b>	<b>ix</b>
<b>Publications</b>	<b>xix</b>
<b>Contents</b>	<b>xxix</b>
<b>List of Tables</b>	<b>xxxix</b>
<b>List of Figures</b>	<b>xxxv</b>
<b>1 Introduction</b>	<b>1</b>
1.1 Motivation and Context . . . . .	1
1.1.1 Spectrum Sensing . . . . .	2
1.1.2 Compressive Covariance Sampling . . . . .	12
1.2 Prior Work and Contributions . . . . .	17
1.2.1 Spectrum Sensing in a Single Channel . . . . .	18
1.2.2 Spectrum Sensing in Multiple Channels . . . . .	21
1.2.3 Spectrum Cartography in Multiple Channels . . . . .	23
1.3 Thesis Structure . . . . .	25
1.4 Notation . . . . .	26

<b>I</b>	<b>Spectrum Sensing in a Single Channel</b>	<b>31</b>
<b>2</b>	<b>Detection of Wireless Microphone Signals Using Multiple Antennas</b>	<b>33</b>
2.1	Problem setting . . . . .	34
2.1.1	Signal Model . . . . .	35
2.1.2	Generalized Likelihood Ratio . . . . .	36
2.2	Multiantenna Detection of BL Signals . . . . .	36
2.2.1	Arbitrary Channel Structure . . . . .	38
2.2.2	Frequency-Flat Channels . . . . .	39
2.3	Multiantenna detection of CM signals . . . . .	40
2.3.1	Arbitrary Channel Structure . . . . .	41
2.3.2	Frequency-Flat Channels . . . . .	41
2.4	Detection of CM Bandlimited Signals . . . . .	42
2.5	Remarks . . . . .	44
2.5.1	Interpretation . . . . .	44
2.5.2	Dealing with an Unknown Carrier Frequency . . . . .	45
2.5.3	Computational Complexity . . . . .	47
2.6	Performance Analysis . . . . .	47
2.6.1	BL Detector . . . . .	48
2.6.2	BLFF Detector . . . . .	49
2.6.3	CM and CMBL Detectors . . . . .	50
2.7	Simulation Results . . . . .	50
2.7.1	Simulation Setting . . . . .	50
2.7.2	Comparison with Existing Detectors . . . . .	52
2.7.3	Performance of the Proposed Detectors . . . . .	53
2.8	Conclusions . . . . .	57
2.A	Computation of the (2,1)-norm . . . . .	58

<b>3</b>	<b>Detection of Constant Magnitude Signals in Time-Varying Channels</b>	<b>61</b>
3.1	Signal Model . . . . .	61
3.2	GLR Detector for Known CM Signals . . . . .	63
3.3	GLR Detector for Unknown CM Signals . . . . .	66
3.3.1	Low-Complexity Approximations . . . . .	67
3.3.2	Numerical Optimization . . . . .	70
3.4	Performance Analysis . . . . .	72
3.5	Simulation Results and Discussion . . . . .	73
3.5.1	Detector for Known CM Signals . . . . .	74
3.5.2	Detectors for Unknown CM Signals . . . . .	75
3.6	Conclusions . . . . .	78
<b>4</b>	<b>Detection of Gaussian Signals in Time-Varying Channels</b>	<b>81</b>
4.1	Observation Model . . . . .	82
4.2	Detectors for Single-Antenna Sensors . . . . .	83
4.2.1	Generalized Likelihood Ratio Test . . . . .	84
4.2.2	Towards Locally Optimal Invariant Tests . . . . .	85
4.3	Detectors for Multiantenna Sensors . . . . .	89
4.3.1	Generalized Likelihood Ratio Test . . . . .	89
4.3.2	EM algorithm . . . . .	90
4.3.3	Rapidly-changing Channels . . . . .	94
4.4	Simulation Results . . . . .	97
4.5	Conclusions . . . . .	101
4.A	Proof of Proposition 4.1 . . . . .	101
<b>II</b>	<b>Spectrum Sensing in Multiple Channels</b>	<b>105</b>
<b>5</b>	<b>Wideband Spectrum Sensing from Compressed Measurements</b>	<b>107</b>

5.1	Wideband Spectral Estimation and Detection . . . . .	108
5.1.1	Power Estimation and Activity Detection . . . . .	109
5.1.2	Complexity of the Exact ML Solution . . . . .	110
5.1.3	Dimensionality Reduction . . . . .	111
5.2	Estimation Algorithms . . . . .	116
5.2.1	The True ML Estimate . . . . .	117
5.2.2	Unconstrained ML Estimation . . . . .	118
5.2.3	Least Squares Estimation . . . . .	120
5.2.4	Estimation Using SPICE . . . . .	121
5.3	Remarks . . . . .	124
5.4	Simulation Results . . . . .	126
5.4.1	Estimation Performance . . . . .	127
5.4.2	Detection Performance . . . . .	128
5.5	Conclusions . . . . .	131
5.A	Proof of Theorem 5.1 . . . . .	132
5.B	Proof of Expression (5.35c) . . . . .	134
<b>6</b>	<b>Sampler Design for Compressive Covariance Sampling</b>	<b>137</b>
6.1	Theoretical Framework . . . . .	137
6.1.1	Interpretation . . . . .	139
6.1.2	Notable Covariance Subspaces . . . . .	140
6.2	Design of Covariance Samplers . . . . .	142
6.2.1	Design of Sparse Samplers . . . . .	143
6.2.2	Design of Dense Samplers . . . . .	144
6.3	Universal Covariance Samplers . . . . .	144
6.3.1	Sparse Samplers . . . . .	145
6.3.2	Dense Samplers . . . . .	148
6.4	Non-Universal Covariance Samplers . . . . .	149

6.4.1	Circulant Covariance Subspace . . . . .	149
6.4.2	Banded Covariance Subspace . . . . .	153
6.5	Asymptotic Regime . . . . .	155
6.6	Discussion . . . . .	156
6.7	Conclusions . . . . .	156
6.A	Proof of Lemma 6.1 . . . . .	157
6.B	Proof of Theorem 6.2 . . . . .	158
6.C	Proof of Lemma 6.6 . . . . .	161
6.D	Proof of Theorem 6.4 . . . . .	163
6.E	Proof of Theorem 6.6 . . . . .	164
6.F	Proof of Theorem 6.7 . . . . .	165
6.G	Proof of Theorem 6.8 . . . . .	166
<b>III</b>	<b>Cartography Learning in Multiple Channels</b>	<b>167</b>
<b>7</b>	<b>Learning Power Spectrum Maps from Compressed Measurements</b>	<b>169</b>
7.1	Problem Formulation . . . . .	170
7.2	Cartography Learning . . . . .	171
7.2.1	Nonparametric Regression . . . . .	173
7.2.2	Semiparametric Regression . . . . .	175
7.3	Extensions . . . . .	180
7.3.1	Extension to Multiple Measurements per Sensor . . . . .	180
7.3.2	Non-uniform Quantization . . . . .	183
7.3.3	Enforcing Non-negativity . . . . .	183
7.4	Online Implementation . . . . .	184
7.5	Implementation Issues . . . . .	187
7.6	Simulation Results . . . . .	188
7.7	Conclusions . . . . .	193

7.A	Acquisition with Pseudo-Random Filters . . . . .	193
7.B	Proof of Proposition 7.1 . . . . .	194
7.C	Proof of Proposition 7.2 . . . . .	196
7.D	Derivation of (7.35) . . . . .	197
7.E	Efficient Matrix Computation for Decoupled Models . . . . .	198
<b>8</b>	<b>Conclusions and Future Work</b>	<b>201</b>
8.1	Conclusions . . . . .	201
8.2	Open Lines and Future Work . . . . .	202
8.2.1	Spectrum Sensing in a Single Channel . . . . .	203
8.2.2	Spectrum Sensing in Multiple Channels . . . . .	204
8.2.3	Spectrum Cartography in Multiple Channels . . . . .	205
	<b>Appendix</b>	<b>207</b>
A.1	Introduction . . . . .	207
A.2	Testing Equality of Covariance Matrices . . . . .	210
A.2.1	Problem Formulation . . . . .	210
A.2.2	Existing Tests . . . . .	212
	Generalized Likelihood Ratio Test . . . . .	212
	Wald Test . . . . .	212
	Locally Asymptotically Optimal Gaussian Test . . . . .	213
	Nagao test . . . . .	213
A.3	Optimal Invariant Test . . . . .	214
A.3.1	Problem Invariances . . . . .	214
A.3.2	Maximal Invariant Statistic . . . . .	215
A.3.3	Most Powerful Invariant Test . . . . .	217
A.4	Locally Optimal Invariant Tests . . . . .	218
A.4.1	Locally Most Powerful Invariant Tests . . . . .	218



A.4.2	Existence of the LMPI Test . . . . .	221
	Case $M = 1$ . . . . .	221
	Case $K = 2$ . . . . .	221
	Case $K = 1$ with known mean . . . . .	221
A.5	Scale test . . . . .	222
A.6	Conclusions . . . . .	223
A.A	Proof of Theorem A.1 . . . . .	223
A.B	Proof of Theorem A.2 . . . . .	225
	A.B.1 Case $M = 1$ . . . . .	227
	A.B.2 Case $M > 1$ . . . . .	227
A.C	Proof of Lemma A.4 . . . . .	230
A.D	Proof of Lemma A.1 . . . . .	230



# List of Tables

1.1	Summary of chapters and contributions. . . . .	26
1.2	Description of some of the symbols used in the thesis. . . . .	27
1.3	Matrix/vector notation. . . . .	28
1.4	Acronyms and abbreviations (1/2). . . . .	29
1.5	Acronyms and abbreviations (2/2). . . . .	30
2.1	Test vectors employed in WM simulation [Clanton et al., 2007]. Frequency units are kHz in all cases. . . . .	51
6.1	Values of $\bar{N}$ for a length- $(N - 1)$ minimal circular sparse ruler ( $\bar{N}_{\text{CSR}}$ ), length- $\lfloor \frac{N}{2} \rfloor$ minimal linear sparse ruler ( $\bar{N}_{\text{HLSR}}$ ) and length- $(N - 1)$ minimal linear sparse ruler ( $\bar{N}_{\text{LSR}}$ ). . . . .	148



# List of Figures

2.1	Comparison of the proposed schemes (CMBL, BLFF, BL and CM) with competing multiantenna detectors. (Test vector 5, $K = 1024$ , $\mathcal{B} = 200$ kHz, $f_s = 6$ MHz, Rayleigh Channel, $\gamma = -20$ dB, $M = 4$ ). . . . .	52
2.2	Comparison of the proposed techniques (CMBL, BLFF, BL and CM) with competing WM detectors. (Test Vector 5, $K = 1024$ , $\mathcal{B} = 200$ kHz, $f_s = 6$ MHz, Rayleigh Channel, $M = 4$ , $P_{FA} = 0.1$ ). . . . .	53
2.3	Influence of the number of antennas in the probability of detection ( $K = 1024$ , $\mathcal{B} = 200$ kHz, $f_s = 6$ MHz, Test Vector 5, Rayleigh Channel, $\gamma = -24$ dB, $P_{FA} = 0.1$ ). . . . .	54
2.4	Probability of detection <i>vs.</i> sampling frequency, which is inversely proportional to the fraction of bandwidth occupied by the WM signal ( $K = 1024$ , $\mathcal{B} = 200$ kHz, $f_s = 200$ kHz, Test Vector 5, Rayleigh Channel, $\gamma = -20$ dB, $M = 4$ , $P_{FA} = 0.1$ ). . . . .	55
2.5	ROC of the BLFF detector for the different test vectors ( $K = 1024$ , $\mathcal{B} = 200$ kHz, $f_s = 6$ MHz, $\gamma = -22$ dB, $M = 4$ ). . . . .	56
2.6	Probability of detection <i>vs.</i> the number of candidate carrier frequencies ( $K = 1024$ , $\mathcal{B} = 200$ kHz, $f_s = 6$ MHz, Test Vector 5, Rayleigh Channel, $M = 4$ , $P_{FA} = 0.1$ ). . . . .	56
3.1	Cost of the original problem in terms of the optimal cost of the SDP (3.39a) ( $K = 32$ , $B = 9$ , $\gamma = 3$ dB, 30 points/cluster). . . . .	70
3.2	Comparison between theoretical and Monte Carlo results for several BEM and Jakes channels ( $K = 32$ , $\gamma = -6$ dB). . . . .	74
3.3	Probability of detection <i>vs.</i> SNR for several BEM and Jakes channels. The Doppler spread of the channel is known ( $K = 32$ , $P_{FA} = 0.1$ ). . . . .	76

3.4	Probability of detection <i>vs.</i> the (known) Doppler spread for several SNR values ( $K = 32$ , $P_{FA} = 0.1$ ). . . . .	76
3.5	Probability of detection <i>vs.</i> the (unknown) Doppler spread for different assumed values of $B$ ( $K = 32$ , $P_{FA} = 0.1$ , $\gamma = 0$ dB). . . . .	77
3.6	ROC curves of the different detectors ( $K = 64$ , $\gamma = 3$ dB, BEM channel with $B = 5$ (Doppler spread = $\pi \times 0.0625$ rad/sample)). . . . .	77
3.7	ROC curves of the different detectors ( $K = 64$ , $\gamma = 3$ dB, BEM channel with $B = 17$ (Doppler spread = $\pi \times 0.250$ rad/sample)). . . . .	79
3.8	Probability of detection <i>vs.</i> SNR for $P_{FA} = 0.1$ ( $K = 64$ samples, BEM channel with $B = 5$ (Doppler spread = $\pi \times 0.0625$ rad/sample)). . . . .	79
3.9	Probability of detection <i>vs.</i> SNR for $P_{FA} = 0.1$ ( $K = 64$ samples, BEM channel with $B = 17$ (Doppler spread = $\pi \times 0.250$ rad/sample)). . . . .	80
3.10	Probability of detection of the PRFP detector <i>vs.</i> the Doppler spread of the channel for different values of $B$ used by the detector ( $K = 32$ , $P_{FA} = 0.1$ , $\gamma = 5$ dB). . . . .	80
4.1	Probability of detection <i>vs.</i> the number of basis functions used in the BEM model when $P_{FA} = 0.10$ ( $K = 128$ , $\gamma = 0$ dB). . . . .	97
4.2	Probability of detection <i>vs.</i> SNR when $P_{FA} = 0.10$ . On the left, the number of basis functions $B$ is set to 3, whereas on the right it is set to 32 ( $K = 32$ ). . . . .	98
4.3	Performance of the proposed detectors <i>vs.</i> the number of samples $K$ and basis functions $B$ when $P_{FA} = 0.10$ and $K = B$ ( $\gamma = 20$ dB). . . . .	99
4.4	$P_D$ for fixed $P_{FA} = 0.10$ ( $K = 20$ , $\gamma = 0$ dB). . . . .	100
4.5	Receiver Operating Characteristics ( $K = 20$ , $M = 4$ , $B = 5$ ). . . . .	100
5.1	Comparison between the true ML solution and a modification of the ML estimate that incorporates averaging and cropping (ACML) ( $K = 325$ , $\alpha = [4, 9, 4, 9, 4, 9, 1]^T$ , dense sampler, $N = 5$ , $\bar{N} = 2$ ). . . . .	114
5.2	PSD estimates for (from left to right) six QAM signals and seven OFDM signals. Many curves overlap since the estimates are close to each other ( $K = 10240$ , dense sampler, $N = 10$ , $\bar{N} = 5$ , $\tilde{L} = 6$ ). . . . .	127
5.3	Comparison of the estimation performance of the different algorithms presented in the chapter ( $\alpha = [4, 9, 1]^T$ , dense sampler, $N = 5$ , $\bar{N} = 2$ , $\tilde{L} = 9$ ). . . . .	128

5.4	A large portion of the samples can be discarded without a meaningful performance loss ( $K = 900$ , $\alpha = [4, 9, 1]^T$ , dense sampler, $N = 30$ , $\tilde{L} = 16$ ). . . . .	129
5.5	Influence of the number of channels in the estimation performance. $\alpha_b = 1$ for $b = 0, 1, \dots, B - 2$ and $\alpha_{B-1} = 10$ ( $K = 5120$ , dense sampler, $N = 10$ , $\bar{N} = 5$ , $\tilde{L} = 11$ ). . . . .	129
5.6	ROC comparing the algorithms of this chapter. ( $K = 300$ , $\alpha = [0.2, 9, 1]^T$ , sparse sampler, $N = 10$ , $\bar{N} = 5$ , $\tilde{L} = 5$ ). . . . .	130
5.7	Influence of the number of channels on the detection performance. $\alpha_0 = 0.4$ , $\alpha_1 = 4$ , $\alpha_{B-1} = 10$ and $\alpha_b = 0$ for $b = 2, 3, \dots, B - 2$ ( $K = 300$ , sparse sampler, $N = 10$ , $\bar{N} = 5$ ). . . . .	131
6.1	Example of a length-10 minimal sparse ruler (above) and length-20 minimal sparse ruler (below). . . . .	147
6.2	Comparison of two length-20 circular sparse rulers. The ruler on the left, with 5 elements, is minimal whereas the one on the right, with 6 elements, is not. . . .	151
7.1	Comparison of the true and estimated maps for $Z = 40$ sensors, $M = 6$ measurements per sensor, 8 bits/measurement, $\lambda = 10^{-7}$ , constant probability quantization and nonnegativity enforcement. . . . .	189
7.2	Effects of compression ( $B = 5$ , $M = 5$ measurements per sensor, uniform quantization, $\sigma_q^2 = 0$ , $\lambda = 10^{-6}$ , nonnegativity not enforced). . . . .	190
7.3	Influence of the extensions discussed in Section 7.3 on the estimation performance ( $B = 5$ , $Z = 40$ , 2 bits/measurement, $\sigma_q^2 = 0$ , $\lambda = 10^{-6}$ ). . . . .	190
7.4	Influence of the measurement noise ( $B = 5$ , $Z = 40$ , $M = 5$ , Gaussian kernel, $\lambda = 10^{-6}$ , nonnegativity not enforced). . . . .	191
7.5	Comparison batch <i>vs.</i> online ( $B = 5$ components, $Z = 30$ sensors, 4 bits/measurement, uniform quantization, $\sigma_q^2 = 0$ , Gaussian kernel, $\lambda = 10^{-6}$ , nonnegativity not enforced). . . . .	192
7.6	Influence of the measurement errors in the convergence of the online algorithm ( $B = 5$ components, $Z = 30$ sensors, 4 bits/measurement, uniform quantization, Gaussian kernel, $\lambda = 10^{-6}$ , nonnegativity not enforced, $\kappa_t = 0.05$ ). . . . .	192





# Chapter 1

## Introduction

In the last few years, we have witnessed an explosive increase in wireless traffic demand. Far from slowing down, this trend is in fact accelerating, and is expected to lead to a ten-fold throughput increase in the next five years [Cisco Systems, 2015]. In correspondence with this growth, the price of licensed bands has rocketed exorbitantly, which suggests that the RF spectrum is becoming a scarce resource. This observation, however, stands in contradiction with recent measurement campaigns, which report that licensed bands remain highly unused for significant periods of time (see e.g. [Federal Communications Commission, 2002, Shared Spectrum Company, 2010]).

This paradoxical situation has been ascribed to the static nature of current spectrum regulation policies [Federal Communications Commission, 2002], where frequency bands are allocated for long periods of time to users which purchase a license. Thus, a dramatic improvement in the RF spectrum exploitation might result from allowing a more flexible and dynamic usage [Zhao and Sadler, 2007].

### 1.1 Motivation and Context

The above concern has spurred on a great deal of research efforts to devise alternatives to current static regulations. In this sense, a diversity of paradigms for *dynamic spectrum access* (DSA) have been proposed in the literature (see [Zhao and Sadler, 2007] and references therein). Among the most remarkable ones is the *hierarchical access model*, which governs the operation of two classes of users: *secondary* users, which are those *without* a license, are allowed to transmit provided the interference they inflict to *primary* users, which are those *with* a license, remains below certain limits. A secondary user can therefore transmit, for instance, if its radiated power

is so low that it is perceived by the primary user below its noise floor; or if no primary user is operating in the same geographical area at that particular time.

In this context, recent regulations in the United States allow unlicensed wireless devices to transmit in broadcast television bands at locations where they are unused by authorized services [Federal Communications Commission, 2008] [Federal Communications Commission, 2010] [Federal Communications Commission, 2011]. Those services — i.e., the primary users — include, among others, television broadcast stations and low-power auxiliary devices, such as wireless microphones (WMs).

Spectrum awareness is therefore of critical importance for secondary users, which must correctly identify their transmission opportunities and set their transmission parameters. While the current state of US regulations establishes that unlicensed users must determine the occupancy state of the radio spectrum by means of a geo-location database, the Federal Communications Commission (FCC) encourages the development of *spectrum sensing* procedures [Yucek and Arslan, 2009, Axell et al., 2012] to detect the presence of the incumbent services, since they are expected to yield significant spectrum efficiency improvements in the future [Federal Communications Commission, 2010]. Furthermore, such procedures are also explicitly demanded by the IEEE 802.22 standard for DSA [IEEE, 2011].

This thesis is primarily concerned with the development of spectrum sensing tools capable of determining the occupancy state of communication channels. This information serves secondary users to set their transmission parameters so that they can coexist with primary users in a DSA environment. Note that, although the terms DSA and *cognitive radio* are oftentimes used as synonyms, they correspond to different concepts. A cognitive radio is an *intelligent* radio that can autonomously reconfigure its operation by learning from and adapting to the communication context [Mitola III and Maguire Jr, 1999, Zhao and Sadler, 2007]. It can be used in any communication scenario, DSA being one of them.

### 1.1.1 Spectrum Sensing

Spectrum sensing encompasses a collection of procedures intended to determine the occupancy state of a — typically wireless — communication channel, based on the observations gathered by one or more *spectrum sensors* [Axell et al., 2012]. For simplicity, we assume throughout that no secondary user is transmitting during the observation window, and hence spectrum sensors may only receive one or more primary signals as well as noise/interference. Note the terminological difference between these two entities: although both may be implemented as a single physical device, a spectrum sensor is concerned with spectrum sensing functions, whereas a secondary user undertakes the functions of transmission and reception of unlicensed communications.

## POWER ESTIMATION AND ACTIVITY DETECTION

Throughout the thesis, we consider two classes of spectrum sensing procedures: those that attempt to determine the power of the primary signal as it arrives at the spectrum sensor and those that simply attempt to establish whether the primary user is active or not.

### Power Estimation

Suppose that a spectrum sensor filters and downconverts a band of interest to baseband. In the simplest scenario, the signal resulting from this operation can be expressed as

$$y = r + w, \quad (1.1)$$

where  $r$  represents a signal term containing the baseband representation of the primary signal after suffering the effects of propagation and  $w$  is noise. At time instant  $t$ , the signals  $y$ ,  $r$  and  $w$  take the values  $y(t)$ ,  $r(t)$  and  $w(t)$  respectively. If there is no ambiguity, the former notation will be used to refer to the signals themselves, seen as functions or stochastic processes, whereas the latter will be used to refer to the evaluation of such functions, seen as scalars or vectors. Unless otherwise stated, random signals will be modeled as wide-sense stationary random processes with zero mean.

Our goal is to provide an estimate of the power of the signal term, defined as  $\eta_0^2 \triangleq \mathbb{E} \{|r(t)|^2\}$ , which can be directly reported to the secondary user or used as an intermediate step for activity detection (see below). Estimates of  $\eta_0^2$  are obtained making use of partial statistical characterizations of the received signal. In particular, suppose that the observations of  $y$  have been generated by a certain model  $\theta$  which is known to be in a given family  $\Theta$  of statistical models. *Estimation* refers to the determination of  $\theta$  based on those observations of  $y$ . Once  $\theta$  is known, so automatically is any other parameter of interest such as  $\eta_0^2$ . Sometimes, even a partial knowledge of  $\theta$  may suffice to reveal the value of such a parameter.

We are interested in constructing functions of the observations of  $y$ , called *estimators*, that return estimates of  $\theta$  or of the parameters of interest. A well-known methodology used throughout to derive such a function is the so-called *maximum likelihood* (ML) rule. If  $p(y; \theta)$  represents the probability density function of the observations under the model  $\theta$ , the ML estimate of  $\theta$  is given by

$$\hat{\theta}(y) = \arg \sup_{\theta \in \Theta} p(y; \theta). \quad (1.2)$$

## Activity Detection

Sometimes the power of the primary signal is not relevant and one is solely interested in determining whether a primary user is active or inactive. In the simplest scenario, one must decide whether the noise-corrupted observations contain a signal term corresponding to a primary transmission or not. Formally, the problem is to decide between two hypotheses:

$$\mathcal{H}_0 : y = w, \quad \mathcal{H}_1 : y = r + w. \quad (1.3)$$

Problems of this kind are the subject of study of *detection theory* [Kay, 1998] and the more general theory of testing statistical hypothesis [Lehmann and Romano, 2005]. In these contexts,  $\mathcal{H}_0$  is referred to as the *null hypothesis* and  $\mathcal{H}_1$  as the *alternative*.

Similarly to power estimation, the decision is made based on a partial statistical characterization of the observations. In this case, there exists a family  $\Theta_{\mathcal{H}_0}$  of models corresponding to  $\mathcal{H}_0$  and a family  $\Theta_{\mathcal{H}_1}$  corresponding to  $\mathcal{H}_1$ , and the goal is to decide whether  $\theta \in \Theta_{\mathcal{H}_0}$  or  $\theta \in \Theta_{\mathcal{H}_1}$ . A *detector* or *test* is a function of the observations which returns a decision on which hypothesis is *active*. This decision is typically made by evaluating a real function  $\mathcal{T}$ , called *test statistic*, and comparing the result against a threshold  $\nu$ :

$$\mathcal{T}(y) \underset{\mathcal{H}_0}{\overset{\mathcal{H}_1}{\gtrless}} \nu. \quad (1.4)$$

The performance of a detector is usually characterized in terms of the two metrics defined next.

- The *probability of false alarm* is defined as

$$P_{\text{FA}}(\theta) \triangleq P_{\theta} \{ \mathcal{T}(y) > \nu \}, \quad \theta \in \Theta_{\mathcal{H}_0}, \quad (1.5)$$

where  $P_{\theta} \{ \cdot \}$  represents probability under the model  $\theta$ . If  $P_{\text{FA}}(\theta) = P_{\text{FA}} \forall \theta$ , that is, if the probability of false alarm does not depend on  $\theta$ , we say that the detector has a *constant false alarm rate* (CFAR) [Kay, 1998].

$P_{\text{FA}}$  corresponds to the probability of deciding that a primary user is transmitting ( $\mathcal{H}_1$ ) when it is not ( $\mathcal{H}_0$ ). Thus, in the long term, it measures the fraction of missed *transmission opportunities*. Since this drastically affects the throughput of the secondary user, it is convenient to keep  $P_{\text{FA}}$  as low as possible.

- The *probability of detection* (also known as the *power of the test*) is defined as

$$P_{\text{D}}(\theta) \triangleq P_{\theta} \{ \mathcal{T}(y) > \nu \}, \quad \theta \in \Theta_{\mathcal{H}_1}. \quad (1.6)$$

It corresponds to the probability of deciding that a primary user is transmitting ( $\mathcal{H}_1$ ) when it is actually doing so. Thus, with probability  $1 - P_D$ , the presence of the primary user is not detected and, consequently, the secondary user may introduce disturbing interference into the primary communication, which suggests keeping  $P_D$  as close to one as possible. It is expected that the upcoming spectrum regulations dictate a minimum  $P_D$  that detectors must guarantee.

Note that there exists a trade-off between  $P_{FA}$  and  $P_D$ : increasing  $\nu$  in (1.4) yields lower values of  $P_{FA}$  and  $P_D$  whereas decreasing  $\nu$  results in higher values. This trade-off can be characterized by the so-called *receiver operating characteristic* (ROC), which is nothing but the probability of detection seen as a function of the probability of false alarm.

In view of the above, it makes sense to seek the tests minimizing  $P_{FA}$  subject to a  $P_D$  constraint. However, due to common practice in detection theory, most works in the spectrum sensing literature adhere to the opposite convention, where the value of  $P_{FA}$  is fixed and  $P_D$  maximized. Unfortunately, even if we focus on the family of CFAR tests whose  $P_{FA}$  does not exceed a certain value, the dependence of  $P_D$  on  $\theta$  makes that, in most cases, none of these tests has a larger  $P_D$  than all the other tests in the family for all  $\theta$ . In other words, for each value of  $\theta$  there is an optimal test, but only in very restricted situations do all values of  $\theta$  lead to the same optimal test. Such a *uniformly most powerful* (UMP) test exists, for instance, when both  $\Theta_{\mathcal{H}_0}$  and  $\Theta_{\mathcal{H}_1}$  contain a single element, say  $\Theta_{\mathcal{H}_0} = \{\theta_{\mathcal{H}_0}\}$  and  $\Theta_{\mathcal{H}_1} = \{\theta_{\mathcal{H}_1}\}$ , in which case it is given by the so-called *likelihood ratio* test, defined as [Lehmann and Romano, 2005, Kay, 1998]

$$\mathcal{G}(y) \triangleq \frac{p(y; \theta_{\mathcal{H}_1})}{p(y; \theta_{\mathcal{H}_0})} \underset{\mathcal{H}_0}{\overset{\mathcal{H}_1}{\gtrless}} \nu, \quad (1.7)$$

where  $\nu$  is adjusted to satisfy the  $P_{FA}$  constraint. However, when the statistical distribution of the observations is only partially known, at least one of the sets  $\Theta_{\mathcal{H}_0}$  and  $\Theta_{\mathcal{H}_1}$  contains more than one element — thus resulting in a *composite* hypothesis test — and such a UMP test may not exist. In those cases, several alternatives exist to design a detector; two of them being introduced next.

- If we consider the family of all tests whose  $P_{FA}$  does not exceed a certain value, it is likely that none of them exhibits the maximum  $P_D(\theta)$  for all values of  $\theta$ . However, if we restrict ourselves to a smaller family, for instance focusing on those tests that satisfy certain additional requirements, a test may exist which is UMP *within* this subfamily. Notable examples include *uniformly most powerful unbiased* or *uniformly most powerful invariant* (UMPI) tests [Lehmann and Romano, 2005].

- A second approach is the so-called *generalized likelihood ratio* (GLR) test, given by:

$$\mathcal{G}(y) \triangleq \frac{\sup_{\theta \in \Theta_{\mathcal{H}_1}} p(y; \theta)}{\sup_{\theta \in \Theta_{\mathcal{H}_0}} p(y; \theta)} \underset{\mathcal{H}_0}{\geq} \nu. \quad (1.8)$$

The ubiquitous presence of this test in detection theory owes to its acceptably good performance in many situations. However, no optimality properties are associated with this test for finite data records. The models in  $\Theta_{\mathcal{H}_0}$  and  $\Theta_{\mathcal{H}_1}$  are typically indexed by a collection of parameters referred to as *unknown deterministic parameters* or *nuisance parameters* [Kay, 1998, Lehmann and Romano, 2005]. Upon comparing (1.2) and (1.8), we find that the values of  $\theta$  attaining the supremum in the denominator and numerator of (1.8) are respectively the ML estimates of  $\theta$  under  $\mathcal{H}_0$  and  $\mathcal{H}_1$ .

## THE ROLE OF THE PRIOR INFORMATION

In the absence of prior information, it is not possible to distinguish signal from noise and, consequently, no detector can be designed with reasonable performance guarantees. It is therefore necessary to exploit some *feature* that makes the signal term different from the noise term.

The most elemental example of such a feature is energy. Suppose that the noise variance  $\sigma^2 \triangleq \mathbb{E}\{|w(t)|^2\}$  is known. If the goal is activity detection, one can merely estimate  $\eta^2 \triangleq \mathbb{E}\{|y(t)|^2\}$  and declare the channel busy if the resulting estimate exceeds  $\sigma^2$  meaningfully. This simple and popular procedure is termed *energy detection* [Kay, 1998] and is optimal in certain settings without further signal structure. In practice, this detector is unable to attain an acceptable performance in low signal-to-noise ratio (SNR) conditions since this would require a highly accurate knowledge of  $\sigma^2$ , which is seldom available in real scenarios [Zeng and Liang, 2009b, Cabric, 2008, Tandra and Sahai, 2008]. The practical interest of this scheme is therefore limited — the FCC, for instance, establishes that any secondary device operating in the television band must be able to detect signals at  $-114$  dBm, which entails SNRs as low as  $-20$  dB [Cabric, 2008, Zeng and Liang, 2009a]. This fact has motivated detectors exploiting other properties of the primary signal, including spectral flatness, amplitude properties, spatial correlation, etc. (see [Yucek and Arslan, 2009, Axell et al., 2012] and the references therein).

In order to tackle this *noise uncertainty problem*, we will focus our attention on spectrum sensing methods that exhibit certain *invariance* properties with respect to scalings of the observations. For complex-valued  $y$ , a test statistic  $\mathcal{T}$  is said to be *invariant* to scalings if  $\mathcal{T}(cy) = \mathcal{T}(y)$  for any  $c \in \mathbb{C}$  [Lehmann and Romano, 2005]. In typical scenarios, such statistics lead to CFAR detectors that are immune to the noise uncertainty problem. On the other hand, in power estimation we will be interested in *equivariant* estimators. An estimator  $\hat{\eta}_0^2$  of  $\eta_0^2$  is

said to be equivariant under scalings if  $\hat{\eta}_0^2(cy) = |c|^2 \hat{\eta}_0^2(y)$  [Lehmann and Romano, 2005].

The performance of any spectrum sensing procedure will drastically depend on the accuracy of the prior information that it exploits. In this thesis we consider several forms of signal structure, which may be classified as follows:

- **Amplitude information:** In some cases, the transmitted primary signal is known to have a *constant magnitude* (CM). This is a common property of practical waveforms: since it relaxes linearity requirements on power amplifiers, inexpensive transmitters can be used. Examples include frequency shift keying (FSK) modulation, continuous-phase modulation (CPM) or Gaussian minimum shift keying (GMSK) modulation, used in the GSM standard. In the context of DSA, this property has a special relevance since WMs typically employ analog frequency modulation (FM), which results in CM waveforms.

In other cases, the amplitude of the transmitted signal may be assumed to follow a Gaussian distribution, which is well motivated in communication scenarios for several reasons: First, many transmission systems employ modulations whose amplitude distribution is approximately Gaussian since this is the one achieving the capacity of additive white Gaussian noise channels. Second, the amplitude of multi-carrier waveforms, which are widespread nowadays, is approximately Gaussian since these signals are linear combinations of many independent — or nearly independent — subcarriers. Third, it is a common working assumption in signal processing and statistics since it leads to tractable models and since many methods designed for Gaussian distributions have an acceptable performance even when there exist considerable departures from Gaussianity [Anderson, 2003, p. 3].

- **Spectral structure:** In many practical scenarios, the knowledge of the power spectrum of the transmitted signal is highly detailed since many transmission systems today obey public standards and regulations. For instance, the waveform features in WiFi, Bluetooth, cellular telephony, digital television, etc., are dictated by the corresponding standard, which specifies roll-off factors, modulations, number of carriers, location of pilots, etc. Other features, such as spectral masks, carrier frequencies, and bandwidths are specified by spectrum regulations. Thus, it is reasonable to assume that the power spectral density (PSD) of the transmitted waveform is approximately known, except possibly for a scaling factor which captures power. Consider, for instance, the case of a signal using QAM, whose PSD is determined up to a scaling by the bandwidth and the roll-off factor of the square root raised cosine pulse, or *orthogonal frequency division multiplexing* (OFDM), where the PSD can be inferred from the location of data and pilot carriers.
- **Channel structure:** Secondary users/spectrum sensors are expected to deploy multiple antennas due to their advantages for communication and spectrum sensing [Taherpour

et al., 2010, Cabric, 2008]. In some cases, for instance, the noise at different antennas is known to be uncorrelated, whereas the primary signal might be highly correlated. This spatial structure provides the sensor with extra information to distinguish signal from noise. Other forms of channel structure is that pertaining to time variations. Due to long observation windows in scenarios with mobility or changes in the propagation medium, the properties of the received signal may vary over time when a primary user is transmitting. Provided noise properties remain constant, this information can be used to detect the presence of a primary waveform.

## SPECTRUM SENSING FORMULATIONS

We may classify spectrum sensing methods in several levels according to how detailed their characterization of the *white space* is [Zhao and Sadler, 2007].

### Spectrum Sensing in a Single Channel

Suppose that we focus our attention on the occupancy state of a specific frequency channel at a particular spatial location. The white space is therefore the unidimensional set of time intervals where no primary user is transmitting. In this setting, a sensor acquires samples of a frequency channel during a certain observation window and uses this information to perform power estimation or activity detection. This thesis is concerned with two problems of this kind:

- *Activity detection of WM signals:* As mentioned earlier, the FCC allows unlicensed wireless devices to operate in the television broadcast spectrum at locations where that spectrum is unused by legacy services, which include, among others, television broadcast stations and WMs. Therefore, it is of critical importance to develop schemes capable of reliably detecting the activity of WMs.
- *Activity detection in time-varying channels:* Suppose that a detector is derived under the assumption that the channel is time invariant. When utilized in a practical scenario, where channels only satisfy this assumption approximately, such a detector will incur a performance loss. Indeed, there is a large swath of applications where such a model becomes unrealistic and channel variations within the observation window should be taken into account. This is the case, for instance, of narrowband wireless communication systems, where the coherence time of the channel may be comparable to the symbol period. Another example can be found in underwater communications, where the typically large Doppler spreads give rise to fast channel variations [Marage and Mori, 2010]. More generally,



the stringent requirements imposed by DSA regulations, which include very low SNR conditions [Cabric, 2008], force detectors to use long observation windows, during which the channel may vary considerably, especially in environments affected by mobility.

### Spectrum Sensing in Multiple Channels

Now suppose that we are interested in the occupancy state of the channels contained in a wide frequency band at a particular spatial location. The white space is therefore the bidimensional set of points in the time-frequency plane where no primary user operates. Sensing multiple channels simultaneously increases the chance of finding a vacant one and enables secondary users to increase their throughput by transmitting on multiple channels at the same time.

Although, in principle, multiple channels can be scanned by applying single-channel procedures independently on a channel-by-channel basis, this approach entails large hardware costs, long sensing times, large power consumption and poor estimation/detection performance. It is therefore preferable to employ statistical procedures that consider multiple channels jointly, these being the subject of study of the so-called *wideband spectrum sensing* (WSS).

In the model used throughout the thesis for WSS, the received signal is given by

$$y = \sum_{b=0}^{B-2} r_b + w, \quad (1.9)$$

where  $r_b$  corresponds to the  $b$ -th primary signal after propagating to the spectrum sensor and  $B - 1$  is the number of primary signals. Note that a single primary user may transmit multiple signals at the same time, as usual in television broadcast bands. However, for the sake of clarity and without any loss of generality, we assume that each signal is transmitted by a different secondary user, although multiple secondary users may be located at the physical position. The two classes of sensing problems considered above can be generalized for the wideband scenario as follows:

- *Power estimation:* The goal is to estimate  $\eta_b^2 \triangleq \mathbb{E} \{|r_b(t)|^2\}$  for all or some indices  $b$ .
- *Activity detection:* Although, in principle, a multiple hypothesis test can be posed, it is customary to focus on a single channel, say

$$\mathcal{H}_0 : r_b = 0, \quad \mathcal{H}_1 : r_b \neq 0. \quad (1.10)$$

Let  $x_b$  denote the  $b$ -th primary signal, which, without any loss of generality, is assumed to be normalized to unit power; and let  $h_b$  represent the impulse response of the linear and

time-invariant channel between the corresponding source and the spectrum sensor. Then, (1.9) becomes

$$y = \sum_{b=0}^{B-2} h_b \star x_b + w, \quad (1.11)$$

where  $\star$  denotes convolution. A more compact representation arises by defining  $\eta_{B-1}^2 \triangleq \mathbb{E}\{|w(t)|^2\}$ , as well as  $h_{B-1}(t) \triangleq \eta_{B-1}\delta(t)$  ( $\delta$  is the Dirac delta function) and  $x_{B-1} \triangleq w/\eta_{B-1}$ :

$$y = \sum_{b=0}^{B-1} h_b \star x_b. \quad (1.12)$$

According to what was explained earlier, it can be assumed that the PSDs of the  $x_b$ , denoted as  $\Xi_b$ , are approximately known. Suppose that all channels  $h_b$  are frequency-flat, which means that we can write  $h_b(t) = \tilde{h}_b\delta(t - t_b)$  for some scalars  $\tilde{h}_b \in \mathbb{C}$ ,  $t_b \in \mathbb{R}$  — frequency-selective channels can be handled similarly by introducing general assumptions [Bazerque and Giannakis, 2010], or at the expense of a higher complexity by artificially decomposing each signal into multiple uncorrelated narrowband components. Without any loss of generality we assume  $t_b = 0$ , so that  $h_b(t) = \tilde{h}_b\delta(t)$ .

If the  $x_b$  are uncorrelated, it is clear that the PSD of  $y$  can be written as

$$\Xi = \sum_{b=0}^{B-1} \alpha_b \Xi_b, \quad (1.13)$$

where  $\alpha_b \triangleq |h_b|^2 = \eta_b^2$  are unknown deterministic parameters. Note that the knowledge of  $\Xi$  is equivalent to the knowledge of the coordinates  $\alpha_b$  if the set of functions  $\{\Xi_b\}_{b=0}^{B-1}$  is linearly independent, in which case (1.13) is called a *basis expansion model* (BEM) for  $\Xi$ . The assumption of linear independence is not limiting in practice: for instance, if two transmitters operate on the same channel using the same PSD — as in *single-frequency networks* —, their signals can be subsumed into a single term in (1.13) since one is not typically interested in the power of individual users but in the overall power of the primary transmissions in a given channel. By defining  $\xi(\tau) \triangleq \mathbb{E}\{y(t)y^*(t-\tau)\}$  and  $\xi_b(\tau) \triangleq \mathbb{E}\{x_b(t)x_b^*(t-\tau)\}$ , we may also write the autocorrelation BEM, related to (1.13) via inverse Fourier transform:

$$\xi = \sum_{b=0}^{B-1} \alpha_b \xi_b. \quad (1.14)$$

The coordinates  $\alpha_b$ , which are nonnegative, contain all relevant information. In particular,

power estimation can be cast as the problem of estimating the  $\alpha_b$ , whereas activity detection can be posed as the hypothesis test

$$\mathcal{H}_0 : \alpha_b = 0, \quad \mathcal{H}_1 : \alpha_b > 0 \quad (1.15)$$

for some  $b$ .

One of the major challenges of WSS is the acquisition of wide frequency bands. Nyquist sampling is oftentimes prohibitive since the cost and power consumption of analog-to-digital converters (ADCs) explosively increase with the sampling rate. Indeed, this can be seen as the bottleneck of WSS. To alleviate this problem, sub-Nyquist techniques have been introduced, leading to the concept of *compressive* WSS (see [Mishali and Eldar, 2009] and references therein). In this context, we will consider two classes of problems:

- *Sensing*: The goal is to determine the occupancy state from compressed measurements of  $y$ . A possible approach is to first reconstruct  $y$ , for instance using compressed sensing [Donoho, 2006, Candès and Wakin, 2008], and then apply a conventional spectrum sensing technique (see [Sun et al., 2013] and references therein). Compression is enabled by assuming certain signal structure, such as sparsity.

Alternatively, one may attempt to obtain the information of interest directly from the compressed observations [Ariananda and Leus, 2012, Lexa et al., 2011]. Bypassing the intermediate step of reconstructing the uncompressed waveform may potentially allow stronger compression ratios and entail performance benefits. Compression is possible since we are solely interested in the second-order statistics of the received signal, such as power, auto-correlation, or PSD; which suffice for power estimation and activity detection purposes. This thesis is concerned with problems of this second kind, which will be addressed from the perspective of *compressive covariance sampling* (CCS) (see Section 1.1.2 below).

- *Compression*: Designing the compression system is nontrivial and requires extensive analysis. In the context of CCS, we are interested in those designs capable of maximizing the compression ratio while preserving all relevant second-order information.

## Spectrum Cartography in Multiple Channels

A more general notion of white space arises by bringing the spatial dimension into the picture: we now aim at monitoring the spectrum usage across time, frequency and space. This information is characterized by the so-called *spectrum maps*, which can be subsequently used to identify the *reusable areas* [Nishimori et al., 2007]. These maps are defined over an area of

interest, which is indexed by a subset of the Euclidean space  $\mathbb{R}^d$ . The dimension  $d$  is application dependent:  $d$  can be set to 1 if, for instance, we wish to monitor the RF spectrum along a railroad or a highway; to 2 if the goal is to create a spectrum map for a flat geographical region; to 3 if we want to monitor the RF spectrum for communication in a city or between aerial vehicles; to 4 if we also want to account for time variations; and so on.

The model to be used arises by introducing the spatial dimension in (1.12). The signal received at location  $\mathbf{z} \in \mathbb{R}^d$  takes the values

$$y(\mathbf{z}; t) = \sum_{b=0}^{B-1} h_b(\mathbf{z}; t) \star x_b(t), \quad (1.16)$$

where  $h_b(\mathbf{z}; t)$  is the impulse response of the channel between the  $b$ -th primary transmitter and a spectrum sensor located at  $\mathbf{z} \in \mathbb{R}^d$ . Likewise, the PSD of  $y$  can be obtained from (1.13) as:

$$\Xi(\mathbf{z}; f) = \sum_{b=0}^{B-1} \alpha_b(\mathbf{z}) \Xi_b(f). \quad (1.17)$$

The goal of spectrum cartography is to estimate the *power spectrum map* or *PSD map*  $\Xi$  given by (1.17). Since the basis functions  $\Xi_b$  are linearly independent, this is equivalent to estimating the  $B$  spatial fields  $\alpha_b$ .

In the spectrum cartography techniques considered in this thesis, the observations gathered by a collection of spectrum sensors deployed across the area of interest are fused to estimate the PSD map. Using multiple sensors and explicitly considering the spatial dimension mitigate the detrimental effects of fading and shadowing on spectrum sensing, and, in particular, alleviate the hidden terminal problem [Quan et al., 2008]. Moreover, including spatial dependence entails further advantages, such as the possibility of exploiting propagation and location prior information.

Other applications besides DSA might profoundly benefit from the knowledge of spectrum maps. Examples include network planning, coverage prediction, interference control, etc., where field measurements may be more effective than prediction via simulation models.

### 1.1.2 Compressive Covariance Sampling

CCS is the workhorse used throughout the thesis to tackle the difficulties of acquiring simultaneously multiple channels that, as a whole, span a wide frequency band. This is possible since the spectrum sensing tasks considered are ultimately concerned with second-order statistics.

In CCS, the second-order statistics of a signal of interest are estimated from a set of com-

pressed observations without an intermediate reconstruction of the uncompressed waveform. Some of these techniques are well-known in signal processing. In particular, the problem of *sparse* power spectrum estimation has been extensively investigated in the literature (see e.g. [Moffet, 1968, Pillai et al., 1985, Abramovich et al., 1998, Abramovich et al., 1999, Pal and Vaidyanathan, 2010]). As for *dense* power spectrum estimation, both parametric [Romero and Leus, 2013b] and nonparametric [Ariananda and Leus, 2012, Yen et al., 2013] approaches have been recently proposed. These techniques have numerous applications in DSA — e.g., spectrum sensing, source localization, frequency estimation, etc.— and beyond DSA (see [Romero et al., 2015d] and references therein).

## COMPRESSIVE ACQUISITION

It is particularly convenient to introduce compression in the acquisition stage since otherwise part of the resources are devoted to acquire data that is afterwards discarded. For this reason, the literature contains many acquisition and reconstruction procedures. Remarkable examples include sub-Nyquist sampling of multiband [Lin and Vaidyanathan, 1998, Herley and Wong, 1999, Venkataramani and Bresler, 2000, Mishali and Eldar, 2010] or multitone [Tropp et al., 2010] signals, compressed sensing [Donoho, 2006, Candès and Wakin, 2008] and array design for aperture synthesis imaging [Hocor and Kassam, 1990, Moffet, 1968, Pillai et al., 1985]. All these approaches use linear compression structures that operate according to the relation

$$\bar{\mathbf{y}} = \Phi \mathbf{y}, \quad (1.18)$$

where  $\mathbf{y} \in \mathbb{C}^K$  represents a vector of uncompressed observations,  $\Phi \in \mathbb{C}^{\bar{K} \times K}$  is the *compression matrix*, *measurement matrix*, or *sampler*; and  $\bar{\mathbf{y}} \in \mathbb{C}^{\bar{K}}$  is the vector of compressed observations. To quantify the compression, we define the *compression ratio*:

$$\rho \triangleq \frac{K}{\bar{K}}. \quad (1.19)$$

It is typically desirable that it be as high as possible.

Two classes of compression structures will be considered:

- *Sparse samplers* are those where  $\Phi$  is a sparse matrix. Commonly,  $\Phi$  is composed of  $\bar{K}$  different rows of the identity matrix  $\mathbf{I}_K$ , thus performing a *component selection* of  $\mathbf{y}$ . If this selection is periodic, which means that  $\Phi$  is a block diagonal matrix whose diagonal blocks are replicas of a certain sparse matrix, it is called *multi-coset sampling*.
- *Dense samplers* are those where  $\Phi$  is a dense matrix. Each component of  $\bar{\mathbf{y}}$  is therefore a

*linear combination* of the components of  $\mathbf{y}$ . In the case of periodic samplers,  $\Phi$  is block diagonal where all diagonal blocks are replicas of a certain dense matrix.

The meaning of each vector in (1.18) depends on the domain where the signal  $y$  is defined:

- *Time-domain signals:* several alternatives have been proposed to replace ADCs — known to be slow, expensive, and power-hungry — by introducing compression. Notable examples include interleaved ADCs [Black and Hodges, 1980], non-uniform sampling and its generalizations [Herley and Wong, 1999, Venkataramani and Bresler, 2000, Wakin et al., 2012], the random demodulator [Laska et al., 2007, Tropp et al., 2010], the modulated wideband converter [Mishali and Eldar, 2010, Mishali and Eldar, 2011] and the random modulator pre-integrator [Yoo et al., 2012, Becker, 2011]. For this reason, we will globally refer to these schemes as *compressive-ADCs* (C-ADCs).

If  $f_s = 1/T_s$  is the Nyquist rate of the signal of interest  $y$  and  $\mathbf{y} \triangleq [y[0], \dots, y[K-1]]^T$ , where  $y[k] = y(kT_s)$ , then the operation of a C-ADC can be described by (1.18). The samples at the output of a C-ADC correspond to the entries of the compressed vector  $\bar{\mathbf{y}} \triangleq [\bar{y}[0], \dots, \bar{y}[\bar{K}-1]]^T$ , which are linear combinations of the entries of  $\mathbf{y}$ . Note, however, that no C-ADC internally acquires the Nyquist samples  $y[k]$  since this would entail precisely the disadvantages of conventional ADCs that they aim to avoid. Nonetheless, working with these samples constitutes a convenient mathematical abstraction.

- *Spatial-domain signals:* In some applications, it is necessary to measure the fine variations of a spatial field, for instance to achieve a high angular resolution in source localization problems. Without compression, a large number of antennas and RF chains are required, which entail large hardware costs and power consumption. It is therefore of critical importance to employ compression techniques that allow cost savings, either by reducing the number of antennas or just the number of RF chains. Their operation can be described by (1.18) if  $\mathbf{y}$  is a vector containing the observations of the *uncompressed* array at a particular time instant and  $\bar{\mathbf{y}}$  represents the vector of compressed observations. As before, the vector  $\mathbf{y}$  does not necessarily have physical existence; it is just a mathematical abstraction.

With sparse sampling (see e.g. [Hocort and Kassam, 1990, Moffet, 1968, Pearson et al., 1990, Wild, 1987, Pillai et al., 1985, Pillai and Haber, 1987, Abramovich et al., 1998, Abramovich et al., 1999, Pal and Vaidyanathan, 2010]), only the antennas corresponding to the non-null columns of  $\Phi$  need to be physically deployed to obtain  $\bar{\mathbf{y}}$ , whereas in dense sampling [Wang et al., 2009, Wang and Leus, 2010, Venkateswaran and van der Veen, 2010], analog combiners are used to reduce the number of RF chains. See [Romero et al., 2015d] for more details.

## Periodic Acquisition

When observation windows for time signals are long, hardware design considerations make it convenient to split a sampling pattern into shorter pieces that are repeated periodically. This amounts to grouping data samples into blocks that are acquired using the same pattern. Note that, despite this block partitioning, subsequent stages may process multiple blocks jointly. Likewise, using periodic arrays in the spatial domain also presents certain advantages [Krieger et al., 2013].

Suppose that  $\mathbf{y}$  is partitioned into  $L$  blocks of  $N \triangleq K/L$  samples<sup>1</sup> as  $\mathbf{y} = [\mathbf{y}^T[0], \dots, \mathbf{y}^T[L-1]]^T$ , with  $\mathbf{y}[l] \in \mathbb{C}^N \forall l$ , and that compressing a block of  $N$  elements produces another block of  $\bar{N}$  elements as

$$\bar{\mathbf{y}}[l] = \check{\Phi} \mathbf{y}[l], \quad l = 0, 1, \dots, L-1, \quad (1.20)$$

where  $\bar{\mathbf{y}}[l] \in \mathbb{C}^{\bar{N}}$  and  $\check{\Phi} \in \mathbb{C}^{\bar{N} \times N}$ . The use of the term *periodicity* owes to the fact that the matrix  $\check{\Phi}$  does not depend on  $l$ . Making  $\bar{\mathbf{y}} \triangleq [\bar{\mathbf{y}}^T[0], \dots, \bar{\mathbf{y}}^T[L-1]]^T$  and

$$\Phi = \mathbf{I}_L \otimes \check{\Phi}, \quad (1.21)$$

where  $\otimes$  represents the Kronecker product, gives again expression (1.18). Since  $\bar{K} = \bar{N}L$ , the compression ratio in the periodic setting takes the form

$$\rho = \frac{K}{\bar{K}} = \frac{N}{\bar{N}}. \quad (1.22)$$

Further conventions are useful when dealing with sparse sampling, in which case, as seen earlier,  $\Phi$  equals a submatrix of  $\mathbf{I}_K$  up to row permutations. For concreteness, assume that the rows of  $\Phi$  are ordered as they are in  $\mathbf{I}_K$ . If  $\mathcal{K} = \{k_0, \dots, k_{\bar{K}-1}\}$  denotes the set containing the indices of the non-null columns of  $\Phi$ , the entries of  $\bar{\mathbf{y}} = \Phi \mathbf{y}$  are given by  $\bar{y}[\bar{k}] = y[k_{\bar{k}}]$ ,  $\bar{k} = 0, 1, \dots, \bar{K}-1$  (see notation conventions in Section 1.4). The set  $\mathcal{N}$ , which contains the indices of the non-null columns of  $\check{\Phi}$ , is related to  $\mathcal{K}$  by

$$\mathcal{K} = \{n + lN, \ n \in \mathcal{N}, l = 0, 1, \dots, L-1\}. \quad (1.23)$$

Loosely speaking, we may say that  $\mathcal{K}$  is periodic with period  $\mathcal{N}$ , or that  $\mathcal{K}$  is the result of an  $L$ -fold *concatenation* of  $\mathcal{N}$ . These sets have cardinality  $|\mathcal{K}| = \bar{K} = \bar{N}L$  and  $|\mathcal{N}| = \bar{N}$  elements.

Note that periodic sampling indeed generalizes non-periodic sampling, since the latter can

---

<sup>1</sup>For simplicity, we assume that  $K$  is an integer multiple of  $L$ .

be retrieved just by making  $L = 1$ . For this reason, most results will be presented for periodic samplers, with occasional comments on the non-periodic setting if needed.

## PROBLEM FORMULATION

Let us first consider the problem of estimating the second-order statistics of the zero-mean random vector  $\mathbf{y} \in \mathbb{C}^K$  from the  $\bar{K}$  linearly compressed observations collected in the vector  $\bar{\mathbf{y}} \in \mathbb{C}^{\bar{K}}$ . The covariance matrix  $\mathbf{\Xi} = \mathbb{E}\{\mathbf{y}\mathbf{y}^H\}$ , which contains this information, is assumed to be a linear combination of the matrices in a given set  $\mathcal{B} = \{\mathbf{\Xi}_0, \mathbf{\Xi}_1, \dots, \mathbf{\Xi}_{B-1}\} \subset \mathbb{C}^{K \times K}$ . Without any loss of generality, we consider real scalars,<sup>2,3</sup> i.e.,

$$\mathbf{\Xi} = \sum_{b=0}^{B-1} \alpha_b \mathbf{\Xi}_b, \quad \text{with } \alpha_b \in \mathbb{R}, \quad (1.24)$$

and  $\mathcal{B}$  is assumed to be a linearly independent set of matrices:

$$\sum_{b=0}^{B-1} \alpha_b \mathbf{\Xi}_b = \sum_{b=0}^{B-1} \alpha'_b \mathbf{\Xi}_b \Rightarrow \alpha_b = \alpha'_b \quad \forall b. \quad (1.25)$$

Thus,  $\mathcal{B}$  is a basis, which means that the decomposition in (1.24) is unique and, consequently, knowing the  $\alpha_b$  is equivalent to knowing  $\mathbf{\Xi}$ .

The prior information captured by  $\mathcal{B}$  restricts the structure of  $\mathbf{\Xi}$ , thus determining how much  $\mathbf{y}$  can be compressed. When no information at all is available,  $\mathbf{\Xi}$  is simply constrained to be Hermitian positive semidefinite and no compression is possible. However, the fact that  $\mathbf{\Xi}$  is necessarily a linear combination of the matrices in  $\mathcal{B}$  may allow for a certain degree of compression. Formally,  $\mathbf{\Xi}$  must be sought in the intersection of the cone of positive semidefinite matrices and the subspace spanned, with real scalars, by  $\mathcal{B}$ :

$$\mathbf{\Xi} \in \mathbb{S}_+ \cap \text{span}_{\mathbb{R}} \mathcal{B}. \quad (1.26)$$

The subspace  $\text{span}_{\mathbb{R}} \mathcal{B}$ , throughout referred to as the *covariance subspace*, captures the prior information available and, intuitively, the smaller its dimension, the stronger the compression that can be reached. Because we are concerned with wide-sense stationary random processes, it will be assumed throughout that the matrices in  $\mathcal{B}$ , and therefore all matrices in the covariance subspace, are Hermitian Toeplitz (HT).

---

<sup>2</sup>The reason why we prefer real scalars is to preserve the Hermitian property. Note that if  $\mathbf{\Xi}_b$  is Hermitian and  $\alpha_b$  is complex, then  $\alpha_b \mathbf{\Xi}_b$  is not necessarily Hermitian.

<sup>3</sup>As opposed to the model for WSS presented earlier, general CCS problems do not necessarily require that the  $\alpha_b$  be nonnegative.



The second-order statistics of  $\bar{\mathbf{y}}$ , arranged in  $\bar{\Xi} \triangleq \mathbb{E}\{\bar{\mathbf{y}}\bar{\mathbf{y}}^H\}$ , and those of  $\mathbf{y}$ , arranged in  $\Xi$ , are related by:

$$\bar{\Xi} = \Phi \Xi \Phi^H = \sum_{b=0}^{B-1} \alpha_b \bar{\Xi}_b, \quad (1.27)$$

where  $\bar{\Xi}_b = \Phi \Xi_b \Phi^H$ . In other words, the expansion coefficients of  $\Xi$  with respect to  $\mathcal{B}$  are those of  $\bar{\Xi}$  with respect to  $\bar{\mathcal{B}} \triangleq \{\bar{\Xi}_0, \bar{\Xi}_1, \dots, \bar{\Xi}_{B-1}\} \subset \mathbb{C}^{\bar{K} \times \bar{K}}$ . The matrices in  $\bar{\mathcal{B}}$  are clearly Hermitian, and it follows from (1.21) that they have a *block Toeplitz* structure with  $\bar{N} \times \bar{N}$  blocks. However, they are not Toeplitz in general. If the compression operation preserves all relevant information, then  $\bar{\mathcal{B}}$  is linearly independent and knowing  $\bar{\Xi}$  is equivalent to knowing the  $\alpha_b$ , which in turn amounts to knowing  $\Xi$ . Conversely, if the compression is so strong that the linear independence is lost, then not all the  $\alpha_b$  can be *identified* and some second-order information about  $\mathbf{y}$  cannot be recovered.

Besides the problem of estimating  $\Xi$ ,— which is a particular instance of the *covariance matching* problem, also known as the *structured covariance estimation* problem [Ottersten et al., 1998, Burg et al., 1982] — we will also consider the design of  $\Phi$ . Our purpose will be to maximize the compression ratio  $\rho$  while guaranteeing that the coordinates  $\alpha_b$  can be identified from the compressed observations.

## 1.2 Prior Work and Contributions

This thesis addresses the spectrum sensing problems introduced at the end of in Section 1.1.1. Although our work is mainly theoretical, a special effort has been made to ensure that the proposed methods meet certain properties that are required for practical application. In particular, none of our techniques necessitates *a priori* knowledge of the noise power. All the proposed detectors are invariant to scalings and all the schemes for spectrum sensing in a single channel are CFAR.<sup>4</sup> This form of invariance also allows fixing the thresholds via Monte Carlo simulation in case that the probability of false alarm cannot be analytically determined [Kay, 1998, Zeng and Liang, 2009b, Chen and Gao, 2011]. Similarly, all our procedures assume that the channel coefficients are unknown, which is motivated by the fact that the SNR may be considerably low and by the fact that primary users do not cooperate with spectrum sensors.

The spectrum sensing problems addressed in this thesis are posed in terms of the models introduced in Section 1.1.1, sometimes in combination with the CCS model from Section 1.1.2. We leverage mathematical tools that fall within detection theory, estimation theory, regression

---

<sup>4</sup>As we will see, CFAR detection is not possible in general for spectrum sensing in multiple channels.

theory, statistical learning theory, and the theory of testing statistical hypotheses; choosing the most appropriate framework on a case-by-case basis.

### 1.2.1 Spectrum Sensing in a Single Channel

As mentioned earlier, we consider two problems of activity detection in channels that contain at most one primary signal: The first deals with detecting the presence of a WM transmission, which is well-motivated in view of recent FCC regulations; the second considers the detection of primary signals in time-varying channels, which is motivated by the long observation windows required in spectrum sensing.

## ACTIVITY DETECTION OF WM SIGNALS

### Prior Work

Both CFAR and non-CFAR detectors<sup>5</sup> have been proposed in the literature to detect the presence of WM waveforms. Among those of the first kind, we mention the detector in [Xu et al., 2008], which makes a decision based on the ratios of consecutive singular values of a Hankel matrix containing the received samples, and the detector in [Hassan and Nasr, 2011], where the decisions of two statistics are combined, one of which is CFAR whereas the other is not, and the threshold is adapted accordingly. Among the non-CFAR detectors, we mention the one in [Chen and Gao, 2011], where the test statistic is the output of a matched filter in the autocorrelation domain; the detectors in [Chen et al., 2008] and [ElRamly et al., 2011], which are, respectively, the maximum of the standard periodogram and Welch periodogram; and the detector in [Gautier et al., 2010], which uses the Teager-Kaiser energy operator to exploit the constant magnitude property of the signal.

All the above detectors assume single-antenna architectures. However, as mentioned in Section 1.1.1, spectrum sensors are expected to deploy multiple antennas, which enable detectors that are fast, resilient to small-scale fading and robust to the noise uncertainty problem. For these reasons, a number of *multiantenna detectors* have been proposed in the past. Some of them exclusively exploit the spatial structure of the signal — this is the case of the detector in [Alamgir et al., 2008], which only exploits the spatial independence of noise, and the detector in [Besson et al., 2006, Taherpour et al., 2010, Wang et al., 2010], which in addition assumes that the signal subspace has dimension one. Generalizations to signal subspaces of larger dimension

---

<sup>5</sup>These detectors are CFAR within the settings where they were proposed because the authors assume that the noise power is known. However, within our setting they are not CFAR since their probability of false alarm depends on the noise power, which is here assumed an unknown parameter (see Section 1.1.1).

were proposed in [Ramírez et al., 2011]. Other schemes exploit both spatial and temporal structure by assuming that the PSD of the primary signal is known up to a scaling [Sala-Álvarez et al., 2012, Vázquez-Vilar et al., 2011b]. It is also worth mentioning the detectors in [Zeng and Liang, 2009a], which capitalize on the fact that the noise process is temporally and spatially uncorrelated.

While the above multiantenna schemes could be readily applied for WM signal detection, none of them can fully exploit the WM signal structure. To the best of our knowledge, no multiantenna detectors have been proposed specifically targeting this class of signals. Moreover, even within single-antenna detectors, none of them is capable of exploiting all the signal structure present in WM waveforms.

## Contributions

**C1.1:** We fill this gap by proposing multiantenna schemes specifically tailored to detect WM signals. The spatial structure and particular properties of WM waveforms are gradually exploited to derive four detectors that trade off performance and complexity: based on the GLR test, each detector is found under a signal model that captures either the fact that the bandwidth of a WM signal never exceeds 200 kHz, the property that WM signals have a constant magnitude, or both. The resulting detectors do not require synchronization with the WM signal and are robust to the noise uncertainty problem as well as to small-scale fading. Using the simulation guidelines proposed by the IEEE 802.22 working group, the novel detectors are shown to outperform previous schemes, thus demonstrating the advantages of exploiting spatial correlation along with the WM signal structure.

## TIME-VARYING CHANNELS

### Prior Work

Previous work on time-varying channels has addressed modeling, estimation, prediction, equalization, coding, waveform design, etc., (see [Hlawatsch and Matz, 2011] and references therein). However, to the best of our knowledge, little effort has been devoted to activity detection. Although some works allow for a certain degree of time variation through adaptive implementations [Wang et al., 2010, Chen et al., 2007], they are not expected to work well under rapidly changing conditions. Moreover, to the best of our knowledge, no scheme in the literature can actually benefit from time variations in the channel to improve its detection performance.

## Contributions

**C2.1:** We consider the problem of detecting CM signals immersed in noise of unknown variance when the propagation channel is frequency-flat and *randomly* time-varying within the observation window. A BEM with random coefficients is used to model time variations [Tsatsanis and Giannakis, 1996a, Giannakis and Tepedelenlioglu, 1998] and a GLR approach is adopted in order to cope with the deterministic nuisance parameters. If the transmitted CM signal is *known*, the resulting scheme can be thought of as a generalization of the well-known matched filter detector [Kay, 1998], to which it reduces for time-invariant channels. Closed-form analytical expressions are found for the distribution of the test statistic under both hypotheses, which allow exact evaluation of the detection performance. If the CM signal is modeled as *unknown deterministic*, a non-convex optimization problem arises. To work out a solution, we propose various low-complexity approximations and an efficient fixed-point iterative method.

**C2.2:** We also consider the problem of detecting *Gaussian* signals immersed in noise of unknown variance when the propagation channel is frequency-flat and time-varying within the observation window. Three detectors are proposed for single-antenna sensors: First, the GLR test is found for the case where the channel is modeled as an *unknown deterministic* parameter with no temporal structure, resulting in the well-known Bartlett test. Then it is shown that, under the transformation group of positive scalings, no *uniformly most powerful invariant* (UMPI) test or *locally most powerful invariant* (LMPI) test exists. Inspired by the likelihood ratio of the *maximal invariant statistic*, two alternative approaches are explored for the low-SNR regime. In the first one, the channel is assigned a prior distribution — hence modeled as *random* — and Bayesian arguments are invoked, whereas in the second one, the channel is expanded using a BEM with *unknown deterministic* coordinates and ML principles are applied. For multiantenna scenarios, we adopt a GLR approach where the channel follows a BEM with *unknown deterministic* coefficients. Since this detection rule requires the knowledge of the ML estimates of the channel coefficients and noise power, which lack closed-form expressions, an *expectation-maximization* (EM) algorithm is proposed compute them numerically.

**C2.3:** It is noted that certain tests for homogeneity of covariance matrices, which aim at declaring whether a set of vector-valued observations gathered from different populations have the same covariance matrix or not, may be applied to detect Gaussian signals in time-varying channels with multiantenna sensors. Motivated by this application and inspired by our analysis of invariant detectors in single-antenna scenarios (see contribution **C2.2**), we look at the general problem of deriving optimal invariant tests for homogeneity of covariance matrices. Because UMPI tests are known to exist only in very restricted conditions, we confine ourselves to locally optimal tests in the challenging scenario of *close hypotheses*, which is of special relevance

in spectrum sensing applications owing to the low-SNR conditions that arise in practical settings. Capturing the invariance requirements in a group of affine transformations and permutations of the populations, we derive the conditions under which a LMPI test exists and find a closed-form expression for its statistic. For completeness, the analysis is then particularized to the so-called *scale test*, where the covariance matrices of all populations are allowed to differ just in a scaling factor.

### 1.2.2 Spectrum Sensing in Multiple Channels

We address two problems pertaining to spectrum sensing in bands where multiple primary users may be operating. First, we consider schemes for power estimation and activity detection in wide frequency bands, where the difficulties of sampling large bandwidths are alleviated by introducing compression in the acquisition stage. Second, we address the design of the compression stage itself.

## WIDEBAND SPECTRUM SENSING

### Prior Work

Previous WSS schemes include [Quan et al., 2009], which takes into account the throughput of the secondary user along with interference constraints on the primary network. The main limitation, however, is that the noise power must be known. This requirement is bypassed in [Taherpour et al., 2008], where noise power is estimated using idle channels. Unfortunately, the existence of such channels is not guaranteed in practice. To overcome this difficulty, [Vázquez-Vilar and López-Valcarce, 2011] capitalizes on spectral prior information about the individual transmissions. However, this scheme requires the acquisition of wideband signals at the Nyquist rate, which may drastically limit the maximum sensed bandwidth if practical power and hardware cost constraints are to be satisfied.

In order to avoid this limitation, one can resort to the scheme from [Ariananda and Leus, 2012], which proposes a nonparametric method for spectrum estimation based on compressed measurements. The spectrum of the uncompressed signal is retrieved by inverting the linear relationship that exists between the second-order statistics at the input and the output of the C-ADC. However, as usual with nonparametric methods [Schölkopf and Smola, 2001], this approach cannot easily accommodate prior information, which is generally available in practice (see Section 1.1.1) and which can allow sampling rate reductions. Moreover, the resulting estimate may be difficult to interpret: while we are ultimately interested in the power of each channel,

this method does not provide such information directly.

## Contributions

**C3:** We propose fully parametric methods for PSD estimation based on the compressed observations reported by a C-ADC and consider their application to power estimation and activity detection. A CCS framework is adopted where a BEM captures the statistical structure of the signal and allows us to formulate the problem in terms of a minimal set of unknown parameters — only the power of each channel and the noise power has to be estimated, which means that, in the absence of further structure, no other WSS method can achieve a smaller sampling rate. The problem statement leads to the well-known covariance matching problem, where existing algorithms are extremely computationally demanding for real-time execution in inexpensive sensors. We develop novel methods capable of achieving a similar performance at a much lower computational cost by exploiting the fact that the covariance matrix of a wide-sense stationary process is Toeplitz together with considerations of the asymptotic theory of circulant matrices to reduce the dimensionality of the resulting optimization problems.

## SAMPLER DESIGN FOR CCS

### Prior Work

Most works in the literature deal with the design of non-periodic sparse samplers for reconstructing the second-order statistics of signals with HT covariance matrices, where the observation is that at least a pair of samples at each possible distance is required [Moffet, 1968, Hoorfar and Kassam, 1990, Pillai et al., 1985, Pal and Vaidyanathan, 2010, Pal and Vaidyanathan, 2011]. This argument leads to the so-called *minimal sparse ruler* problem, analyzed in [Rédei and Rényi, 1949, Leech, 1956, Wichmann, 1963, Wild, 1987, Pearson et al., 1990, Linebarger et al., 1993] and shown to result in optimal designs for direction finding in [Pillai et al., 1985]. Suboptimal yet more structured schemes were proposed in [Wichmann, 1963, Pearson et al., 1990, Linebarger et al., 1993, Pumphrey, 1993, Pal and Vaidyanathan, 2010, Pal and Vaidyanathan, 2012].

Designs for periodic sampling in banded covariance subspaces (see definition in Chapter 6) were proposed in [Ariananda and Leus, 2012, Domínguez-Jiménez and González-Prelcic, 2013] based on the conditions for unique reconstruction of a least squares (LS) algorithm [Ariananda and Leus, 2012]. Non-periodic sparse sampling in circulant subspaces was considered in [Yen et al., 2013], where the authors present a suboptimal design based on an estimation algorithm

that they propose<sup>6</sup>.

To the best of our knowledge, the maximum compression ratio remains an open problem in many cases of interest; and most existing results rely on the usage of specific reconstruction algorithms. Furthermore, their formulation is not general enough to accommodate periodic samplers, dense samplers, or prior information.

## Contributions

**C4.1:** We present a formal and general framework, irrespective of any algorithm, that establishes the conditions for a compression pattern to be *admissible* and defines the maximum compression ratio based on abstract criteria.

**C4.2:** We provide simple tools to assess admissibility for all linear and certain non-linear covariance parameterizations. Particularly, we show that the positive semidefinite nature of covariance matrices *does not* generally allow greater compression ratios.

**C4.3:** Maximum compression ratios are found for some of the most relevant linear covariance parameterizations. Moreover, our proofs are constructive, thus providing optimal designs. Novel designs include:

- periodic and nonperiodic sparse samplers for circulant and banded covariance subspaces,
- periodic sparse samplers for Toeplitz subspaces,
- periodic and nonperiodic dense samplers for Toeplitz, circulant and banded subspaces.

### 1.2.3 Spectrum Cartography in Multiple Channels

Bringing the spatial dimension into the picture is highly beneficial since it allows us to capture prior information about propagation and localization, and mitigates the effects of fading and shadowing. Although we exclusively investigate cartography techniques for power estimation, an extension for activity detection can be performed following the approach described in Chapter 5.

## Prior Work

Several algorithms have been proposed for spatial (and possibly temporal) interpolation of power measurements, including kriging [Alaya-Feki et al., 2008], a modification of orthogonal

---

<sup>6</sup>The initial statement in [Yen et al., 2013] uses periodic sampling, but their considerations in the frequency domain lead to non-periodic sampling.

matching pursuit [Jayawickrama et al., 2013], sparse Bayesian learning [Huang et al., 2015] and dictionary learning [Kim et al., 2011b, Kim and Giannakis, 2013]. However, since these techniques can only deal with a single power component, estimating PSD maps requires proceeding independently on a band-by-band basis, which incurs in a suboptimal estimation performance, especially if spectral prior information is available. Moreover, these schemes cannot separate the contribution of signal and noise to the overall power, and, in some cases, sensors must implement filter banks or periodograms, which require complex hardware architectures.

The frequency dimension was introduced for the first time in [Bazerque and Giannakis, 2010], where the PSD is modeled using a BEM. Several improvements were described afterwards in [Dall’Anese et al., 2012]. In [Bazerque et al., 2011], an overcomplete BEM is used to model uncertainties in the frequency domain, and regression via *thin-plate splines* (TPS) is applied along the spatial dimensions. Unfortunately, these techniques suffer from the large amount of data required by the sensors to report their measurements and from the complexity of their acquisition systems, especially when sampling wide frequency bands. The collaborative scheme in [Mehanna and Sidiropoulos, 2013, Mehanna, 2014] circumvents these limitations by proposing an extremely simple architecture where measurements are quantized to a single bit. However, this approach is unable to capture variations across space and, therefore, to provide spectrum maps.

An intimately related problem is that of channel-gain map estimation, which can be used to obtain PSD maps at the expense of further prior information and processing [Kim et al., 2011a, Dall’Anese et al., 2011]. However, to the best of our knowledge, existing techniques do not consider dependence along the frequency dimension and require active sensing, where sensors transmit pilot signals.

## Contributions

**C5.1:** We propose a family of spectrum cartography methods that solve many of the practical limitations of the aforementioned techniques. They rely on simple sensor architectures capable of acquiring wide frequency bands and sending strongly compressed measurements to the *fusion center* (FC), which robustly constructs PSD maps. For the reasons mentioned earlier, these maps are *parametrically* modeled along the frequency dimension using a BEM. On the other hand, based on the framework of *reproducing kernel Hilbert spaces* (RKHS) of vector-valued functions proposed in [Micchelli and Pontil, 2005], spatial dependence is treated from a *nonparametric* perspective, where the weights  $\alpha_b(\mathbf{z})$  are seen as scalar fields which must be jointly estimated via nonparametric regression.



**C5.2:** In order to improve the flexibility and interpretability of the map estimate, and to enable the exploitation of spatial and propagation prior information, we then adopt a *semiparametric* approach along the spatial dimension. A regression method is proposed by generalizing the setting in [Micchelli and Pontil, 2005] to the semiparametric case. To the best of our knowledge, except for some particular cases which include TPS in [Wang et al., 2001, Bazerque et al., 2011], this is the first effort to consider semiparametric regression in RKHSs of vector-valued functions from a general perspective. The resulting technique, although derived in the context of spectrum cartography, can be used in many other applications where a vector field is to be estimated using the observations gathered by a collection of sensors.

An interesting connection is established between spectrum cartography and statistical learning theory. Specifically, the regression problems can be cast as *support vector machines* (SVMs) [Schölkopf and Smola, 2001, Cherkassky and Mulier, 2007, Smola and Schölkopf, 2004, Smola et al., 1998]. This conclusion, which is not surprising, means that the proposed estimates inherit the properties of SVMs, which are known 1) to be universal approximators firmly grounded on the statistical learning theory and 2) to provide sparse representations of their estimates. The latter property is especially convenient for spectrum cartography applications since it simplifies the evaluation of PSD maps.

**C5.3:** Finally, an online implementation for the non-parametric regression method is provided based on stochastic gradient descent in the RKHS [Kivinen et al., 2004, Audiffren and Kadri, 2013]. A novel representation of the vector field, which can also be of application in any problem of nonparametric estimation with sensor networks, is proposed to avoid truncating the estimate expansions.

## 1.3 Thesis Structure

The main content of this thesis is structured in 8 chapters, arranged in three parts, and one appendix. Part I, which comprises Chapters 2, 3 and 4, considers spectrum sensing in a single channel. Part II, deals with WSS in Chapter 5 and with the fundamental problem of sampler design in Chapter 6. Part III, which includes Chapter 7, pertains to spectrum cartography. Finally, Chapter 8 provides some conclusions and future lines. Each chapter is self-contained and can be read separately after the present introduction. The topic in the Appendix is covered independently of the rest of the thesis, since its fundamental considerations and conclusions go beyond spectrum sensing applications. A summary of this structure is provided in Table 1.1.

Part	Chapter	Contribution
I	2	C1
I	3	C2.1
I	4	C2.2
II	5	C3
II	6	C4
III	7	C5
Appendix		C2.3

Table 1.1: Summary of chapters and contributions.

## 1.4 Notation

Throughout the thesis, lowercase is used for scalars, boldface lowercase for vectors and boldface uppercase for matrices. All vectors are assumed to be column vectors unless otherwise stated. Sets, matrices and vectors are indexed starting from zero. For instance, the entries of a  $P \times Q$  matrix  $\mathbf{A}$  are indexed as:

$$\mathbf{A} = \begin{bmatrix} a_{0,0} & a_{0,1} & \dots & a_{0,Q-1} \\ \vdots & \vdots & \ddots & \vdots \\ a_{P-1,0} & a_{P-1,1} & \dots & a_{P-1,Q-1} \end{bmatrix}. \quad (1.28)$$

The  $d$ -th diagonal refers to the entries  $(i, j)$  with  $j - i = d$ , where  $d$  is a negative, null or positive integer. The rest of the notation conventions are summarized in Tables 1.2 and 1.3. Acronyms and abbreviations are provided in Tables 1.4 and 1.5.

Symbol	Description
$\triangleq$	Equality by definition
$ \mathcal{A} $	Cardinality of the set $\mathcal{A}$
$\phi(\mathcal{A})$	Image of the set $\mathcal{A}$ through the function $\phi$
$j$	Imaginary unit ( $j = \sqrt{-1}$ )
$\angle x$	Phase of $x \in \mathbb{C}$
$\propto$	Related by a monotone increasing transformation not depending on the observations
$!$	factorial
$!!$	double factorial
$(x)_K$	Remainder of the integer division of $x \in \mathbb{Z}$ by $K$ : $(x)_K$ is the only element in the set $\{x + lK, l \in \mathbb{Z}\} \cap \{0, \dots, K-1\}$
$\text{span}_{\mathbb{F}} \mathcal{A}$	Span of the set of matrices $\mathcal{A}$ with scalars in the field $\mathbb{F}$ : $\text{span}_{\mathbb{F}} \mathcal{A} = \{\mathbf{A} \in \mathbb{C}^{P \times P} : \mathbf{A} = \sum_b \alpha_b \mathbf{A}_b, \mathbf{A}_b \in \mathcal{A}, \alpha_b \in \mathbb{F}\}$
$\dim_{\mathbb{F}} \mathcal{B}$	$\mathbb{F}$ -dimension of set $\mathcal{B}$ : smallest $n \in \mathbb{N}$ such that there exists some $\mathcal{A}$ with $ \mathcal{A}  = n$ such that $\mathcal{B} \subset \text{span}_{\mathbb{F}} \mathcal{A}$
$\mathbb{P}\{\cdot\}$	Probability
$\mathbb{E}\{\cdot\}$	Expectation
$\mathcal{CN}$	Circularly-symmetric complex Gaussian distribution
$\mathcal{N}$	Real Gaussian distribution
$\mathcal{F}$	F-distribution
$\chi^2$	$\chi^2$ -distribution
$\mathcal{CW}$	Complex central Wishart distribution
$\star$	Convolution
$\delta(t)$	Dirac delta
$\delta[t]$	Kronecker delta

Table 1.2: Description of some of the symbols used in the thesis.

Symbol	Description
$\mathbf{1}_K$	$K \times 1$ vector of all ones
$\mathbf{0}_K$	$K \times 1$ vector of all zeros
$\mathbf{e}_{K,i}$	$K \times 1$ vector with a 1 at the $i$ -th position and zeros elsewhere
$\mathbf{E}_{i,j}$	Matrix with all zeros except for a 1 at the position $(i, j)$
$\mathbf{I}_K$	Identity matrix of dimension $K$
$(\mathbf{v})_k$	$k$ -th entry of the vector $\mathbf{v}$
$(\mathbf{A})_{k,l}$	$(k, l)$ entry of the matrix $\mathbf{A}$
$\text{diag}\{\mathbf{v}\}$	Diagonal matrix with the entries of the vector $\mathbf{v}$ on its diagonal
$\text{diag}\{\mathbf{A}\}$	Vector with the diagonal entries of matrix $\mathbf{A}$
$\text{vec}$	Column-wise vectorization: if $\mathbf{A} = [\mathbf{a}_0, \dots, \mathbf{a}_{K-1}]$ , then $\text{vec}(\mathbf{A}) = [\mathbf{a}_0^T, \dots, \mathbf{a}_{K-1}^T]^T$
superscript $T$	Transpose
superscript $*$	Complex conjugate
superscript $H$	Conjugate and transpose
$\otimes$	Kronecker product [Bernstein, 2009]
$\mathbf{A} \odot \mathbf{B}$	Khatri-Rao product of $\mathbf{A} = [\mathbf{a}_0, \dots, \mathbf{a}_{K-1}]$ and $\mathbf{B} = [\mathbf{b}_0, \dots, \mathbf{b}_{K-1}]$ : $\mathbf{A} \odot \mathbf{B} = [\mathbf{a}_0 \otimes \mathbf{b}_0, \dots, \mathbf{a}_{K-1} \otimes \mathbf{b}_{K-1}]$
$\mathbf{A} \circ \mathbf{B}$	Entry-wise (Hadamard) product: $(\mathbf{A} \circ \mathbf{B})_{i,j} = (\mathbf{A})_{i,j}(\mathbf{B})_{i,j}$
$\ \cdot\ _F$	Frobenius norm
$\ \cdot\ _p$	$\ell^p$ -norm
$\ \cdot\ $	$\ell^2$ -norm
$\ \mathbf{A}\ _{p,q}$	Operator norm, defined as $\max_{\mathbf{x}} \ \mathbf{A}\mathbf{x}\ _q$ subject to $\ \mathbf{x}\ _p = 1$
$ \mathbf{A} $	Determinant of the matrix $\mathbf{A}$
$\text{Tr}(\mathbf{A})$	Trace of the matrix $\mathbf{A}$
$\text{etr}\{\mathbf{A}\}$	Abbreviation for $\exp\{\text{Tr}(\mathbf{A})\}$
$\lambda_n(\mathbf{A})$	$n$ -th largest eigenvalue of $\mathbf{A}$
$\mathbf{a} \succeq \mathbf{b}$	Generalized inequality/partial ordering with respect to the nonnegative orthant: $\mathbf{a} \succeq \mathbf{b} \Leftrightarrow (\mathbf{a})_i \geq (\mathbf{b})_i \forall i$
$\mathbf{A} \geq \mathbf{0}$	$\mathbf{A}$ is positive semidefinite
$\mathbf{A} > \mathbf{0}$	$\mathbf{A}$ is positive definite

Table 1.3: Matrix/vector notation.

Acronym/Abbreviation	Meaning
ADC	Analog-to-digital converter
BEM	Basis expansion model
BL	Bandlimited
BLCM	Bandlimited and constant magnitude
C-ADC	Compressive ADC
CCS	Compressive Covariance Sampling
CFAR	Constant false alarm rate
CM	Constant magnitude
CPD	Conditionally positive definite
CPM	Continuous-phase modulation
CPQ	Constant-probability quantization
CRB	Cramér-Rao bound
DFT	Discrete Fourier transform
DSA	Dynamic spectrum access
EM	Expectation-maximization
FC	Fusion center
FCC	Federal Communications Commission
FFT	Fast Fourier transform
FIR	Finite impulse response
FM	Frequency modulation
FSK	Frequency-shift keying
GK	Generalized kurtosis/Gaussian kernel
GLR	Generalized likelihood ratio
GMSK	Gaussian minimum shift keying
GSM	Global System for Mobile
HT	Hermitian Toeplitz
iff	if and only if
IFFT	Inverse fast Fourier transform
KKT	Karush-Kuhn-Tucker

Table 1.4: Acronyms and abbreviations (1/2).

Acronym/Abbreviation	Meaning
LIKES	Likelihood-based estimation of sparse parameters
LMPI	Locally most powerful invariant
LOS	Line-of-sight
LS	Least squares
MC	Monte Carlo
ML	Maximum likelihood
MSE	Mean squared error
NLOS	Non-line-of-sight
NORMA	Naive Online $R_{\text{reg}}$ Minimization Algorithm
OFDM	Orthogonal frequency-division multiplexing
ONORMA	Operator NORMA
PSD	Power spectral density
RKHS	Reproducing kernel Hilbert space
ROC	Receiver operating characteristic
SCM	Sample covariance matrix
SDP	Semidefinite program
SMO	Sequential minimal optimization
SNR	Signal-to-noise ratio
SOCp	Second-order cone program
SPICE	Sparse iterative covariance-based estimation
s.t.	subject to
SVM	Support vector machine
TPS	Thin-plate splines
ULA	Uniform linear array
UMP	Uniformly most powerful
UMPI	Uniformly most powerful invariant
UQ	Uniform quantization
WM	Wireless microphone
WSS	Wideband spectrum sensing

Table 1.5: Acronyms and abbreviations (2/2).

## Part I

# Spectrum Sensing in a Single Channel





## Chapter 2

# Detection of Wireless Microphone Signals Using Multiple Antennas

The purpose of this chapter is to devise detection schemes capable of fully exploiting both the spatial structure and the available signal prior information to reliably detect the activity of WMs. As explained in Section 1.2.1, no detector for WM signals has been proposed for multiantenna sensors, while no multiantenna detector has been specifically tailored to detect the activity of this class of signals. Even within single-antenna detectors, none of them exploits the whole structure of WM waveforms.

In the IEEE 802.22 standard [IEEE, 2011], a 6 MHz TV channel is scanned for the presence of TV and WM signals, among others. This motivates the acquisition of 6 MHz-chunks over which a batch of detection algorithms for different kinds of primary signals is applied. Since WM transmissions are confined to a bandwidth of 200 kHz [Clanton et al., 2007, Gautier et al., 2010, Erpek et al., 2011], it is reasonable to take advantage of the fact that the signal to be detected has a small bandwidth relative to the 6 MHz channel. In other words, we may exploit the fact that the signal is *bandlimited* (BL). Moreover, regulations dictate that the carrier frequency of WM transmissions must be an integer multiple of 25 kHz away from the channel edge [Federal Communications Commission, 2012], meaning that the set of candidate frequency locations of WM signals are known *a priori*. Additionally, WM waveforms typically employ analog frequency modulation (FM) [Chen and Gao, 2011, Clanton et al., 2007], and therefore their complex lowpass equivalent exhibits a constant magnitude (CM).

We consider these two features, namely the BL and CM properties, along with spatial information in order to develop several multiantenna detectors for WMs. These detectors differ in the amount of prior information they exploit, providing the system designer with different trade-offs between performance and complexity. In order to cope with the unknown param-

ters, our derivations are based on evaluating the GLR test under different signal models. The deterministic approach adopted, by which the signal term is modeled as an unknown deterministic parameter [Kay, 1998, Besson et al., 2006], enables us to find detectors which require no assumptions about the statistical distribution of the transmitted signal or channel, and allows to gradually incorporate prior information about WM signals while keeping the problem mathematically tractable.

Our detectors generalize those in [Derakhtian et al., 2009a, Derakhtian et al., 2009b, Besson et al., 2006, Taherpour et al., 2010, Wang et al., 2010] and were especially inspired by the work in [Derakhtian et al., 2009a, Derakhtian et al., 2009b]. Besides spectrum sensing, these schemes can also be used in other settings where the activity of BL or CM signals needs to be detected (see Section 1.1.1).

The rest of this chapter is organized as follows. The problem is formulated in Section 2.1, where the deterministic signal model is presented. We then derive several detectors that exploit different degrees of prior information:

- In Section 2.2, we derive the GLR test for the case where only the BL property is exploited, resulting in the simplest of all detectors proposed in this chapter. Next, we consider this property along with the spatial rank-1 structure of the channel to derive another GLR detector.
- In Section 2.3, the CM property is used together with the rank-1 space structure to derive a third detector.
- Capitalizing on the spatial structure along with the BL and CM properties, a GLR detector is developed in Section 2.4. Albeit the most computationally demanding, this scheme provides the best performance since it exploits all the available prior information.

Some common considerations and implementation issues are discussed in Section 2.5. Next, performance is analytically evaluated in Section 2.6. In Section 2.7, we assess performance using the simulation guidelines for WMs proposed by the IEEE 802.22 working group and finally provide some concluding remarks in Section 2.8.

## 2.1 Problem setting

We start by generalizing the signal model from Section 1.1.1 to represent the observations acquired by a spectrum sensor with multiple antennas.

### 2.1.1 Signal Model

Consider a spectrum sensor that observes a certain frequency channel using  $M$  antennas. If a WM signal  $x^*$  is present, then the signal received by the  $m$ -th antenna is given by:<sup>1</sup>

$$y_m = h_m \star x^* + w_m, \quad m = 0, \dots, M-1. \quad (2.1)$$

The sensor collects  $K$  samples  $y_m[k] = y_m(kT_s)$ ,  $k = 0, \dots, K-1$ , from each antenna, producing:

$$\begin{aligned} y_m[k] &= h_m[k] \star x^*[k] + w_m[k], \quad m = 0, 1, \dots, M-1, \\ k &= 0, 1, \dots, K-1, \end{aligned}$$

where the  $h_m[k]$ ,  $x^*[k]$ , and  $w_m[k]$  denote, respectively, the samples of  $h_m$ ,  $x^*$ , and  $w_m$ . The noise processes  $w_m$  are assumed zero-mean, circularly symmetric jointly Gaussian, and temporally and spatially white with variance  $\sigma^2$ , which implies that  $E\{w_m[k]w_{m'}^*[k']\} = \sigma^2\delta[m-m']\delta[k-k']$ .

Let  $\mathbf{h}[k] \triangleq [h_0[k], \dots, h_{M-1}[k]]^T$  and  $\mathbf{r}[k] \triangleq \mathbf{h}[k] \star x^*[k] = \sum_{k'} \mathbf{h}[k']x^*[k-k']$ . Introducing the  $M \times K$  matrix  $\mathbf{R} \triangleq [\mathbf{r}[0], \dots, \mathbf{r}[K-1]]$ , we can arrange all samples in matrix form and write

$$\mathbf{Y} = \mathbf{R} + \mathbf{W}, \quad (2.2)$$

where the  $(m, k)$  entries of  $\mathbf{Y}$  and  $\mathbf{W}$  are respectively  $y_m[k]$  and  $w_m[k]$ .

The activity detection problem can be cast as a test of the null hypothesis  $\mathcal{H}_0$  that the observations contain only noise, i.e.  $\mathbf{Y} = \mathbf{W}$ , against the alternative  $\mathcal{H}_1$  stating that there is both signal and noise, i.e.  $\mathbf{Y} = \mathbf{R} + \mathbf{W}$ . The transmitted signal samples  $x^*[k]$ , the channel coefficients  $h_m[k]$  and the noise power  $\sigma^2$  are modeled as unknown deterministic parameters, which will allow us to gradually introduce the prior information available about  $x^*$  and  $h_m$ . In view of this assumption, the observations in  $\mathbf{Y}$  are Gaussian distributed and satisfy  $E_{\mathcal{H}_0}\{\mathbf{Y}\} = \mathbf{0}$  and  $E_{\mathcal{H}_1}\{\mathbf{Y}\} = \mathbf{R}$ , where  $E_{\mathcal{H}_i}\{\cdot\}$  denotes expectation under hypothesis  $\mathcal{H}_i$ .

Let

$$\hat{\mathbf{S}}_0 \triangleq \frac{1}{K} \mathbf{Y} \mathbf{Y}^H, \quad \hat{\mathbf{S}}_1 \triangleq \frac{1}{K} (\mathbf{Y} - \mathbf{R})(\mathbf{Y} - \mathbf{R})^H \quad (2.3)$$

respectively denote the  $M \times M$  sample spatial covariance matrices under  $\mathcal{H}_0$  and  $\mathcal{H}_1$ . Then the probability density function of the observations under  $\mathcal{H}_i$ ,  $i \in \{0, 1\}$ , is given by

$$p_{\mathcal{H}_i}(\mathbf{Y}) = \left[ \frac{1}{(\pi\sigma^2)^M} \exp \left[ -\frac{1}{\sigma^2} \text{Tr}(\hat{\mathbf{S}}_i) \right] \right]^K. \quad (2.4)$$

---

<sup>1</sup>We conjugate the signal component  $x$  for notational convenience.

### 2.1.2 Generalized Likelihood Ratio

In order to cope with the presence of unknown parameters, we consider the GLR test, whose statistic is given by

$$\mathcal{G}(\mathbf{Y}) \triangleq \frac{\sup_{\sigma^2, \mathbf{R}} p_{\mathcal{H}_1}(\mathbf{Y}; \sigma^2, \mathbf{R})}{\sup_{\sigma^2} p_{\mathcal{H}_0}(\mathbf{Y}; \sigma^2)}. \quad (2.5)$$

Under either  $\mathcal{H}_0$  or  $\mathcal{H}_1$ , it is readily found (see e.g. [Anderson, 2003, Lemma 3.2.2]) that the value of  $\sigma^2$  maximizing (2.4) — i.e., the ML estimate of  $\sigma^2$  — is

$$\hat{\sigma}_i^2 = \frac{1}{M} \text{Tr}(\hat{\mathbf{S}}_i), \quad i = 0, 1. \quad (2.6)$$

Substituting (2.6) in (2.4) yields

$$p_{\mathcal{H}_i}(\mathbf{Y}; \hat{\sigma}_i^2) = \left[ \pi e \cdot \text{Tr}(\hat{\mathbf{S}}_i) \right]^{-MK},$$

which after substitution in (2.5) produces

$$\mathcal{G}(\mathbf{Y}) = \left[ \frac{\text{Tr}(\hat{\mathbf{S}}_0)}{\inf_{\mathbf{R}} \text{Tr}(\hat{\mathbf{S}}_1(\mathbf{R}))} \right]^{MK}. \quad (2.7)$$

The following sections address the minimization of  $\text{Tr}(\hat{\mathbf{S}}_1(\mathbf{R}))$  under several models for  $\mathbf{R}$  that incorporate different degrees of prior information, thus determining the feasible set of such optimization problems.

## 2.2 Multiantenna Detection of BL Signals

Let us assume that the transmitted signal has a known bandwidth  $\mathcal{B}$ , measured in radians per sample. In the case of WM signals, we know that

$$\mathcal{B} = \frac{2\pi \cdot 200 \text{ kHz}}{f_s}, \quad (2.8)$$

where, recall from Chapter 1,  $f_s = 1/T_s$  is the sampling rate. The central frequency  $\omega_c$  is not known, but it is assumed to belong in a finite set  $\Omega_c$  of candidate central frequencies. For WM

signals, this set is given by

$$\Omega_c = \left\{ \frac{2\pi f_k}{f_s}, k = 0, 1, \dots, k_{\max} \right\}, \quad (2.9)$$

where  $f_k \triangleq f_e + k \cdot 25$  kHz for  $f_e$  the minimum carrier frequency, which is related to the edge of the TV channel [Federal Communications Commission, 2012]. For the sake of clarity, we start by considering the case where this set has only one element, i.e., its cardinality  $|\Omega_c|$  equals one, in which case  $\omega_c$  can be regarded as known. The case  $|\Omega_c| > 1$  will be discussed in Section 2.5.2.

Let us particularize (2.7) to the BL case by noting that

$$\text{Tr}(\hat{\mathbf{S}}_1(\mathbf{R})) = \frac{1}{K} \sum_{k=0}^{K-1} \|\mathbf{y}[k] - \mathbf{r}[k]\|^2, \quad (2.10)$$

where  $\mathbf{y}[k]$  and  $\mathbf{r}[k]$  respectively denote the  $k$ -th column of  $\mathbf{Y}$  and  $\mathbf{R}$ . By virtue of Parseval's identity,

$$\text{Tr}(\hat{\mathbf{S}}_1(\mathbf{R})) = \frac{1}{K^2} \sum_{n=0}^{K-1} \|\mathbf{y}(e^{j\omega_n}) - \mathbf{r}(e^{j\omega_n})\|^2, \quad (2.11)$$

where  $\omega_n \triangleq \frac{2\pi}{K}n$  and the DFT vectors  $\mathbf{y}(e^{j\omega_n})$  and  $\mathbf{r}(e^{j\omega_n})$  are given by

$$\mathbf{y}(e^{j\omega_n}) \triangleq \sum_{k=0}^{K-1} \mathbf{y}[k] e^{-j\omega_n k}, \quad \mathbf{r}(e^{j\omega_n}) \triangleq \sum_{k=0}^{K-1} \mathbf{r}[k] e^{-j\omega_n k}.$$

Let us assume, without any loss of generality, that the frequency support of  $x^*[k]$ , and therefore that of  $\mathbf{r}[k]$ , is contained in the first  $B$  DFT coefficients<sup>2</sup> ( $B = \lfloor \frac{K}{2\pi} \mathcal{B} \rfloor$ ). Then (2.11) can be written as the sum of two terms:

$$\text{Tr}(\hat{\mathbf{S}}_1(\mathbf{R})) = \frac{1}{K^2} \sum_{n=0}^{B-1} \|\mathbf{y}(e^{j\omega_n}) - \mathbf{r}(e^{j\omega_n})\|^2 + \frac{1}{K^2} \sum_{n=B}^{K-1} \|\mathbf{y}(e^{j\omega_n})\|^2. \quad (2.12)$$

The rest of this section is devoted to addressing the minimization of the first term in the right-hand side of (2.12), which is the only one that depends on  $\mathbf{R}$ , under two scenarios. First, an arbitrary channel impulse response  $\mathbf{h}[k]$  is assumed, which implies that the signal term  $\mathbf{r}[k]$  is unstructured. This will result in the simplest of the detectors proposed in this chapter — it

---

<sup>2</sup> Strictly speaking, the received sequence is only approximately bandlimited since we observe a finite number of samples  $K$ . Nevertheless, throughout this chapter it is assumed that  $K$  is sufficiently large so that windowing effects can be neglected and the signal can be regarded as truly bandlimited. This is justified by the fact that, in practice, stringent low-SNR detectability requirements cannot be met with small values of  $K$ .

only exploits the BL property. Later, a frequency-flat channel assumption will induce a rank-1 spatial structure, resulting in a second detector with better performance but higher complexity.

### 2.2.1 Arbitrary Channel Structure

Applying Parseval's identity again to the first term on the right side of (2.12) yields

$$\frac{1}{K^2} \sum_{n=0}^{B-1} \|\mathbf{y}(e^{j\omega_n}) - \mathbf{r}(e^{j\omega_n})\|^2 = \frac{1}{K} \sum_{k=0}^{K-1} \|\mathbf{y}_f[k] - \mathbf{h}[k] \star x^*[k]\|^2, \quad (2.13)$$

where  $\mathbf{y}_f[k]$  represents a filtered version of  $\mathbf{y}[k]$  obtained by setting to zero all out-of-band DFT coefficients, i.e.,

$$\mathbf{y}_f[k] \triangleq \frac{1}{K} \sum_{n=0}^{B-1} \mathbf{y}(e^{j\omega_n}) e^{j\omega_n k}. \quad (2.14)$$

Clearly, expression (2.13), and consequently (2.12), is minimized when  $\mathbf{y}_f[k] = \mathbf{h}[k] \star x^*[k]$ . Since no structure about  $\mathbf{h}[k]$  is assumed, it is clearly possible to select  $x^*[k]$  and  $\mathbf{h}[k]$  to satisfy this condition. The resulting minimizer, denoted as  $\hat{\mathbf{R}}$ , is in fact the ML estimate of the signal term (see Section 1.1.1). From (2.12), it follows that

$$\begin{aligned} \text{Tr}(\hat{\mathbf{S}}_1(\hat{\mathbf{R}})) &= \frac{1}{K^2} \sum_{n=0}^{K-1} \|\mathbf{y}(e^{j\omega_n})\|^2 \\ &= \frac{1}{K^2} \sum_{n=0}^{K-1} \|\mathbf{y}(e^{j\omega_n})\|^2 - \frac{1}{K^2} \sum_{n=0}^{B-1} \|\mathbf{y}(e^{j\omega_n})\|^2, \end{aligned}$$

which, in the time domain, becomes

$$\text{Tr}(\hat{\mathbf{S}}_1(\hat{\mathbf{R}})) = \frac{1}{K} \sum_{k=0}^{K-1} \|\mathbf{y}[k]\|^2 - \frac{1}{K} \sum_{k=0}^{K-1} \|\mathbf{y}_f[k]\|^2. \quad (2.15)$$

Similarly to  $\mathbf{Y}$  and  $\hat{\mathbf{S}}_0$ , one can define

$$\mathbf{Y}_f \triangleq \begin{bmatrix} \mathbf{y}_f[0] & \mathbf{y}_f[1] & \cdots & \mathbf{y}_f[K-1] \end{bmatrix}, \quad (2.16a)$$

$$\hat{\mathbf{S}}_0^f \triangleq \frac{1}{K} \mathbf{Y}_f \mathbf{Y}_f^H. \quad (2.16b)$$

In that case, (2.15) becomes  $\text{Tr}(\hat{\mathbf{S}}_1(\hat{\mathbf{R}})) = \text{Tr}(\hat{\mathbf{S}}_0) - \text{Tr}(\hat{\mathbf{S}}_0^f)$  and (2.7) reduces to

$$\mathcal{G}_{\text{BL}}(\mathbf{Y}) = \left[ \frac{\text{Tr}(\hat{\mathbf{S}}_0)}{\text{Tr}(\hat{\mathbf{S}}_0) - \text{Tr}(\hat{\mathbf{S}}_0^f)} \right]^{MK}. \quad (2.17)$$

Since two test statistics related by a monotonically increasing transformation define the same test as long as the thresholds are properly set [Kay, 1998, Lehmann and Romano, 2005], testing  $\mathcal{G}_{\text{BL}}(\mathbf{Y})$  in (2.17) amounts to testing

$$\mathcal{T}_{\text{BL}}(\mathbf{Y}) \triangleq \frac{\text{Tr}(\hat{\mathbf{S}}_0^f)}{\text{Tr}(\hat{\mathbf{S}}_0)} = \frac{\|\mathbf{Y}_f\|_F^2}{\|\mathbf{Y}\|_F^2}, \quad (2.18)$$

where  $\|\cdot\|_F$  denotes the Frobenius norm. Henceforth, the test associated with the statistic in (2.18) will be referred to as the BL detector since this is the only property that it exploits. Note that it simply measures the ratio of the in-band energy to the total energy.

### 2.2.2 Frequency-Flat Channels

As the WM signal is narrowband relative to the 6 MHz operational bandwidth, the channel response can be regarded as frequency-flat.<sup>3</sup> This produces a rank-1 channel structure which, without any loss of generality, can be expressed by writing  $\mathbf{R} = \mathbf{h}\mathbf{x}^H$ , where  $\mathbf{h} \in \mathbb{C}^M$  and  $\mathbf{x} \triangleq [x[0], x[1], \dots, x[K-1]]^T$ . This reads in the frequency domain as  $\mathbf{r}(e^{j\omega_n}) = x^*(e^{-j\omega_n})\mathbf{h}$ , where  $x(e^{j\omega_n}) \triangleq \sum_{k=0}^{K-1} x[k]e^{-j\omega_n k}$ . Therefore, optimizing with respect to  $\mathbf{R}$  amounts to optimizing with respect to  $x(e^{j\omega_n})$  and  $\mathbf{h}$ . We first find the minimum of

$$\|\mathbf{y}(e^{j\omega_n}) - \mathbf{r}(e^{j\omega_n})\|^2 = \|\mathbf{y}(e^{j\omega_n}) - x^*(e^{-j\omega_n})\mathbf{h}\|^2 \quad (2.19)$$

with respect to  $x(e^{j\omega_n})$  for each  $\omega_n$ , with  $n = 0, \dots, B-1$ . This is a typical least squares (LS) problem, with solution given by

$$\inf_{x(e^{j\omega_n})} \|\mathbf{y}(e^{j\omega_n}) - x^*(e^{-j\omega_n})\mathbf{h}\|^2 = \|\mathbf{y}(e^{j\omega_n})\|^2 - \frac{|\mathbf{h}^H \mathbf{y}(e^{j\omega_n})|^2}{\|\mathbf{h}\|^2}. \quad (2.20)$$

---

<sup>3</sup>Note that the distance between antennas is set in the order of half the wavelength of the carrier frequency. Since the bandwidth of the WM signal is much smaller than this carrier frequency, the relative delay that different frequencies in the support of the WM signal experience when arriving at different antennas is small and, as a result, we may adopt the usual narrowband assumption, by which the complex baseband representation of the signal received by one antenna differs from another in a complex scaling factor.

Substituting (2.20) in (2.12) yields

$$\text{Tr} \left( \hat{\mathbf{S}}_1(\hat{\mathbf{x}}, \mathbf{h}) \right) = \frac{1}{K^2} \sum_{n=0}^{K-1} \|\mathbf{y}(e^{j\omega_n})\|^2 - \frac{1}{K^2} \sum_{n=0}^{B-1} \frac{|\mathbf{h}^H \mathbf{y}(e^{j\omega_n})|^2}{\|\mathbf{h}\|^2}, \quad (2.21)$$

or, in the time domain,

$$\begin{aligned} \text{Tr} \left( \hat{\mathbf{S}}_1(\hat{\mathbf{x}}, \mathbf{h}) \right) &= \frac{1}{K} \sum_{k=0}^{K-1} \|\mathbf{y}[k]\|^2 - \frac{1}{K} \frac{\|\mathbf{h}^H \mathbf{Y}_f\|^2}{\|\mathbf{h}\|^2} \\ &= \text{Tr} \left( \hat{\mathbf{S}}_0 \right) - \frac{\mathbf{h}^H \hat{\mathbf{S}}_0^f \mathbf{h}}{\|\mathbf{h}\|^2}. \end{aligned} \quad (2.22)$$

The vector  $\mathbf{h}$  minimizing (2.22) is given by the principal eigenvector of  $\hat{\mathbf{S}}_0^f$ . Hence,

$$\inf_{\mathbf{h}} \text{Tr} \left( \hat{\mathbf{S}}_1(\hat{\mathbf{x}}, \mathbf{h}) \right) = \text{Tr} \left( \hat{\mathbf{S}}_0 \right) - \lambda_1 \left( \hat{\mathbf{S}}_0^f \right), \quad (2.23)$$

where  $\lambda_1(\mathbf{A})$  denotes the largest eigenvalue of  $\mathbf{A}$ . Substituting (2.23) in (2.7) yields

$$\mathcal{G}_{\text{BLFF}}(\mathbf{Y}) = \left[ \frac{\text{Tr} \left( \hat{\mathbf{S}}_0 \right)}{\text{Tr} \left( \hat{\mathbf{S}}_0 \right) - \lambda_1 \left( \hat{\mathbf{S}}_0^f \right)} \right]^{MK}.$$

For detection purposes, this statistic is equivalent to (recall our notational conventions from Section 1.4):

$$\mathcal{T}_{\text{BLFF}}(\mathbf{Y}) \triangleq \frac{\lambda_1 \left( \hat{\mathbf{S}}_0^f \right)}{\text{Tr} \left( \hat{\mathbf{S}}_0 \right)} = \frac{\|\mathbf{Y}_f\|_{2,2}^2}{\|\mathbf{Y}\|_F^2}, \quad (2.24)$$

From now on, we will refer to the test defined by this statistic as the bandlimited frequency-flat detector (BLFF). Observe that (2.24) reduces to the well-known multiantenna detector from [Besson et al., 2006, Taherpour et al., 2010, Wang et al., 2010] when the signal is not bandlimited, i.e., when  $B = K$ , which yields  $\hat{\mathbf{S}}_0^f = \hat{\mathbf{S}}_0$ . In that case, the only property that these detectors exploit is the rank-1 spatial structure.

### 2.3 Multiantenna detection of CM signals

In this section we derive the GLR detector that only exploits the CM property of the WM signal. To do so, we minimize  $\text{Tr}(\hat{\mathbf{S}}_1(\mathbf{R}))$  assuming that the transmitted signal  $x[k]$  has this property,



although it may not be bandlimited. As it turns out, the existence of the GLR depends on whether the assumption of frequency-flat channel applies or not.

### 2.3.1 Arbitrary Channel Structure

From expression (2.10), it is possible to write

$$\text{Tr} \left( \hat{\mathbf{S}}_1(\mathbf{R}) \right) = \frac{1}{K} \sum_{k=0}^{K-1} \| \mathbf{y}[k] - \mathbf{h}[k] \star x^*[k] \|^2. \quad (2.25)$$

Due again to the fact that no structure is imposed on  $\mathbf{h}[k]$ , it follows that (2.25) can be made zero: for example, pick  $x^*[k]$  as any CM signal with no spectral zeros, and choose each entry of  $\mathbf{h}[k]$  as the signal whose DFT spectrum equals that of the corresponding entry of  $\mathbf{y}[k]$  divided by the spectrum of  $x^*[k]$ . Thus, the denominator of (2.7) vanishes and no GLR exists for this case. This makes sense since the CM property of the transmitted signal, which is the only feature exploited in this case, is wiped out after passing through a frequency-selective channel.

### 2.3.2 Frequency-Flat Channels

Now assume that the channel is frequency flat, which, as seen in Section 2.2.2, means that one may write  $\mathbf{R} = \mathbf{h}\mathbf{x}^H$ . In order to explicitly represent the CM property of the transmitted signal, let us adopt the notation  $\mathbf{x}(\boldsymbol{\varphi}) \triangleq [e^{j\varphi_0}, e^{j\varphi_1}, \dots, e^{j\varphi_{K-1}}]^T$ , where  $\boldsymbol{\varphi} \triangleq [\varphi_0, \varphi_1, \dots, \varphi_{K-1}]^T$ . Note that there is no loss of generality in assuming unit magnitude, since any scaling factor can be subsumed in the unknown channel vector  $\mathbf{h}$ . Noting that  $\mathbf{x}^H(\boldsymbol{\varphi})\mathbf{x}(\boldsymbol{\varphi}) = K$  yields

$$\text{Tr} \left( \hat{\mathbf{S}}_1(\mathbf{h}, \boldsymbol{\varphi}) \right) = \frac{1}{K} [\text{Tr} (\mathbf{Y}\mathbf{Y}^H) - 2 \text{Re} \{ \mathbf{h}^H \mathbf{Y} \mathbf{x}(\boldsymbol{\varphi}) \} + K \|\mathbf{h}\|^2]. \quad (2.26)$$

The ML estimate of  $\boldsymbol{\varphi}$  is given by

$$\hat{\boldsymbol{\varphi}} = \arg \sup_{\boldsymbol{\varphi}} \text{Re} \{ \mathbf{h}^H \mathbf{Y} \mathbf{x}(\boldsymbol{\varphi}) \} \quad (2.27a)$$

$$= \arg \sup_{\boldsymbol{\varphi}} \text{Re} \left\{ \sum_{k=0}^{K-1} e^{j\varphi_k} \mathbf{h}^H \mathbf{y}[k] \right\}, \quad (2.27b)$$

which results in  $\hat{\varphi}_k = -\angle(\mathbf{h}^H \mathbf{y}[k])$ . The optimal value of the above expression is therefore  $\sum_k |\mathbf{h}^H \mathbf{y}[k]| = \|\mathbf{Y}^H \mathbf{h}\|_1$ . Substituting this back in (2.26) gives

$$\text{Tr} \left( \hat{\mathbf{S}}_1(\mathbf{h}, \hat{\boldsymbol{\varphi}}) \right) = \frac{1}{K} [\text{Tr} (\mathbf{Y}\mathbf{Y}^H) - 2\|\mathbf{Y}^H \mathbf{h}\|_1 + K \|\mathbf{h}\|^2]. \quad (2.28)$$

In order to minimize this expression with respect to  $\mathbf{h}$ , write  $\mathbf{h} = c \cdot \tilde{\mathbf{h}}$ , with  $c > 0$  and  $\|\tilde{\mathbf{h}}\| = 1$ . The optimal value of  $c$  is readily found to be  $\hat{c} = \frac{1}{K} \|\mathbf{Y}^H \tilde{\mathbf{h}}\|_1$ . Using this expression, the ML estimate of the spherical component  $\tilde{\mathbf{h}}$  is seen to be

$$\hat{\tilde{\mathbf{h}}} = \arg \sup_{\tilde{\mathbf{h}}} \|\mathbf{Y}^H \tilde{\mathbf{h}}\|_1 \quad \text{s.t.} \quad \|\tilde{\mathbf{h}}\| = 1. \quad (2.29)$$

The solution to this problem,  $\|\mathbf{Y}^H\|_{2,1} \triangleq \|\mathbf{Y}^H \hat{\tilde{\mathbf{h}}}\|_1$  is known as the *operator norm*, *dual norm*, or *subordinate norm* to the vector  $\ell^2$ - and  $\ell^1$ -norms [Demmel, 1997, Golub and Van Loan, 1996, Boyd and Vandenberghe, 2004, Kolmogorov and Fomin, 1970]. An iterative method for solving this constrained optimization problem is presented in Appendix 2.A. Substituting this solution produces

$$\text{Tr} \left( \hat{\mathbf{S}}_1(\hat{\mathbf{h}}, \hat{\varphi}) \right) = \frac{1}{K} \left[ \|\mathbf{Y}\|_F^2 - \frac{1}{K} \|\mathbf{Y}^H\|_{2,1}^2 \right]. \quad (2.30)$$

Finally, using (2.30) in (2.7) gives

$$\mathcal{G}_{\text{CM}}(\mathbf{Y}) = \left[ \frac{\|\mathbf{Y}\|_F^2}{\|\mathbf{Y}\|_F^2 - \frac{1}{K} \|\mathbf{Y}^H\|_{2,1}^2} \right]^{MK}, \quad (2.31)$$

which is a monotonically increasing function of the equivalent test statistic

$$\mathcal{T}_{\text{CM}}(\mathbf{Y}) \triangleq \frac{\|\mathbf{Y}^H\|_{2,1}^2}{\|\mathbf{Y}\|_F^2}. \quad (2.32)$$

The detector defined by the statistic in (2.32) will be referred to as the CM detector since it exploits the CM property. Although it also exploits the rank-1 structure of the signal term, we will dismiss this fact in the notation since, as seen in Section 2.3.1, no GLR detector exists that exploits the CM property if the channel structure is arbitrary.

## 2.4 Detection of CM Bandlimited Signals

We now consider the complete model, which captures the entire prior knowledge about the WM signal. Regarding the minimization of  $\text{Tr} \left( \hat{\mathbf{S}}_1(\mathbf{R}) \right)$ , it can be readily shown, analogously to Section 2.3.1, that if an arbitrary channel impulse response is assumed, then the CM constraint on the signal still allows to make zero the signal term within the frequency support of the transmitted signal. However, in this case the denominator of (2.7) does not vanish because of the contribution of the out-of-band noise, thus resulting in a well-defined GLR statistic.

The resulting test turns out to be equivalent to the BL detector in (2.18). This is consistent with our findings in Section 2.3.1: since passing a CM signal through a frequency selective channel destroys the CM property at the channel output, it is reasonable that the corresponding detector should not exploit such a property. However, the situation is different with frequency-flat channels, as discussed next.

Let us start by noting that the fact that the signal is bandlimited allows us to write the trace of the sample covariance matrix again as in (2.12). However, the optimization with respect to  $\mathbf{r}(e^{j\omega_n})$  now has to take into account the CM feature, which is a time-domain property. As we will see, a solution can be found by confining ourselves to the frequency support of  $\mathbf{x}(e^{j\omega_n})$ .

As seen in Section 2.2.1, for frequency-flat channels we may write  $\mathbf{r}(e^{j\omega_n}) = x^*(e^{-j\omega_n})\mathbf{h}$ , which means that the first term in the right-hand side of (2.12) becomes

$$\frac{1}{K^2} \sum_{n=0}^{B-1} \|\mathbf{y}(e^{j\omega_n}) - \mathbf{r}(e^{j\omega_n})\|^2 = \frac{1}{K^2} \sum_{n=0}^{B-1} \|\mathbf{y}(e^{j\omega_n}) - x^*(e^{-j\omega_n})\mathbf{h}\|^2. \quad (2.33)$$

Now let  $\rho \triangleq K/B$  and, for a signal  $z[k]$ , let  $z_d[k]$  denote the result of ideally<sup>4</sup> bandpass filtering  $z[k]$  to the interval  $[0, 2\pi/\rho]$  followed by a downsampling operation<sup>5</sup> by a factor  $\rho$  (see, e.g., [Vaidyanathan, 2003]). Then one has  $z(e^{j\omega}) = \rho \cdot z_d(e^{j\omega\rho})$  for  $\omega \in [0, 2\pi/\rho]$ , which means that (2.33) can be rewritten as

$$\frac{1}{K^2} \sum_{n=0}^{B-1} \|\mathbf{y}(e^{j\omega_n}) - \mathbf{r}(e^{j\omega_n})\|^2 = \frac{\rho^2}{K^2} \sum_{n=0}^{B-1} \|\mathbf{y}_d(e^{j\frac{2\pi n}{K}\rho}) - x_d^*(e^{-j\frac{2\pi n}{K}\rho})\mathbf{h}\|^2 \quad (2.34a)$$

$$= \frac{1}{B} \sum_{k=0}^{B-1} \|\mathbf{y}_d[k] - x_d^*[k]\mathbf{h}\|^2, \quad (2.34b)$$

where (2.34b) follows from Parseval's identity (note that the sequences  $\mathbf{y}_d[k]$ ,  $x_d[k]$  have length  $K/\rho = B$ ). By introducing

$$\hat{\mathbf{S}}_1^d \triangleq \frac{1}{B} (\mathbf{Y}_d - \mathbf{h}\mathbf{x}_d^H) (\mathbf{Y}_d - \mathbf{h}\mathbf{x}_d^H)^H \in \mathbb{C}^{M \times M}, \quad (2.35)$$

where

$$\mathbf{Y}_d \triangleq \begin{bmatrix} \mathbf{y}_d[0] & \mathbf{y}_d[1] & \cdots & \mathbf{y}_d[B-1] \end{bmatrix} \in \mathbb{C}^{M \times B}, \quad (2.36a)$$

$$\mathbf{x}_d \triangleq \begin{bmatrix} x_d[0] & x_d[1] & \cdots & x_d[B-1] \end{bmatrix}^T \in \mathbb{C}^B, \quad (2.36b)$$

<sup>4</sup>Note that some performance degradation may be expected in practice due to the usage of non-ideal filters.

<sup>5</sup>Note that if  $\rho$  is not an integer, a previous interpolation step may be required.

(2.34b) becomes

$$\frac{1}{K^2} \sum_{n=0}^{B-1} \|\mathbf{y}(e^{j\omega_n}) - \mathbf{r}(e^{j\omega_n})\|^2 = \text{Tr} \left( \hat{\mathbf{S}}_1^d(\mathbf{h}, \mathbf{x}_d) \right), \quad (2.37)$$

Because decimation preserves the CM property of a signal, the problem of minimizing (2.37) with respect to  $\mathbf{h}$  and  $\mathbf{x}_d$  subject to the CM constraint on  $\mathbf{x}_d$  is analogous to the problem found in Section 2.3.2. Therefore, the same approach can be applied, resulting in the following minimum value for (2.37):

$$\text{Tr} \left( \hat{\mathbf{S}}_1^d(\hat{\mathbf{h}}, \hat{\mathbf{x}}_d) \right) = \frac{1}{B} \left[ \text{Tr} (\mathbf{Y}_d \mathbf{Y}_d^H) - \frac{1}{B} \|\mathbf{Y}_d^H\|_{2,1}^2 \right]. \quad (2.38)$$

Substituting (2.38) back in (2.12) yields

$$\text{Tr} \left( \hat{\mathbf{S}}_1(\hat{\mathbf{R}}) \right) = \frac{1}{B} \left[ \text{Tr} (\mathbf{Y}_d \mathbf{Y}_d^H) - \frac{1}{B} \|\mathbf{Y}_d^H\|_{2,1}^2 \right] + \frac{1}{K} \text{Tr} (\mathbf{Y} \mathbf{Y}^H) - \frac{1}{K} \text{Tr} (\mathbf{Y}_f \mathbf{Y}_f^H),$$

where, recall,  $\mathbf{Y}_f$  is the filtered data matrix from (2.16a). Hence, the GLR statistic becomes

$$\mathcal{G}_{\text{CMBL}}(\mathbf{Y}) = \left[ \frac{\|\mathbf{Y}\|_F^2}{\rho \left( \|\mathbf{Y}_d\|_F^2 - \frac{1}{B} \|\mathbf{Y}_d^H\|_{2,1}^2 \right) + \|\mathbf{Y}\|_F^2 - \|\mathbf{Y}_f\|_F^2} \right]^{MK}. \quad (2.39)$$

The corresponding detector, which exploits the whole prior information about WM signals, will be referred to as the CM bandlimited detector (CMBL). It is expected to offer the best performance of all the detectors presented in this chapter, although this is at the expense of the highest computational complexity.

## 2.5 Remarks

### 2.5.1 Interpretation

All the detectors for bandlimited signals derived in previous sections have the same general form: all of them can be written as

$$\mathcal{G}(\mathbf{Y}) = \left[ \frac{\hat{\sigma}_{\text{tot}}^2}{\hat{\sigma}_{\text{in}}^2 + \hat{\sigma}_{\text{out}}^2} \right]^{MK}, \quad (2.40)$$

where  $\hat{\sigma}_{\text{tot}}^2 = \text{Tr}(\hat{\mathbf{S}}_0)$  is an estimate of the total power of the observations, whereas  $\hat{\sigma}_{\text{in}}^2$  and  $\hat{\sigma}_{\text{out}}^2$  are, respectively, estimates of the in-band and out-of-band *noise* powers.

An alternative form, which was already used in (2.18) and (2.24), follows from noting that an estimate of the in-band signal power can be obtained as  $\hat{\eta}_0^2 = \hat{\sigma}_{\text{tot}}^2 - (\hat{\sigma}_{\text{in}}^2 + \hat{\sigma}_{\text{out}}^2)$ . Thus (2.40) can be rewritten as  $\mathcal{G}(\mathbf{Y}) = [\sigma_{\text{tot}}^2 / (\hat{\sigma}_{\text{tot}}^2 - \hat{\eta}_0^2)]^{MK}$ , which is equivalent to the statistic  $\mathcal{T}(\mathbf{Y}) = \hat{\eta}_0^2 / \hat{\sigma}_{\text{tot}}^2$ . The proposed detectors are seen to use different estimates  $\hat{\eta}_0^2$ :

- The BL detector uses  $\hat{\eta}_0^2 = \text{Tr}(\hat{\mathbf{S}}_0^f)$ , i.e., all the in-band power is ascribed to the signal component. Consequently,  $\hat{\sigma}_{\text{in}}^2 = 0$ .
- The BLFF detector uses  $\hat{\eta}_0^2 = \lambda_1(\hat{\mathbf{S}}_0^f)$ , which is an (actually biased) estimator of the power in the principal eigenspace of the filtered covariance matrix. The prior information being exploited here is the rank-1 structure of the signal subspace.
- From the denominator in (2.39), it can be seen that the CMBL detector uses  $\hat{\eta}_0^2 = \|\mathbf{Y}_f\|_F^2 - \rho \|\mathbf{Y}_d\|_F^2 + \rho B^{-1} \|\mathbf{Y}_d^H\|_{2,1}^2$ . For large  $K$ , the energy of the downsampled sequence  $\mathbf{y}_d[k]$  relates to that of the filtered sequence  $\mathbf{y}_f[k]$  as  $\|\mathbf{Y}_d\|_F^2 \approx \frac{1}{\rho} \|\mathbf{Y}_f\|_F^2$  [Vaidyanathan, 2003], and therefore  $\hat{\eta}_0^2 \approx \rho B^{-1} \|\mathbf{Y}_d^H\|_{2,1}^2$ . This observation suggests the following modification of the statistic in (2.39):

$$\mathcal{G}_{\text{CMBL}}(\mathbf{Y}) \approx \left[ \frac{\|\mathbf{Y}\|_F^2}{\|\mathbf{Y}\|_F^2 - \frac{\rho}{B} \|\mathbf{Y}_d^H\|_{2,1}^2} \right]^{MK}, \quad (2.41)$$

which, for detection purposes, is equivalent to

$$\mathcal{T}_{\text{CMBL}}(\mathbf{Y}) \triangleq \frac{\|\mathbf{Y}_d^H\|_{2,1}^2}{\|\mathbf{Y}\|_F^2}. \quad (2.42)$$

Clearly, the statistic in (2.42) has a lower computational complexity than that in (2.39). Moreover, empirical results reveal that the modified CMBL test improves the detection performance with respect to that of the original formulation (2.39) and reduces the influence of the particular choice of the filters used for band selection and decimation. Note that (2.42) reduces to (2.32) when the BL assumption is dropped, since in that case one has  $\mathbf{Y}_d = \mathbf{Y}$ .

### 2.5.2 Dealing with an Unknown Carrier Frequency

In practice, the carrier frequency of the WM signal is not known. Similarly to detectors for WM signals [Chen and Gao, 2011], the GLR statistics for the BL and CMBL detectors need,

therefore, to be maximized with respect to this carrier frequency parameter  $\omega_c$  over the set  $\Omega_c$  of candidate values. From (2.9), the number of candidate carrier frequencies  $|\Omega_c|$  in a 6 MHz TV channel is 237. Since  $|\Omega_c|$  has a considerable impact on the computational complexity of some of the proposed detectors (see Section 2.5.3 below), it is convenient to devise a simplification.

In this respect, the above detectors present an important advantage over previous schemes in the literature, e.g. [Chen and Gao, 2011]: since the carrier frequency is not explicitly used by the detector, it is possible to divide the 6 MHz channel in a reduced number of overlapping intervals with bandwidth larger than 200 kHz. This operation reduces  $|\Omega_c|$  and increases the bandwidth  $\mathcal{B}$  of each segment, which allows a significant reduction in computational complexity at the expense of some degradation in performance. Interestingly, as will be seen in Section 2.7, the loss incurred by this approach is small provided that the number of subbands is large enough.

We also remark that some of the proposed detectors allow further simplifications when performing a series of evaluations for different central frequencies  $\omega_c \in \Omega_c$ . Consider first the BL statistic (2.18), for which one must compute

$$\text{Tr}(\hat{\mathbf{S}}_0^f) = \frac{1}{K^2} \sum_{n=0}^{K-1} G_{\omega_c}(e^{j\omega_n}) \|\mathbf{y}(e^{j\omega_n})\|^2 \quad (2.43)$$

for all  $\omega_c \in \Omega_c$ , where  $G_{\omega_c}(e^{j\omega_n})$  denotes the frequency response of a bandpass filter satisfying  $G_{\omega_c}(e^{j\omega_n}) = 1$  for the  $B$  bins centered at  $\omega_c$  and zero otherwise. Thus, it suffices to compute the DFT of the observations and then store the squared magnitudes  $\|\mathbf{y}(e^{j\omega_n})\|^2$ ; after that, only  $B - 1$  additions per candidate central frequency are required.

As for the BLFF statistic (2.24), it is seen that  $\lambda_1(\hat{\mathbf{S}}_0^f)$  must be computed for each  $\omega_c$ . Let  $\mathbf{F} \in \mathbb{C}^{K \times K}$  be the Fourier matrix, which means that  $\mathbf{c}^T \mathbf{F}$  is the DFT of the row vector  $\mathbf{c}^T$ . Note that  $\mathbf{F}^H \mathbf{F} = \mathbf{F} \mathbf{F}^H = K \mathbf{I}_K$ . Then, it is clear that  $\mathbf{Y}_f = \frac{1}{K} \tilde{\mathbf{Y}} \mathbf{G}_{\omega_c} \mathbf{F}^H$ , where  $\tilde{\mathbf{Y}} = \mathbf{Y} \mathbf{F}$  contains the DFT of the observations and  $\mathbf{G}_{\omega_c} \triangleq \text{diag}\{G_{\omega_c}[0], \dots, G_{\omega_c}[K-1]\}$ . Therefore  $\hat{\mathbf{S}}_0^f = \frac{1}{K} \mathbf{Y}_f \mathbf{Y}_f^H = \frac{1}{K^2} \tilde{\mathbf{Y}} \mathbf{G}_{\omega_c} \mathbf{G}_{\omega_c}^H \tilde{\mathbf{Y}}^H$ . Since  $\lambda_1(\hat{\mathbf{S}}_0^f) = \frac{1}{K^2} \lambda_1(\tilde{\mathbf{Y}} \mathbf{G}_{\omega_c} \mathbf{G}_{\omega_c}^H \tilde{\mathbf{Y}}^H) = \frac{1}{K^2} \lambda_1(\mathbf{G}_{\omega_c}^H \tilde{\mathbf{Y}}^H \tilde{\mathbf{Y}} \mathbf{G}_{\omega_c})$ , one can first compute the matrix  $\tilde{\mathbf{Y}}^H \tilde{\mathbf{Y}}$  and then, for each  $\omega_c \in \Omega_c$ , select the suitable rows and columns to evaluate the largest eigenvalue.

Finally, the CMBL statistic (2.42) requires the computation of  $\|\mathbf{Y}_d^H\|_{2,1}^2$  for each  $\omega_c \in \Omega_c$ . If  $\rho = K/B$  is an integer,<sup>6</sup> then  $\mathbf{Y}_d$  can be directly obtained as  $\mathbf{Y}_d = \mathbf{Y}_f \mathbf{\Gamma} = \frac{1}{K} \tilde{\mathbf{Y}} \mathbf{G}_{\omega_c} \mathbf{F}^H \mathbf{\Gamma}$ , where  $\mathbf{\Gamma} \in \mathbb{C}^{K \times B}$  is a decimation matrix containing the appropriate  $B$  columns of the  $K \times K$  identity matrix. If  $\rho$  is not an integer, but  $\rho = \rho_1/\rho_2$  with  $\rho_1, \rho_2$  coprime, then  $\mathbf{Y}_d$  can still be obtained from  $\mathbf{Y}_f$  by first upsampling by a factor  $\rho_2$ , followed by appropriate bandpass filtering and finally downsampling by a factor  $\rho_1$ . Once  $\mathbf{Y}_d$  is obtained, the computation of  $\|\mathbf{Y}_d^H\|_{2,1}^2$

<sup>6</sup>This is the typical case, since for WMs in 6 MHz bands, this factor is  $\rho = 6 \text{ MHz}/200 \text{ kHz} = 30$ .

can be addressed as shown in Appendix 2.A.

### 2.5.3 Computational Complexity

According to what was explained in Section 2.5.2, the BL detector requires the computation of  $\|\mathbf{y}(e^{j\omega_n})\|^2$  for  $n = 0, \dots, K-1$ . This requires  $M$  fast Fourier transforms (FFTs), with complexity  $O(MK \log K)$ , and the computation of  $K$  squared magnitudes of vectors in  $\mathbb{C}^M$ , which is  $O(MK)$ . After that, just a few additions are needed, which means that the complexity of the BL detector is  $O(MK \log K)$ .

Besides the  $M$  FFTs, the BLFF detector requires the computation of  $\tilde{\mathbf{Y}}^H \tilde{\mathbf{Y}}$ , which is  $O(MK^2)$ . Then a total of  $|\Omega_c|$  eigenvalues must be computed, for example using the standard power method with  $I$  iterations, resulting in a complexity of  $O(I|\Omega_c|B^2)$ . We therefore conclude that the BLFF detector has complexity  $O(\max(I|\Omega_c|B^2, MK^2))$ , which is higher than the complexity of the BL detector.

As for the CM detector, its complexity is dominated by that of the computation of  $\|\mathbf{Y}^H\|_{2,1}$ . Using the algorithm proposed in Appendix 2.A with  $I$  iterations, it can be seen that this operation is  $O(IM^2K)$ .

The number of operations required by the CMBL detector is the largest one since the computations must be performed in the time domain. This means that one FFT and  $|\Omega_c|$  inverse FFTs (IFFTs) are required, resulting in a complexity of  $O(|\Omega_c|MK \log K)$ . The execution of the power method requires, in this case,  $O(|\Omega_c|IM^2K/B)$  operations, whereas further computations may require up to  $O(M^2K)$ . Therefore, the complexity of the CMBL detector is  $O(|\Omega_c|MK \log K)$ .

## 2.6 Performance Analysis

Characterizing the detection performance of the schemes introduced in this chapter is of paramount importance. This section considers those cases where analytic evaluation is possible. For more involved scenarios, we resort to Monte Carlo simulations, as described in Section 2.7.

### 2.6.1 BL Detector

The exact distribution of the BL detector (2.18) when  $|\Omega_c| = 1$  can be obtained as follows. Note from (2.43) that the BL statistic can be rewritten as

$$\mathcal{T}_{\text{BL}}(\mathbf{Y}) = \frac{\sum_{n=0}^{K-1} G(e^{j\omega_n}) \|\mathbf{y}(e^{j\omega_n})\|^2}{\sum_{n=0}^{K-1} G(e^{j\omega_n}) \|\mathbf{y}(e^{j\omega_n})\|^2 + \sum_{n=0}^{K-1} (1 - G(e^{j\omega_n})) \|\mathbf{y}(e^{j\omega_n})\|^2},$$

where again  $G(e^{j\omega_n}) = 1$  if the  $n$ -th bin is within the passband and zero otherwise. Hence, an equivalent statistic is given by

$$\mathcal{T}'_{\text{BL}}(\mathbf{Y}) = \frac{\sum_{n=0}^{K-1} G(e^{j\omega_n}) \|\mathbf{y}(e^{j\omega_n})\|^2}{\sum_{n=0}^{K-1} (1 - G(e^{j\omega_n})) \|\mathbf{y}(e^{j\omega_n})\|^2} \quad (2.44a)$$

$$= \frac{\sum_{n=0}^{B-1} \|\mathbf{y}(e^{j\omega_n})\|^2}{\sum_{n=B}^{K-1} \|\mathbf{y}(e^{j\omega_n})\|^2}, \quad (2.44b)$$

where in (2.44b) it has been assumed, without any loss of generality, that the passband comprises the bins with indices  $n = 0, 1, \dots, B-1$ .

Let  $\mathbf{w}[k]$  denote the  $k$ -th column of the noise matrix  $\mathbf{W}$  and let

$$\mathbf{w}(e^{j\omega_n}) \triangleq \sum_{k=0}^{K-1} \mathbf{w}[k] e^{-j\omega_n k}.$$

Then, (2.44b) can be rewritten as

$$\mathcal{T}'_{\text{BL}}(\mathbf{Y}) = \frac{\sum_{n=0}^{B-1} \|\mathbf{r}(e^{j\omega_n}) + \mathbf{w}(e^{j\omega_n})\|^2}{\sum_{n=B}^{K-1} \|\mathbf{w}(e^{j\omega_n})\|^2}, \quad (2.45)$$

since  $\mathbf{r}(e^{j\omega_n}) = \mathbf{0}$  for  $n \geq B$ . The distribution of (2.45) follows by noting that  $\mathbf{r}(e^{j\omega_n})$  is deterministic whereas  $\mathbf{w}(e^{j\omega_n})$  is Gaussian. Hence, the numerator is a scaled non-central  $\chi^2$  random variable, whereas the denominator is central  $\chi^2$ . Thus,  $\frac{K-B}{B} \mathcal{T}'_{\text{BL}}(\mathbf{Y})$  is a non-central F-distributed random variable with non-centrality parameter  $\lambda = \frac{2}{K\sigma^2} \sum_n \|\mathbf{r}(e^{j\omega_n})\|^2 = \frac{2}{\sigma^2} \text{Tr}(\mathbf{R}\mathbf{R}^H)$  and degrees of freedom  $n_1 = 2MB$  and  $n_2 = 2M(K-B)$ . Clearly, one has that  $\lambda = 0$  under  $\mathcal{H}_0$  and  $\lambda > 0$  under  $\mathcal{H}_1$ .

Therefore, if  $F_{\lambda, n_1, n_2}$  denotes the cumulative distribution function corresponding to the F-distribution, it is clear that, once a threshold  $\nu'$  is fixed for the test

$$\frac{K-B}{B} \mathcal{T}'_{\text{BL}}(\mathbf{Y}) \underset{\mathcal{H}_0}{\overset{\mathcal{H}_1}{\gtrless}} \nu', \quad (2.46)$$



the probability of false alarm will be given by  $P_{\text{FA}} = 1 - F_{0,n_1,n_2}(\nu')$  whereas the probability of detection will be  $P_{\text{D}} = 1 - F_{\lambda,n_1,n_2}(\nu')$ . Combining both expressions gives the ROC:

$$P_{\text{D}} = 1 - F_{\lambda,n_1,n_2}(F_{0,n_1,n_2}^{-1}(1 - P_{\text{FA}})) \quad (2.47)$$

These expressions provide a complete characterization of the performance of the BL detector and allow to set the threshold  $\nu'$  in order to attain any target  $P_{\text{FA}}$  or  $P_{\text{D}}$ .

### 2.6.2 BLFF Detector

The evaluation of the distribution of the BLFF statistic turns out to be considerably more involved. Under  $\mathcal{H}_0$ , one can asymptotically approximate  $\text{Tr}(\hat{\mathbf{S}}_0) \approx M\sigma^2$  for large  $K$  [Taherpour et al., 2010], which means that (2.24) becomes

$$\mathcal{T}_{\text{BLFF}}(\mathbf{Y}) \approx \frac{\lambda_1(\mathbf{Y}_f \mathbf{Y}_f^H)}{MK\sigma^2} = \frac{\lambda_1(\mathbf{Y}_f^H \mathbf{Y}_f)}{MK\sigma^2}. \quad (2.48)$$

This test can thus be equivalently defined as the one deciding  $\mathcal{H}_1$  when

$$MK^2 \cdot \mathcal{T}_{\text{BLFF}}(\mathbf{Y}) = \frac{K}{\sigma^2} \lambda_1(\mathbf{Y}_f^H \mathbf{Y}_f) > \nu', \quad (2.49)$$

for some threshold  $\nu'$ . In order to compute the probability of false alarm, we note that under  $\mathcal{H}_0$  the observations  $\mathbf{Y}_f$  are the result of filtering white noise with a bandpass filter of bandwidth  $\mathcal{B}$ . Using the notation introduced in Section 2.5.2, this means that  $\mathbf{Y}_f^H = \frac{1}{K} \mathbf{F} \mathbf{G}_{\omega_c} \mathbf{F}^H \mathbf{W}^H$  under  $\mathcal{H}_0$ . Therefore, the columns of  $\mathbf{Y}_f^H$  are independent Gaussian random vectors with zero mean and covariance matrix  $\frac{\sigma^2}{K^2} \mathbf{F} \mathbf{G}_{\omega_c} \mathbf{F}^H$ , and the product  $\mathbf{Y}_f^H \mathbf{Y}_f$  follows a complex central Wishart distribution with  $M$  degrees of freedom:

$$\frac{K^2}{\sigma^2} \mathbf{Y}_f^H \mathbf{Y}_f \sim \mathcal{CW}(\mathbf{F} \mathbf{G}_{\omega_c} \mathbf{F}^H, M). \quad (2.50)$$

The density of the largest eigenvalue of this matrix is given by [Zanella et al., 2009, expression (41)], where we must note that the scale matrix  $\mathbf{F} \mathbf{G}_{\omega_c} \mathbf{F}^H$  in (2.50) has two eigenvalues: 1 with multiplicity  $B$ , and 0 with multiplicity  $K - B$ . If  $f_{\text{BLFF}}$  denotes such density, the probability of false alarm is given by

$$P_{\text{FA}} = 1 - \int_0^{\nu'} f_{\text{BLFF}}(t) dt \quad (2.51)$$

which enables us to set the threshold  $\nu'$  for a prescribed  $P_{\text{FA}}$ .

The computation of the probability of detection involves finding the distribution of the largest eigenvalue of the matrix  $\mathbf{Y}_f^H \mathbf{Y}_f$ , which is non-central Wishart distributed under  $\mathcal{H}_1$ . To the best of our knowledge, no simple method is known to compute the marginal density of the largest eigenvalue of a non-central correlated complex Wishart matrix where the eigenvalues of the scale matrix have multiplicity greater than one (see [Couillet and Debbah, 2011, Sec. 2.1] and references therein, also [Zanella et al., 2009]). It is therefore more convenient to assess the performance via Monte Carlo simulation, as described in Section 2.6.3.

### 2.6.3 CM and CMBL Detectors

From (2.32), (2.39) and (2.42), we see that the detectors exploiting the CM property rely on the (2,1)-subordinate matrix norm of a correlated Gaussian matrix. To the best of our knowledge, the distribution of this norm remains an open problem in statistics/random matrix theory, which means that the threshold of these detectors cannot be determined analytically. However, due to their invariance to scalings, the distributions of the corresponding statistics under  $\mathcal{H}_0$  are independent of the noise power and, consequently, the threshold required to obtain some target  $P_{FA}$  can be computed off-line using Monte Carlo simulation.

## 2.7 Simulation Results

Among the detection schemes proposed in the literature, only the statistical performance of a few of them has been exactly characterized in terms of analytical expressions. Most of them have been analyzed either approximately, asymptotically, or even heuristically. Notable exceptions include the energy detector [Kay, 1998] and, in this chapter, the BL detector. This means that comparisons between different schemes should not be carried out in terms of analytical expressions; instead we must rely on Monte Carlo simulation. In this section, we analyze the performance of the proposed and existing schemes in the context of WM signal detection, following the guidelines of the IEEE 802.22 Working Group [Clanton et al., 2007].

### 2.7.1 Simulation Setting

The guidelines in [Clanton et al., 2007] consider six simulation scenarios, termed *test vectors*, which are summarized in Table 2.1. The frequency-modulated analog WM signal  $x^*(t)$ , gener-

#	Description	$f_{\text{mod}}$	$\Delta f$	Fading
1	Outdoor, LOS, Silent	32	5	No
2	Outdoor, LOS, Soft Speaker	3.9	15	No
3	Outdoor, LOS, Loud Speaker	13.4	32.6	No
4	Indoor, NLOS, Silent	32	5	Yes
5	Indoor, NLOS, Soft Speaker	3.9	15	Yes
6	Indoor, NLOS, Loud Speaker	13.4	32.6	Yes

Table 2.1: Test vectors employed in WM simulation [Clanton et al., 2007]. Frequency units are kHz in all cases.

ated according to

$$x^*(t) = \exp \left\{ j \left( 2\pi f_c t + \frac{\Delta f}{f_{\text{mod}}} \sin(2\pi f_{\text{mod}} t) \right) \right\},$$

where  $\Delta f$  is the frequency deviation and  $f_{\text{mod}}$  is the modulating frequency, is then sampled at rate  $f_s = 6$  MHz unless otherwise stated. Channels are frequency-flat in all cases; with line-of-sight (LOS) propagation for vectors 1-3 and non-line-of-sight (NLOS) propagation for vectors 4-6.

Since [Clanton et al., 2007] just considers single-antenna sensors, we generalize those guidelines to multi-antenna settings. For LOS channels we assume a uniform linear array (ULA) with half-wavelength spacing:  $\mathbf{h} = \alpha^{1/2} \cdot [1, e^{j\psi}, e^{j2\psi}, \dots, e^{j(M-1)\psi}]^T$ , where  $\psi \sim \mathcal{U}(0, \pi)$  is a random phase and  $\alpha$  the power of the signal term. For NLOS scenarios, Rayleigh fading is implemented with  $\mathbf{h} \sim \mathcal{CN}(\mathbf{0}, \alpha \mathbf{I})$ . The SNR (per antenna) is defined as

$$\gamma \triangleq \frac{\mathbb{E} \{ |h_m|^2 \}}{\mathbb{E} \{ |w_m[k]|^2 \}} = \frac{\alpha}{\sigma^2}. \quad (2.52)$$

We consider SNR values around  $-20$  dB, which corresponds to a highly demanding scenario for WM detection (see e.g., [Cabric, 2008, Zeng and Liang, 2009a]). Under these conditions, simulations reveal that the proposed BL, BLFF and CMBL detectors necessitate sensing times in the order of a fraction of millisecond — depending on several factors such as the number of antennas — in order to satisfy typical performance requirements in 6 MHz channels.

In Section 2.7.2, we compare the proposed detectors with a representative part of the competing schemes. Our results show the advantages of simultaneously exploiting the WM signal features along with the spatial structure. In Section 2.7.3, we then focus on the novel detectors, illustrating their performance in a wide variety of scenarios.

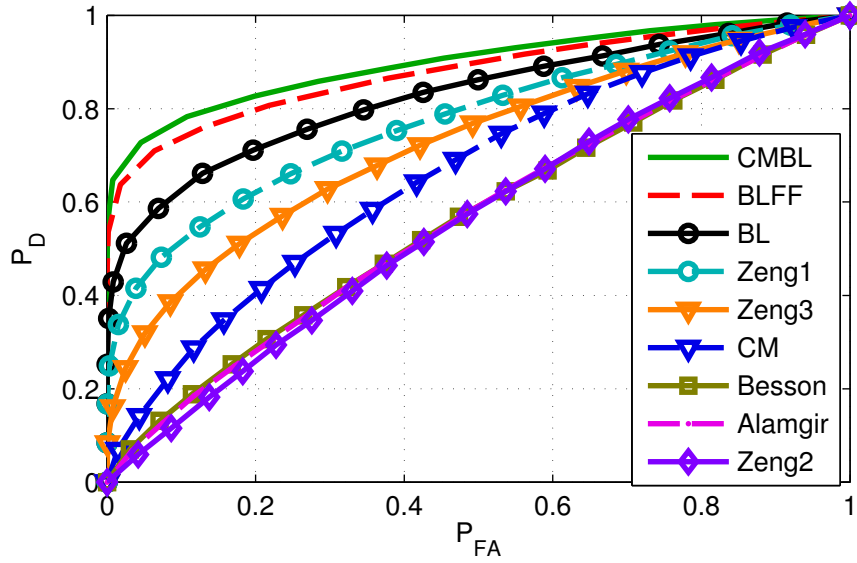


Figure 2.1: Comparison of the proposed schemes (CMBL, BLFF, BL and CM) with competing multiantenna detectors. (Test vector 5,  $K = 1024$ ,  $B = 200$  kHz,  $f_s = 6$  MHz, Rayleigh Channel,  $\gamma = -20$  dB,  $M = 4$ ).

### 2.7.2 Comparison with Existing Detectors

We consider sensors with  $M = 4$  antennas that gather  $K = 1024$  samples per antenna (corresponding to an observation time of 0.17 ms) in a setting defined by Test Vector 5. The central frequency is randomly generated with a uniform distribution over  $\Omega_c$ , which contains the 237 frequencies where a WM may transmit. Figure 2.1 shows the ROC of the proposed detectors along with the sphericity detector (Alamgir *et al.* [Alamgir et al., 2008]), the detector from [Besson et al., 2006, Taherpour et al., 2010, Wang et al., 2010] (labeled as Besson), and three detectors by Zeng *et al.*: Zeng 1 [Zeng and Liang, 2009a, Algorithm 1], Zeng 2 [Zeng and Liang, 2009a, Algorithm 2] and Zeng 3 [Zeng and Liang, 2009b]. Although the last three detectors are considered in the IEEE 802.22 standard for the problem at hand, only Zeng 3 is specifically tailored for detecting WM signals<sup>7</sup> [IEEE, 2011].

We recall that, for a given  $P_{FA}$ , detector A is said to *perform better* than detector B in a given setting if  $P_D$  is higher for detector A than for detector B. In Figure 2.1 it is seen that the three proposed multiantenna WM detectors that exploit the bandwidth information (BL, BLFF and CMBL) outperform all of the previous detectors in the literature. On the other hand,

<sup>7</sup>Note that, although the detectors by Zeng *et al.* were proposed in the IEEE 802.22 standard for single-antenna detection, we are considering the multiantenna extensions given by the authors. This, together with the fact that these detectors stem from heuristic considerations, explains why in the multiantenna scenario of Figure 2.1, Zeng 3 performs worse than Zeng 1.

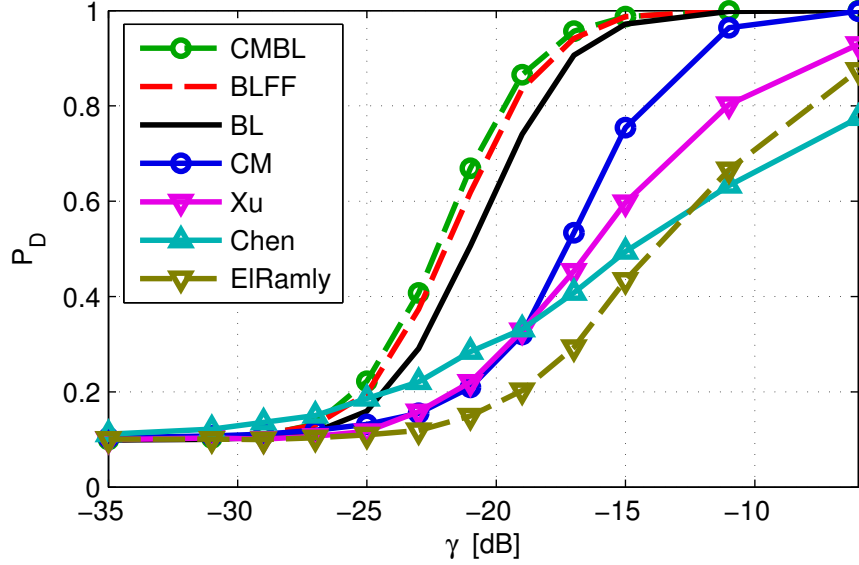


Figure 2.2: Comparison of the proposed techniques (CMBL, BLFF, BL and CM) with competing WM detectors. (Test Vector 5,  $K = 1024$ ,  $\mathcal{B} = 200$  kHz,  $f_s = 6$  MHz, Rayleigh Channel,  $M = 4$ ,  $P_{FA} = 0.1$ ).

the CM detector is outperformed by Zeng 1 and Zeng 3, which rely on space-time correlation. This shows that temporal correlation is more important than the CM property for WM signal detection.

We next compare the proposed detectors with existing single-antenna WM detectors. Figure 2.2 depicts the probability of detection *vs.* SNR when the thresholds are adjusted to obtain  $P_{FA} = 0.1$  with all detectors. The proposed schemes are considered along with the detector by Xu *et al.* [Xu et al., 2008], the detector by ElRamly *et al.* [ElRamly et al., 2011] and the one by Chen *et al.* [Chen and Gao, 2011]. The advantages of using multiple antennas are clear: not only is the  $P_D$  of the multiantenna detectors better, but also the *rate* at which  $P_D$  increases.<sup>8</sup> Among the four detectors proposed, the performance of the CM detector shows a significant gap with respect to the other three. This effect will be further analyzed in Section 2.7.3.

### 2.7.3 Performance of the Proposed Detectors

In order to independently illustrate the impact of each parameter on the detection performance, we vary a single parameter at a time while fixing the others to keep the setting as simple as possible. In particular, we start assuming that  $\Omega_c = \{2\pi f_c/f_s\}$ , i.e., the only candidate frequency is the carrier frequency. Later, we consider the influence of the cardinality of this set and the

<sup>8</sup>This is related to the notion of *diversity* in multiantenna communications [Vázquez-Vilar et al., 2011a].

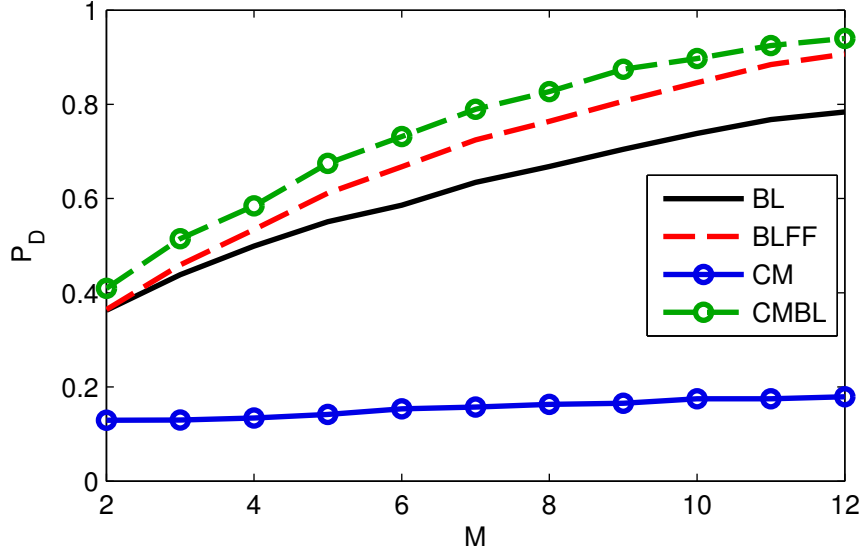


Figure 2.3: Influence of the number of antennas in the probability of detection ( $K = 1024$ ,  $\mathcal{B} = 200$  kHz,  $f_s = 6$  MHz, Test Vector 5, Rayleigh Channel,  $\gamma = -24$  dB,  $P_{FA} = 0.1$ ).

technique explained at the beginning of Section 2.5.2. Figure 2.3 shows the influence of the number of antennas  $M$  on the probability of detection for fixed  $P_{FA} = 0.1$  and  $\gamma = -24$  dB. With the exception of the CM detector, the proposed schemes exhibit a significant improvement as  $M$  becomes larger, thus showing that in this setting the BL property is more useful for detection purposes than the CM property. This effect can be ascribed to the small *fractional bandwidth* of the WM signal ( $200 \text{ kHz}/6 \text{ MHz} = 1/30$ ). With larger fractional bandwidths, the advantage of the BL property over the CM property diminishes. This is illustrated in Figure 2.4, where the probability of detection is depicted *vs.* the sampling frequency in the range  $200 \text{ kHz} \leq f_s \leq 2 \text{ MHz}$  for  $P_{FA} = 0.1$ . With fixed WM signal bandwidth ( $b = 200 \text{ kHz}$ ), the net effect is the variation of the fractional bandwidth  $b/f_s$ . In the extreme case where  $f_s = 200 \text{ kHz}$  the sampled signal ceases to be bandlimited, and it is observed that the detectors exploiting the CM property show a better  $P_D$  than those which do not. In fact, the BL detector is unable to detect the signal at all since the only property it exploits is absent in the signal. The performance of the BLFF at this point is slightly better since it exploits the spatial correlation. As the sampling rate is increased, the fractional bandwidth of the signal decreases, and thus the BL property becomes more relevant. Note that the performance of the CM detector is not affected by the fractional bandwidth, as could be expected. In addition, the  $P_D$  of the BLFF and CMBL detectors approach each other for sufficiently small fractional bandwidths; in particular, for  $f_s = 30 \cdot 200 \text{ kHz} = 6 \text{ MHz}$ , the performance of both schemes is similar, although the computational cost of the former is considerably lower.

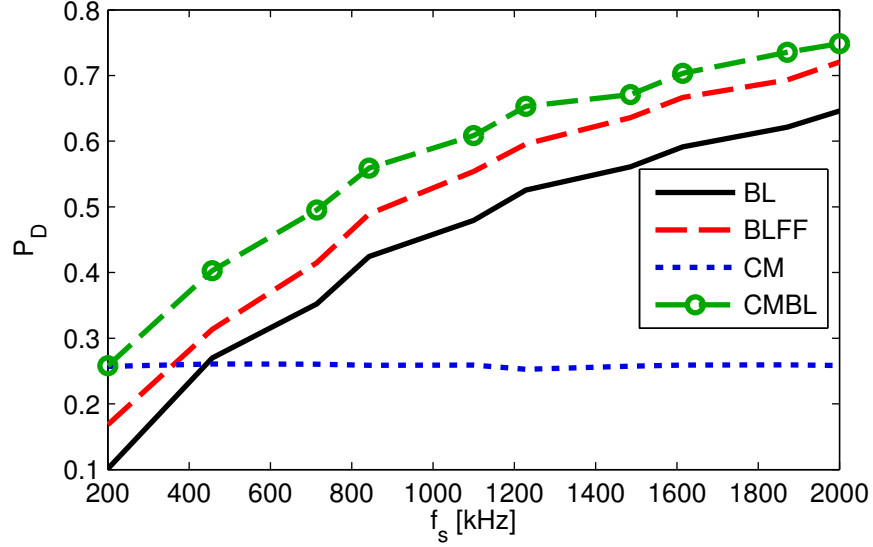


Figure 2.4: Probability of detection *vs.* sampling frequency, which is inversely proportional to the fraction of bandwidth occupied by the WM signal ( $K = 1024$ ,  $\mathcal{B} = 200$  kHz,  $f_s = 200$  kHz, Test Vector 5, Rayleigh Channel,  $\gamma = -20$  dB,  $M = 4$ ,  $P_{FA} = 0.1$ ).

Next we complete the performance evaluation in terms of the simulation scenarios of Table 2.1. Figure 2.5 shows the ROC curves corresponding to the six test vectors for the BLFF detector when  $\gamma = -22$  dB and the number of antennas is  $M = 4$ . It is observed that the probability of detection does not meaningfully depend on the parameters of the WM signal (modulating frequency and frequency deviation). It is the channel model which essentially determines the performance of the detector to a larger extent. This agrees with intuition, since detecting a signal in the presence of an LOS component should be easier than when operating in NLOS conditions. Although not shown for brevity, a similar behavior is observed for the BL, CM, and CMBL detectors.

To close this section we analyze the tradeoff discussed in Section 2.5.2 by considering multiple candidate carrier frequency values, *i.e.*,  $|\Omega_c| > 1$ . As pointed out, it is not strictly necessary to scan the 237 central frequencies using the theoretical bandwidth of 200 kHz. Instead, we can reduce the number of candidate frequency intervals by increasing their width. In the experiment reported in Figure 2.6, this approach is followed by dividing the 6 MHz channel into  $|\Omega_c|$  intervals. Specifically, for  $|\Omega_c| = n$  intervals, we consider the following candidate carrier frequency set and bandwidth:

$$\Omega_c^{(n)} = \left\{ \frac{2\pi}{n}k, \quad k = 0, 1, \dots, n-1 \right\}, \quad \mathcal{B}^{(n)} = \frac{2\pi}{n}. \quad (2.53)$$

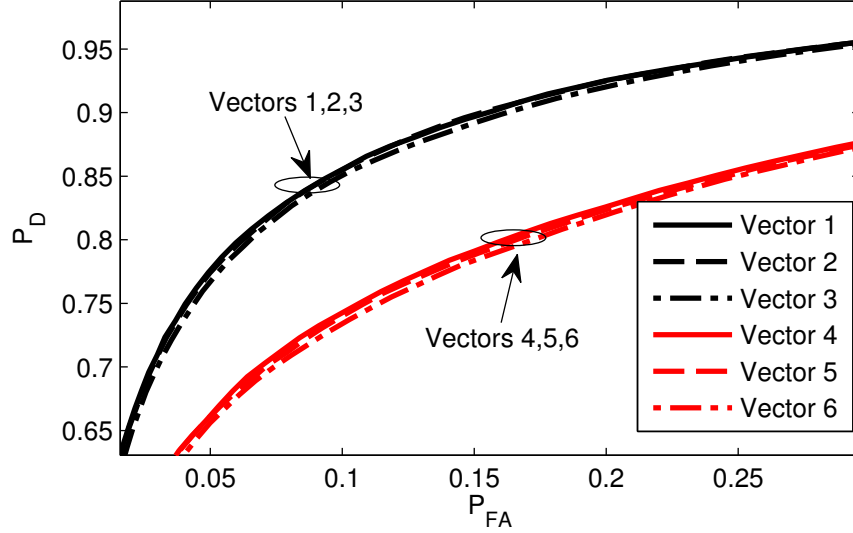


Figure 2.5: ROC of the BLFF detector for the different test vectors ( $K = 1024$ ,  $\mathcal{B} = 200$  kHz,  $f_s = 6$  MHz,  $\gamma = -22$  dB,  $M = 4$ ).

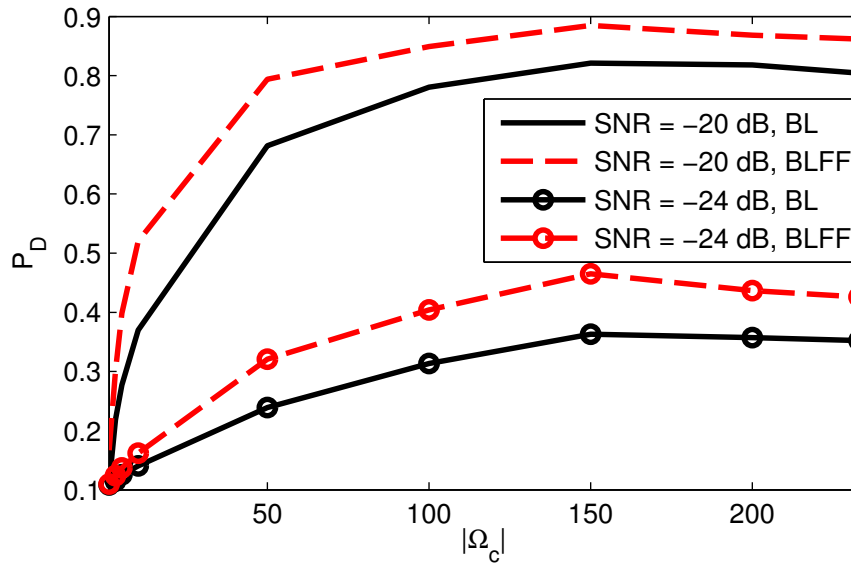


Figure 2.6: Probability of detection *vs.* the number of candidate carrier frequencies ( $K = 1024$ ,  $\mathcal{B} = 200$  kHz,  $f_s = 6$  MHz, Test Vector 5, Rayleigh Channel,  $M = 4$ ,  $P_{FA} = 0.1$ ).



When the WM signal is present, its carrier frequency is set to  $f_c = 0$ . It is observed in Figure 2.6 that the probability of detection stabilizes when  $|\Omega_c|$  is large enough. This observation allows computational savings at a small performance loss, since the complexity of some of the proposed schemes increases linearly with the number of candidate frequency intervals. Of course, other choices for  $\Omega_c^{(n)}$  and  $\mathcal{B}^{(n)}$  different from (2.53) may be preferable in practice depending on the desired tradeoff. It is also observed that the probability of detection slightly decreases after  $|\Omega_c|$  is about 150. This may be explained with the following argument: since the number of candidate frequencies is too high, the probability that the actual frequency is erroneously estimated becomes larger.

## 2.8 Conclusions

The protection of WM communications is a requirement imposed by the FCC for emerging DSA systems in the TV band. Whereas no previous WM detector considers the use of multiple antennas, none of the multiantenna detectors in the literature has been specifically designed for WM signals. In order to fill this gap we have developed four GLR-based multiantenna detectors which exploit a number signal features. The computational load of these detectors increases with the amount of WM signal structure that they exploit, and therefore they offer different tradeoffs between performance and complexity.

The proposed schemes do not require synchronization with the potentially present WM signal, and are robust to the noise uncertainty problem as well as to small-scale fading due to the use of multiple antennas. Moreover, they do not require information that is not available in practice, such as the channel coefficients, the transmitted signal, or the noise power. The detection performance was characterized analytically and using Monte Carlo simulations, where we observed that the proposed schemes are well behaved and outperform previous detectors, in particular those proposed in the IEEE 802.22 standard for WM detection.

The work in this chapter has been published on the IEEE Transactions on Vehicular Technology [Romero and López-Valcarce, 2014b] and presented in part in the *12th IEEE International Workshop on Signal Processing Advances in Wireless Communications (SPAWC 2011)* [Romero and López-Valcarce, 2011b] and in the *4th IEEE International Workshop on Computational Advances in Multi-Sensor Adaptive Processing (CAMSAP 2011)* [Romero and López-Valcarce, 2011a].

## 2.A Computation of the (2,1)-norm

Consider the constrained maximization problem (2.29). The cost can be written explicitly as

$$\begin{aligned} J(\tilde{\mathbf{h}}) = \|\mathbf{Y}^H \tilde{\mathbf{h}}\|_1 &= \sum_{k=0}^{K-1} |\mathbf{y}^H[k] \tilde{\mathbf{h}}| \\ &= \sum_{k=0}^{K-1} \sqrt{\tilde{\mathbf{h}}^H \mathbf{y}[k] \mathbf{y}^H[k] \tilde{\mathbf{h}}}. \end{aligned} \quad (2.54)$$

One must maximize (2.54) subject to  $\tilde{\mathbf{h}}^H \tilde{\mathbf{h}} = 1$ . Let us decompose  $\tilde{\mathbf{h}}$  in its real and imaginary parts as

$$\tilde{\mathbf{h}} = \tilde{\mathbf{h}}_R + j\tilde{\mathbf{h}}_I \quad (2.55)$$

and let us define the complex gradient  $\nabla_{\tilde{\mathbf{h}}}$  as

$$\nabla_{\tilde{\mathbf{h}}} = \nabla_{\tilde{\mathbf{h}}_R} + j\nabla_{\tilde{\mathbf{h}}_I}. \quad (2.56)$$

The corresponding Lagrangian is

$$\Lambda(\tilde{\mathbf{h}}, \lambda) \triangleq J(\tilde{\mathbf{h}}) - \frac{\lambda}{2}(\tilde{\mathbf{h}}^H \tilde{\mathbf{h}} - 1), \quad (2.57)$$

where  $\lambda$  is the Lagrange multiplier. Note that the gradient of the constraint is  $2\tilde{\mathbf{h}}$ , which does not vanish on the unit sphere  $\|\tilde{\mathbf{h}}\|_2 = 1$ . It follows that all feasible points are regular, and any local extremum of the constrained problem must satisfy the first-order necessary conditions  $\nabla_{\tilde{\mathbf{h}}} \Lambda(\tilde{\mathbf{h}}, \lambda) = 0$ ,  $\nabla_{\lambda} \Lambda(\tilde{\mathbf{h}}, \lambda) = 0$ , which are readily seen to yield  $\nabla_{\tilde{\mathbf{h}}} J(\tilde{\mathbf{h}}) = \lambda \tilde{\mathbf{h}}$ ,  $\tilde{\mathbf{h}}^H \tilde{\mathbf{h}} = 1$ . The gradient of  $J$  is given by

$$\nabla_{\tilde{\mathbf{h}}} J(\tilde{\mathbf{h}}) = \sum_{k=0}^{K-1} \frac{\mathbf{y}[k] \mathbf{y}^H[k]}{|\mathbf{y}^H[k] \tilde{\mathbf{h}}|} \tilde{\mathbf{h}} = \mathbf{C}(\tilde{\mathbf{h}}) \cdot \tilde{\mathbf{h}}, \quad (2.58)$$

where we have introduced the  $M \times M$  matrix

$$\mathbf{C}(\tilde{\mathbf{h}}) \triangleq \sum_{k=0}^{K-1} \frac{\mathbf{y}[k] \mathbf{y}^H[k]}{|\mathbf{y}^H[k] \tilde{\mathbf{h}}|} = \mathbf{Y} \mathbf{D}^{-1}(\tilde{\mathbf{h}}) \mathbf{Y}^H, \quad (2.59)$$

with  $\mathbf{D}(\tilde{\mathbf{h}}) \triangleq \text{diag} \{ |\mathbf{y}^H[0]\tilde{\mathbf{h}}|, \dots, |\mathbf{y}^H[K-1]\tilde{\mathbf{h}}| \}$ . Note that  $\mathbf{C}(\tilde{\mathbf{h}})$  is positive (semi)definite, and that the cost (2.54) can be written as  $J(\tilde{\mathbf{h}}) = \tilde{\mathbf{h}}^H \mathbf{C}(\tilde{\mathbf{h}}) \tilde{\mathbf{h}}$ .

The first-order necessary conditions then read as

$$\mathbf{C}(\tilde{\mathbf{h}})\tilde{\mathbf{h}} = \lambda\tilde{\mathbf{h}}, \quad \tilde{\mathbf{h}}^H \tilde{\mathbf{h}} = 1. \quad (2.60)$$

Thus we see that at any extremum of the constrained problem,  $\tilde{\mathbf{h}}$  must be a unit-norm eigenvector of  $\mathbf{C}(\tilde{\mathbf{h}})$ . The corresponding eigenvalue is the attained cost, i.e.  $J(\tilde{\mathbf{h}}) = \tilde{\mathbf{h}}^H \mathbf{C}(\tilde{\mathbf{h}}) \tilde{\mathbf{h}} = \lambda$ . These conditions do not reveal whether  $\lambda$  corresponds to the largest, smallest, or an intermediate eigenvalue of  $\mathbf{C}(\tilde{\mathbf{h}})$ . However, by examining the high SNR case, for which  $\mathbf{Y} \approx \mathbf{h}\mathbf{x}^H(\varphi)$ , one sees that  $\mathbf{C}(\tilde{\mathbf{h}}) = \mathbf{Y}\mathbf{D}^{-1}(\tilde{\mathbf{h}})\mathbf{Y}^H \approx [\mathbf{x}^H(\varphi)\mathbf{D}^{-1}(\tilde{\mathbf{h}})\mathbf{x}(\varphi)]\mathbf{h}\mathbf{h}^H$ , i.e. a rank-1 matrix, whose eigenvector associated to the largest eigenvalue is the true channel vector  $\mathbf{h}$  (independently of  $\tilde{\mathbf{h}}$ ). Therefore, it makes sense to consider numerical methods for the computation of the principal eigenvector of a matrix, and then update the matrix at each iteration by using the eigenvector estimate from the previous step. For example, the standard power method [Golub and Van Loan, 1996] can be suitably modified in this manner, see Algorithm 2.1.

A reasonable initializer for any numerical method of this kind is the eigenvector associated with the largest eigenvalue of  $\mathbf{Y}\mathbf{Y}^H$ , since this is the solution to (2.29) if we relax the  $\ell^1$ -norm to the  $\ell^2$ -norm in the cost function. In addition, since all elements of  $\mathbf{x}(\varphi)$  have unit magnitude, in the high SNR regime one has  $\mathbf{D}(\tilde{\mathbf{h}}) \approx |\mathbf{h}^H \tilde{\mathbf{h}}| \mathbf{I}_K$ , which means that  $\mathbf{C}(\tilde{\mathbf{h}}) \approx \frac{1}{|\mathbf{h}^H \tilde{\mathbf{h}}|} \mathbf{Y}\mathbf{Y}^H$ , and thus the eigenvectors of  $\mathbf{C}(\tilde{\mathbf{h}})$  and  $\mathbf{Y}\mathbf{Y}^H$  should lie close to each other.

---

**Algorithm 2.1** Modified Power Method

---

```

Set  $\tilde{\mathbf{h}}_0$  = principal eigenvector of  $\mathbf{Y}\mathbf{Y}^H$ 
for  $i = 1$  to  $I$  do
     $\mathbf{v}_i = \mathbf{C}(\tilde{\mathbf{h}}_{i-1})\tilde{\mathbf{h}}_{i-1}$ 
     $\tilde{\mathbf{h}}_i = \frac{\mathbf{v}_i}{\|\mathbf{v}_i\|}$ 
end for
Set  $\hat{\mathbf{h}} = \tilde{\mathbf{h}}_I$ 

```

---



## Chapter 3

# Detection of Constant Magnitude Signals in Time-Varying Channels

This chapter addresses the problem of deciding on the presence of a CM waveform in noise of unknown variance when the propagation channel introduces time-varying frequency-flat Rayleigh fading. Relying on a BEM, we exploit the fact that the Doppler spectrum of the channel is typically low pass [Tsatsanis and Giannakis, 1996a, Giannakis and Tepedelenlioğlu, 1998].

We first consider activity detection in the case where the transmitted sequence is known, which arises, for example, if the primary user transmits a pilot sequence. The resulting GLR test generalizes the well-known matched filter detector to time-varying scenarios [Kay, 1998, Cabric, 2008]. We then focus on the case of unknown transmitted signals, where the GLR requires the solution of a difficult non-convex problem. We present one numerical method and various approximations with different performance/complexity trade-offs. The performance of the proposed detectors is investigated both analytically and via Monte Carlo simulation.

### 3.1 Signal Model

As explained in Section 1.1.1, time-varying channels arise in many spectrum sensing applications because the stringent requirements imposed by spectrum regulations force sensors to acquire long observation windows. This situation is exacerbated when the signal of interest is narrowband, since the low sampling rates used entail long observation times. For this reason, it seems reasonable to assume that the channel is frequency-flat. The received signal can thus be

written as

$$y = h \cdot x + w, \quad (3.1)$$

where  $\cdot$  denotes point-wise multiplication. The signal  $x$  has a constant magnitude and, without any loss of generality, it can be assumed to satisfy  $|x(t)| = 1 \forall t$ . Thus, the power of the signal term  $h \cdot x$  is given by

$$\eta_0^2 \triangleq \mathbb{E} \{ |h(t) \cdot x(t)|^2 \} = \mathbb{E} \{ |h(t)|^2 |x(t)|^2 \} = \mathbb{E} \{ |h(t)|^2 \}. \quad (3.2)$$

A spectrum sensor collects  $K$  samples of  $y$ , which can be expressed as (see Section 1.1.1):

$$y[k] = h[k] \cdot x[k] + w[k], \quad k = 0, 1, \dots, K-1. \quad (3.3)$$

If we define  $\mathbf{y} \triangleq [y[0], \dots, y[K-1]]^T$  and  $\mathbf{x} \triangleq [x[0], \dots, x[K-1]]^T$ , then  $\mathbf{y}$  can be written in vector/matrix form as

$$\mathbf{y} = \mathbf{X}\mathbf{h} + \mathbf{w}, \quad (3.4)$$

where  $\mathbf{X} \triangleq \text{diag} \{ \mathbf{x} \}$ ,  $\mathbf{h} \triangleq [h[0], \dots, h[K-1]]^T$ , and  $\mathbf{w} \triangleq [w[0], \dots, w[K-1]]^T$ . Note that, as a result of the CM property, one has that  $\mathbf{X}^H \mathbf{X} = \mathbf{I}_K$ . The noise vector  $\mathbf{w}$  is assumed zero-mean circularly symmetric complex Gaussian with  $\mathbb{E} \{ \mathbf{w} \mathbf{w}^H \} = \sigma^2 \mathbf{I}_K$ . The parameters  $\eta_0^2$  and  $\sigma^2$  are regarded as unknown deterministic. Recall that the SNR is defined as

$$\gamma \triangleq \frac{\eta_0^2}{\sigma^2}. \quad (3.5)$$

The time variations of the channel are captured by a BEM with  $B$  orthonormal basis functions  $\beta_b \in \mathbb{C}^K$  and random coefficients  $\alpha_b$  which, upon defining  $\boldsymbol{\alpha} \triangleq [\alpha_0, \dots, \alpha_{B-1}]^T$  and  $\mathbf{B}_0 \triangleq [\beta_0, \dots, \beta_{B-1}]$ , can be written as:

$$\mathbf{h} = \sum_{b=0}^{B-1} \alpha_b \beta_b = \mathbf{B}_0 \boldsymbol{\alpha}. \quad (3.6)$$

Note that  $\mathbf{B}_0$  satisfies  $\mathbf{B}_0^H \mathbf{B}_0 = \mathbf{I}_B$ . The vector  $\boldsymbol{\alpha}$  is assumed zero-mean circularly symmetric complex Gaussian with  $\mathbb{E} \{ \boldsymbol{\alpha} \boldsymbol{\alpha}^H \} = \eta_0^2 \frac{K}{B} \mathbf{I}_B$ , where the factor  $K/B$  ensures that  $K^{-1} \mathbb{E} \{ \|\mathbf{y}\|_2^2 \} = \eta_0^2 + \sigma^2$ . The channel vector  $\mathbf{h}$  is therefore Gaussian distributed, which models Rayleigh fading.

Although any orthonormal basis can be used, of particular relevance is the model where the columns of  $\mathbf{B}_0$  are given by the  $B$  elements of lowest frequency in the Fourier basis [Tsatsanis

and Giannakis, 1996b, Leus, 2004], in which case  $\mathbf{B}_0$  is given by

$$\mathbf{B}_0 = [\mathbf{f}_0 \ \mathbf{f}_1 \ \cdots \ \mathbf{f}_{\tilde{B}} \ \mathbf{f}_{K-\tilde{B}} \ \cdots \ \mathbf{f}_{K-1}], \quad (3.7)$$

where  $\tilde{B} \triangleq \frac{B-1}{2}$  ( $B$  is assumed odd) and

$$\mathbf{f}_b \triangleq \frac{1}{\sqrt{K}} \begin{bmatrix} 1 & e^{j\frac{2\pi}{K}b} & \cdots & e^{j\frac{2\pi}{K}b(K-1)} \end{bmatrix}^T. \quad (3.8)$$

The complete Fourier matrix will be denoted as  $\mathbf{F} \triangleq [\mathbf{f}_0, \dots, \mathbf{f}_{K-1}]$ . For future reference, note that, since  $\mathbf{f}_{K-b} = \mathbf{f}_b^*$ ,  $1 \leq b \leq \tilde{B}$ , the entries of the matrix

$$\mathbf{B}_0 \mathbf{B}_0^H = \sum_{b=0}^{B-1} \beta_b \beta_b^H = \mathbf{f}_0 \mathbf{f}_0^H + 2 \sum_{b=1}^{\tilde{B}} \text{Re} \{ \mathbf{f}_b \mathbf{f}_b^H \} \quad (3.9)$$

are real valued. Moreover, since  $\mathbf{B}_0 \mathbf{B}_0^H = \mathbf{F} \mathbf{D}_0 \mathbf{F}^H$ , where  $\mathbf{D}_0 \triangleq \text{diag} \left\{ [\mathbf{1}_{\tilde{B}+1}^T \ \mathbf{0}_{K-B}^T \ \mathbf{1}_{\tilde{B}}^T]^T \right\}$ , one has that

$$\mathbb{E} \{ \mathbf{h} \mathbf{h}^H \} = \eta_0^2 \frac{K}{B} \mathbf{B}_0 \mathbf{B}_0^H = \mathbf{F} \left[ \eta_0^2 \frac{K}{B} \mathbf{D}_0 \right] \mathbf{F}^H, \quad (3.10)$$

which means that the PSD of the channel is asymptotically given by the diagonal of the matrix  $\eta_0^2(K/B)\mathbf{D}_0$  [Gray, 2006]. The channel is therefore a low-pass random process of bandwidth  $2\pi\tilde{B}/K$ , which is proportional to the maximum Doppler shift. This allows us to select  $B$  based on some (possibly conservative) estimate of this parameter.

### 3.2 GLR Detector for Known CM Signals

The problem of activity detection can be cast as the following hypothesis test:

$$\mathcal{H}_0 : \mathbf{y} = \mathbf{w}, \quad \mathcal{H}_1 : \mathbf{y} = \mathbf{X} \mathbf{h} + \mathbf{w}. \quad (3.11)$$

When  $\mathbf{x}$  is known, the GLR statistic is

$$\mathcal{G}_{\mathbf{x}}(\mathbf{y}) \triangleq \frac{\sup_{\eta_0^2 \geq 0, \sigma^2 \geq 0} p_{\mathcal{H}_1}(\mathbf{y}; \eta_0^2, \sigma^2)}{\sup_{\sigma^2 \geq 0} p_{\mathcal{H}_0}(\mathbf{y}; \sigma^2)}. \quad (3.12)$$

The density of  $\mathbf{y}$  under  $\mathcal{H}_0$ , which is given by

$$p_{\mathcal{H}_0}(\mathbf{y}; \sigma^2) = \frac{1}{(\pi\sigma^2)^K} \exp \left\{ -\frac{1}{\sigma^2} \|\mathbf{y}\|^2 \right\}, \quad (3.13)$$

attains its maximum for  $\hat{\sigma}^2 = \frac{1}{K} \|\mathbf{y}\|^2$ . On the other hand, the density of  $\mathbf{y}$  under  $\mathcal{H}_1$  is

$$p_{\mathcal{H}_1}(\mathbf{y}; \eta_0^2, \sigma^2) = \frac{1}{\pi^K |\boldsymbol{\Xi}|} \exp \{ -\mathbf{y}^H \boldsymbol{\Xi}^{-1} \mathbf{y} \}, \quad (3.14)$$

where

$$\boldsymbol{\Xi} = \eta_0^2 \frac{K}{B} \mathbf{X} \mathbf{B}_0 \mathbf{B}_0^H \mathbf{X}^H + \sigma^2 \mathbf{I}_K \quad (3.15)$$

is the covariance matrix<sup>1</sup> of  $\mathbf{y}$ . Taking logarithms, we find that maximizing (3.14) with respect to  $\eta_0^2$  and  $\sigma^2$  amounts to minimizing

$$\mathbf{y}^H \boldsymbol{\Xi}^{-1} \mathbf{y} + \log |\boldsymbol{\Xi}|. \quad (3.16)$$

Let  $\mathbf{B}_1 \in \mathbb{C}^{K \times (K-B)}$  be a matrix with orthonormal columns that satisfies  $\mathbf{B}_0^H \mathbf{B}_1 = \mathbf{0}$ . Then, it is clear that  $\mathbf{B} \triangleq [\mathbf{B}_0 \ \mathbf{B}_1]$  is unitary and  $\mathbf{B}_0 = \mathbf{B} [\mathbf{I}_B \ \mathbf{0}]^T$ . Since  $\mathbf{X}\mathbf{B}$  is also unitary, it follows from (3.15) that  $\boldsymbol{\Xi} = \mathbf{X}\mathbf{B} \mathbf{D}_1 \mathbf{B}^H \mathbf{X}^H$  is an eigenvalue decomposition of  $\boldsymbol{\Xi}$ , where

$$\mathbf{D}_1 \triangleq \begin{bmatrix} (\frac{K}{B}\eta_0^2 + \sigma^2) \mathbf{I}_B & \mathbf{0} \\ \mathbf{0} & \sigma^2 \mathbf{I}_{K-B} \end{bmatrix}. \quad (3.17)$$

Therefore, with  $\mathbf{z} \triangleq \mathbf{B}^H \mathbf{X}^H \mathbf{y} = [z_0, z_1, \dots, z_{K-1}]^T$ , minimizing (3.16) amounts to minimizing  $\mathbf{z}^H \mathbf{D}_1^{-1} \mathbf{z} + \log |\mathbf{D}_1|$ . Let us introduce the quantities

$$\hat{\eta}_{\text{in}}^2 \triangleq \frac{1}{B} \sum_{i=0}^{B-1} |z_i|^2 = \frac{1}{B} \|\mathbf{B}_0^H \mathbf{X}^H \mathbf{y}\|_2^2 \quad (3.18a)$$

$$\hat{\eta}_{\text{out}}^2 \triangleq \frac{1}{K-B} \sum_{i=B}^{K-1} |z_i|^2 = \frac{1}{K-B} \|\mathbf{B}_1^H \mathbf{X}^H \mathbf{y}\|_2^2, \quad (3.18b)$$

which respectively represent, if the Fourier basis is used, the estimated average power inside and outside of the Doppler bandwidth of the channel. Note that the received energy is given by

---

<sup>1</sup>The dependence of  $\boldsymbol{\Xi}$  with  $\eta_0^2$  and  $\sigma^2$  is not explicitly written so as not to overburden the notation, but must be kept in mind.



$\|\mathbf{y}\|_2^2 = B\hat{\eta}_{\text{in}}^2 + (K - B)\hat{\eta}_{\text{out}}^2$ . From (3.18) it follows that

$$\begin{aligned} \mathbf{z}^H \mathbf{D}_1^{-1} \mathbf{z} + \log |\mathbf{D}_1| &= (K - B) \left[ \frac{\hat{\eta}_{\text{out}}^2}{\sigma^2} + \log \sigma^2 \right] \\ &+ B \left[ \frac{\hat{\eta}_{\text{in}}^2}{\frac{K}{B}\eta_0^2 + \sigma^2} + \log \left( \frac{K}{B}\eta_0^2 + \sigma^2 \right) \right]. \end{aligned} \quad (3.19)$$

The minimizer of (3.19), subject to  $\eta_0^2 \geq 0$  and  $\sigma^2 \geq 0$ , can be seen to be

$$(\hat{\eta}^2, \hat{\sigma}^2) = \begin{cases} (0, \vartheta \hat{\eta}_{\text{in}}^2 + (1 - \vartheta) \hat{\eta}_{\text{out}}^2) & \text{if } \hat{\eta}_{\text{out}}^2 \geq \hat{\eta}_{\text{in}}^2, \\ (\vartheta(\hat{\eta}_{\text{in}}^2 - \hat{\eta}_{\text{out}}^2), \hat{\eta}_{\text{out}}^2) & \text{if } \hat{\eta}_{\text{out}}^2 < \hat{\eta}_{\text{in}}^2, \end{cases} \quad (3.20)$$

where

$$\vartheta \triangleq \frac{B}{K} \quad (3.21)$$

is the *fractional bandwidth*.

The log-GLR thus becomes

$$\log \mathcal{G}_{\mathbf{x}}(\mathbf{y}) = \begin{cases} K \cdot \log \frac{\text{A.M.}}{\text{G.M.}}, & \text{if } \hat{\eta}_{\text{in}}^2 > \hat{\eta}_{\text{out}}^2, \\ 0, & \text{otherwise,} \end{cases} \quad (3.22)$$

where A.M. and G.M. stand for "arithmetic mean" and "geometric mean" respectively, and are defined as

$$\text{A.M.} \triangleq \vartheta \hat{\eta}_{\text{in}}^2 + (1 - \vartheta) \hat{\eta}_{\text{out}}^2, \quad (3.23a)$$

$$\text{G.M.} \triangleq (\hat{\eta}_{\text{in}}^2)^\vartheta (\hat{\eta}_{\text{out}}^2)^{1-\vartheta}. \quad (3.23b)$$

It is readily checked that  $K \log \frac{\text{A.M.}}{\text{G.M.}}$  depends on the data only through the ratio  $\hat{\eta}_{\text{in}}^2 / \hat{\eta}_{\text{out}}^2$ , and moreover, it is a monotonically increasing function of  $\hat{\eta}_{\text{in}}^2 / \hat{\eta}_{\text{out}}^2$  in the range  $\hat{\eta}_{\text{in}}^2 / \hat{\eta}_{\text{out}}^2 \geq 1$ . Hence, the GLR test is equivalent to

$$\frac{\hat{\eta}_{\text{in}}^2}{\hat{\eta}_{\text{out}}^2} \underset{\mathcal{H}_0}{\overset{\mathcal{H}_1}{\gtrless}} \nu', \quad (3.24)$$

where  $\nu' \geq 1$  is a threshold.

This test is intuitively satisfying: the first step in the detection process is to correlate the received waveform with a scaled version of the transmitted signal, obtaining the vector  $\mathbf{X}^H \mathbf{y}$ . This operation preserves the noise statistics and removes the effects of the signal: now the signal term allows to directly observe the time variations of the channel. After that, the representation

of this vector in terms of the orthonormal basis  $\mathbf{B}$  is obtained as  $\mathbf{z} = \mathbf{B}^H(\mathbf{X}^H \mathbf{y})$ . If the BEM uses the Fourier basis, then  $\mathbf{z}$  is the DFT of  $\mathbf{X}^H \mathbf{y}$ , and  $\hat{\eta}_{\text{in}}^2$ ,  $\hat{\eta}_{\text{out}}^2$  are the result of averaging the periodogram over the corresponding frequency bins. The GLR test then compares these two values.

The time-invariant case is recovered by setting  $B = 1$  and  $\mathbf{B}_0 = \frac{1}{\sqrt{K}} \mathbf{1}_K$ . In that case, we have  $z_0 = \frac{1}{\sqrt{K}} \mathbf{1}_K^T \mathbf{X}^H \mathbf{y} = \frac{1}{\sqrt{K}} \mathbf{x}^H \mathbf{y}$ , which yields

$$\hat{\eta}_{\text{in}}^2 = |z_0|^2 = \frac{1}{K} |\mathbf{x}^H \mathbf{y}|^2 \quad (3.25)$$

and

$$\hat{\eta}_{\text{out}}^2 = \frac{1}{K-1} [||\mathbf{z}||^2 - |z_0|^2] = \frac{1}{K-1} [||\mathbf{y}||^2 - \frac{1}{K} |\mathbf{x}^H \mathbf{y}|^2]. \quad (3.26)$$

Thus, the GLR detector is equivalent to  $|\mathbf{x}^H \mathbf{y}|^2 / ||\mathbf{y}||^2 \gtrless_{\mathcal{H}_0}^{\mathcal{H}_1} \nu'$  for some  $\nu'$ , which is the matched filter detector normalized by the total observed power, which accounts for the lack of knowledge about the noise variance. Consequently, the GLR test from (3.24) is a generalization of the matched filter for time-varying channels [Kay, 1998].

### 3.3 GLR Detector for Unknown CM Signals

Clearly, when  $\mathbf{x}$  is not known, the GLR test can be written as

$$\mathcal{G}(\mathbf{y}) = \sup_{\mathbf{x} \in \mathcal{M}^K} \mathcal{G}_{\mathbf{x}}(\mathbf{y}) \gtrless_{\mathcal{H}_0}^{\mathcal{H}_1} \nu, \quad (3.27)$$

with  $\mathcal{G}_{\mathbf{x}}$  given by (3.22) and with  $\mathcal{M}^K \triangleq \{\mathbf{x} \in \mathbb{C}^K : |x[k]| = 1, \forall k\}$  the set of unit-magnitude signals of length  $K$ . Since  $\mathcal{G}_{\mathbf{x}}$  is a monotonically increasing function of  $\hat{\eta}_{\text{in}}^2 / \hat{\eta}_{\text{out}}^2$ , it suffices to maximize this ratio with respect to  $\mathbf{x}$ . Moreover, since

$$\frac{\hat{\eta}_{\text{in}}^2}{\hat{\eta}_{\text{out}}^2} = (K - B) \frac{\hat{\eta}_{\text{in}}^2}{||\mathbf{y}||_2^2 - B \hat{\eta}_{\text{in}}^2} \quad (3.28)$$

is increasing in  $\hat{\eta}_{\text{in}}^2$ , the problem boils down to maximizing  $\hat{\eta}_{\text{in}}^2$ . Defining  $\mathbf{Y} \triangleq \text{diag}\{\mathbf{y}\}$  enables us to rewrite (3.18a) as

$$B \hat{\eta}_{\text{in}}^2 = ||\mathbf{B}_0^T \mathbf{Y}^H \mathbf{x}||^2 = \mathbf{x}^H \mathbf{C} \mathbf{x}, \quad (3.29)$$

where  $\mathbf{C} \triangleq \mathbf{Y}\mathbf{B}_0^*\mathbf{B}_0^T\mathbf{Y}^H$  is  $K \times K$  positive semidefinite with rank  $B$ . Consequently, the problem reduces to maximizing  $\mathbf{x}^H\mathbf{C}\mathbf{x}$  subject to the CM constraint  $\mathbf{x} \in \mathcal{M}^K$ :

$$\hat{\mathbf{x}} = \arg \sup_{\mathbf{x} \in \mathcal{M}^K} \mathbf{x}^H\mathbf{C}\mathbf{x}. \quad (3.30)$$

The problem (3.30) can be solved in closed form when  $B = 1$ . In that case,  $\mathbf{C} = \mathbf{c}\mathbf{c}^H$  is a rank-1 matrix, where  $\mathbf{c} = \mathbf{Y}\boldsymbol{\beta}_0^*$ . Therefore,  $\mathbf{x}^H\mathbf{C}\mathbf{x} = |\mathbf{c}^H\mathbf{x}|^2 \leq \|\mathbf{c}\|_1^2$ , with equality when  $\angle x[k] = \angle(\mathbf{c})_k + C, \forall k$ , with  $C$  any real constant. Using the Fourier basis, where  $\sqrt{K}\boldsymbol{\beta}_0^* = \mathbf{1}_K$ , the GLR detector becomes that for CM signals in time-invariant channels [Derakhtian et al., 2009b]. On the other hand, as far as we know no closed-form expression exists for  $\hat{\mathbf{x}}$  in (3.30) when  $B > 1$ , which means that the GLR statistic has to be approximated or numerically evaluated. Both alternatives are discussed next.

### 3.3.1 Low-Complexity Approximations

We now investigate several approximations and bounds for the objective in (3.30). Remarkably, all these approaches yield the correct solution to the problem if  $B = 1$ , although they are not necessarily equivalent if  $B > 1$ .

#### Largest Eigenvalue of $\mathbf{C}$

Since  $\|\mathbf{x}\|_2^2 = K$  for all  $\mathbf{x} \in \mathcal{M}^K$ , one can relax the constraint in (3.30) to obtain:

$$\begin{aligned} &\text{maximize} && \mathbf{x}^H\mathbf{C}\mathbf{x} \\ &\text{s.t.} && \|\mathbf{x}\|_2^2 = K. \end{aligned}$$

The maximum is given by  $\lambda_{\max}(\mathbf{C}) \cdot K$ , where  $\lambda_{\max}(\cdot)$  denotes the largest eigenvalue. This constitutes an upper bound on  $\hat{\mathbf{x}}^H\mathbf{C}\hat{\mathbf{x}}$ . Hence, one can think of approximating

$$\hat{\eta}_{\text{in}}^2 \approx \hat{\eta}_{\text{in,L1}}^2 \triangleq \frac{K}{B} \lambda_{\max}(\mathbf{C}). \quad (3.31)$$

### $\ell^1$ -Norm of Principal Eigenvector

Since the original problem is easily solvable when  $B = 1$ , consider a rank-1 approximation of  $\mathbf{C}$  in terms of its principal unit-norm eigenvector  $\mathbf{v}$ , i.e.,  $\mathbf{C} \approx \lambda_{\max}(\mathbf{C})\mathbf{v}\mathbf{v}^H$ . This leads to

$$\mathbf{x}^H \mathbf{C} \mathbf{x} \approx \lambda_{\max}(\mathbf{C}) \cdot |\mathbf{v}^H \mathbf{x}|^2 \leq \lambda_{\max}(\mathbf{C}) \cdot \|\mathbf{v}\|_1^2 \quad (3.32)$$

with equality attained for  $\angle x[k] = \angle(\mathbf{v})_k + C, \forall k$ . As a result, one can approximate

$$\hat{\eta}_{\text{in}}^2 \approx \hat{\eta}_{\text{in,L1n1}}^2 \triangleq \frac{1}{B} \lambda_{\max}(\mathbf{C}) \|\mathbf{v}\|_1^2. \quad (3.33)$$

### Phase Relaxation

By writing  $\mathbf{x} = [e^{j\varphi_0}, e^{j\varphi_1}, \dots, e^{j\varphi_{K-1}}]^T$ , it is clear that

$$\mathbf{x}^H \mathbf{C} \mathbf{x} = \sum_{k=0}^{K-1} \sum_{l=0}^{K-1} c_{kl} e^{j(\varphi_l - \varphi_k)} \quad (3.34)$$

with  $c_{kl} \triangleq (\mathbf{C})_{k,l}$ . Since  $\mathbf{C}$  is Hermitian, (3.34) can be rewritten in terms of the elements on and below the diagonal as

$$\mathbf{x}^H \mathbf{C} \mathbf{x} = \sum_{k=0}^{K-1} c_{kk} + 2 \operatorname{Re} \left\{ \sum_{k=1}^{K-1} \sum_{l=0}^{k-1} c_{kl} e^{-j\varphi_{kl}} \right\}, \quad (3.35)$$

where  $\varphi_{kl} \triangleq \varphi_k - \varphi_l$ . Although only  $K$  degrees of freedom are available to choose the  $\varphi_{kl}$ , we can relax this requirement and regard all of the  $\varphi_{kl}$ ,  $l < k$  as free parameters, thus having  $K(K-1)/2$  degrees of freedom. In doing so, the  $\varphi_{kl}$  maximizing (3.35) satisfy  $\varphi_{kl} = \angle c_{kl}$ , resulting in the following bound:

$$\mathbf{x}^H \mathbf{C} \mathbf{x} \leq \sum_{k=0}^{K-1} \sum_{l=0}^{K-1} |c_{kl}|. \quad (3.36)$$

Therefore, it is reasonable to approximate

$$\hat{\eta}_{\text{in}}^2 \approx \hat{\eta}_{\text{in,PR}}^2 \triangleq \frac{1}{B} \sum_{k=0}^{K-1} \sum_{l=0}^{K-1} |c_{kl}|. \quad (3.37)$$

### Phases of the Principal Eigenvector

If we were to approximate  $\hat{\mathbf{x}}$  rather than  $\hat{\eta}_{\text{in}}^2$ , an argument similar to the one leading to  $\hat{\eta}_{\text{in,L1}}^2$  could be applied. If  $\mathbf{v}$  is the principal eigenvector of  $\mathbf{C}$ , then

$$\hat{\eta}_{\text{in}}^2 \approx \hat{\eta}_{\text{in,PPE}}^2 \triangleq \frac{1}{B} \mathbf{x}_{\text{PPE}}^H \mathbf{C} \mathbf{x}_{\text{PPE}}, \quad (3.38)$$

where the  $k$ -th component of  $\mathbf{x}_{\text{PPE}}$  is given by  $(\mathbf{v})_k / |(\mathbf{v})_k|$ .

### Semidefinite Relaxation

As suggested in [Gholam et al., 2011], upon noting that  $\mathbf{x}^H \mathbf{C} \mathbf{x} = \text{Tr}(\mathbf{C} \mathbf{x} \mathbf{x}^H) = \text{Tr}(\mathbf{C} \tilde{\mathbf{X}})$ , where  $\tilde{\mathbf{X}} \triangleq \mathbf{x} \mathbf{x}^H$ , one can relax the (non-convex) rank-1 constraint on  $\tilde{\mathbf{X}}$  to produce the following semidefinite program (SDP):

$$\text{maximize} \quad \text{Tr}(\mathbf{C} \tilde{\mathbf{X}}) \quad (3.39a)$$

$$\text{s.t.} \quad \text{diag}\{\tilde{\mathbf{X}}\} = \mathbf{1}_K \quad (3.39b)$$

$$\tilde{\mathbf{X}} \in \mathbb{S}_+, \quad (3.39c)$$

where  $\mathbb{S}_+$  denotes the cone of positive semidefinite matrices. One can find a solution using any convex solver, and then retrieve an estimate  $\mathbf{x} \in \mathcal{M}^K$  from the optimal  $\tilde{\mathbf{X}}$ , e.g., by taking the phases of its principal eigenvector.

Disappointingly, although two different matrices  $\tilde{\mathbf{X}}_1$  and  $\tilde{\mathbf{X}}_2$  may be very close to the optimum of (3.39a), the associated vector estimates  $\mathbf{x}_1$  and  $\mathbf{x}_2$  may result in considerably different costs, i.e.  $\mathbf{x}_1^H \mathbf{C} \mathbf{x}_1$  may significantly differ from  $\mathbf{x}_2^H \mathbf{C} \mathbf{x}_2$ . This is illustrated in Figure 3.1, where the cost of the original non-convex problem is represented *vs.* the cost of the SDP. Every cluster of points corresponds to a particular realization of the matrix  $\mathbf{C}$ , whereas each point is the result of solving the SDP with a different initialization. The fact that in many instances the points in each cluster are spread vertically is an indication of the phenomenon described above. This has an effect on the performance of the resulting detectors, as we have observed via simulations: the probability of detection strongly depends on the initializations and parameters of the convex solver, resulting in a quite erratic and unpredictable behavior. For this reason, this approach will not be pursued further.

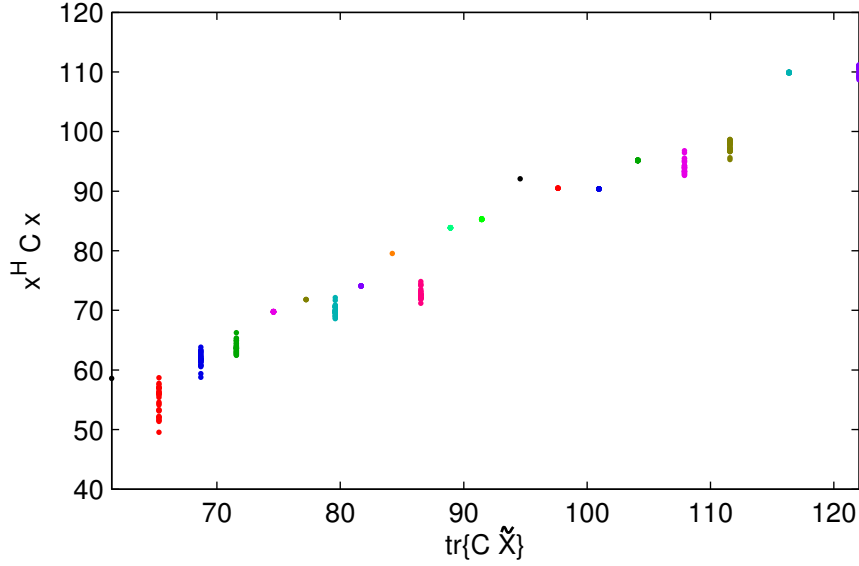


Figure 3.1: Cost of the original problem in terms of the optimal cost of the SDP (3.39a) ( $K = 32$ ,  $B = 9$ ,  $\gamma = 3$  dB, 30 points/cluster).

### 3.3.2 Numerical Optimization

Although  $\mathbf{C}$  is positive semidefinite, and thus  $\mathbf{x}^H \mathbf{C} \mathbf{x}$  is a convex function of  $\mathbf{x}$ , the feasible set of (3.30) is clearly non-convex, which prevents us from using a convex solver. Since the computational efficiency is a major requirement for the algorithm to be implemented in practice, one can think of employing a simple method for local search such as a gradient ascent or a fixed-point iterative algorithm. However, although gradient ascent methods enjoy local convergence for properly selected step size sequences, the design of those sequences may be tricky. For this reason, we abandon this approach in favor of fixed-point iterative methods. This class of methods aim at solving a system of equations by iteratively updating each variable in such a way that one of the equations is satisfied. In our case, we construct this system by setting the gradient of the cost equal to zero.

Consider the unconstrained problem that results from substituting  $\mathbf{x} = [e^{j\varphi_0}, e^{j\varphi_1}, \dots, e^{j\varphi_{K-1}}]^T$  in  $\mathbf{x}^H \mathbf{C} \mathbf{x}$ . Taking the derivatives with respect to  $\boldsymbol{\varphi} \triangleq [\varphi_0, \varphi_1, \dots, \varphi_{K-1}]^T$  yields

$$\nabla_{\boldsymbol{\varphi}} = 2 \operatorname{Im} \{ \mathbf{X}^* \mathbf{C} \mathbf{x} \}. \quad (3.40)$$

Based on this expression, we propose the iterative method listed as Algorithm 3.1, where  $\mathbf{c}_k^H$  denotes the  $k$ -th row of  $\mathbf{C}$ . Several remarks are in order:

**Algorithm 3.1** Fixed-Point iteration

---

```

1: Set initial vector  $\mathbf{x}$ 
2: repeat
3:   for  $k = 0$  to  $K - 1$  do
4:     Set  $\varphi_k = \angle(\mathbf{c}_k^H \mathbf{x})$ 
5:     Set  $x[k] = \exp\{j\varphi_k\}$ 
6:   end for
7: until stopping criterion is satisfied
8: Set  $\hat{\eta}_{\text{in}}^2 = \frac{1}{B} \mathbf{x}^H \mathbf{C} \mathbf{x}$ 

```

---

- One can readily check that the gradient (3.40) vanishes at any fixed point of this iteration.
- No parameter tuning is required.
- The variables  $\varphi_k$  and  $x[k]$  are overwritten at each iteration of the outer loop.
- There are two nested loops instead of just one for stability reasons. Each component in  $\mathbf{x}$  is updated one at a time rather than all together. In other words, to compute  $x[k]$  during the  $i$ -th iteration of the outer loop, the values of  $x[0], x[1] \dots x[k-1]$  corresponding to the outer  $i$ -th iteration and the values of  $x[k], x[k+1] \dots x[K-1]$  corresponding to the  $(i-1)$ -th iteration are used in the right hand side of the expression in line 4. This prevents oscillations without introducing additional complexity.
- No stability problems have been observed in all our experiments, where the proposed algorithm invariably converges to a maximum of the original cost.
- A candidate stopping criterion, used in Section 3.5.2, is whether the norm of the gradient exceeds some certain tolerance  $\epsilon$ .

Since the optimization problem is not convex, multiple local optima may exist, which means that the choice of the initial iterate is critical to find the global maximum. One may attempt to make that choice following the same lines as in Section 3.3.1. However, none of these approaches yield valid initializers as seen next. First, the arguments leading to (3.31), (3.33) and (3.37) merely bound the cost without producing an approximation for  $\hat{\mathbf{x}}$ . Second, if the matrix  $\mathbf{B}_0 \mathbf{B}_0^H$  is real-valued, the vector  $\mathbf{x}_{\text{PPE}}$  used in (3.38) is a saddle point, where the gradient is zero but the objective is not maximized: indeed, it can be shown that, for real-valued  $\mathbf{B}_0 \mathbf{B}_0^H$ , the gradient vanishes at those CM vectors obtained by retaining the phases of the components of any eigenvector of  $\mathbf{C}$  associated with a non-null eigenvalue; and it can be numerically checked by evaluating the Hessian matrix that these CM vectors are not, in general, maxima but saddle points. As pointed out in Section 3.1,  $\mathbf{B}_0 \mathbf{B}_0^H$  is real for Fourier bases, which discourages using

this approach. Finally, the approximation using semidefinite relaxation is not reliable as an initializer for the reasons discussed there.

Having dismissed all approximations from Section 3.3.1, we must consider other alternatives. One possibility to obtain an initial estimate for  $\boldsymbol{\varphi}$  is to project the solution of the phase-relaxed problem onto the feasible set. This can be accomplished by forming an overdetermined system of equations with the relationships  $\varphi_{kl} = \varphi_k - \varphi_l, k > l$  and solving it via LS. Specifically, one may compute

$$\hat{\boldsymbol{\varphi}} = \arg \inf_{\boldsymbol{\varphi}} \|\mathbf{\Gamma}\boldsymbol{\varphi} - \boldsymbol{\varphi}_{\text{PR}}\|^2, \quad (3.41)$$

where  $\boldsymbol{\varphi}_{\text{PR}}$  is a  $K(K-1)/2$ -element vector whose entries are the phases  $\varphi_{kl} = \angle c_{kl}, k > l$ , and  $\mathbf{\Gamma}$  is a  $K(K-1)/2 \times K$  matrix whose  $i$ -th row is of the form

$$[ 0 \quad \dots \quad 0 \quad 1 \quad 0 \quad \dots \quad 0 \quad -1 \quad 0 \quad \dots \quad 0 ], \quad (3.42)$$

where the non-null coefficients are placed in such a way that the relationships  $\varphi_{kl} = \varphi_k - \varphi_l, k > l$ , are imposed. Note that the sum of the columns of  $\mathbf{\Gamma}$  is the zero vector, i.e.,  $\mathbf{\Gamma}\mathbf{1}_K = \mathbf{0}_{K(K-1)/2}$ . This reflects the fact that the relationships above are invariant to any constant added to the  $\varphi_k \forall k$ . To sidestep this issue, we fix  $\varphi_1 = 0$  so that we can drop the first column of  $\mathbf{\Gamma}$  and the first row of  $\boldsymbol{\varphi}$ . The resulting  $\mathbf{\Gamma}$  has full rank and the solution of (3.41) is unique.

### 3.4 Performance Analysis

We next characterize the performance of the detector for known CM signals from (3.24). Since  $\mathbf{z} = \mathbf{B}^H \mathbf{X}^H \mathbf{y}$  is zero-mean Gaussian with diagonal covariance  $\mathbf{D}_1$  given by (3.17),  $\hat{\eta}_{\text{in}}^2$  and  $\hat{\eta}_{\text{out}}^2$  are the sum of squared magnitudes of complex zero-mean i.i.d. Gaussian random variables. Thus, it can be readily checked that:

$$\begin{aligned} k_{\text{in},0} \hat{\eta}_{\text{in}}^2 &\sim \chi^2(2B) \text{ under } \mathcal{H}_0, \text{ where } k_{\text{in},0} \triangleq 2B/\sigma^2, \\ k_{\text{in},1} \hat{\eta}_{\text{in}}^2 &\sim \chi^2(2B) \text{ under } \mathcal{H}_1, \text{ where } k_{\text{in},1} \triangleq 2B/\left(\frac{K}{B}\eta_0^2 + \sigma^2\right), \\ k_{\text{out}} \hat{\eta}_{\text{out}}^2 &\sim \chi^2(2(K-B)) \text{ under } \mathcal{H}_0 \text{ and } \mathcal{H}_1, \text{ where } k_{\text{out}} \triangleq 2(K-B)/\sigma^2, \end{aligned}$$

where  $\chi^2(d)$  denotes a chi-square distribution with  $d$  degrees of freedom. The GLR test statistic  $\hat{\eta}_{\text{in}}^2/\hat{\eta}_{\text{out}}^2$  is, therefore, the quotient of two independent chi-square random variables, which is



$F$ -distributed [Papoulis and Pillai, 2002]. Hence, under  $\mathcal{H}_0$ ,

$$\frac{k_{\text{in},0} \hat{\eta}_{\text{in}}^2 / (2B)}{k_{\text{out}} \hat{\eta}_{\text{out}}^2 / (2(K-B))} = \frac{\hat{\eta}_{\text{in}}^2}{\hat{\eta}_{\text{out}}^2} \sim \mathcal{F}(2B, 2(K-B)),$$

and, under  $\mathcal{H}_1$ ,

$$\frac{k_{\text{in},1} \hat{\eta}_{\text{in}}^2 / (2B)}{k_{\text{out}} \hat{\eta}_{\text{out}}^2 / (2(K-B))} = \frac{\vartheta}{\gamma + \vartheta} \frac{\hat{\eta}_{\text{in}}^2}{\hat{\eta}_{\text{out}}^2} \sim \mathcal{F}(2B, 2(K-B)),$$

where  $\gamma$  and  $\vartheta$  respectively denote the SNR and fractional bandwidth (see (3.5) and (3.21)). Let  $F_{B,K}(x)$  denote the cumulative distribution function of an  $\mathcal{F}(2B, 2(K-B))$  random variable. Then, the probabilities of detection and false alarm can be written as

$$P_D = 1 - F_{B,K} \left( \frac{\vartheta}{\gamma + \vartheta} \nu' \right), \quad P_{\text{FA}} = 1 - F_{B,K}(\nu'). \quad (3.43)$$

Eliminating the threshold  $\nu'$  from (3.43) gives the ROC:

$$P_D = 1 - F_{B,K} \left( \frac{\vartheta}{\gamma + \vartheta} \cdot F_{B,K}^{-1}(1 - P_{\text{FA}}) \right). \quad (3.44)$$

Observe that, as expected, the probability of detection is an increasing function of the SNR  $\gamma$  for fixed  $P_{\text{FA}}$ .

### 3.5 Simulation Results and Discussion

Since analytic performance evaluation is only tractable for certain detectors and under simple scenarios, in this section we assess the performance of the proposed techniques using Monte Carlo simulation. In our experiments, the transmitted signal is generated as  $x[k] = e^{j\varphi_k}$ , where the  $\varphi_k$  are independent and identically distributed random variables with uniform distribution over  $(0, 2\pi)$ . Two flat-fading Rayleigh channel models are used to generate  $\mathbf{h}$ :

- **BEM channel:**  $\mathbf{h}$  is generated using the model from Section 3.1:  $\mathbf{h}$  is given by  $\mathbf{h} = \mathbf{B}_0 \boldsymbol{\alpha}$ , where  $\mathbf{B}_0$  is the Fourier basis from (3.7) and  $\boldsymbol{\alpha}$  is Gaussian distributed with zero mean and  $\text{E}\{\boldsymbol{\alpha} \boldsymbol{\alpha}^H\} = \eta_0^2 \frac{K}{B} \mathbf{I}_B$ . The parameter  $B$  controls the Doppler spread, which is given by  $\omega_d = \frac{B-1}{2} \frac{2\pi}{K}$  — recall that  $B$  is assumed an odd integer.
- **Jakes model:**  $\mathbf{h}$  is generated using the popular dense scatterer model (also known as Jakes model) [Hlawatsch and Matz, 2011, Goldsmith, 2005]: the vector  $\mathbf{h}$  is Gaussian

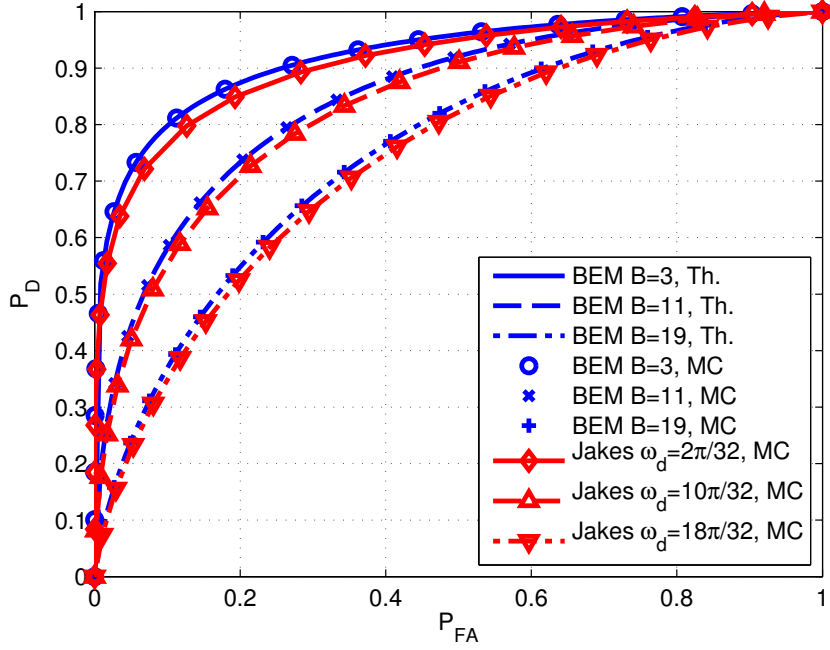


Figure 3.2: Comparison between theoretical and Monte Carlo results for several BEM and Jakes channels ( $K = 32$ ,  $\gamma = -6$  dB).

distributed with zero mean and Toeplitz covariance matrix given by

$$(\mathbb{E} \{ \mathbf{h} \mathbf{h}^H \})_{i,j} = J_0(\omega_d(i - j)), \quad (3.45)$$

where  $\omega_d$  is the Doppler spread of the channel and  $J_0(x)$  is the following Bessel function:

$$J_0(x) \triangleq \frac{1}{\pi} \int_0^\pi e^{-jx \cos \theta} d\theta. \quad (3.46)$$

On the sensor side, the test statistics are evaluated using the Fourier basis from Section 3.1, where the number of basis functions, denoted as  $B$ , is selected based on prior knowledge. To separately investigate the influence of each parameter, we start by assuming that the sensor exactly knows the Doppler spread  $\omega_d$  of the channel and selects  $B = 1 + \lceil \frac{K\omega_d}{\pi} \rceil$ . Later on, we will consider the effects of using different values of  $B$ .

### 3.5.1 Detector for Known CM Signals

We first consider the detector for known CM signals presented in Section 3.2. The ROC of this detector is shown in Figure 3.2 for both channel models and several Doppler spreads. For BEM

channels, the observations follow the same model as assumed by the detector, and hence the simulation results (MC) perfectly agree with (3.44) (Th.). As expected, when the observations are generated using the Jakes model, the performance degrades, although just slightly. This effect is also illustrated in Figure 3.3, where the probability of detection is represented *vs.* the SNR for fixed false alarm rate  $P_{\text{FA}} = 0.1$ . The SNR penalty incurred with Jakes channels is in the order of 0.5 dB for this example.

The impact of the Doppler spread on the performance is shown in Figure 3.4. It is seen that  $P_{\text{D}}$  decreases as  $\omega_d$  becomes larger, even when the latter is perfectly known. In fact, for  $\omega_d = \pi$ , which is the largest Doppler spread possible, one has  $P_{\text{D}} = P_{\text{FA}}$  and the detector becomes useless. This is because in that case the distributions of  $\mathbf{y}$  under both hypotheses coincide.

To analyze the case in which the actual value of the Doppler spread is not available to the detector, we show in Figure 3.5 the probability of detection *vs.* the actual Doppler spread for several values of  $B$  used in the detector (Ass.  $B$ ). Although the matched filter detector — that is, the GLR detector with  $B = 1$  — is the best choice for time-invariant channels, its performance quickly degrades as soon as fading is introduced. As intuition suggests, Figure 3.5 shows that overestimating the true Doppler spread is less detrimental than underestimating it.

### 3.5.2 Detectors for Unknown CM Signals

We now consider detection of unknown CM waveforms and compare the low-complexity approximations from Section 3.3.1 and the fixed-point iteration with *phase relaxation*-based initialization (PRFP) from Section 3.3.2. For the latter, we use a tolerance value  $\epsilon = 10^{-3}$  in the stopping criterion.

Figures 3.6 and 3.7 show the ROC of the proposed detectors for a BEM channel with  $B = 5$  and  $B = 17$ , respectively. The curve labeled as "KS" corresponds to the detector for known CM signals from Section 3.2 and provides a performance upper bound for the other detectors. As expected, the PRFP detector exhibits the best performance among those detectors without knowledge of the signal, although this is at the expense of the highest computational cost. The low complexity approximations are seen to perform quite similarly and suffer from a larger performance loss relative to PRFP as  $B$  (and hence the Doppler spread) is increased.

In order to illustrate the influence of the SNR, Figures 3.8 and 3.9 show the probability of detection for fixed false alarm rate *vs.* the SNR  $\gamma$  in the same settings as Figures 3.6 and 3.7, respectively. Note that the performance loss incurred by the PRFP detector due to the lack of knowledge about the transmitted signal is approximately 10 dB. We also note the presence of a performance ceiling for the low-complexity approximations, that is, for given  $K$  and  $B$ , there

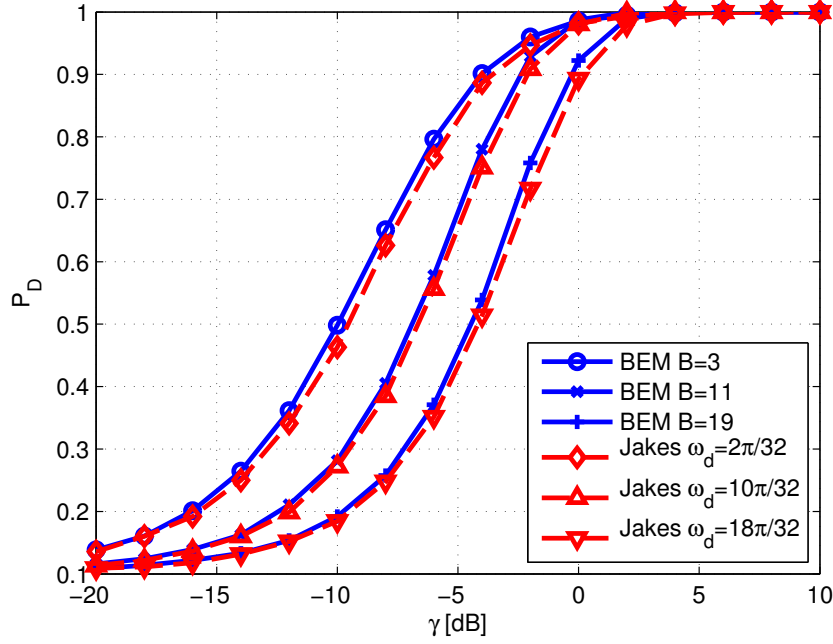


Figure 3.3: Probability of detection *vs.* SNR for several BEM and Jakes channels. The Doppler spread of the channel is known ( $K = 32$ ,  $P_{FA} = 0.1$ ).

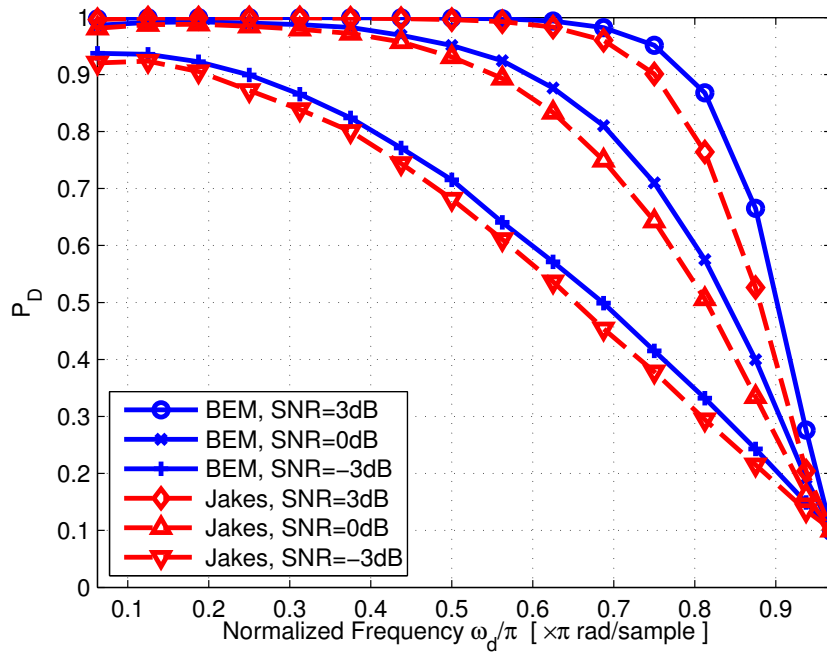


Figure 3.4: Probability of detection *vs.* the (known) Doppler spread for several SNR values ( $K = 32$ ,  $P_{FA} = 0.1$ ).

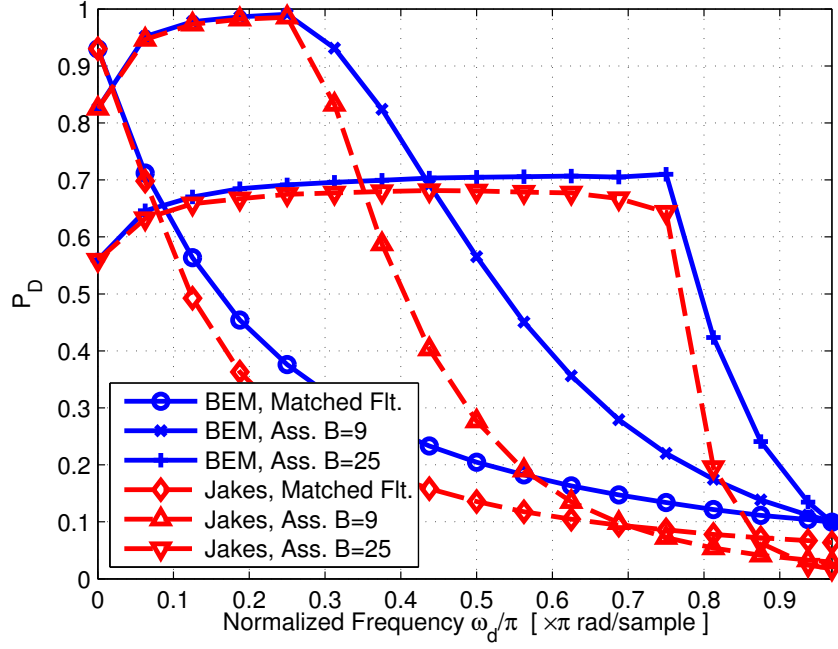


Figure 3.5: Probability of detection *vs.* the (unknown) Doppler spread for different assumed values of  $B$  ( $K = 32$ ,  $P_{FA} = 0.1$ ,  $\gamma = 0$  dB).

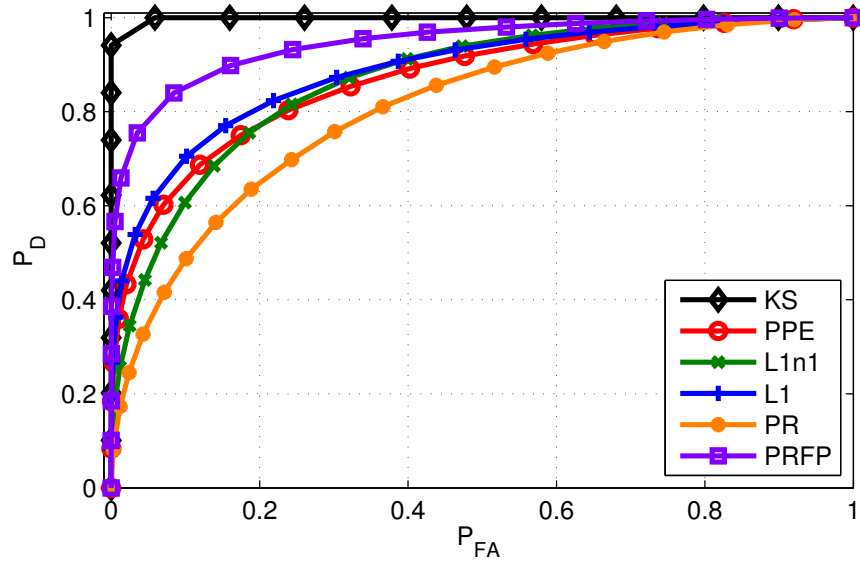


Figure 3.6: ROC curves of the different detectors ( $K = 64$ ,  $\gamma = 3$  dB, BEM channel with  $B = 5$  (Doppler spread =  $\pi \times 0.0625$  rad/sample)).

exists an upper bound on  $P_D$  that cannot be exceeded even if the SNR becomes arbitrarily large.

Finally, Figure 3.10 uses the PRFP detector to illustrate two different effects. First, as in Section 3.5.1, it is exemplified using the Jakes channel that the scheme is robust to mismatches in the channel model. Second, the influence of the value of  $B$  assumed by the detector is similar to that observed in Figure 3.5.

## 3.6 Conclusions

We have proposed several schemes for activity detection in time-varying channels when the transmitted signal is known to have a constant magnitude. Channel variations are captured by a BEM with random coefficients. If the transmitted sequence is known, then the GLR detector is a generalization of the matched filter detector that compares the energy measured inside and outside of the Doppler bandwidth of the channel. If the transmitted sequence is unknown, then the GLR detector requires the solution of a non-convex problem. Several low-complexity approximations were proposed along with a fixed-point method that finds a local optimum of that problem.

It has been observed through simulations that the probability of detection of the low-complexity approximations remains bounded away from 1 even when the SNR goes to infinity, an effect which is more pronounced as the Doppler spread of the channel increases. We have also observed the importance of not underestimating the Doppler spread of the channel.

This work of this chapter has been presented in part in the *37th IEEE International Conference on Acoustics, Speech and Signal Processing (ICASSP 2012)* [Romero et al., 2012a] and in the *3rd International Workshop on Cognitive Information Processing (CIP 2012)* [Romero and López-Valcarce, 2012].

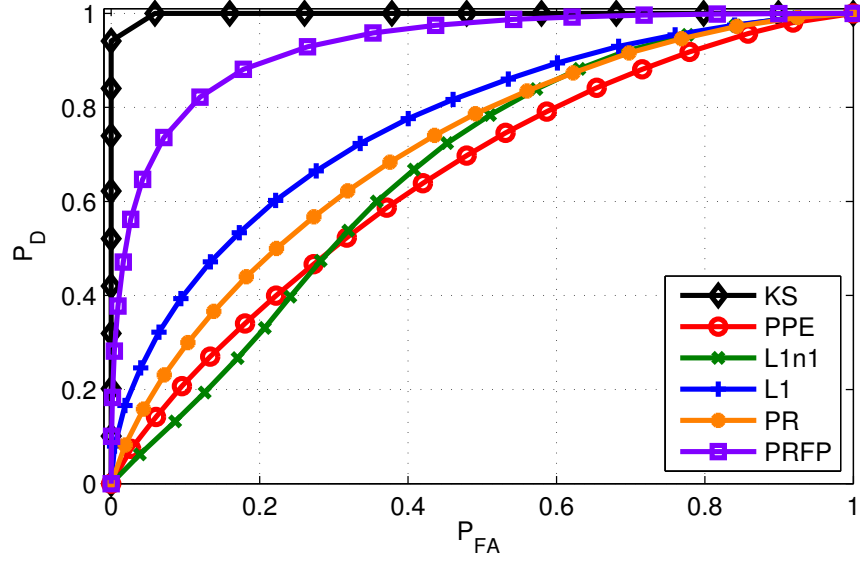


Figure 3.7: ROC curves of the different detectors ( $K = 64$ ,  $\gamma = 3$  dB, BEM channel with  $B = 17$  (Doppler spread  $= \pi \times 0.250$  rad/sample)).

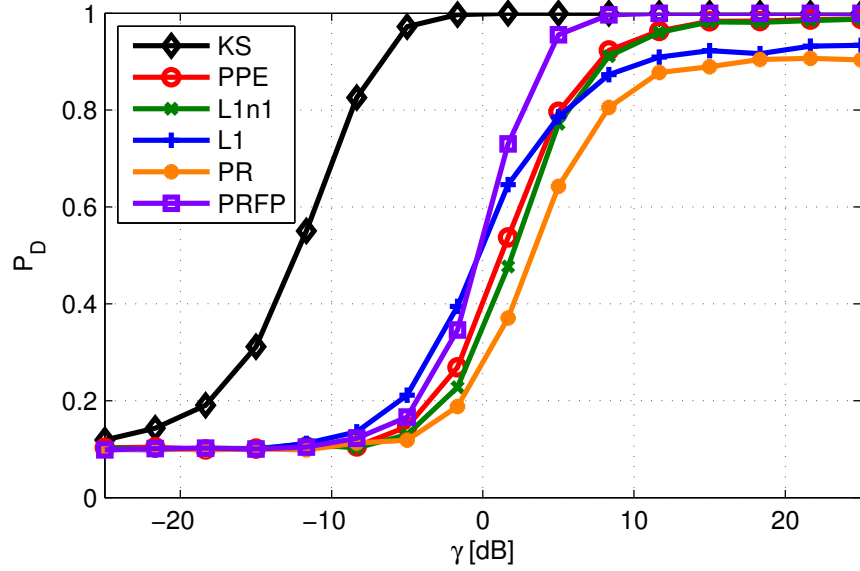


Figure 3.8: Probability of detection *vs.* SNR for  $P_{FA} = 0.1$  ( $K = 64$  samples, BEM channel with  $B = 5$  (Doppler spread  $= \pi \times 0.0625$  rad/sample)).

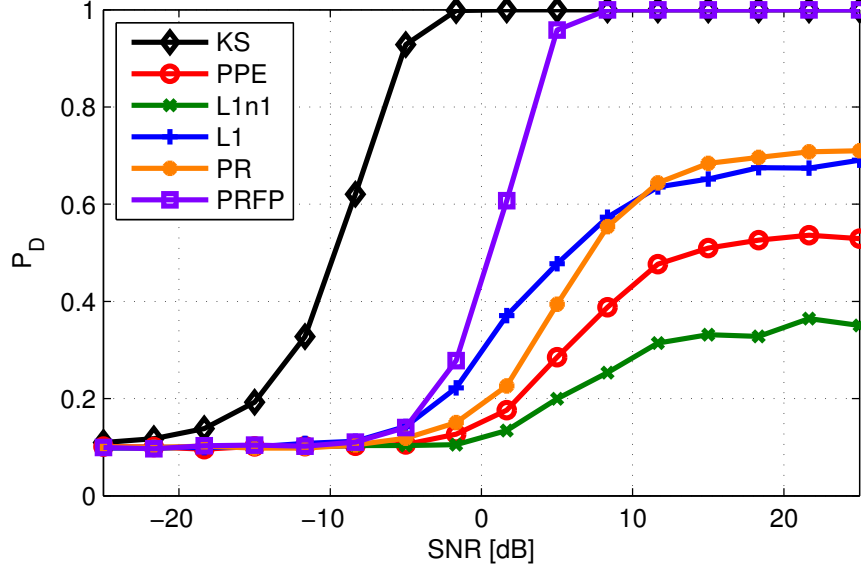


Figure 3.9: Probability of detection *vs.* SNR for  $P_{FA} = 0.1$  ( $K = 64$  samples, BEM channel with  $B = 17$  (Doppler spread  $= \pi \times 0.250$  rad/sample)).

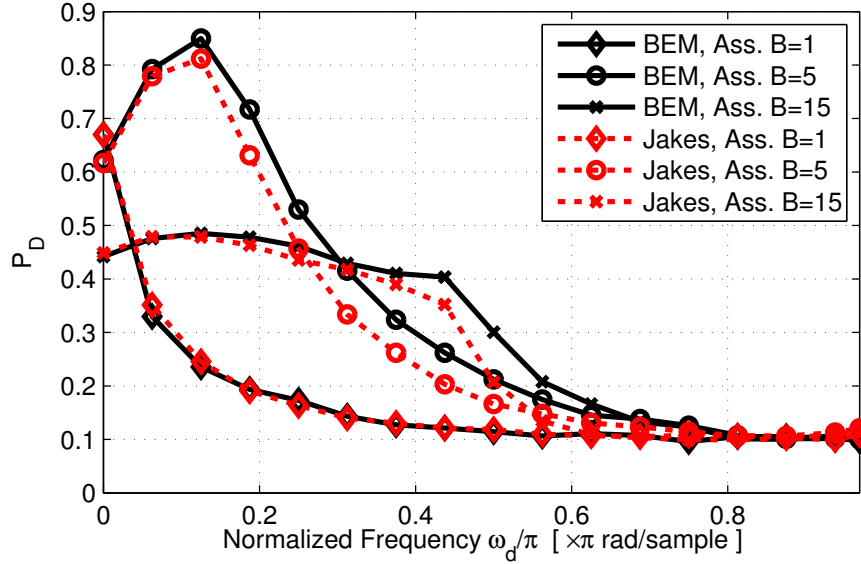


Figure 3.10: Probability of detection of the PRFP detector *vs.* the Doppler spread of the channel for different values of  $B$  used by the detector ( $K = 32$ ,  $P_{FA} = 0.1$ ,  $\gamma = 5$  dB).



## Chapter 4

# Detection of Gaussian Signals in Time-Varying Channels

In this chapter, we consider the problem of detecting the activity of primary signals with Gaussian distribution observed in noise of unknown variance after passing through a frequency-flat and time-varying channel. We start considering three single-antenna detectors, which arise from three alternative formulations of the problem. First, we derive the GLR detector for the case where the flat-fading channel is deterministic and unknown and has no temporal structure. Second, we attempt to find optimal invariant tests under the group of positive scalings by deriving the likelihood ratio of the maximal invariant statistic; but it is found that no such a test exists, even in the low-SNR scenario. Inspired by the derivation of this likelihood ratio, we propose two different detectors: the first assumes a prior distribution for the channel taps and derives a test from Bayesian considerations, whereas the second models the channel using a BEM with unknown deterministic coefficients and proceeds in a GLRT-like fashion.

We then consider activity detection using sensors with multiple antennas. Time variations are captured by a BEM where the unknown deterministic coefficients are decoupled from one antenna to another [Ma and Giannakis, 2002]. As opposed to Chapter 3, in this approach the basis vectors need not be orthogonal. One may consider, for instance, discrete prolate spheroidal sequences [Zemen and Mecklenbrauker, 2005], complex exponentials [Giannakis and Tepedelenlioğlu, 1998, Tsatsanis and Giannakis, 1996b, Leus, 2004], Karhunen-Loeve orthogonal expansion functions [Senol et al., 2005] or simply polynomials [Hijazi and Ros, 2009]. The GLR test requires the ML estimates of the noise power and BEM coefficients, which must be obtained numerically. To this end, we propose the direct application of the *expectation-maximization* (EM) algorithm.

## 4.1 Observation Model

Let us start by generalizing the model from Chapter 3 to the multiantenna scenario. Suppose that a spectrum sensor is monitoring a particular frequency channel using  $M$  antennas and that the  $m$ -th antenna receives the signal

$$y_m = h_m \cdot x + w_m, \quad (4.1)$$

where  $w_m$  and  $h_m$  respectively represent the noise process at the  $m$ -th antenna and the frequency-flat channel between the single-antenna primary user and the  $m$ -th antenna of the spectrum sensor. The  $K$  samples obtained from each antenna can be arranged in the matrix  $\mathbf{Y} \in \mathbb{C}^{M \times K}$ , where the  $m$ -th row corresponds to the  $m$ -th antenna and the  $k$ -th column corresponds to the  $k$ -th time instant. Similarly, we form the matrices  $\mathbf{H}$  and  $\mathbf{W}$ , whose  $(m, k)$  entries are respectively the samples  $h_m[k]$  and  $w_m[k]$ , and the vector  $\mathbf{x}$ , whose  $k$ -th entry is the sample  $x[k]$ . Thus, we may write

$$\mathbf{Y} = \mathbf{H}\mathbf{X} + \mathbf{W}, \quad (4.2)$$

where  $\mathbf{X} \triangleq \text{diag}\{\mathbf{x}\} \in \mathbb{C}^{K \times K}$ . It is assumed that the samples  $x[k]$  form a sequence of independent complex Gaussian circularly symmetric random variables with zero mean and unit variance, i.e.,  $\mathbf{x} \sim \mathcal{CN}(\mathbf{0}, \mathbf{I}_K)$  (see motivation in Section 1.1.1). The noise is assumed spatially and temporally white, independent of  $x[k]$ , where the samples  $w_m[k]$  are independent and identically distributed with  $w_m[k] \sim \mathcal{CN}(0, \sigma^2)$ . The noise power  $\sigma^2$  is regarded as an unknown deterministic parameter.

It is also convenient to define the column-wise vectorizations  $\mathbf{y} \triangleq \text{vec } \mathbf{Y}$  and  $\mathbf{w} \triangleq \text{vec } \mathbf{W}$  so that we can rewrite (4.2) as

$$\mathbf{y} = \mathbf{G}\mathbf{x} + \mathbf{w} \quad (4.3)$$

where  $\mathbf{G} \in \mathbb{C}^{MK \times K}$  is given by

$$\mathbf{G} \triangleq \begin{bmatrix} \mathbf{g}[0] & \mathbf{0} & \dots & \mathbf{0} \\ \mathbf{0} & \mathbf{g}[1] & \dots & \mathbf{0} \\ \vdots & \vdots & \ddots & \vdots \\ \mathbf{0} & \mathbf{0} & \dots & \mathbf{g}[K-1] \end{bmatrix}, \quad (4.4)$$

with  $\mathbf{g}[k] \in \mathbb{C}^M$  representing the  $k$ -th column of  $\mathbf{H}$ . Thus, the covariance matrix of the obser-

variations can be written as

$$\mathbf{\Xi} \triangleq \mathbb{E} \{ \mathbf{y} \mathbf{y}^H \} = \mathbf{G} \mathbf{G}^H + \sigma^2 \mathbf{I}_{MK}, \quad (4.5)$$

which means that the probability density function of  $\mathbf{y}$  is simply

$$p_{\mathcal{H}_1}(\mathbf{y}; \mathbf{G}, \sigma^2) = \frac{\exp \{ -\mathbf{y}^H \mathbf{\Xi}^{-1} \mathbf{y} \}}{\pi^{KM} |\mathbf{\Xi}|}. \quad (4.6)$$

When no primary signal is present, the probability density function reduces to  $p_{\mathcal{H}_0}(\mathbf{y}; \sigma^2) \triangleq p_{\mathcal{H}_1}(\mathbf{y}; \mathbf{G} = \mathbf{0}, \sigma^2)$ . With these definitions in mind, one can pose the activity detection problem as the following test:

$$\mathcal{H}_0 : \mathbf{Y} = \mathbf{W}, \quad \mathcal{H}_1 : \mathbf{Y} = \mathbf{H} \mathbf{X} + \mathbf{W}. \quad (4.7)$$

The detectors to be derived based on this model exploit the spatial structure and time variations of the channel. If the sensor has a single antenna and the channel is time-invariant, it can be seen from (4.5) and (4.6) that  $\mathbf{G} \mathbf{G}^H$  and  $\sigma^2$  are not identifiable, which in turn means that the two hypotheses in (4.7) are indistinguishable. Therefore, the proposed schemes will benefit from time variation.

## 4.2 Detectors for Single-Antenna Sensors

Suppose that  $M = 1$  and form the vector

$$\boldsymbol{\eta} \triangleq [|h_0[0]|^2, \dots, |h_0[K-1]|^2]^T. \quad (4.8)$$

Then, the covariance matrix of the observations can be written as

$$\mathbf{\Xi} = \text{diag} \{ \boldsymbol{\eta} \} + \sigma^2 \mathbf{I}_K, \quad (4.9)$$

and the probability density function from (4.6) becomes

$$p_{\mathcal{H}_1}(\mathbf{y}; \boldsymbol{\eta}, \sigma^2) = \frac{1}{\pi^K \prod_{k=0}^{K-1} (|h_0[k]|^2 + \sigma^2)} \exp \left\{ - \sum_{k=0}^{K-1} \frac{|y_0[k]|^2}{|h_0[k]|^2 + \sigma^2} \right\}. \quad (4.10)$$

We next derive several detectors for single-antenna sensors following two philosophies. First, we rely on a GLR approach to develop a detector for rapidly-changing channels. Second, we

attempt to find an optimal test within the family of tests that are invariant to positive scalings. Since no such test exists, we consider two alternative approaches that result in usable detectors.

### 4.2.1 Generalized Likelihood Ratio Test

The GLR test in the single-antenna case is given by

$$\mathcal{G}(\mathbf{y}) = \frac{\sup_{\sigma^2 \geq 0} p_{\mathcal{H}_0}(\mathbf{y}; \sigma^2)}{\sup_{\boldsymbol{\eta} \in \mathcal{E}, \sigma^2 \geq 0} p_{\mathcal{H}_1}(\mathbf{y}; \boldsymbol{\eta}, \sigma^2)} \stackrel{\mathcal{H}_0}{\geq} \nu, \quad (4.11)$$

where  $\mathcal{E}$  denotes the set of feasible channel power gain vectors  $\boldsymbol{\eta}$  allowed by the model; for instance, the set of vectors allowed by a BEM.

It can be easily seen that the maximizer of the density in the numerator, i.e., the ML estimate of  $\sigma^2$  under  $\mathcal{H}_0$ , is given by  $\hat{\sigma}^2 = \frac{1}{K} \sum_{k=0}^{K-1} |y_0[k]|^2$ . To obtain the values of  $\boldsymbol{\eta}$  and  $\sigma^2$  maximizing the density in the denominator, i.e., the ML estimates under  $\mathcal{H}_1$ , one must solve:

$$\underset{\boldsymbol{\eta} \in \mathcal{E}, \sigma^2}{\text{minimize}} \sum_{k=0}^{K-1} \left[ \log(|h_0[k]|^2 + \sigma^2) + \frac{|y_0[k]|^2}{|h_0[k]|^2 + \sigma^2} \right], \quad (4.12)$$

which is not convex and therefore difficult to solve in general. In Section 4.3, we will develop an EM method, which can be used with single-antenna or multiantenna sensors, to find a solution to this problem numerically when the channel follows a BEM. Here, we will focus on the limiting case without any particular temporal structure, i.e.,  $\mathcal{E} = \mathbb{R}_+^K$ . Specifically, it can be seen that the ML estimates in that scenario satisfy

$$|\hat{h}_0[k]|^2 + \hat{\sigma}^2 = |y_0[k]|^2, \quad k = 0, \dots, K-1, \quad (4.13)$$

and result in the following GLR statistic ( $\propto$  denotes equality up to a monotonically increasing transformation not depending on the observations)

$$\mathcal{G}(\mathbf{c}) = \frac{\left( \prod_{k=0}^{K-1} |y_0[k]|^2 \right)^{1/K}}{\frac{1}{K} \sum_{k=0}^{K-1} |y_0[k]|^2} \propto \mathcal{T}_{\text{AM/GM}}(\mathbf{c}) \triangleq \prod_{k=0}^{K-1} c[k], \quad (4.14)$$

where

$$c[k] \triangleq \frac{|y_0[k]|^2}{\sum_{k'=0}^{K-1} |y_0[k']|^2} \quad (4.15)$$

and

$$\mathbf{c} \triangleq [c[0], \dots, c[K-1]]^T. \quad (4.16)$$

Recall that two statistics related by a monotonically increasing transformation not depending on the observations define equivalent tests.

From (4.14), it follows that the GLR test computes the geometric over arithmetic mean ratio of the *instantaneous power* and compares the result against a threshold. This is the well-known Bartlett test [Bartlett, 1937] for equality of variances. Ratios of this kind are also encountered in other contexts under the names of *spectral flatness measure* or *Wiener entropy* [Johnston, 1988]. Note that the GLR test rejects the null hypothesis  $\mathcal{H}_0$  for low values of  $\mathcal{G}(\mathbf{c})$  in (4.14), which satisfies  $0 \leq \mathcal{G}(\mathbf{c}) \leq 1$ . The exact and asymptotic distributions of  $\mathcal{G}$  can be obtained as particular cases of the results in [Glaser, 1976].

#### 4.2.2 Towards Locally Optimal Invariant Tests

Although the GLR approach usually results in simple and intuitive tests with acceptable performance, it is not generally UMP [Kay, 1998, Lehmann and Romano, 2005, Scharf, 1991] (see Section 1.1.1). In fact, a UMP test seldom exists. We next pursue a different approach, where an optimal test is sought within a constrained family (see Section 1.1.1). Specifically, we focus on the class of tests which are invariant under scaling transformations.

The most powerful member of the family of invariant tests, if exists, is called *UMP invariant* (UMPI), and it can be seen that its statistic is a *maximal invariant* (see [Lehmann and Romano, 2005]; also the Appendix). Although in order to find a UMPI test one can seek a maximal invariant statistic and then compute its likelihood ratio, this operation is considerably involved in most cases. A simpler approach relies on the application of Wijsman's theorem [Wijsman, 1967], which states that, under mild assumptions, this likelihood ratio can be obtained by integrating the densities under both hypotheses over the group of transformations defining the problem invariances. Since, in this chapter, our interest will center on invariance to positive scalings (see the Appendix for a more general case), the likelihood ratio of the maximal invariant statistic will be given by

$$\mathcal{L}(\mathbf{y}; \boldsymbol{\eta}, \sigma^2) = \frac{\int_0^\infty p_{\mathcal{H}_1}(a\mathbf{y}; \boldsymbol{\eta}, \sigma^2) a^{2K} da}{\int_0^\infty p_{\mathcal{H}_0}(a\mathbf{y}; \sigma^2) a^{2K} da}, \quad (4.17)$$

where  $a \in \mathbb{R}_+$  is a scale factor and  $a^{2K}$  represents the Jacobian of the transformation. Since  $\mathcal{L}$  is invariant to scalings of  $\mathbf{y}$ , one can scale this vector by a factor of  $1/\sqrt{\sum_k |y_0[k]|^2}$  without changes in  $\mathcal{L}$ . After doing this operation, it can be seen that the denominator of (4.17) becomes

a constant and, consequently,

$$\mathcal{L}(\mathbf{y}; \boldsymbol{\eta}, \sigma^2) = \mathcal{L}(\mathbf{c}; \boldsymbol{\eta}, \sigma^2) \propto \int_0^\infty \prod_{k=0}^{K-1} \frac{a^2}{\sigma^2 + |h_0[k]|^2} \exp \left\{ -\frac{a^2 \mathbf{c}[k]}{\sigma^2 + |h_0[k]|^2} \right\} da, \quad (4.18)$$

where  $\mathbf{c}$  has been defined in (4.16). Using the change of variable  $a \leftarrow \sigma a$ , it follows that

$$\mathcal{L}(\mathbf{c}; \boldsymbol{\eta}, \sigma^2) \propto \mathcal{L}'(\mathbf{c}; \boldsymbol{\gamma}) \triangleq \int_0^\infty \prod_{k=0}^{K-1} \frac{a^2}{1 + \gamma[k]} \exp \left\{ -\frac{a^2 \mathbf{c}[k]}{1 + \gamma[k]} \right\} da, \quad (4.19)$$

where

$$\gamma[k] \triangleq \frac{|h_0[k]|^2}{\sigma^2} \quad (4.20)$$

and

$$\boldsymbol{\gamma} \triangleq [\gamma[0], \dots, \gamma[K-1]]^T. \quad (4.21)$$

Since the tests defined by the right-hand side of (4.19) for all values of the unknown parameter  $\boldsymbol{\gamma}$  are not equivalent, we conclude that there exists no UMPI test [Lehmann and Romano, 2005, Scharf, 1991] associated with this invariance group.

However, there is still the possibility that if we focus on the case of *close hypotheses*, which in this setting means low SNR ( $\boldsymbol{\gamma} \approx \mathbf{0}$ ), a *locally most powerful invariant* (LMPI) test may exist. To find it, we approximate the statistic  $\mathcal{L}'$  in (4.19) using a second-order Taylor expansion with respect to  $\boldsymbol{\gamma}$ . This operation yields

$$\mathcal{L}'(\mathbf{c}; \boldsymbol{\gamma}) \approx \int_0^\infty a^{2K} e^{-a^2} \Psi(a, \mathbf{c}, \boldsymbol{\gamma}) da, \quad (4.22)$$

where

$$\begin{aligned} \Psi(a, \mathbf{c}, \boldsymbol{\gamma}) &\triangleq 1 + (a^2 \mathbf{c} - \mathbf{1})^T \boldsymbol{\gamma} \\ &\quad + \frac{1}{2} \boldsymbol{\gamma}^T [(a^2 \mathbf{c} - \mathbf{1})(a^2 \mathbf{c} - \mathbf{1})^T - \text{diag} \{a^2 \mathbf{c} - \mathbf{1}\}] \boldsymbol{\gamma}. \end{aligned} \quad (4.23)$$

Since this expression still depends on unknown parameters, we also conclude that no LMPI test exists for this invariance group. A more in-depth study of the existence of (locally) optimal invariant tests in more general scenarios is provided in the Appendix. In the rest of this section, we propose two tests based on the local approximation (4.22): The first one introduces a prior distribution on the channel and proceeds in a Bayesian-like fashion, whereas the second one

assumes a BEM for the channel and proposes a detector inspired by the ML philosophy.

### BAYESIAN APPROACH

The introduction of a prior distribution on the channel coefficients clearly induces a prior on  $\gamma$ . If  $p_\gamma$  denotes the density of such a prior distribution and  $E_\gamma\{\Psi\} \triangleq \int \Psi(a, \mathbf{c}, \gamma') p_\gamma(\gamma') d\gamma'$ , one may consider using the following test statistic:

$$\mathcal{T}_{\text{Bayes}}(\mathbf{c}) \triangleq E_\gamma\{\mathcal{L}'(\mathbf{c}; \gamma)\} = \int_0^\infty a^{2K} e^{-a^2} E_\gamma\{\Psi\} da. \quad (4.24)$$

We now assume that  $\boldsymbol{\mu}_\eta \triangleq E\{\boldsymbol{\eta}\}$  is proportional to the vector of all ones and  $\boldsymbol{\Xi}_\eta \triangleq E\{(\boldsymbol{\eta} - \boldsymbol{\mu}_\eta)(\boldsymbol{\eta} - \boldsymbol{\mu}_\eta)^T\}$  has a constant diagonal, which is the case, for instance, if the sequence of instantaneous channel power gains  $|h_0[k]|^2$  is a wide-sense stationary process. Taking these two facts into account and noting from (4.15) and (4.16) that  $\mathbf{c}^T \mathbf{1} = 1$ , we find that

$$E_\gamma\{\Psi(a, \mathbf{c}, \gamma)\} \propto a^2 \mathbf{c}^T \boldsymbol{\Xi}_\eta \mathbf{c} - 2\mathbf{1}^T \boldsymbol{\Xi}_\eta \mathbf{c}. \quad (4.25)$$

Thus,  $\mathcal{T}_{\text{Bayes}}(\mathbf{c})$  is a linear combination of a quadratic and a linear term:

$$\mathcal{T}_{\text{Bayes}}(\mathbf{c}) \propto v_2 \mathbf{c}^T \boldsymbol{\Xi}_\eta \mathbf{c} - 2v_1 \mathbf{1}^T \boldsymbol{\Xi}_\eta \mathbf{c}. \quad (4.26)$$

where  $v_2 = \int_0^\infty a^{2K+2} e^{-a^2} da$  and  $v_1 = \int_0^\infty a^{2K} e^{-a^2} da$ . The first constant can be computed as

$$v_2 = \int_0^\infty a^{2K+2} e^{-a^2} da \quad (4.27a)$$

$$= \frac{1}{2} \int_{-\infty}^\infty a^{2K+2} e^{-a^2} da \quad (4.27b)$$

$$= \frac{\sqrt{\pi}}{2} E_a\{a^{2K+2}\} \quad (4.27c)$$

$$= \frac{\sqrt{\pi}}{2^{K+2}} (2K+1)!!, \quad (4.27d)$$

where (4.27b) follows from the fact that the integrand is an even function of  $a$ , the expectation in (4.27c) is with respect to a random variable  $a \sim \mathcal{N}(0, 1/2)$ , and  $!!$  denotes double factorial.<sup>1</sup> Applying a similar procedure to obtain  $v_1$  yields  $v_1 = (1/2)(2K+1)v_2$ . Therefore,

$$\mathcal{T}_{\text{Bayes}}(\mathbf{c}) \propto \mathbf{c}^T \boldsymbol{\Xi}_\eta \mathbf{c} - (2K+1) \mathbf{1}^T \boldsymbol{\Xi}_\eta \mathbf{c}. \quad (4.28)$$

---

<sup>1</sup>Recall that the double factorial of a positive odd integer  $n$  is the product of all odd integers between 1 and  $n$  inclusive.

In the limiting case of independent channel gains  $h_0[k]$ , where the matrix  $\Xi_\eta$  has the form  $\Xi_\eta = \lambda \mathbf{I}_K$  with  $\lambda$  a positive constant, we obtain

$$\mathcal{T}_{\text{Bayes}}(\mathbf{c}) \propto \mathcal{T}_{\text{GK}}(\mathbf{c}) \triangleq \|\mathbf{c}\|_2^2 = \frac{\|\mathbf{y}\|_4^4}{\|\mathbf{y}\|_2^4}, \quad (4.29)$$

where "GK" stands for *generalized kurtosis* and whose meaning is explained below.

Interestingly, this test statistic was obtained in the context of testing for homogeneity of covariance matrices following a completely different approach [Nagao, 1973] (see also the Appendix). The test statistic can be seen as a monotone function of the sample excess kurtosis [Ollila et al., 2011] and exploits the fact that the observations  $y_0[k]$  follow a Gaussian distribution under the null hypothesis  $\mathcal{H}_0$  and a *leptokurtic* distribution (with kurtosis  $\kappa = 3\text{Var}[|h_0[k]|^2]/\text{E}^2\{|h_0[k]|^2\} > 0$ ) under the alternative  $\mathcal{H}_1$ .

## DETERMINISTIC APPROACH VIA ORTHONORMAL BEM

Let us decompose the vector  $\mathbf{h}_0^H \triangleq [h_0[0], \dots, h_0[K-1]]$ , which collects the coefficients of the zeroth row of  $\mathbf{H}$ , as  $\mathbf{h}_0 = \|\mathbf{h}_0\|_2 \tilde{\mathbf{h}}_0$ , or equivalently,  $\gamma = \|\gamma\|_1 \tilde{\gamma}$ , where  $\|\tilde{\gamma}\|_1 = \tilde{\gamma}^T \mathbf{1} = 1$ . Noting that in the low-SNR scenario ( $\|\gamma\|_1 \ll 1$ ) the quadratic term in (4.23) is negligible allows us to write

$$\Psi(a, \mathbf{c}, \|\gamma\|_1, \tilde{\gamma}) \approx 1 + \|\gamma\|_1 (a^2 \mathbf{c} - \mathbf{1})^T \tilde{\gamma}. \quad (4.30)$$

To capture the structure present in the time-variations of the channel, assume that  $\mathbf{h}_0$  follows a BEM with unknown deterministic parameters. Specifically, suppose that  $\tilde{\mathbf{h}}_0$  is given by  $\tilde{\mathbf{h}}_0 = \mathbf{B}_0 \tilde{\alpha}_0$ , where  $\mathbf{B}_0$  has orthonormal columns and  $\tilde{\alpha}_0$  is an unknown deterministic vector satisfying  $\|\tilde{\alpha}_0\|_2 = 1$ . To maximize  $\Psi$  with respect to  $\tilde{\alpha}_0$ , note that

$$\Psi(a, \mathbf{c}, \|\gamma\|_1, \tilde{\gamma}) \propto \mathbf{c}^T \tilde{\gamma} = \tilde{\alpha}_0^H \mathbf{B}_0^H \mathbf{C} \mathbf{B}_0 \tilde{\alpha}_0, \quad (4.31)$$

where  $\mathbf{C} = \text{diag}(\mathbf{c})$ . Thus, we can see that our problem reduces to the maximization of the correlation between the sequences of normalized *instantaneous power* observations  $c[k]$  and the instantaneous SNR  $\gamma[k]$ , which resembles the idea of subspace matched detectors [Scharf, 1991]. Clearly, the maximizer of (4.31) with respect to  $\tilde{\alpha}_0$  is given by the principal eigenvector of  $\mathbf{B}_0^H \mathbf{C} \mathbf{B}_0$ , and results in the test statistic

$$\mathcal{T}_{\text{EV}}(\mathbf{c}) = \lambda_{\max}(\mathbf{B}_0^H \mathbf{C} \mathbf{B}_0). \quad (4.32)$$



Note that this test decides  $\mathcal{H}_1$  for large values of  $\mathcal{T}_{\text{EV}}$  and, in the limiting case with no temporal channel structure (with  $\mathbf{B}_0$  a complete basis), the statistic reduces to the largest element of  $\mathbf{c}$ .

### 4.3 Detectors for Multiantenna Sensors

In this section, we rely on a BEM with unknown deterministic coefficients to derive a GLR detector. It will be shown that such a detector cannot properly operate if the channel has no structure, and alternative schemes will be discussed for such a scenario.

#### 4.3.1 Generalized Likelihood Ratio Test

In the BEM adopted in this section, a different collection of coefficients captures the time variations of the channel at each antenna [Ma and Giannakis, 2002]. That is, if  $\mathbf{h}_m^H$  denotes the  $m$ -th row of  $\mathbf{H}$ , we apply the expansion

$$\mathbf{h}_m = \sum_{b=0}^{B-1} \beta_b \alpha_{b,m}, \quad (4.33)$$

where  $\beta_b \in \mathbb{C}^K$  is the  $b$ -th basis vector and  $\alpha_{b,m}$  is the corresponding coefficient, regarded as an unknown deterministic parameter. Expression (4.33) can also be written as  $\mathbf{h}_m = \mathbf{B}_0 \boldsymbol{\alpha}_m$ , where  $\mathbf{B}_0 = [\beta_0, \beta_1, \dots, \beta_{B-1}] \in \mathbb{C}^{K \times B}$  and  $\boldsymbol{\alpha}_m = [\alpha_{0,m}, \alpha_{1,m}, \dots, \alpha_{B-1,m}]^T \in \mathbb{C}^B$  or, more compactly, as  $\mathbf{H}^H = \mathbf{B}_0 \mathbf{A}$ , where  $\mathbf{A} = [\boldsymbol{\alpha}_0, \boldsymbol{\alpha}_1, \dots, \boldsymbol{\alpha}_{M-1}] \in \mathbb{C}^{B \times M}$ . The GLR statistic can therefore be written as

$$\mathcal{G}(\mathbf{y}) = \frac{\sup_{\mathbf{A}, \sigma^2 \geq 0} p_{\mathcal{H}_1}(\mathbf{y}; \mathbf{A}, \sigma^2)}{\sup_{\sigma^2 \geq 0} p_{\mathcal{H}_0}(\mathbf{y}; \sigma^2)}. \quad (4.34)$$

It can be easily seen that the maximizer of the denominator, i.e., the ML estimate of  $\sigma^2$  under  $\mathcal{H}_0$ , is given by  $\hat{\sigma}^2 = (MK)^{-1} \|\mathbf{y}\|^2 = (MK)^{-1} \text{Tr}(\mathbf{Y}\mathbf{Y}^H)$ . On the other hand, the maximizers of the numerator, i.e., the ML estimates of  $\mathbf{A}$  and  $\sigma^2$  under  $\mathcal{H}_1$ , cannot be obtained in closed-form, to the best of our knowledge. For this reason, we next consider an EM method capable of computing the pair  $\theta \triangleq (\mathbf{A}, \sigma^2)$  numerically.

### 4.3.2 EM algorithm

The EM algorithm is an iterative method proposed by Dempster *et al.* [Dempster et al., 1977] for the numerical computation of ML estimates. It enjoys, as its most appealing property, local convergence. Moreover, as opposed to methods like gradient descent, no parameter needs to be tuned. The key observation is that optimizing the numerator of (4.34) with respect to  $\theta$  would be much easier if we knew the transmitted sequence  $\mathbf{x}$ . We thus may form the so-called *complete data* vector  $\mathbf{z}$ :

$$\mathbf{z} \triangleq \begin{bmatrix} \mathbf{x} \\ \mathbf{y} \end{bmatrix} = \begin{bmatrix} \mathbf{0}_K & \mathbf{I}_K \\ \mathbf{I}_{MK} & \mathbf{G} \end{bmatrix} \begin{bmatrix} \mathbf{w} \\ \mathbf{x} \end{bmatrix}. \quad (4.35)$$

This vector is clearly Gaussian distributed with probability density function

$$p(\mathbf{z}; \theta) = \frac{\exp \{-\mathbf{z}^H \boldsymbol{\Xi}_z^{-1} \mathbf{z}\}}{\pi^{K(M+1)} |\boldsymbol{\Xi}_z|}, \quad (4.36)$$

where

$$\boldsymbol{\Xi}_z \triangleq \mathbb{E} \{\mathbf{z} \mathbf{z}^H\} = \begin{bmatrix} \mathbf{I}_K & \mathbf{G}^H \\ \mathbf{G} & \sigma^2 \mathbf{I}_{MK} + \mathbf{G} \mathbf{G}^H \end{bmatrix}. \quad (4.37)$$

Note that  $p(\mathbf{z}; \theta)$  is clearly related to the numerator of (4.34) via

$$\int p(\mathbf{z}; \theta) d\mathbf{x} = p_{\mathcal{H}_1}(\mathbf{y}; \theta). \quad (4.38)$$

Given a guess  $\underline{\theta}$  for the vector of true parameters, every iteration of the EM algorithm obtains a refined estimate  $\theta_*$  as  $\theta_* = \arg \sup_{\theta} J(\theta | \underline{\theta})$  (maximization step), where  $J(\theta | \underline{\theta}) \triangleq \mathbb{E} \{\log p(\mathbf{z}; \theta) | \mathbf{y}; \underline{\theta}\}$  (expectation step). This procedure is repeated by taking the output  $\theta_*$  of each iteration as the input  $\underline{\theta}$  of the next one. In the sequel, we will describe the operations performed in each iteration using the *under-bar* notation to represent the input parameters and the asterisk notation to represent the output parameters.

#### EXPECTATION STEP

In view of (4.36), it is clear that the expectation in  $J(\theta | \underline{\theta})$  can be expanded as

$$J(\theta | \underline{\theta}) = -K(M+1) \log \pi - \log |\boldsymbol{\Xi}_z| - \mathbb{E} \{\mathbf{z}^H \boldsymbol{\Xi}_z^{-1} \mathbf{z} | \mathbf{y}; \underline{\theta}\}. \quad (4.39)$$

On the other hand, using the properties of the Schur complement [Bernstein, 2009] we find that  $|\Xi_z| = \sigma^{2MK}$  and

$$\Xi_z^{-1} = \frac{1}{\sigma^2} \begin{bmatrix} \sigma^2 \mathbf{I}_K + \mathbf{G}^H \mathbf{G} & -\mathbf{G}^H \\ -\mathbf{G} & \mathbf{I}_{MK} \end{bmatrix}. \quad (4.40)$$

Combining these expressions we obtain, after some algebra,

$$J(\theta|\theta) \propto -MK \log \sigma^2 - \frac{\text{Tr}(\mathbf{G}^H \mathbf{G} \Upsilon_{x|y}) - 2 \text{Re} \left\{ \boldsymbol{\mu}_{x|y}^H \mathbf{G}^H \mathbf{y} \right\} + \mathbf{y}^H \mathbf{y}}{\sigma^2} \quad (4.41)$$

where  $\Upsilon_{x|y} = \text{E} \{ \mathbf{x} \mathbf{x}^H | \mathbf{y}, \theta \}$  and  $\boldsymbol{\mu}_{x|y} = \text{E} \{ \mathbf{x} | \mathbf{y}, \theta \}$ . Since  $\mathbf{w}$  and  $\mathbf{x}$  are independent and thus jointly Gaussian, the values of  $\Upsilon_{x|y}$  and  $\boldsymbol{\mu}_{x|y}$  can be easily computed using (4.35) and [Kay, 1993, Sec. 10.5]; on the one hand,

$$\boldsymbol{\mu}_{x|y} = \mathbf{G}^H (\sigma^2 \mathbf{I}_{MK} + \mathbf{G} \mathbf{G}^H)^{-1} \mathbf{y}. \quad (4.42)$$

Applying the matrix inversion lemma [Bernstein, 2009], it follows that

$$(\sigma^2 \mathbf{I}_M + \underline{\mathbf{g}}[k] \underline{\mathbf{g}}^H[k])^{-1} = \frac{1}{\sigma^2} \left[ \mathbf{I}_M - \frac{\underline{\mathbf{g}}[k] \underline{\mathbf{g}}^H[k]}{\sigma^2 + \|\underline{\mathbf{g}}[k]\|^2} \right], \quad (4.43)$$

which means that (4.42) becomes

$$\boldsymbol{\mu}_{x|y} = (\sigma^2 \mathbf{I}_K + \mathbf{G}^H \mathbf{G})^{-1} \mathbf{G}^H \mathbf{y}. \quad (4.44)$$

For convenience, let us also define  $\mathbf{D}_{x|y} = \text{diag} \boldsymbol{\mu}_{x|y}$  and

$$\mathbf{U} = \begin{bmatrix} \mathbf{y}[0] & \mathbf{0} & \dots & \mathbf{0} \\ \mathbf{0} & \mathbf{y}[1] & \dots & \mathbf{0} \\ \vdots & \vdots & \ddots & \vdots \\ \mathbf{0} & \mathbf{0} & \dots & \mathbf{y}[K-1] \end{bmatrix}, \quad (4.45)$$

where  $\mathbf{y}[k]$  is the  $k$ -th column of  $\mathbf{Y}$ . Then, it is clear that

$$\mathbf{D}_{x|y} = (\sigma^2 \mathbf{I}_K + \mathbf{G}^H \mathbf{G})^{-1} \mathbf{G}^H \mathbf{U}. \quad (4.46)$$

On the other hand

$$\Upsilon_{x|y} = \Xi_{x|y} + \boldsymbol{\mu}_{x|y} \boldsymbol{\mu}_{x|y}^H, \quad (4.47)$$

where [Kay, 1993, Sec. 10.5]

$$\begin{aligned}\Xi_{x|y} &= \mathbb{E} \{ (x - \mu_{x|y})(x - \mu_{x|y})^H | y, \theta \} \\ &= \mathbf{I}_K - \mathbf{G}^H (\sigma^2 \mathbf{I}_{MK} + \mathbf{G}\mathbf{G}^H)^{-1} \mathbf{G},\end{aligned}\quad (4.48)$$

but, using (4.43) again, (4.48) simplifies to

$$\Xi_{x|y} = \sigma^2 (\sigma^2 \mathbf{I}_K + \mathbf{G}^H \mathbf{G})^{-1}, \quad (4.49)$$

which is much easier to compute. Finally, since the cost function  $J(\theta|\theta)$  only depends on the values on the diagonal of  $\Upsilon_{x|y}$ , we will replace this matrix with

$$\tilde{\Upsilon}_{x|y} \triangleq \Xi_{x|y} + \mathbf{D}_{x|y} \mathbf{D}_{x|y}^H, \quad (4.50)$$

which is equal to  $\Upsilon_{x|y}$  on the diagonal and zero elsewhere.

## MAXIMIZATION STEP

In this section, we shall maximize (4.41) with respect to  $\sigma^2$  and  $\mathbf{G}$ , subject to the constraints that  $\sigma^2 \geq 0$  and  $\mathbf{H} = \mathbf{A}^H \mathbf{B}_0^H$  for some  $\mathbf{A}$ . For a given  $\mathbf{G}$ , the maximizer with respect to  $\sigma^2$  is

$$\sigma_*^2 = \frac{\text{Tr}(\mathbf{G}^H \mathbf{G} \tilde{\Upsilon}_{x|y}) - 2 \text{Re} \left\{ \mu_{x|y}^H \mathbf{G}^H \mathbf{y} \right\} + \mathbf{y}^H \mathbf{y}}{MK} \quad (4.51)$$

and results in

$$\sup_{\sigma^2} Q(\theta|\theta) \propto -\text{Tr}(\mathbf{G}^H \mathbf{G} \tilde{\Upsilon}_{x|y}) + 2 \text{Re} \left\{ \mu_{x|y}^H \mathbf{G}^H \mathbf{y} \right\}, \quad (4.52)$$

which, denoting the  $m$ -th row of  $\mathbf{Y}$  by  $\mathbf{y}_m^H$ , can be expressed as

$$\sup_{\sigma^2} Q(\theta|\theta) \propto - \sum_{m=0}^{M-1} \left[ \mathbf{h}_m^H \tilde{\Upsilon}_{x|y} \mathbf{h}_m - 2 \text{Re} \left\{ \mathbf{y}_m^H \mathbf{D}_{x|y}^H \mathbf{h}_m \right\} \right]. \quad (4.53)$$

Recalling that  $\mathbf{h}_m = \mathbf{B}_0 \alpha_m$  enables us to rewrite the right hand side as

$$- \sum_{m=0}^{M-1} \left[ \alpha_m^H \mathbf{B}_0^H \tilde{\Upsilon}_{x|y} \mathbf{B}_0 \alpha_m - 2 \text{Re} \left\{ \mathbf{y}_m^H \mathbf{D}_{x|y}^H \mathbf{B}_0 \alpha_m \right\} \right]. \quad (4.54)$$

Maximizing this expression with respect to  $\alpha_m$  yields

$$\alpha_{m,*} = (B_0^H \tilde{\Upsilon}_{x|y} B_0)^{-1} B_0^H D_{x|y} y_m \quad (4.55)$$

or, alternatively,

$$A_* = (B_0^H \tilde{\Upsilon}_{x|y} B_0)^{-1} B_0^H D_{x|y} Y^H. \quad (4.56)$$

The resulting EM method is summarized as Algorithm 4.1.

---

**Algorithm 4.1** Expectation-Maximization

---

```

Initialize  $\sigma^2$  and  $\underline{H}$ 
while stopping_criterion==FALSE do
  • E-STEP:
     $D_{x|y} = (\sigma^2 \mathbf{I}_K + \underline{G}^H \underline{G})^{-1} \underline{G}^H U$ 
     $\tilde{\Upsilon}_{x|y} = \sigma^2 (\sigma^2 \mathbf{I}_K + \underline{G}^H \underline{G})^{-1} + D_{x|y} D_{x|y}^H$ 
  • M-STEP:
     $H_* = Y D_{x|y}^H B_0 (B_0^H \tilde{\Upsilon}_{x|y} B_0)^{-1} B_0^H$ 
     $\sigma_*^2 = \frac{1}{MK} \text{Tr} \left( \underline{G}^H \underline{G} \tilde{\Upsilon}_{x|y} - 2 \text{Re} \left\{ D_{x|y}^H \underline{G}^H U \right\} + U^H U \right)$ 
  • UPDATE:
     $\sigma^2 \leftarrow \sigma_*^2$ 
     $\underline{H} \leftarrow H_*$ 
end while
```

---

## INITIALIZATION

The EM iteration presented above can be initialized in a number of different ways. Fortunately, we have observed in all our experiments that the detection performance does not depend meaningfully on the particular choice among those described next.

One possibility arises by assuming that  $\mathbf{X} = \mathbf{I}_K$ , which implies that the minimum-variance unbiased estimate for  $\mathbf{A}$  is given by  $\hat{\mathbf{A}} = (B_0^H B_0)^{-1} B_0^H \mathbf{Y}^H$ . A different option is to assume that the channel is time invariant: if  $\beta_0 \propto \mathbf{1}_K$ , then  $\mathbf{A}$  is of the form  $\mathbf{A} = [\alpha_0, \mathbf{0}, \dots, \mathbf{0}]^H$ , which implies that the ML estimate of  $\alpha_0$  is given by  $\hat{\alpha}_0 = v \cdot \mathbf{v}$ , where  $v$  is a constant depending on the trace and largest eigenvalue of the spatial sample covariance matrix  $\hat{\mathbf{S}} \triangleq \mathbf{Y} \mathbf{Y}^H / K$  and  $\mathbf{v}$  is the principal eigenvector [Besson et al., 2006, Taherpour et al., 2010, Wang et al., 2010].

As an initial value for  $\sigma^2$ , it seems reasonable to take

$$\underline{\sigma}^2 = \max \left[ \epsilon, \frac{\|\mathbf{Y}\|_F^2 - \|\mathbf{B}_0 \mathbf{A}\|_F^2}{MK} \right], \quad (4.57)$$

where  $\epsilon$  is a small positive constant, required to avoid negative variance estimates.

### 4.3.3 Rapidly-changing Channels

Let us consider the scenario where the channel has no known structure to exploit, which occurs for instance when  $B = K$  in the BEM above. In that case, we have the following result:

**PROPOSITION 4.1.** *Let  $M > 1$ . If the channel is deterministic with no structure, that is, the only information available about  $\mathbf{H}$  is that it is contained in  $\mathbb{C}^{M \times K}$ , then, with probability one, the ML estimates of  $\mathbf{g}[k]$  and  $\sigma^2$  under hypothesis  $\mathcal{H}_1$  satisfy*

$$\|\hat{\mathbf{g}}[k]\|^2 = \|\mathbf{y}[k]\|^2, \quad k = 0, \dots, K-1, \quad (4.58)$$

$$\hat{\sigma}^2 = 0 \quad (4.59)$$

and the GLR statistic becomes  $\mathcal{G}(\mathbf{y}) = \infty$ .

*Proof.* See Appendix 4.A. □

Consequently, in such a case the GLR test decides  $\mathcal{H}_1$  with probability one irrespective of the observations, which renders this detector useless. However, this phenomenon is not exclusive to the case without structure: it takes place, for example, whenever we use our multiantenna BEM and  $B$  is large enough. To see that, we note that the same arguments used to establish Proposition 4.1 (see Appendix 4.A) can be used to conclude that the GLR statistic becomes infinite when  $M > 1$  and the channel structure is such that the expression

$$\|\mathbf{y}[k]\|^2 = \sigma^2 + \|\mathbf{g}[k]\|^2 \quad (4.60)$$

is satisfied for some  $\sigma^2 \geq 0$  and some candidate channel matrix  $\mathbf{G}$  as in (4.4). To show that this is possible even for  $B < K$ , let us invoke the well-known *Fejer-Riesz spectral factorization theorem* [Papoulis, 1977]:

**THEOREM 4.1.** *Let  $\tilde{B}$  be a nonnegative integer and let*

$$V(e^{j\omega}) \triangleq \sum_{k=-2\tilde{B}}^{2\tilde{B}} v[k] e^{-j\omega k} \quad (4.61)$$

be a function taking nonnegative values in  $0 \leq \omega < 2\pi$ . Then, there exists a function

$$\tilde{H}(e^{j\omega}) = \sum_{b=-\tilde{B}}^{\tilde{B}} \tilde{h}[b] e^{-j\omega b} \quad (4.62)$$

such that  $V(e^{j\omega}) = |\tilde{H}(e^{j\omega})|^2$  for all  $\omega$ .

Let  $\sigma^2$  be such that  $\|\mathbf{y}[k]\|^2 - \sigma^2 \geq 0$  for all  $k$  and assume that there exist  $M$  nonnegative functions of the form

$$V_m(e^{j\omega}) \triangleq \sum_{k=-2\tilde{B}}^{2\tilde{B}} v_m[k] e^{-j\omega k} \quad (4.63)$$

satisfying

$$\|\mathbf{y}[k]\|^2 - \sigma^2 = \sum_{m=0}^{M-1} V_m(e^{j\frac{2\pi}{K}k}) \quad (4.64)$$

for  $k = 0, \dots, K-1$ . Then, according to Theorem 4.1, there exist  $M$  functions

$$\tilde{H}_m(e^{j\omega}) = \sum_{b=-\tilde{B}}^{\tilde{B}} \tilde{h}_m[b] e^{-j\omega b}, \quad m = 0, \dots, M-1 \quad (4.65)$$

satisfying that  $|\tilde{H}_m(e^{j\omega})|^2 = V_m(e^{j\omega})$  for all  $\omega$  and, in particular,  $|\tilde{H}_m(e^{j\frac{2\pi}{K}k})|^2 = V_m(e^{j\frac{2\pi}{K}k})$  for  $k = 0, \dots, K-1$ . In that case, (4.64) becomes

$$\|\mathbf{y}[k]\|^2 - \sigma^2 = \sum_{m=0}^{M-1} |\tilde{H}_m(e^{j\frac{2\pi}{K}k})|^2. \quad (4.66)$$

Now recall that  $\mathbf{g}[k] \triangleq [(\mathbf{H})_{0,k}, \dots, (\mathbf{H})_{M-1,k}]^T$ . Thus, if there exists a candidate channel matrix  $\mathbf{H}$  satisfying  $(\mathbf{H})_{m,k} = \tilde{H}_m^*(e^{j\frac{2\pi}{K}k})$ , the condition (4.60) holds and the GLR becomes infinite. As shown next, this is possible when  $\mathbf{H}$  follows a BEM  $\mathbf{H}^H = \mathbf{B}_0 \mathbf{A}$  if  $\mathbf{B}_0$  contains the  $B = 2\tilde{B} + 1$  columns of the Fourier matrix with lowest frequencies (see (3.7) and (3.8)). In that

case, we find that

$$\begin{aligned}
(\mathbf{H})_{m,k}^* &= \frac{1}{\sqrt{K}} \left[ e^{-j\frac{2\pi}{K}\tilde{B}k} \alpha_{\tilde{B}+1,m} + e^{-j\frac{2\pi}{K}(\tilde{B}-1)k} \alpha_{\tilde{B}+2,m} + \dots + e^{-j\frac{2\pi}{K}k} \alpha_{B-1,m} \right. \\
&\quad \left. + \alpha_{0,m} + e^{j\frac{2\pi}{K}k} \alpha_{1,m} + e^{j\frac{2\pi}{K}2k} \alpha_{2,m} + \dots + e^{j\frac{2\pi}{K}\tilde{B}k} \alpha_{\tilde{B},m} \right] \\
&= \sum_{b=1}^{\tilde{B}} \frac{\alpha_{B-b,m}}{\sqrt{K}} e^{-j\frac{2\pi}{K}bk} + \sum_{b=-\tilde{B}}^0 \frac{\alpha_{-b,m}}{\sqrt{K}} e^{-j\frac{2\pi}{K}bk}.
\end{aligned} \tag{4.67}$$

Comparing (4.65) and (4.67), it follows that one can obtain  $\tilde{H}_m^*(e^{j\frac{2\pi}{K}k}) = (\mathbf{H})_{m,k}$  by setting

$$(\mathbf{A})_{b,m} = \alpha_{b,m} = \begin{cases} \sqrt{K} \cdot \tilde{h}_m[-b] & \text{if } b = 0, \dots, \tilde{B} \\ \sqrt{K} \cdot \tilde{h}_m[B-b] & \text{if } b = \tilde{B} + 1, \dots, B-1. \end{cases} \tag{4.68}$$

To sum up, when the nonnegative functions  $V_m(e^{j\omega})$  satisfying (4.64) exist, the condition (4.60) is satisfied and  $\mathcal{G}(\mathbf{y}) = \infty$ . Thus, the question is under which conditions the  $V_m(e^{j\omega})$  exist. Clearly, they exist with nonzero probability whenever  $4\tilde{B} + 1 = 2B - 1 \geq K$ , which amounts to saying that  $B \geq (K+1)/2$ . As seen in Proposition 4.1, they exist with probability one if  $B = K$ . In between these two values, these functions exist with a certain nonzero probability, whereas for  $B < (K+1)/2$  they exist with probability zero. Since the existence of those functions is not, in principle, connected with the presence of a primary user, this effect is detrimental for the detection performance, which discourages the use of the GLR test for channels with little or no structure. In other words, the GLR test can only properly exploit the structure of the channel if it is sufficiently *parsimonious*, but not if the channel is unstructured or, equivalently, rapidly-changing. Devising detectors for this class of channels requires further research in this direction, which we leave as a future line.

In this regard, we point out that possible approaches to activity detection when the channel structure is completely unknown may consider applying tests for homogeneity of covariance: note that, if  $\mathbf{H}$  is assumed deterministic, the covariance matrices of the columns of  $\mathbf{Y}$  in (4.2) are all the same under  $\mathcal{H}_0$ , while they differ under  $\mathcal{H}_1$ . Thus, the presence of a primary signal may be detected by looking at this feature. Although we will not embark in the task of applying those tests to activity detection, in the Appendix we move a step forward in this research direction by deriving (locally) optimal invariant tests for homogeneity of covariance. As mentioned earlier, this class of tests may be of paramount importance in practical applications. Other tests that can be used in this context are also reviewed in the Appendix.



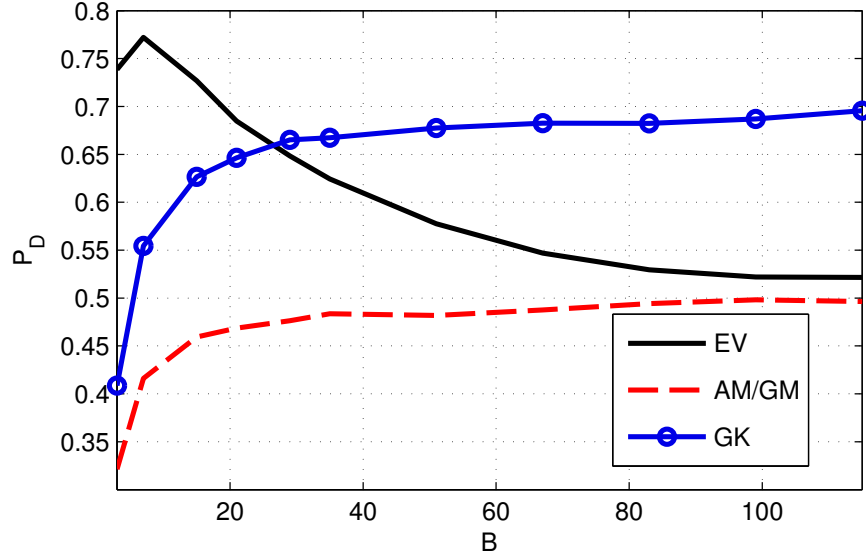


Figure 4.1: Probability of detection *vs.* the number of basis functions used in the BEM model when  $P_{FA} = 0.10$  ( $K = 128$ ,  $\gamma = 0$  dB).

## 4.4 Simulation Results

In this section, we provide a Monte Carlo simulation study that illustrates the performance of the proposed methods. The transmitted signal and the noise samples are generated as described in Section 4.1. On the other hand, the channel is generated using the BEM model from Section 4.3.1, where  $\mathbf{h}_m = \mathbf{B}_0 \boldsymbol{\alpha}_m$ . The basis matrix  $\mathbf{B}_0$  is composed of the  $B$  columns with lowest frequency in the unitary Fourier matrix (see (3.7)), which results in a Doppler spread of  $\omega_d = \frac{B-1}{2} \frac{2\pi}{K}$ . The coordinate vectors  $\boldsymbol{\alpha}_m$  are generated as independent random vectors with distribution  $\boldsymbol{\alpha}_m \sim \mathcal{CN}(\mathbf{0}, \eta_0^2 \frac{K}{B} \mathbf{I}_B)$ , which implies that  $\mathbf{h}_m$  is Rayleigh. Since

$$\mathbb{E} \{ \|\mathbf{H}\mathbf{X}\|_F^2 \} = \mathbb{E} \{ \text{Tr}(\mathbf{A}^H \mathbf{B}_0^H \mathbf{X} \mathbf{X}^H \mathbf{B}_0 \mathbf{A}) \} \quad (4.69a)$$

$$= \mathbb{E} \{ \text{Tr}(\mathbf{B}_0^H \mathbf{X} \mathbf{X}^H \mathbf{B}_0 \mathbf{A} \mathbf{A}^H) \} \quad (4.69b)$$

$$= \frac{\eta_0^2 K M}{B} \text{Tr}(\mathbf{B}_0^H \mathbf{I}_K \mathbf{B}_0 \mathbf{I}_B) \quad (4.69c)$$

$$= \eta_0^2 K M, \quad (4.69d)$$

the average SNR per antenna is given by

$$\gamma \triangleq \frac{\mathbb{E} \{ \|\mathbf{H}\mathbf{X}\|_F^2 \}}{\mathbb{E} \{ \|\mathbf{W}\|_F^2 \}} = \frac{\eta_0^2 K M}{\sigma^2 K M} = \frac{\eta_0^2}{\sigma^2}. \quad (4.70)$$

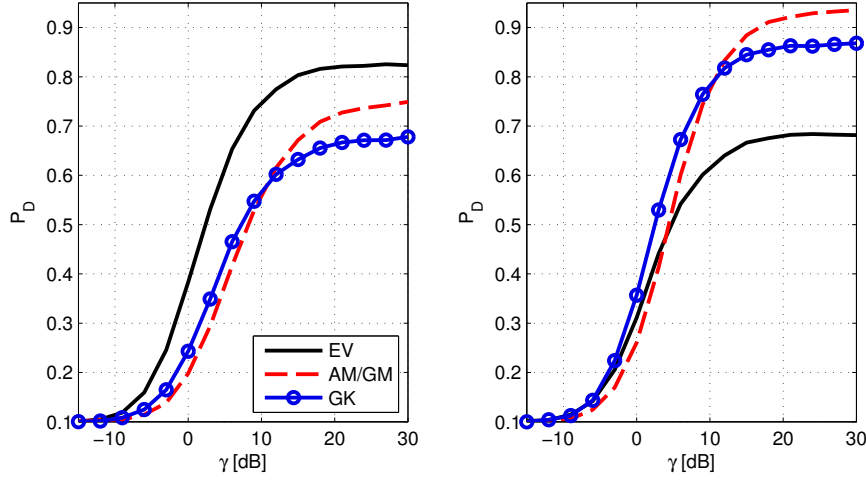


Figure 4.2: Probability of detection *vs.* SNR when  $P_{\text{FA}} = 0.10$ . On the left, the number of basis functions  $B$  is set to 3, whereas on the right it is set to 32 ( $K = 32$ ).

In order for our results to be as general as possible, a different  $\mathbf{H}$  is generated at every Monte Carlo run. This operation does not affect the probability of false alarm and naturally averages the probability of detection over the different realizations of the channel.

We first perform a few simple experiments to assess the performance of the AM/GM, GK and EV detectors from Section 4.2. Note that, among these detectors, only EV requires the knowledge of  $B$ ; the others assume that the channel is fast-varying. Figure 4.1 depicts the probability of detection *vs.* the number of basis functions  $B$  when  $P_{\text{FA}} = 0.1$ . As expected, both the GK and AM/GM detectors improve for larger Doppler spreads. On the other hand, the EV is negatively affected by fast variations of the channel. Interestingly, for a large Doppler spread, the probability of detection for AM/GM and EV is roughly the same, but both detectors are outperformed by GK: this effect can be intuitively explained by noting that the product of two Gaussian distributed random variables — in particular  $h$  and  $x$  — is leptokurtic and GK exploits precisely this feature (see Section 4.2.2).

Another interesting effect is observed in Figure 4.2, which represents the probability of detection *vs.* the SNR for fixed  $P_{\text{FA}} = 0.1$  and two values of  $B$ . For large SNR, the EV detector shows the highest  $P_D$  when the channel is slow-varying ( $B = 3$ ), as seen in the left panel; while the situation is reversed when the channel is fast-varying ( $B = 32$ ), as seen in the right panel. On the other hand, the superiority of EV and GK, which assume low  $\gamma$ , is manifest in the low-SNR regime. Finally, it is also noted that  $P_D$  is bounded away from 1 even when the SNR approaches infinity. To elucidate this effect, in Figure 4.3 we represent  $P_D$  *vs.*  $K$  and  $B$  for fixed  $P_{\text{FA}} = 0.1$  and  $K = B$ , which corresponds to rapidly-changing channels. The SNR was chosen

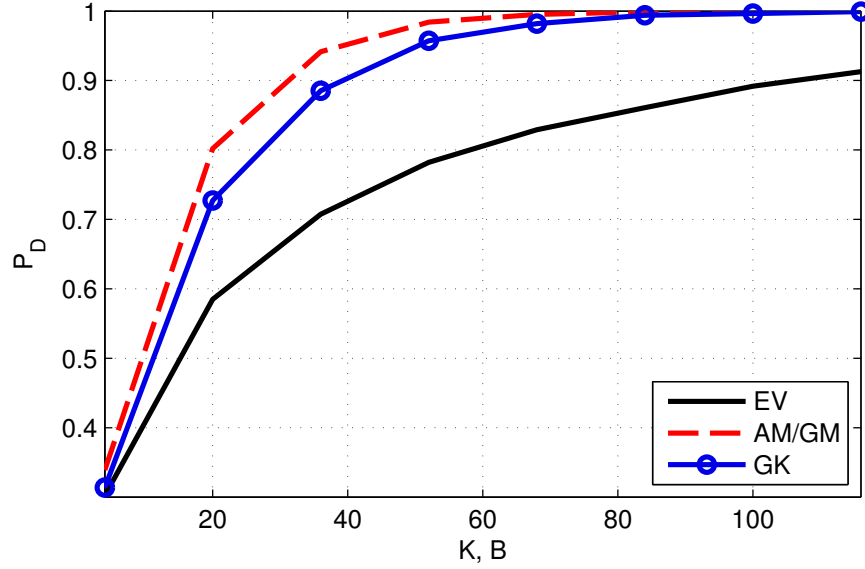
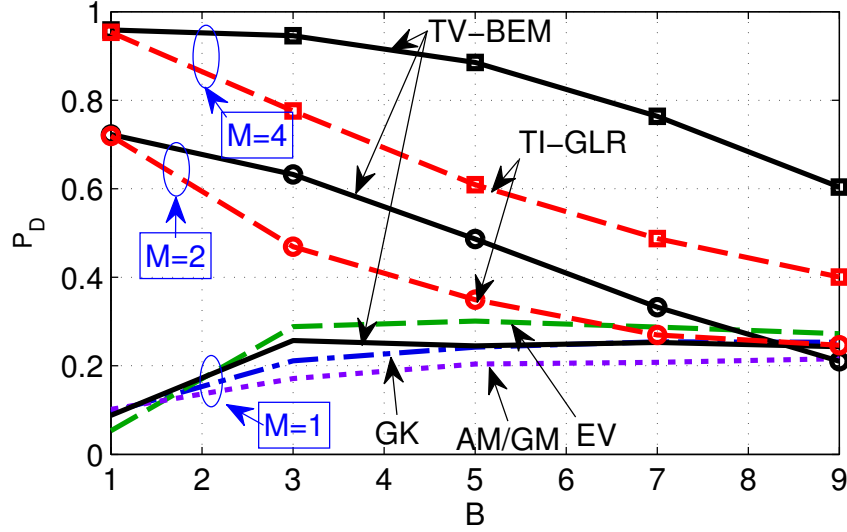
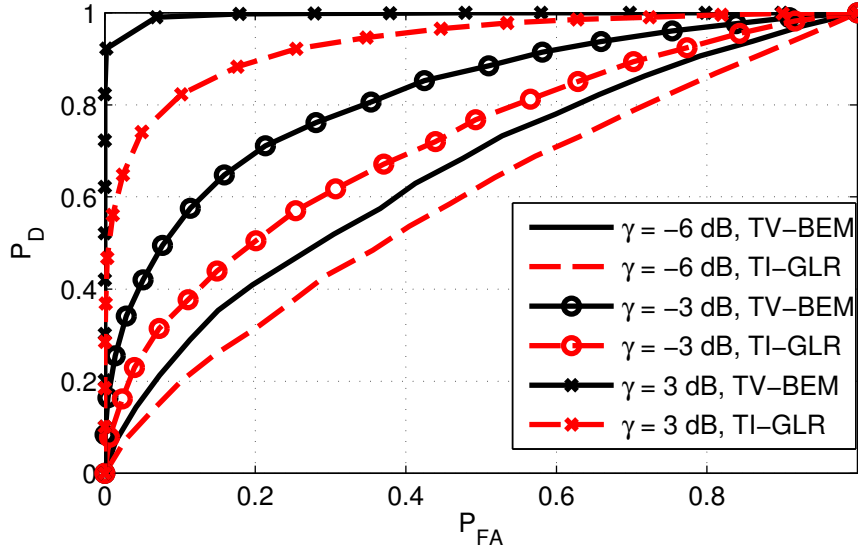


Figure 4.3: Performance of the proposed detectors *vs.* the number of samples  $K$  and basis functions  $B$  when  $P_{FA} = 0.10$  and  $K = B$  ( $\gamma = 20$  dB).

high so that the curves are close to their asymptotic forms in the high-SNR regime. In view of this figure, we conclude that  $P_D$  will not approach 1 unless the data record is long enough. This can be interpreted from the perspective of homogeneity of covariance mentioned earlier: it is not possible to reliably decide whether a collection of samples have the same variance if we do not observe a sufficiently large number of them.

To appreciate the advantages of using multiple antennas, in Figure 4.4, we show the probability of detection *vs.*  $B$  for different numbers of antennas. The GLR detector from Section 4.3, denoted as TV-GLR, is compared with the detectors from Section 4.2 and the GLR detector for time-invariant channels from [Besson et al., 2006, Taherpour et al., 2010, Wang et al., 2010], denoted as TI-GLR. We observe that, when  $B > 1$ , the time variations of the channel are successfully exploited by the TV-GLR detector, which moreover attains the same performance as TI-GLR when the channel is time-invariant ( $B = 1$ ) as a result of the exploitation of the spatial structure. Note that in the single antenna case ( $M = 1$ ), the detector from Section 4.3, which is the GLR detector for this scenario, does not necessarily perform better than all the detectors from Section 4.2.

Finally, Figure 4.5 shows the ROC of the TV-GLR and TI-GLR detectors when  $K = 20$  samples,  $M = 4$  antennas and  $B = 5$  basis vectors, for three different SNR values. It is observed that a significant improvement arises from exploiting the time variations of the channel.

Figure 4.4:  $P_D$  for fixed  $P_{FA} = 0.10$  ( $K = 20$ ,  $\gamma = 0$  dB).Figure 4.5: Receiver Operating Characteristics ( $K = 20$ ,  $M = 4$ ,  $B = 5$ ).

## 4.5 Conclusions

We have presented several methods to detect the presence of Gaussian signals observed in noise of unknown power after passing a time-varying channel. For single-antenna sensors, we considered the GLR detector for channels with no structure, which results in the well known AM/GM test, and we sought an optimal test within the family of tests invariant to positive scalings, which turned out not to exist. However, we used the likelihood ratio of the maximal invariant statistic to propose, based on Bayesian and ML criteria, two additional detectors. For multiantenna sensors, we adopted a BEM for the channel coefficients and derived the GLR test, which requires the solution of a non-convex problem. An EM algorithm was proposed to solve that problem numerically. We also showed that the GLR test cannot be used with channels without structure or, in general, for rapidly-changing channels. In those cases, one must resort to alternative schemes, such as the tests for homogeneity of covariances considered in the Appendix. Finally, we analyzed the performance of the proposed detectors via Monte Carlo simulation, which revealed the convenience of exploiting the time variations of the channel.

This work was presented in part in the *IEEE Statistical Signal Processing Workshop (SSP 2012)* [Romero et al., 2012b] and in the *14th IEEE International Workshop on Signal Processing Advances for Wireless Communications (SPAWC 2013)* [Romero and López-Valcarce, 2013].

## 4.A Proof of Proposition 4.1

The GLR statistic is given by

$$\mathcal{G}(\mathbf{y}) = \frac{\sup_{\mathbf{G}, \sigma^2 \geq 0} p_{\mathcal{H}_1}(\mathbf{y}; \mathbf{G}, \sigma^2)}{\sup_{\sigma^2 \geq 0} p_{\mathcal{H}_0}(\mathbf{y}; \sigma^2)}. \quad (4.71)$$

It can be readily seen that the denominator takes, with probability one, a positive finite value. From (4.5) and (4.6), it follows that

$$p_{\mathcal{H}_1}(\mathbf{y}; \mathbf{G}, \sigma^2) = \prod_{k=0}^{K-1} \frac{\exp \{ -\mathbf{y}^H[k] \boldsymbol{\Xi}^{-1}[k] \mathbf{y}[k] \}}{\pi^M |\boldsymbol{\Xi}[k]|}, \quad (4.72)$$

where  $\boldsymbol{\Xi}[k] = \mathbf{g}[k] \mathbf{g}^H[k] + \sigma^2 \mathbf{I}_M$ . Using [Bernstein, 2009, Fact 2.16.3], we find that

$$|\boldsymbol{\Xi}[k]| = \sigma^{2M} \left( 1 + \frac{\|\mathbf{g}[k]\|^2}{\sigma^2} \right). \quad (4.73)$$

From (4.72), (4.43) and (4.73) it follows that

$$-\log p_{\mathcal{H}_1}(\mathbf{y}; \mathbf{G}, \sigma^2) = -\sum_{k=0}^{K-1} \log \frac{\exp \{ -\mathbf{y}^H[k] \mathbf{\Xi}^{-1}[k] \mathbf{y}[k] \}}{\pi^M |\mathbf{\Xi}[k]|} \quad (4.74a)$$

$$= \sum_{k=0}^{K-1} \mathbf{y}^H[k] \mathbf{\Xi}^{-1}[k] \mathbf{y}[k] + M \log \pi + \log(|\mathbf{\Xi}[k]|) \quad (4.74b)$$

$$= \sum_{k=0}^{K-1} \frac{\|\mathbf{y}[k]\|^2}{\sigma^2} - \frac{|\mathbf{y}^H[k] \mathbf{g}[k]|^2}{\sigma^2(\sigma^2 + \|\mathbf{g}[k]\|^2)} + M \log \pi \\ + M \log(\sigma^2) + \log \left( 1 + \frac{\|\mathbf{g}[k]\|^2}{\sigma^2} \right) \quad (4.74c)$$

Let us decompose  $\mathbf{g}[k] = u_k \tilde{\mathbf{g}}[k]$ , where  $\tilde{\mathbf{g}}[k]$  satisfies  $\|\tilde{\mathbf{g}}[k]\| = 1$  and  $u_k$  is real and non-negative. Then, (4.74c) can be rewritten as

$$-\log p_{\mathcal{H}_1}(\mathbf{y}; \{\tilde{\mathbf{g}}[k]\}_k, \{u_k\}_k, \sigma^2) = \sum_{k=0}^{K-1} \frac{\|\mathbf{y}[k]\|^2}{\sigma^2} - \frac{u_k^2 |\mathbf{y}^H[k] \tilde{\mathbf{g}}[k]|^2}{\sigma^2(\sigma^2 + u_k)} + M \log \pi \\ + M \log(\sigma^2) + \log \left( 1 + \frac{u_k}{\sigma^2} \right). \quad (4.75)$$

The minimizer of (4.75) with respect to  $\tilde{\mathbf{g}}[k]$  is clearly given by

$$\hat{\mathbf{g}}[k] = \frac{\mathbf{y}[k]}{\|\mathbf{y}[k]\|} \quad (4.76)$$

and results in

$$-\log p_{\mathcal{H}_1}(\mathbf{y}; \{\hat{\mathbf{g}}[k]\}_k, \{u_k\}_k, \sigma^2) = \sum_{k=0}^{K-1} \frac{\|\mathbf{y}[k]\|^2}{\sigma^2} - \frac{u_k^2 \|\mathbf{y}[k]\|^2}{\sigma^2(\sigma^2 + u_k)} + M \log \pi \\ + M \log(\sigma^2) + \log \left( 1 + \frac{u_k}{\sigma^2} \right) \quad (4.77a)$$

$$= \sum_{k=0}^{K-1} \frac{\|\mathbf{y}[k]\|^2}{\sigma^2 + u_k} + M \log \pi + M \log(\sigma^2) + \log \left( 1 + \frac{u_k}{\sigma^2} \right). \quad (4.77b)$$

Setting the derivative of this expression with respect to  $u_k$  equal to zero gives the condition

$$\|\mathbf{y}[k]\|^2 = \sigma^2 + u_k, \quad (4.78)$$

and noting that each term in the sum of (4.77b) is decreasing for  $u_k < \|\mathbf{y}[k]\|^2 - \sigma^2$ , implies that the ML estimate of  $u_k$  is given by

$$\hat{u}_k = \max(0, \|\mathbf{y}[k]\|^2 - \sigma^2), \quad k = 0, \dots, K-1. \quad (4.79)$$

Assume that  $\sigma^2 \leq \|\mathbf{y}[k]\|^2$  for all  $k$ . In that case we obtain from (4.77b) that

$$-\log p_{\mathcal{H}_1}(\mathbf{y}; \hat{\mathbf{G}}, \sigma^2) = K + KM \log \pi + K(M-1) \log(\sigma^2) + \sum_{k=0}^{K-1} \log \|\mathbf{y}[k]\|^2 \quad (4.80)$$

Since  $M > 1$  by hypothesis, it follows from (4.80) that the ML estimate of  $\sigma^2$  is  $\hat{\sigma}^2 = 0$ , which agrees with the assumption that  $\sigma^2 \leq \|\mathbf{y}[k]\|^2$  for all  $k$ . It also follows from (4.80) that the resulting GLR statistic is unbounded.





## Part II

# Spectrum Sensing in Multiple Channels



## Chapter 5

# Wideband Spectrum Sensing from Compressed Measurements

We now assume that a spectrum sensor acquires a wide frequency band comprising a large number of frequency channels, where primary users may be operating. To avoid the large cost and power consumption associated with Nyquist sampling, the received signal is acquired by means of a C-ADC (see Section 1.1.2). Based on the observation of this wideband signal, the goal is to perform power estimation and activity detection. To this end, we adopt the multi-channel model from Section 1.1.1 and the compression model from Section 1.1.2.

Starting from a Gaussian assumption — see motivation in Section 1.1.1 —, we address various spectrum sensing tasks from an ML perspective. Next, this assumption is dropped and several non-ML criteria are considered to develop estimation methods capable of working either in Gaussian or non-Gaussian scenarios.

We pursue an entirely parametric approach, where the second-order statistics of the observations follow a BEM whose expansion coefficients contain all the information of interest. The set of parameters to estimate is minimal, which favors performance, interpretability and compression. Although this formulation lends itself to the application of well-known algorithms for structured covariance estimation/covariance matching, their high complexity limits their applicability to real-world scenarios — spectrum sensors should be implementable as low-end devices where algorithms minimize their sensing and processing time, both for optimizing the exploitation of transmission opportunities and for saving energy resources [Axell et al., 2012, Zhao and Sadler, 2007]. To circumvent this limitation, we base our methods on a technique to reduce the dimension of the problem in the *covariance domain* that we present in Section 5.1. It capitalizes on the redundancy present in the covariance matrix of a wide-sense stationary process and on

the fact that most information is usually concentrated on the first few autocorrelation lags.

In Section 5.2, we review and modify some well-known structured covariance estimation algorithms so that they can work in our setting, and we exploit the aforementioned technique to propose efficient approximations that achieve similar performance at a much lower computational cost. Although the asymptotic characterization of the resulting methods is relatively simple — consistency can be established based on simple arguments —, analytic performance evaluation is intractable for finite data records. For this reason, we resort to Monte Carlo simulation in Section 5.4 in order to assess the performance of the proposed methods.

## 5.1 Wideband Spectral Estimation and Detection

We adopt the WSS signal model from Section 1.1.1 and the compression model from Section 1.1.2. Specifically, the compressed observations  $\bar{\mathbf{y}} \in \mathbb{C}^{\bar{K}}$  provided by a C-ADC were seen to be given by  $\bar{\mathbf{y}} = \Phi \mathbf{y}$ , where  $\mathbf{y} \triangleq [y[0], \dots, y[K-1]]^T$  collects the Nyquist samples of the received signal  $y$  and  $\Phi = \mathbf{I}_L \otimes \tilde{\Phi}$  is the compression matrix of the C-ADC.<sup>1</sup> The second-order statistics of  $y$  are captured by (1.14), which in this case particularizes as

$$\Xi = \sum_{b=0}^{B-1} \alpha_b \Xi_b, \quad (5.1)$$

where  $\Xi \triangleq \mathbb{E}\{\mathbf{y}\mathbf{y}^H\} \in \mathbb{C}^{K \times K}$  and  $\Xi_b \triangleq \mathbb{E}\{\mathbf{x}_b \mathbf{x}_b^H\} \in \mathbb{C}^{K \times K}$  contain the second-order statistics of  $\mathbf{y}$  and  $\mathbf{x}_b$ . The latter collects the Nyquist samples of the signal  $x_b$  transmitted by the  $b$ -th user:  $\mathbf{x}_b \triangleq [x_b[0], \dots, x_b[K-1]]^T$ . The known and linearly independent set of matrices  $\mathcal{B} = \{\Xi_0, \dots, \Xi_{B-1}\}$  is the basis of the covariance subspace, in which  $\Xi$  is equivalently represented by its non-negative coordinates  $\alpha_b$ . From (5.1), the compressed statistics are clearly related by

$$\bar{\Xi} = \Phi \Xi \Phi^H = \sum_{b=0}^{B-1} \alpha_b \bar{\Xi}_b, \quad (5.2)$$

where  $\bar{\Xi}_b = \Phi \Xi_b \Phi^H$ . We assume that  $\Phi$  is properly designed so that the set  $\bar{\mathcal{B}} = \{\bar{\Xi}_0, \dots, \bar{\Xi}_{B-1}\}$  is also linearly independent — otherwise the coordinates  $\alpha_b$  are not identifiable (see Chapter 6). Since the transmitted signals  $x_b$  are wide-sense stationary processes, the matrices  $\Xi_b$ , and consequently  $\Xi$ , are Hermitian Toeplitz (HT). Furthermore, since the  $x_b$  are power-normalized, the entries on the main diagonal of the  $\Xi_b$  equal 1.

Recall that the C-ADC individually compresses input blocks of  $N$  samples to produce

---

<sup>1</sup>Recall that the samples in  $\mathbf{y}$  do not have physical existence (see Chapter 1).

output blocks of  $\bar{N}$  samples. For convenience,  $\Xi$  is partitioned into  $N \times N$  blocks as

$$\Xi = \begin{bmatrix} \Xi[0] & \Xi^H[1] & \dots & \Xi^H[L-1] \\ \Xi[1] & \Xi[0] & \dots & \Xi^H[L-2] \\ \vdots & \vdots & \ddots & \vdots \\ \Xi[L-1] & \Xi[L-2] & \dots & \Xi[0] \end{bmatrix},$$

where  $\Xi[l] \triangleq \mathbb{E} \{ \mathbf{y}[l' + l] \mathbf{y}^H[l'] \} \forall l'$  is the covariance matrix of  $\mathbf{y}[l] \triangleq [y[lN], y[lN+1], \dots, y[lN+(N-1)]]^T$ . Similarly,  $\Xi_b$  is partitioned into the  $N \times N$  blocks  $\Xi_b[l] \triangleq \mathbb{E} \{ \mathbf{x}_b[l' + l] \mathbf{x}_b^H[l'] \} \forall l'$ , where  $\mathbf{x}_b[l] \triangleq [x_b[lN], x_b[lN+1], \dots, x_b[lN+(N-1)]]^T$ . In the compressed domain,  $\bar{\Xi}$  and  $\bar{\Xi}_b$  can be similarly partitioned into the  $\bar{N} \times \bar{N}$  blocks  $\bar{\Xi}[l] = \check{\Phi} \Xi[l] \check{\Phi}^H$  and  $\bar{\Xi}_b[l] = \check{\Phi} \Xi_b[l] \check{\Phi}^H$ , respectively. Although these blocks are not Toeplitz,  $\bar{\Xi}$  and  $\bar{\Xi}_b$  have a *block Toeplitz* structure. In addition, because all the matrices in  $\bar{\mathcal{B}}$  are assumed positive definite, the non-negativity of the coordinates  $\alpha_b$  means that  $\bar{\Xi}$  is positive definite as well.

### 5.1.1 Power Estimation and Activity Detection

In this chapter we are concerned with both spectrum sensing formulations from Section 1.1.1. In power estimation, the goal is to estimate  $\boldsymbol{\alpha} \succeq \mathbf{0}$ , which contains the power of all channels. In activity detection, we are interested in deciding on the presence of a primary user in a specific channel  $b$ . Without any loss of generality, we assume  $b = 0$ , which results in the following test:

$$\mathcal{H}_0 : \alpha_0 = 0, \quad \mathcal{H}_1 : \alpha_0 > 0. \quad (5.3)$$

In order to cope with the presence of the unknown parameters  $\alpha_b$ ,  $b = 1, 2, \dots, B-1$ , we follow a GLR approach to derive the detectors in this chapter.

We start by assuming that the transmitted signals  $x_b$  are zero-mean circularly symmetric complex Gaussian distributed, and therefore the second-order statistics introduced above entirely characterize the statistical distribution of the observations  $\bar{\mathbf{y}}$ . Their probability density function is given by

$$p(\bar{\mathbf{y}}; \boldsymbol{\alpha}) = \frac{\exp \{ -\bar{\mathbf{y}}^H \bar{\Xi}^{-1} \bar{\mathbf{y}} \}}{\pi^{\bar{N}L} |\bar{\Xi}|}. \quad (5.4)$$

Although  $\bar{\Xi}$  depends on  $\boldsymbol{\alpha}$ , we dismiss the notation  $\bar{\Xi}(\boldsymbol{\alpha})$  in favor of clarity.

Under the Gaussian assumption, obtaining the ML estimate  $\hat{\boldsymbol{\alpha}}_{ML} = \arg \sup_{\boldsymbol{\alpha}} p(\bar{\mathbf{y}}; \boldsymbol{\alpha})$  is a particular instance of the so-called *covariance matching* or *structured covariance estimation* problem, and requires non-convex optimization. Although this problem has been widely ana-

lyzed, no closed-form solution has been found. Because the existing numerical methods (see e.g. [Burg et al., 1982, Ottersten et al., 1998]) are not well-fitted to the specifics of our problem, in part due to the computational burden they require, we will develop several efficient yet accurate alternatives.

On the other hand, the GLR statistic is given by

$$\mathcal{G}(\bar{\mathbf{y}}) = \frac{p(\bar{\mathbf{y}}; \hat{\boldsymbol{\alpha}}_{\mathcal{H}_1})}{p(\bar{\mathbf{y}}; \hat{\boldsymbol{\alpha}}_{\mathcal{H}_0})} = \frac{|\bar{\boldsymbol{\Xi}}(\hat{\boldsymbol{\alpha}}_{\mathcal{H}_0})|}{|\bar{\boldsymbol{\Xi}}(\hat{\boldsymbol{\alpha}}_{\mathcal{H}_1})|} \frac{\exp\{-\bar{\mathbf{y}}^H \bar{\boldsymbol{\Xi}}^{-1}(\hat{\boldsymbol{\alpha}}_{\mathcal{H}_1}) \bar{\mathbf{y}}\}}{\exp\{-\bar{\mathbf{y}}^H \bar{\boldsymbol{\Xi}}^{-1}(\hat{\boldsymbol{\alpha}}_{\mathcal{H}_0}) \bar{\mathbf{y}}\}}, \quad (5.5)$$

where the vectors  $\hat{\boldsymbol{\alpha}}_{\mathcal{H}_0}$  and  $\hat{\boldsymbol{\alpha}}_{\mathcal{H}_1}$  respectively denote the ML estimates of  $\boldsymbol{\alpha}$  under hypotheses  $\mathcal{H}_0$  and  $\mathcal{H}_1$ . In particular,  $\hat{\boldsymbol{\alpha}}_{\mathcal{H}_0}$  is the maximizer of (5.4) subject to  $\alpha_0 = 0$  and  $\alpha_b \geq 0$ ,  $b = 1, \dots, B-1$ , whereas  $\hat{\boldsymbol{\alpha}}_{\mathcal{H}_1}$  is the maximizer of (5.4) subject to  $\alpha_0 > 0$  and  $\alpha_b \geq 0$ ,  $b = 1, \dots, B-1$ . For concreteness, but without any loss of generality, we only discuss the estimation of  $\boldsymbol{\alpha}$  subject to the constraint that all the  $\alpha_b$  are non-negative. Note that both the estimation of  $\hat{\boldsymbol{\alpha}}_{\mathcal{H}_0}$  and  $\hat{\boldsymbol{\alpha}}_{\mathcal{H}_1}$  can be formulated as particular instances of this problem: in the first case, it is easy to see that  $\hat{\boldsymbol{\alpha}}_{\mathcal{H}_0}$  can be obtained in this way just by removing  $\bar{\boldsymbol{\Xi}}_0$  from  $\bar{\boldsymbol{\mathcal{B}}}$ ; in the second case, no modifications are required since, except for degenerate cases, the likelihood function is continuous in  $\alpha_0$ , which means that using the constraint  $\alpha_0 > 0$  amounts to using the constraint  $\alpha_0 \geq 0$ .

### 5.1.2 Complexity of the Exact ML Solution

The complexity of obtaining the exact ML estimates using existing methods is prohibitive in spectrum sensing applications, even in those cases where the size of the compressed data record  $\bar{K} \triangleq \bar{N}L$  is of the order of a few hundreds. This is due to the fact that  $\bar{K}$  is also the size of the covariance matrices involved, and typical algorithms need to evaluate their inverses and determinants at each iteration. Moreover, numerical instabilities force algorithms to perform multiple checks at every iteration, which slows down the execution even more. To see this, let us look at the problem from an alternative perspective.

Observe that expression (5.4) can also be written in terms of the sample covariance matrix (SCM)  $\bar{\mathbf{y}}\bar{\mathbf{y}}^H$  as

$$p(\bar{\mathbf{y}}; \boldsymbol{\alpha}) = \frac{\exp\{-\text{Tr}(\bar{\boldsymbol{\Xi}}^{-1} \bar{\mathbf{y}}\bar{\mathbf{y}}^H)\}}{\pi^{\bar{N}L} |\bar{\boldsymbol{\Xi}}|}. \quad (5.6)$$

The problem is therefore to find a matrix  $\bar{\boldsymbol{\Xi}}$  maximizing the metric in (5.6), which is a measure of fit between  $\bar{\mathbf{y}}\bar{\mathbf{y}}^H$  and  $\bar{\boldsymbol{\Xi}}$ . This matrix has to be sought in the feasible set, which is the intersection of the subspace of  $\bar{K} \times \bar{K}$  matrices spanned by  $\bar{\boldsymbol{\mathcal{B}}}$  and the cone of positive definite matrices. Note that if  $\bar{\boldsymbol{\Xi}}$  is not positive definite or, more generally, invertible, then expression (5.6) cannot be

even evaluated. A conventional iterative algorithm will move across the feasible set ensuring that the iterate stays far enough from the boundary of the cone (i.e., the set of singular positive semidefinite matrices); otherwise it could become unstable. This goal is particularly hampered by the fact that this iterate is attracted by  $\bar{\mathbf{y}}\bar{\mathbf{y}}^H$ , which is exactly on that boundary — note that  $\bar{\mathbf{y}}\bar{\mathbf{y}}^H$  has one positive eigenvalue with multiplicity 1 and a null eigenvalue with multiplicity  $\bar{K} - 1$ .

### 5.1.3 Dimensionality Reduction

As opposed to many statistical problems where the computational cost increases linearly or sub-linearly with the number of samples, a larger  $\bar{K}$  here *increases the dimension* of the underlying optimization problem, forcing us to work with larger matrices, whose determinants and inverses become increasingly ill-conditioned and difficult to compute. Moreover, the problem described in Section 5.1.2 will persist regardless of  $\bar{K}$ . Intuition suggests attempting to approximate the ML solution by replacing the *raw* SCM  $\bar{\mathbf{y}}\bar{\mathbf{y}}^H$  with a *modified version* satisfying two properties:

- **Fixed dimension:** the size of the modified SCM should not increase with the number of samples. It must be kept small enough to facilitate the evaluation of the likelihood function.
- **Non-singular:** the modified SCM should be full rank whenever the number of samples is large enough. This would overcome the problem described in Section 5.1.2.

In addition, observe that the raw covariance matrix  $\bar{\mathbf{y}}\bar{\mathbf{y}}^H$  does not even have the block structure of  $\bar{\mathbf{\Xi}}$ , which also suggests looking for a modified SCM of that particular form. The asymptotic theory of Toeplitz matrices will give us some insight into how to accomplish this search.

### AVERAGING THE SCM

Suppose that  $\mathbf{T}$  is the Toeplitz covariance matrix of a wide-sense stationary random process. The associated autocorrelation sequence contains the coefficients in the first row and column of  $\mathbf{T}$  set in the proper order. Without confining ourselves to covariance matrices, a *correlation sequence* may be similarly associated with any Toeplitz matrix by selecting the corresponding coefficients of the first row and column.

Given a sequence of  $n \times n$  Toeplitz covariance matrices  $\{\mathbf{T}_n\}$  satisfying that the Fourier transform of the associated correlation sequences exists, it is possible to find a sequence of  $n \times n$  circulant matrices  $\{\mathbf{C}_n\}$  which is *asymptotically equivalent* [Gray, 2006]. Particularly, if

two sequences  $\{\mathbf{T}_n\}$  and  $\{\mathbf{C}_n\}$  are asymptotically equivalent, then the products  $\text{Tr}(\mathbf{T}_n^{-1}\mathbf{A}_n)$  and  $\text{Tr}(\mathbf{C}_n^{-1}\mathbf{A}_n)$  will converge to the same value provided that  $\{\mathbf{A}_n\}$  is a sequence of matrices bounded in some norm. The sequences of determinants  $|\mathbf{T}_n|$  and  $|\mathbf{C}_n|$  will also have the same limit as long as these matrices are non-singular. Since these are the only operations we are going to perform with these matrices, we will allow ourselves to say that the sequence of matrices  $\{\mathbf{T}_n\}$  is *asymptotically circulant* or, for a finite  $n$ , *approximately circulant*. Likewise, since any circulant matrix can be diagonalized by the vectors of the Fourier basis, we can also say that these are, asymptotically (or approximately), the eigenvectors of  $\mathbf{T}_n$ .

With this in mind, we may say that, as  $\bar{K}$  becomes large,  $\bar{\Xi}$  becomes *approximately block circulant* and, consequently, it will remain approximately the same after a circular rotation of the block-rows and block-columns. Formally, this operation can be expressed as  $\mathbf{R}_l \bar{\Xi} \mathbf{R}_l^T \approx \bar{\Xi}$ , where  $\mathbf{R}_l$  denotes the matrix performing a block-row circular rotation of the  $l$ -th order, i.e.,  $\mathbf{R}_l = \check{\mathbf{R}}_l \otimes \mathbf{I}_{\bar{N}}$  where

$$\check{\mathbf{R}}_l \triangleq \begin{bmatrix} \mathbf{0}_{L-1}^T & 1 \\ \mathbf{I}_{L-1} & \mathbf{0}_{L-1} \end{bmatrix}^l. \quad (5.7)$$

This enables us to approximate the density of the observations as

$$p(\bar{\mathbf{y}}; \boldsymbol{\alpha}) = \frac{\exp\{-\text{Tr}(\bar{\Xi}^{-1}\bar{\mathbf{y}}\bar{\mathbf{y}}^H)\}}{\pi^{\bar{K}}|\bar{\Xi}|} \quad (5.8a)$$

$$\approx \frac{\exp\{-\text{Tr}((\mathbf{R}_l \bar{\Xi} \mathbf{R}_l^T)^{-1}\bar{\mathbf{y}}\bar{\mathbf{y}}^H)\}}{\pi^{\bar{K}}|\bar{\Xi}|}, \quad (5.8b)$$

where we have made use of the fact that the squared determinant  $|\mathbf{R}_l|^2$  is one. Noting that

$$\text{Tr}((\mathbf{R}_l \bar{\Xi} \mathbf{R}_l^T)^{-1}\bar{\mathbf{y}}\bar{\mathbf{y}}^H) = \text{Tr}(\bar{\Xi}^{-1} \mathbf{R}_l^T \bar{\mathbf{y}}\bar{\mathbf{y}}^H \mathbf{R}_l),$$

for all  $l = 0, 1, \dots, L-1$  shows that  $\text{Tr}(\bar{\Xi}^{-1}\bar{\mathbf{y}}\bar{\mathbf{y}}^H)$  can actually be approximated as

$$\begin{aligned} \text{Tr}(\bar{\Xi}^{-1}\bar{\mathbf{y}}\bar{\mathbf{y}}^H) &\approx \frac{1}{L} \sum_{l=0}^{L-1} \text{Tr}(\bar{\Xi}^{-1} \mathbf{R}_l^T \bar{\mathbf{y}}\bar{\mathbf{y}}^H \mathbf{R}_l) \\ &= \text{Tr}(\bar{\Xi}^{-1} \hat{\mathbf{S}}_{\text{av}}), \end{aligned}$$

where we have defined the *averaged SCM* as  $\hat{\mathbf{S}}_{\text{av}} = \frac{1}{L} \sum_l \mathbf{R}_l^T \bar{\mathbf{y}}\bar{\mathbf{y}}^H \mathbf{R}_l$ . In other words, we have



that

$$p(\bar{\mathbf{y}}; \boldsymbol{\alpha}) \approx \frac{\exp \left\{ -\text{Tr} \left( \bar{\boldsymbol{\Xi}}^{-1} \hat{\mathbf{S}}_{\text{av}} \right) \right\}}{\pi^{\bar{K}} |\bar{\boldsymbol{\Xi}}|}. \quad (5.9)$$

This means that<sup>2</sup> averaging along the *modular* block-diagonals of the SCM, where the  $d$ -th modular diagonal comprises the blocks at positions  $(l, l')$  with  $(l' - l)_L = d$ , has a small influence on the likelihood function. However, since in our case  $\bar{\boldsymbol{\Xi}}$  is not block-circulant but block-Toeplitz, one may prefer to simply average along the actual block-diagonals, i.e., to make

$$\hat{\mathbf{S}}_{\text{av}} = \begin{bmatrix} \hat{\mathbf{S}}[0] & \hat{\mathbf{S}}^H[1] & \dots & \hat{\mathbf{S}}^H[L-1] \\ \hat{\mathbf{S}}[1] & \hat{\mathbf{S}}[0] & \dots & \hat{\mathbf{S}}^H[L-2] \\ \vdots & \vdots & \ddots & \vdots \\ \hat{\mathbf{S}}[L-1] & \hat{\mathbf{S}}[L-2] & \dots & \hat{\mathbf{S}}[0] \end{bmatrix}, \quad (5.10)$$

where  $\hat{\mathbf{S}}[l] \triangleq \frac{1}{M_l} \sum_m \bar{\mathbf{y}}[m+l] \bar{\mathbf{y}}^H[m]$  for  $M_l$  a constant that may depend on  $l$ . If  $M_l = L$ , then  $\hat{\mathbf{S}}_{\text{av}}$  is actually composed of the coefficients of the traditional biased estimates of the autocorrelation/crosscorrelation of the processes  $\{\bar{\mathbf{y}}[l\bar{N} + \bar{n}]\}_l$  for  $\bar{n} = 0, \dots, \bar{N} - 1$  [Stoica and Moses, 2005]. On the other hand, if  $M_l = L - l$ , then  $\hat{\mathbf{S}}_{\text{av}}$  is composed of the coefficients in the traditional unbiased estimate, which may be more justified in general since in that case  $M_l$  also represents the length of the  $l$ -th block-diagonal of  $\hat{\mathbf{S}}_{\text{av}}$ , i.e., the number of terms averaged. The use of either of these estimates will guarantee that  $\hat{\mathbf{S}}[l]$  is a consistent estimator for  $\bar{\boldsymbol{\Xi}}[l]$  for fixed  $l$  as  $K \rightarrow \infty$  [Lehmann and Casella, 1998]. Note that the blocks of the raw estimate  $\bar{\mathbf{y}} \bar{\mathbf{y}}^H$ , however, lack this property. In terms of the interpretation of Section 5.1.2, consistency means that this *averaged* SCM becomes *closer*, as  $K$  becomes large, to the feasible set where  $\bar{\boldsymbol{\Xi}}$  must be sought, and intuition suggests that this is numerically convenient. A further advantage of  $\hat{\mathbf{S}}_{\text{av}}$  is that it presents the same block structure as  $\bar{\boldsymbol{\Xi}}$ .

## CROPPING THE COVARIANCE MATRIX

Now that averaging has been motivated by arguing that it barely impacts the likelihood function, two observations are in order: First, due to the block-Toeplitz structure of the covariance matrix and the averaged SCM, most coefficients are replicated several times. This redundancy becomes smaller as we move away from the main diagonal, which suggests that the importance of the blocks  $\bar{\boldsymbol{\Xi}}[l]$  and  $\hat{\mathbf{S}}[l]$  decreases with increasing  $l$ . Second, the coefficients of  $\hat{\mathbf{S}}_{\text{av}}$  that are closer to the diagonal have a lower estimation variance for fixed  $\bar{K}$  and, consequently, are more *reliable*.

---

<sup>2</sup>Note that we have unintentionally derived the exact ML estimate of  $\bar{\boldsymbol{\Xi}}$  for the case where  $\bar{\boldsymbol{\Xi}}$  is known to be block-circulant.

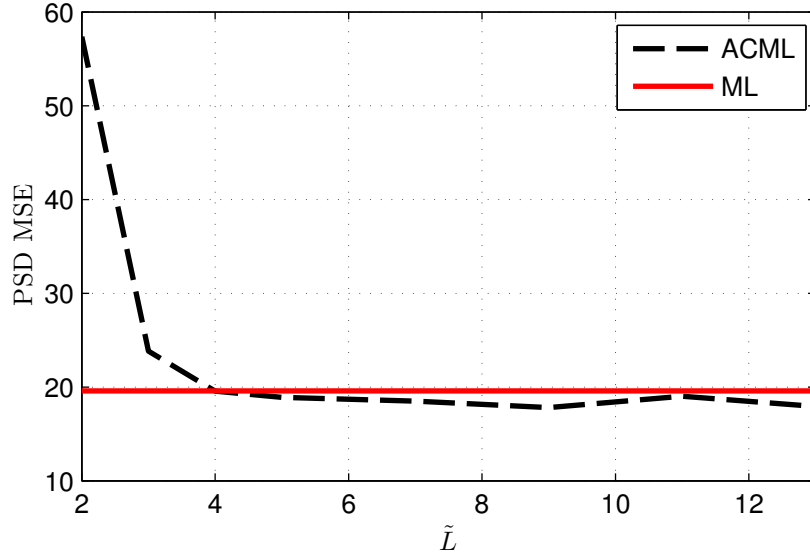


Figure 5.1: Comparison between the true ML solution and a modification of the ML estimate that incorporates averaging and cropping (ACML) ( $K = 325$ ,  $\alpha = [4, 9, 4, 9, 4, 9, 1]^T$ , dense sampler,  $N = 5$ ,  $\tilde{N} = 2$ ).

These remarks suggest truncating both  $\bar{\Xi}$  and  $\hat{\mathbf{S}}_{\text{av}}$ , disregarding the blocks  $\bar{\Xi}[l]$  and  $\hat{\mathbf{S}}[l]$  for large  $l$ . In particular, one may only retain the first  $\tilde{L}$  autocorrelation lags, which correspond to the blocks  $\bar{\Xi}[0], \bar{\Xi}[1], \dots, \bar{\Xi}[\tilde{L} - 1]$  of  $\bar{\Xi}$  and the blocks  $\hat{\mathbf{S}}[0], \hat{\mathbf{S}}[1], \dots, \hat{\mathbf{S}}[\tilde{L} - 1]$  of  $\hat{\mathbf{S}}_{\text{av}}$ . The resulting *averaged and cropped* SCM has dimension  $\tilde{N}\tilde{L} \times \tilde{N}\tilde{L}$  and can be written as

$$\hat{\mathbf{S}} \triangleq \begin{bmatrix} \hat{\mathbf{S}}[0] & \hat{\mathbf{S}}^H[1] & \dots & \hat{\mathbf{S}}^H[\tilde{L} - 1] \\ \hat{\mathbf{S}}[1] & \hat{\mathbf{S}}[0] & \dots & \hat{\mathbf{S}}^H[\tilde{L} - 2] \\ \vdots & \vdots & \ddots & \vdots \\ \hat{\mathbf{S}}[\tilde{L} - 1] & \hat{\mathbf{S}}[\tilde{L} - 2] & \dots & \hat{\mathbf{S}}[0] \end{bmatrix}. \quad (5.11)$$

An analogous structure applies to the cropped version of  $\bar{\Xi}$ , which will also be denoted as  $\bar{\Xi}$  since no ambiguity is possible. Similar techniques were previously used in the literature (see e.g. [Ariananda and Leus, 2012, Zeng and Liang, 2009a, Zeng and Liang, 2009b]) where, like here,  $\tilde{L}$  is regarded as a design parameter.

In view of the above discussion, one may use averaging and cropping to approximate the ML estimate by the maximizer of

$$p(\bar{\mathbf{y}}; \alpha) \approx \frac{\exp \left\{ -\text{Tr} \left( \bar{\Xi}^{-1} \hat{\mathbf{S}} \right) \right\}}{\pi^{\tilde{K}} |\bar{\Xi}|}. \quad (5.12)$$

Figure 5.1 compares the mean squared error (MSE) of the ML estimate of the PSD, obtained via maximization of (5.8a) (full red line) with the MSE of the approximate ML estimate obtained via maximization of (5.12) (dashed black line) in a scenario where the received signal  $y$  is composed of six bandpass signals with non-overlapping spectra of power  $[4, 9, 4, 9, 4, 9]$  and white noise of unit power. A compression ratio of  $\rho = 3/2$  results from the application of a compression matrix  $\check{\Phi} \in \mathbb{C}^{2 \times 3}$ , which is generated using independent Gaussian variables for each entry. More details about these computations can be found in Section 5.4. We observe that a value of  $\tilde{L} = 4$  is enough to obtain an estimation performance similar to ML. For larger values, the MSE of the two compared techniques is roughly the same.

## PARAMETER SELECTION

The algorithms presented in subsequent sections rely on the modified SCM and, in some cases, they require that this matrix satisfy certain properties: sometimes, it must be positive semidefinite because its square root needs to be evaluated; in other cases, its inverse must exist or its determinant must be different from zero. Since these properties depend on the choice of  $K$ ,  $\bar{N}$ ,  $N$  and  $\tilde{L}$ , it is therefore convenient to establish which combinations of these parameters yield positive semidefinite or invertible matrices. The following theorem, whose proof can be found in Appendix 5.A, provides this information.

**THEOREM 5.1.** *Let  $\hat{\mathbf{S}}$  be the averaged and cropped SCM from (5.11) and let  $\bar{\mathbf{y}}$  have a continuous distribution. Then, we have the following:*

1. *If the values of  $M_l$  correspond to the biased estimator of the autocorrelation, that is  $M_l = L$ , then  $\hat{\mathbf{S}}$  is positive semidefinite.*
2. *If the values of  $M_l$  correspond to the biased estimator of the autocorrelation, that is  $M_l = L$ , we have that*

$$\text{rank}(\hat{\mathbf{S}}) = \min(L + \tilde{L} - 1, \bar{N}\tilde{L})$$

*with probability one.*

3. *If the values of  $M_l$  correspond to the unbiased estimator of the autocorrelation, that is  $M_l = L - l$ , we have that*

$$\text{rank}(\hat{\mathbf{S}}) = \min(L\tilde{L}, \bar{N}\tilde{L}) = \tilde{L} \min(L, \bar{N})$$

*with probability one.*

In our setting, the hypothesis that  $\bar{\mathbf{y}}$  is distributed according to a continuous probability distribution<sup>3</sup> holds provided that the covariance matrix  $\bar{\mathbf{\Xi}}$  is full rank. The reason for such an assumption is that the proof takes advantage of the fact that  $\bar{\mathbf{y}}[l]$  and  $\bar{\mathbf{y}}[l']$ ,  $l \neq l'$ , are linearly independent with probability 1 if this hypothesis is satisfied.

The first part of the theorem guarantees that  $\hat{\mathbf{S}}$  is positive semidefinite if the biased estimate is used, but the same cannot be said in the unbiased case, where  $\hat{\mathbf{S}}$  may have negative eigenvalues. Intuitively, the reason is that the coefficients far from the main diagonal may be considerably large due to the small number of samples averaged and the low value of  $M_l$ .

From the second part, we conclude that  $L + \tilde{L} - 1$  has to be greater than or equal to  $\bar{N}\tilde{L}$  in order for  $\hat{\mathbf{S}}$  to be invertible in the biased case. This establishes a lower bound on the number of samples required:

$$K \geq N[\bar{N}\tilde{L} - \tilde{L} + 1]. \quad (5.13)$$

As stated by the third part, this lower bound is smaller for the unbiased estimate, where it equals the product  $N\bar{N}$ . Interestingly, since  $\tilde{L}$  does not have an influence on whether  $\hat{\mathbf{S}}$  is full rank or not, this parameter can be freely adjusted in the unbiased case.

Finally, note that there is a further restriction on the values that these design parameters can take on. In particular, the coefficients  $\alpha_b$  must remain identifiable after the observations are compressed. This issue is related to the design of  $\Phi$  and will be investigated in detail in Chapter 6.

## 5.2 Estimation Algorithms

In this section, we start by detailing how to approximate the ML estimate at a low computational cost. Later, the Gaussian assumption is dropped and several estimators are discussed for more general scenarios. As seen in Section 5.1.1, evaluating the GLR requires the numerical computation of two vector estimates, one under each hypothesis, and their substitution in (5.5). Since no simplification is possible, we defer further discussions about activity detection to Section 5.4.

---

<sup>3</sup>Formally, we say that a distribution  $\mu$  is continuous if it is *absolutely continuous with respect to Lebesgue measure*, that is,  $\mu(B) = 0$  for all Borel sets of  $\mathbb{C}^{N \times N}$  with zero Lebesgue measure [Billingsley, 1995]. Intuitively, this means that there are no probability *masses*.

### 5.2.1 The True ML Estimate

In order to find the ML estimate of  $\alpha$ , one must maximize (5.4) with respect to  $\alpha$  over the non-negative orthant  $\{\alpha : \alpha \succeq \mathbf{0}\}$ . Equivalently, one may minimize the negative of the log-likelihood function:

$$\Lambda(\alpha) = \log |\bar{\Xi}| + \text{Tr} (\bar{\Xi}^{-1} \bar{\mathbf{y}} \bar{\mathbf{y}}^H). \quad (5.14)$$

To do so, numerical methods such as *likelihood-based estimation of sparse parameters* (LIKES) can be utilized. This algorithm was proposed in [Stoica and Babu, 2012] for rank-1 SCMs in the context of sparse-parameter estimation and subsequently extended to the full-rank case in [Babu and Stoica, 2012]. Although both works assume that the matrices in  $\bar{\mathcal{B}}$  are rank-1, the scheme carries over to the general case, as discussed next.

LIKES is based on the *minimization-majorization principle*, which locally majorizes the cost by a convex function at each iteration and minimizes this function to obtain the next estimate. Suppose that the current iterate is given by  $\underline{\alpha}$ . Since the first term in (5.14) is concave and the second convex, it suffices to majorize the first one by its tangent plane at  $\alpha = \underline{\alpha}$ :

$$\begin{aligned} \log |\bar{\Xi}| &\leq \log |\bar{\Xi}| + \sum_{b=0}^{B-1} \text{Tr} (\bar{\Xi}^{-1} \bar{\Xi}_b) (\alpha_b - \underline{\alpha}_b) \\ &= \log |\bar{\Xi}| - \bar{K} + \sum_{b=0}^{B-1} \text{Tr} (\bar{\Xi}^{-1} \bar{\Xi}_b) \alpha_b, \end{aligned} \quad (5.15)$$

where the parameters with the *under-bar* notation are those associated with  $\underline{\alpha}$ . Therefore, the cost in (5.14) can be majorized as

$$\Lambda(\alpha) \leq \log |\bar{\Xi}| - \bar{K} + \bar{\mathbf{y}}^H \bar{\Xi}^{-1} \bar{\mathbf{y}} + \sum_{b=0}^{B-1} \text{Tr} (\bar{\Xi}^{-1} \bar{\Xi}_b) \alpha_b.$$

Hence, one must solve the program

$$\underset{\alpha \succeq \mathbf{0}}{\text{minimize}} \quad \bar{\mathbf{y}}^H \bar{\Xi}^{-1} \bar{\mathbf{y}} + \sum_{b=0}^{B-1} \text{Tr} (\bar{\Xi}^{-1} \bar{\Xi}_b) \alpha_b \quad (5.16)$$

at every iteration. As we will see in Section 5.2.4, the objective in (5.16) mimics the SPICE objective with  $\beta_b = \text{Tr} (\bar{\Xi}^{-1} \bar{\Xi}_b)$ . LIKES is an algorithm that iteratively uses SPICE to refine its current estimate. As summarized in Algorithm 5.1, the weight vector  $\beta = [\beta_0, \dots, \beta_{B-1}]^T$  is computed and SPICE executed at every iteration.

**Algorithm 5.1**  $\alpha = \text{LIKES}(\bar{\mathbf{y}})$ 


---

```

Initialize  $\alpha = [\alpha_0, \dots, \alpha_{B-1}]^T$ 
while stopping_criterion == FALSE do
  •  $\bar{\Xi} \leftarrow \sum_b \alpha_b \bar{\Xi}_b$ 
  •  $\beta_b \leftarrow \text{Tr}(\bar{\Xi}^{-1} \bar{\Xi}_b)$ ,  $b = 0, \dots, B-1$ 
  •  $\alpha \leftarrow \text{SPICE\_ITERATION}(\beta, \bar{\mathbf{y}})$ 
end while

```

---

Unfortunately, both the matrix inversion needed for the computation of  $\beta$  and the execution of SPICE are slow operations for vectors  $\bar{\mathbf{y}}$  of moderate sizes. Following the guidelines from Section 5.1, we propose to replace the  $\bar{K} \times \bar{K}$  SCM  $\bar{\mathbf{y}}\bar{\mathbf{y}}^H$  in (5.14) by its averaged and cropped version  $\hat{\mathbf{S}}$ , which is just  $\bar{N}\tilde{L} \times \bar{N}\tilde{L}$ . Recall that the matrices  $\bar{\Xi}$  and  $\bar{\Xi}_b$  must be cropped accordingly so that their dimensions are consistent with  $\hat{\mathbf{S}}$ . Although the resulting algorithm, henceforth referred to as *simplified*-LIKES (SLIKES), does not provide the exact ML estimate, it enables a considerable reduction of the computational time. It can be shown that the expressions for SLIKES are the same as those presented earlier if we replace  $\bar{\mathbf{y}}$  by  $\hat{\mathbf{S}}^{1/2}$  and  $\bar{\mathbf{y}}^H \bar{\Xi}^{-1} \bar{\mathbf{y}}$  by  $\text{Tr}\{\hat{\mathbf{S}}^{H/2} \bar{\Xi}^{-1} \hat{\mathbf{S}}^{1/2}\}$ , where  $\hat{\mathbf{S}}^{1/2}$  is an  $\bar{N}\tilde{L} \times \bar{N}\tilde{L}$  matrix satisfying that  $\hat{\mathbf{S}}^{1/2} \hat{\mathbf{S}}^{H/2} = \hat{\mathbf{S}}$ .

Unfortunately, in order for the square root  $\hat{\mathbf{S}}^{1/2}$  to exist, the modified SCM needs to be positive semidefinite which, in turn, means that the unbiased estimate of the autocorrelation cannot be used (c.f. Section 5.1.3). However, since the biased estimate is expected to bias the estimate of  $\alpha$ , it is convenient to devise an algorithm capable of operating on the unbiased sample estimate yet based on the ML philosophy. Hinging on the idea of relaxing the positivity constraints  $\alpha_b \geq 0$ , the next section proposes such an algorithm, which in addition requires fewer samples to operate.

### 5.2.2 Unconstrained ML Estimation

Since  $\Lambda(\alpha)$  in (5.14) is twice differentiable, relaxing the constraint  $\alpha \succeq \mathbf{0}$  enables us to find a minimum just by setting the gradient equal to zero. By noting that  $\bar{\Xi} = \sum_b \alpha_b \bar{\Xi}_b$ , it is possible to write

$$\frac{\partial \Lambda(\alpha)}{\partial \alpha_b} = \text{Tr}(\bar{\Xi}^{-1} \bar{\Xi}_b) - \text{Tr}(\bar{\Xi}^{-1} \bar{\Xi}_b \bar{\Xi}^{-1} \bar{\mathbf{y}} \bar{\mathbf{y}}^H). \quad (5.17)$$

Due to the regularity of this function, the gradient vanishes when a minimum of  $\Lambda(\alpha)$  is attained. Setting the right side of (5.17) to zero and applying some algebraic manipulations, this condition

becomes

$$\text{Tr}((\bar{\Xi}^{-1} - \bar{\Xi}^{-1} \bar{\mathbf{y}} \bar{\mathbf{y}}^H \bar{\Xi}^{-1}) \bar{\Xi}_b) = 0 \quad \forall b. \quad (5.18)$$

To the best of our knowledge, no analytical solution has been found for this non-linear system of equations. In fact, even for the simple case where the  $\bar{\Xi}_b$  are Toeplitz, one must resort to numerical computations [Fuhrmann, 1991]. A method that can be used is the celebrated *inverse iteration algorithm* (IIA) from [Burg et al., 1982]. However, similarly to LIKES, IIA suffers from a high complexity, especially for moderate  $\bar{K}$ , and may easily become unstable, which demands intense efforts to stay in the positive definite region (see Section 5.1.2).

Since the condition in (5.18) can be rewritten as

$$\text{Tr}((\bar{\Xi} - \bar{\mathbf{y}} \bar{\mathbf{y}}^H) \bar{\Xi}^{-1} \bar{\Xi}_b \bar{\Xi}^{-1}) = 0 \quad \forall b, \quad (5.19)$$

a possibility to refine an estimate  $\underline{\alpha}$  is to set  $\bar{\Xi}^{-1} = \bar{\Xi}^{-1}$  and compute the  $\alpha$  satisfying

$$\text{Tr}((\bar{\Xi} - \bar{\mathbf{y}} \bar{\mathbf{y}}^H) \bar{\Xi}^{-1} \bar{\Xi}_b \bar{\Xi}^{-1}) = 0 \quad \forall b. \quad (5.20)$$

This expression can be rewritten as  $\mathbf{A}\alpha = \mathbf{c}$ , where

$$[\mathbf{A}]_{b,b'} = \text{Tr}(\bar{\Xi}^{-1} \bar{\Xi}_b \bar{\Xi}^{-1} \bar{\Xi}_{b'}) \quad (5.21a)$$

$$[\mathbf{c}]_b = \text{Tr}(\bar{\Xi}^{-1} \bar{\Xi}_b \bar{\Xi}^{-1} \bar{\mathbf{y}} \bar{\mathbf{y}}^H) \quad (5.21b)$$

for  $b, b' = 0, \dots, B-1$ . The IIA algorithm from [Burg et al., 1982] iteratively uses this system of equations to refine the previous estimate  $\underline{\alpha}$ . Since the solution  $\alpha_* = \mathbf{A}^{-1} \mathbf{c}$  may fall out of the feasible region, the update rule sets the new iterate to  $\underline{\alpha} + \kappa \mathbf{d}$ , where  $\mathbf{d} = \alpha_* - \underline{\alpha}$  and  $\kappa$  is a factor that simultaneously ensures that  $\underline{\alpha} + \kappa \mathbf{d}$  is in the feasible region of the unconstrained problem<sup>4</sup> and the objective is reduced with respect to  $\underline{\alpha}$ .

Although this algorithm converges to a local minimum, it is seen from (5.21a) that the  $\bar{K} \times \bar{K}$  matrix  $\bar{\Xi}$  must be inverted and its determinant evaluated at every iteration. Since the computational cost of these operations may be prohibitive in many practical settings, even for moderate values of  $\bar{K}$ , a sensible approximation is to substitute the raw SCM  $\bar{\mathbf{y}} \bar{\mathbf{y}}^H$  by its averaged and cropped version  $\hat{\mathbf{S}}$ . The resulting algorithm will be referred to as the *simplified IIA* (SIIA) and, depending on our choice for  $\tilde{L}$ , may achieve considerable computational cost reductions. The resulting procedure is summarized as Algorithm 5.2.

---

<sup>4</sup> Note that, in the unconstrained problem, it is necessary to check that  $\bar{\Xi}$  is positive definite. This is not the case in the constrained setting since the positive definiteness of  $\bar{\Xi}$  is guaranteed by the fact that  $\alpha_b \geq 0 \quad \forall b$  — recall that the  $\bar{\Xi}_b$  are positive definite.

**Algorithm 5.2**  $\alpha = \text{SIIA}(\hat{\mathbf{S}})$ 


---

```

Initialize  $\alpha = [\alpha_0, \dots, \alpha_{B-1}]^T$ 
while stopping_criterion == FALSE do
  •  $\bar{\Xi} \leftarrow \sum_b \alpha_b \bar{\Xi}_b$ 
  •  $[\mathbf{A}]_{b,b'} \leftarrow \text{Tr}(\bar{\Xi}^{-1} \bar{\Xi}_b \bar{\Xi}^{-1} \bar{\Xi}_{b'})$ 
  •  $[\mathbf{c}]_b \leftarrow \text{Tr}(\bar{\Xi}^{-1} \bar{\Xi}_b \bar{\Xi}^{-1} \hat{\mathbf{S}})$ 
  •  $\alpha_* \leftarrow \mathbf{A}^{-1} \mathbf{c}$ 
  •  $\mathbf{d} \leftarrow \alpha_* - \alpha$ 
  • Choose  $\kappa$  as explained
  •  $\alpha \leftarrow \alpha + \kappa \mathbf{d}$ 
end while

```

---

As an initialization, we propose to approximate  $\bar{\Xi}^{-1} \approx \hat{\mathbf{S}}^{-1}$  in (5.19) so that the initial value for  $\alpha$  can be chosen as the solution to the following linear system of equations:

$$\text{Tr}((\bar{\Xi} - \hat{\mathbf{S}}) \hat{\mathbf{S}}^{-1} \bar{\Xi}_b \hat{\mathbf{S}}^{-1}) = 0 \quad \forall b. \quad (5.22)$$

or, equivalently

$$\sum_{b'} \alpha_{b'} \text{Tr}(\hat{\mathbf{S}}^{-1} \bar{\Xi}_b \hat{\mathbf{S}}^{-1} \bar{\Xi}_{b'}) = \text{Tr}(\hat{\mathbf{S}}^{-1} \bar{\Xi}_b) \quad \forall b.$$

Finally note that, since this algorithm is designed to solve the unconstrained ML problem, we shall not expect that all the components of the resulting  $\alpha$  be non-negative. A discussion on the implications of this fact is deferred to Section 5.3. Note as well that even though the SIIA can be several times faster than the IIA, the computations involved can still be too burdensome for some applications. The next section alleviates this issue by proposing two simpler algorithms that rely on an LS approximation.

### 5.2.3 Least Squares Estimation

Note that the condition in (5.18) can be rewritten as

$$\text{Tr}(\bar{\Xi}^{-1} (\mathbf{I}_{\bar{K}} - \bar{\mathbf{y}} \bar{\mathbf{y}}^H \bar{\Xi}^{-1}) \bar{\Xi}_b) = 0 \quad \forall b,$$

which would immediately hold if one had  $\bar{\mathbf{y}} \bar{\mathbf{y}}^H \bar{\Xi}^{-1} = \mathbf{I}_{\bar{K}}$ . This suggests approximating  $\bar{\Xi} \approx \bar{\mathbf{y}} \bar{\mathbf{y}}^H$  somehow, for example in the least squares sense, i.e., one may use the vector  $\alpha$  that minimizes the Frobenius distance  $\|\bar{\mathbf{y}} \bar{\mathbf{y}}^H - \bar{\Xi}\|_F^2$ . However,  $\bar{\mathbf{y}} \bar{\mathbf{y}}^H \bar{\Xi}^{-1}$  is a poor approximation of  $\mathbf{I}_{\bar{K}}$  since  $\bar{\mathbf{y}} \bar{\mathbf{y}}^H$  is rank one. Thus, it is not surprising that better results are obtained, in general, when



$\bar{\mathbf{y}}\bar{\mathbf{y}}^H$  is replaced by the averaged and cropped  $\hat{\mathbf{S}}$  which, apart from being of higher rank, shares the block structure of  $\bar{\mathbf{\Xi}}_b$ . This improves the consistency of the approximation and allows to consider only one representative from each block-diagonal in the Frobenius criterion. By defining

$$\hat{\mathbf{s}} \triangleq \text{vec} \begin{bmatrix} \tilde{M}_{\tilde{L}-1} \hat{\mathbf{S}}^H[\tilde{L}-1] \\ \vdots \\ \tilde{M}_1 \hat{\mathbf{S}}^H[1] \\ \tilde{M}_0 \hat{\mathbf{S}}[0] \\ \tilde{M}_1 \hat{\mathbf{S}}[1] \\ \vdots \\ \tilde{M}_{\tilde{L}-1} \hat{\mathbf{S}}[\tilde{L}-1] \end{bmatrix} \quad \text{and} \quad \mathbf{v}_b \triangleq \text{vec} \begin{bmatrix} \tilde{M}_{\tilde{L}-1} \bar{\mathbf{\Xi}}_b^H[\tilde{L}-1] \\ \vdots \\ \tilde{M}_1 \bar{\mathbf{\Xi}}_b^H[1] \\ \tilde{M}_0 \bar{\mathbf{\Xi}}_b[0] \\ \tilde{M}_1 \bar{\mathbf{\Xi}}_b[1] \\ \vdots \\ \tilde{M}_{\tilde{L}-1} \bar{\mathbf{\Xi}}_b[\tilde{L}-1] \end{bmatrix},$$

where  $\tilde{M}_l \triangleq \tilde{L} - l$  accounts for the number of times the  $l$ -th block is present in  $\hat{\mathbf{S}}$  or  $\bar{\mathbf{\Xi}}_b$ , the problem of minimizing  $\|\hat{\mathbf{S}} - \bar{\mathbf{\Xi}}\|_F^2$  can be stated as the LS program

$$\min_{\boldsymbol{\alpha}} \|\hat{\mathbf{s}} - \mathbf{V}\boldsymbol{\alpha}\|^2, \quad (5.23)$$

where  $\mathbf{V} \triangleq [\mathbf{v}_0, \mathbf{v}_1, \dots, \mathbf{v}_{B-1}]$ . Considering the blocks  $\hat{\mathbf{S}}[l]$  along with their Hermitian versions  $\hat{\mathbf{S}}[l]^H$  naturally imposes that  $\alpha_b \in \mathbb{R}$ . Although this yields a compact representation, a more efficient choice when computing this solution is to separately consider real and imaginary parts.

For simplicity and efficiency, we may think of solving (5.23) without enforcing  $\boldsymbol{\alpha} \succeq \mathbf{0}$ . The resulting solution is given by  $\boldsymbol{\alpha}_{WLS} \triangleq \mathbf{V}^\dagger \hat{\mathbf{s}}$ , where WLS stands for *weighted least squares*<sup>5</sup>. This algorithm simply projects the modified SCM onto the space spanned by the  $B$  basis matrices in  $\bar{\mathbf{\Xi}}_b$ . On the other hand, if the constraint  $\boldsymbol{\alpha} \succeq \mathbf{0}$  is enforced, the resulting algorithm is termed *constrained WLS* (CWLS). Note that both these algorithms are equally well motivated even if the underlying distribution is not Gaussian. They resemble the parametric counterpart of the LS algorithm from [Ariananda and Leus, 2012].

### 5.2.4 Estimation Using SPICE

SPICE is a collection of algorithms that cast the problem of sparse parameter estimation as an optimization program of the form

$$\underset{\boldsymbol{\alpha} \succeq \mathbf{0}}{\text{minimize}} \quad \text{Tr}(\mathbf{U}^H \bar{\mathbf{\Xi}}^{-1} \mathbf{U}) + \beta^T \boldsymbol{\alpha}, \quad (5.24)$$

---

<sup>5</sup>Simulations reveal that, in most cases, WLS works better than the pure LS, which is the result of making  $\tilde{M}_k = 1 \forall k$ . However, for brevity, we omit the discussion of this algorithm.

where  $\mathbf{U}$  is either a matrix or a column vector whose dimensions are consistent with  $\bar{\mathbf{\Xi}}$ , and  $\beta \succ 0$  is a vector of the same length as  $\alpha$ . These algorithms are derived in [Stoica et al., 2011a, Stoica et al., 2011c, Stoica et al., 2011b, Stoica and Babu, 2012, Babu and Stoica, 2012] under different conditions, where the program (5.24) is solved as a second-order cone program (SOCP) or in a fixed-point fashion. Although, to the best of our knowledge, no SPICE algorithm has been proposed for the case where the basis matrices  $\bar{\mathbf{\Xi}}_b$  have a rank greater than one, an extension, summarized here as Algorithm 5.3, can be readily found.

---

**Algorithm 5.3**  $\alpha = \text{SPICE\_ITERATION}(\beta, \mathbf{U})$ 


---

```

Initialize  $\alpha = [\alpha_0, \dots, \alpha_{B-1}]^T$ 
while stopping_criterion == FALSE do
    •  $\bar{\mathbf{\Xi}} \leftarrow \sum_b \alpha_b \bar{\mathbf{\Xi}}_b$ 
    •  $\mathbf{C}_b \leftarrow \alpha_b \bar{\mathbf{\Xi}}_b^{H/2} \bar{\mathbf{\Xi}}^{-1} \mathbf{U}, \quad b = 0, \dots, B-1$ 
    •  $c_b \leftarrow \text{Tr}(\mathbf{C}_b^H \mathbf{C}_b), \quad b = 0, \dots, B-1$ 
    •  $\alpha_b \leftarrow \sqrt{c_b / \beta_b}, \quad b = 0, \dots, B-1$ 
end while

```

---

Note that Algorithm 5.3 contains the operations needed in the corresponding line of Algorithm 5.1. In the case of LIKES we set  $\mathbf{U} = \bar{\mathbf{y}}$  whereas in the case of SLIKES  $\mathbf{U}$  is set to  $\hat{\mathbf{S}}^{1/2}$ . In the remainder of this section we apply SPICE directly to our problem, first considering the raw SCM  $\bar{\mathbf{y}}\bar{\mathbf{y}}^H$  and then the averaged and cropped version  $\hat{\mathbf{S}}$ . The first algorithm will be simply referred to as SPICE whereas the second one will be dubbed *simplified* SPICE (SSPICE).

In [Stoica et al., 2011a, Stoica et al., 2011c], the so-called extended invariance principle [Ottersten et al., 1998] is invoked to simplify the problem of covariance matching, achieving an estimate that asymptotically matches the ML solution. This estimate, which is also seen to work in the non-Gaussian case [Stoica and Babu, 2012], is the minimizer of the following criterion [Stoica et al., 2011a]

$$\|\bar{\mathbf{\Xi}}^{-1/2}(\hat{\mathbf{R}} - \bar{\mathbf{\Xi}})\|_F^2, \quad (5.25)$$

where  $\hat{\mathbf{R}} = \bar{\mathbf{y}}\bar{\mathbf{y}}^H$  if the observations are composed of exactly one realization  $\bar{\mathbf{y}}$ , or [Stoica et al., 2011c]

$$\|\bar{\mathbf{\Xi}}^{-1/2}(\hat{\mathbf{S}}_0 - \bar{\mathbf{\Xi}})\hat{\mathbf{S}}_0^{-1/2}\|_F^2, \quad (5.26)$$

if the number of realizations available is such that a full-rank SCM  $\hat{\mathbf{S}}_0$  can be constructed. Note that the statistical motivation for (5.26) is stronger than for (5.25) [Stoica et al., 2011c]. Since in our setting only a single realization is available, we will replace  $\hat{\mathbf{S}}_0$  by the averaged and cropped  $\hat{\mathbf{S}}$  in order to apply this second criterion.

### STANDARD SPICE

When  $\hat{\mathbf{R}} = \bar{\mathbf{y}}\bar{\mathbf{y}}^H$ , expression (5.25) can be expanded as

$$\text{Tr}(\bar{\Xi}) + \|\bar{\mathbf{y}}\|^2 \cdot \bar{\mathbf{y}}^H \bar{\Xi}^{-1} \bar{\mathbf{y}} - 2\|\bar{\mathbf{y}}\|^2, \quad (5.27)$$

so that the problem becomes

$$\underset{\alpha \succeq 0}{\text{minimize}} \quad \bar{\mathbf{y}}^H \bar{\Xi}^{-1} \bar{\mathbf{y}} + \frac{\text{Tr}(\bar{\Xi})}{\|\bar{\mathbf{y}}\|^2}. \quad (5.28)$$

Clearly, (5.28) is a particular case of (5.24) where  $\mathbf{U} = \bar{\mathbf{y}}$  and  $\beta_b = \text{Tr}(\bar{\Xi}_b) / \|\bar{\mathbf{y}}\|^2$  and can be solved using Algorithm 5.3.

### SIMPLIFIED SPICE

As mentioned above, we propose to apply SPICE over the averaged and cropped SCM  $\hat{\mathbf{S}}$ . Using simple algebra, it can be seen that the problem of minimizing (5.26), with  $\hat{\mathbf{R}}$  replaced by  $\hat{\mathbf{S}}$ , can be rewritten as

$$\underset{\alpha \succeq 0}{\text{minimize}} \quad \text{Tr}(\hat{\mathbf{S}}^{H/2} \bar{\Xi}^{-1} \hat{\mathbf{S}}^{1/2}) + \text{Tr}(\hat{\mathbf{S}}^{-1} \bar{\Xi}). \quad (5.29)$$

This is a particular instance of (5.24) where  $\mathbf{U} = \hat{\mathbf{S}}^{1/2}$  and  $\beta_b = \text{Tr}(\hat{\mathbf{S}}^{-1} \bar{\Xi}_b)$ , and can be efficiently solved using Algorithm 5.3. The resulting estimator will be referred to as *simplified SPICE* (SSPICE).

Although (standard) SPICE is an efficient method in the context of array processing and spectral analysis for line-spectrum/direction of arrival estimation [Stoica et al., 2011c, Stoica et al., 2011b, Stoica and Babu, 2012, Babu and Stoica, 2012], the need to invert a  $\bar{K} \times \bar{K}$  matrix at each iteration makes its application to spectrum sensing difficult. For concreteness, and since we have observed that the rank-1 criterion in (5.25) does not yield a good estimation performance in our experiments, we will only consider SSPICE in the rest of the chapter. Note that this fact agrees with the claim in [Stoica et al., 2011a] stating that, although the minimizer of (5.25) provides a good indication of the sparsity pattern of  $\alpha$ , it does not result in good estimates for the coefficients  $\alpha_b$  themselves.

### 5.3 Remarks

#### NON-NEGATIVITY CONSTRAINTS

Among the above algorithms, SIIA and WLS do not enforce the constraint  $\alpha \succeq \mathbf{0}$ . The resulting estimates may thus contain negative entries  $\alpha_b$ , which may be set to zero in order to reconstruct the power spectrum or to evaluate the GLR statistic.

#### SCM SELECTION

Based on the biased and unbiased traditional estimates of the autocorrelation of  $\bar{y}$ , we proposed two ways of constructing an averaged and cropped SCM, each one with different properties (see Section 5.1.3). A simple guideline to choose the proper averaging method to be used with one of the proposed algorithms is to look at whether it allows  $\hat{\mathbf{S}}$  to have negative eigenvalues or not. In the latter case, arising in SLIKES and SSPICE, only the biased estimate can be used, since this is the only one guaranteeing this requirement (c.f. Theorem 5.1). In the former case, either method will work.

The choice of the parameters  $N, \bar{N}, L$  and  $\tilde{L}$  must fit the application requirements and guarantee the properties that the considered algorithm requires of  $\hat{\mathbf{S}}$ . Besides the issue described in the previous paragraph, one must take care to ensure that  $\hat{\mathbf{S}}$  is invertible when needed. To this end, Theorem 5.1 can be used to determine whether a particular candidate combination of parameters is allowed. In practice, since the values of  $\bar{N}$  and  $N$  are imposed by the C-ADC, one may only be allowed to set  $L$  and  $\tilde{L}$ . The former can be adjusted to satisfy performance requirements, whereas the latter can be used to trade performance for complexity. According to our experience, good values for  $\tilde{L}$  are those that make the product  $\bar{N}\tilde{L}$  a few times greater than  $B$ .

#### CONVERGENCE AND CONSISTENCY

From an optimization point of view, all algorithms described above enjoy interesting convergence properties. For instance, LIKES guarantees convergence to a local minimum of the negative log-likelihood function since the cost is always decreased at each iteration [Stoica and Babu, 2012]. A similar argument establishes local convergence for SLIKES. This property is also satisfied by the IIA, where each iteration provides an *improving direction* [Burg et al., 1982] and the step size should be selected so that the cost is decreased. Moreover, since the arguments in [Burg et al., 1982] assume a general positive definite SCM, it is clear that they remain valid if the

modified SCM is used, thus showing local convergence for SIIA. Regarding non-ML algorithms, note that both WLS and CWLS arise from convex criteria, which means that they can be solved using convex solvers, which are globally convergent. As for SPICE, global convergence of the alternating algorithm is established in [Stoica et al., 2011a]. For SSPICE, global convergence follows from the arguments in [Stoica et al., 2011c].

The consistency of the algorithms employing the modified SCM, namely SLIKES, SIIA, WLS, CWLS and SSPICE, can be informally established based on the following argument: for fixed  $\tilde{L}$ , the averaged and cropped SCM  $\hat{\mathbf{S}}$  is a consistent estimator for the cropped  $\bar{\mathbf{\Xi}}$ , which means that  $\hat{\mathbf{S}}$  converges in probability to  $\bar{\mathbf{\Xi}}$  for  $\bar{K} \rightarrow \infty$ . Consistency then follows by noting that the criteria used by these algorithms are minimized for  $\bar{\mathbf{\Xi}} = \hat{\mathbf{S}}$  whenever  $\hat{\mathbf{S}}$  falls in the feasible set, i.e., provided that  $\hat{\mathbf{S}}$  is in the span of  $\bar{\mathbf{B}}$  with non-negative coefficients. Thus, as  $\hat{\mathbf{S}}$  becomes closer and closer to the feasible region, the resulting estimate becomes closer to  $\bar{\mathbf{\Xi}}$ .

## CFAR DETECTION

Note from (5.2), (5.3) and (5.4) that the distribution of the observations under  $\mathcal{H}_0$  depends on the  $\alpha_b$ . This implies that, in general, the distribution of a test statistic under  $\mathcal{H}_0$ , including the GLR from (5.5), will depend on the parameters of the model. Even if the statistic is invariant to scalings, its distribution under  $\mathcal{H}_0$  will depend on the  $\alpha_b$  whenever  $B > 2$ . Therefore, it is difficult to set the test threshold to satisfy a typical  $P_{\text{FA}}$  requirement since the values of the  $\alpha_b$ ,  $b = 1, \dots, B - 1$ , are unknown in practice. Fortunately, we expect that the influence of these parameters on the distribution of  $\mathcal{G}$  is relatively small if different channels have different frequency supports, and thus one may approximately achieve a target  $P_{\text{FA}}$ .

In any case, one may argue that any detector for spectrum sensing faces similar difficulties. Although (see Chapter 1) searching for the test that maximizes  $P_{\text{D}}$  within the family of tests with a given  $P_{\text{FA}}$  is a widespread convention, spectrum regulations in practice will not set  $P_{\text{FA}}$  but  $P_{\text{D}}$ , which motivates proceeding in the opposite direction: search for the test that minimizes  $P_{\text{FA}}$  within the family of tests with a given  $P_{\text{D}}$ . However, specifying  $P_{\text{D}}$  is difficult — a complete set of parameters such as signal power, noise power, SNR, the power of adjacent channels, etc, must be given as well. Thus, the practical difficulty faced by our GLR detector is not larger than the one faced by any other detector. We leave it as a future research line to investigate possible means of dealing with this issue.

## 5.4 Simulation Results

Although it was simple to establish the good asymptotic properties of the presented algorithms, performance assessment for finite  $K$  is not so immediate, especially for detection, where an analytical evaluation is intractable. For this reason, in this section we accomplish this task via Monte Carlo simulation.

All the algorithms to be considered use the averaged and cropped version of the SCM except for LIKES and IIA, which are sometimes presented for the sake of comparison. In all simulations, SLIKES and SSPICE operate on the biased SCM, while the rest of algorithms (SIIA, WLS and CWLS) use its unbiased counterpart. Both dense and sparse samplers are considered. The former are generated by drawing the entries of  $\check{\Phi}$  from independent zero-mean complex Gaussian distributions with unit variance. In order to provide our results with more generality, this procedure is repeated at every Monte Carlo iteration so that the final performance measures are averaged over this family of sampling matrices. For sparse samplers, we use the multi-coset pattern generated by a length-10 minimal sparse ruler, which corresponds to (see also Section 1.1.2 and Chapter 6):

$$\check{\Phi} = \begin{bmatrix} 1 & 0 & 0 & 0 & 0 & 0 & 0 & 0 & 0 & 0 \\ 0 & 1 & 0 & 0 & 0 & 0 & 0 & 0 & 0 & 0 \\ 0 & 0 & 0 & 0 & 1 & 0 & 0 & 0 & 0 & 0 \\ 0 & 0 & 0 & 0 & 0 & 0 & 0 & 1 & 0 & 0 \\ 0 & 0 & 0 & 0 & 0 & 0 & 0 & 0 & 0 & 1 \end{bmatrix}. \quad (5.30)$$

The general setting is depicted in Figure 5.2, where the true PSD is shown along with the reconstructed PSD. The latter is obtained by substituting the corresponding estimate of  $\alpha$  in (1.13). The sensed band contains six 4-QAM signals, seven OFDM signals and white noise. The power of the signals is given by  $\alpha_b = 3 \times (b \bmod 3 + 1)$ ,  $b = 0, 1, \dots, 12$ , whereas the noise power is set to  $\alpha_{13} = 10$ . The QAM signals use a root raised cosine pulse with a roll-off factor of 0.3. The OFDM signal uses 512 subcarriers, where the last and first 50 are set to zero; a cyclic prefix with length 1/4 of the symbol period, and a 4-QAM constellation in each subcarrier. We observe that, although the distribution of these signals is not exactly Gaussian — especially in the case of the QAM signals —, all the schemes are still capable of estimating the power of each channel with acceptable accuracy.

In order not to confine ourselves to specific modulations, in the remaining simulations we generate the samples  $x_b[k]$  by passing zero-mean circularly symmetric white Gaussian noise of power  $\alpha_b$  through an energy-normalized bandpass prototype FIR filter with 31 coefficients

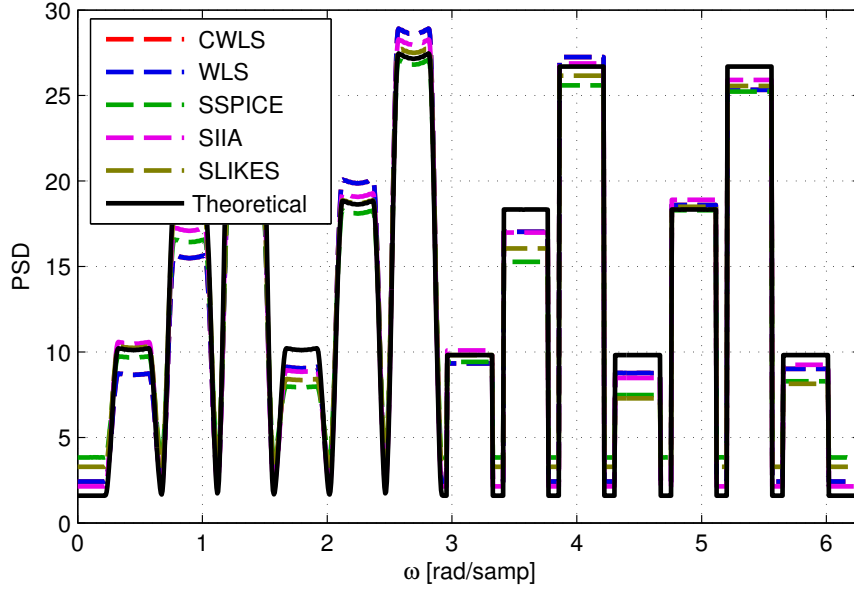


Figure 5.2: PSD estimates for (from left to right) six QAM signals and seven OFDM signals. Many curves overlap since the estimates are close to each other ( $K = 10240$ , dense sampler,  $N = 10$ ,  $\bar{N} = 5$ ,  $\tilde{L} = 6$ ).

and bandwidth  $0.4\pi$  rad/samp, except when a large number of channels is considered, where the order is increased and the bandwidth reduced to avoid frequency overlap<sup>6</sup>. The resulting signals are then shifted to uniformly spaced carrier frequencies via multiplication by a complex exponential. The last signal  $x_{B-1}$  is in all cases white Gaussian noise.

#### 5.4.1 Estimation Performance

We start by illustrating the consistency of the proposed schemes. In Figure 5.3, the MSE of the reconstructed PSD is represented *vs.*  $K$  along with the CRB, which is obtained by applying a linear transformation [Kay, 1993, Sec. 3.8] to the bound for  $\alpha$  from [Stoica and Moses, 2005, Stoica and Babu, 2011]. Note that  $\alpha$  necessarily satisfies  $\alpha \succeq \mathbf{0}$ , which means that the constrained CRB must be used. However, it is shown in [Gorman and Hero, 1990] that this bound coincides with the unconstrained CRB at those points where  $\alpha \succ \mathbf{0}$ . For simplicity, in this experiment we only consider points satisfying the latter condition. The MSE is estimated as the squared Euclidean distance between the reconstructed and the theoretical PSD, normalized by the number of PSD samples. Thus, the MSE is measured in squared units of power per radian.

<sup>6</sup>Note that the proposed schemes can be used without modification even if the channels overlap.

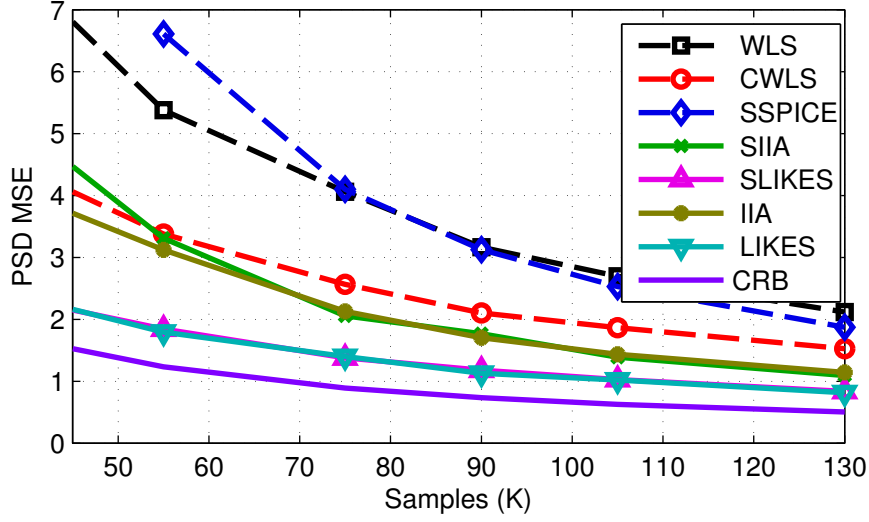


Figure 5.3: Comparison of the estimation performance of the different algorithms presented in the chapter ( $\alpha = [4, 9, 1]^T$ , dense sampler,  $N = 5$ ,  $\bar{N} = 2$ ,  $\bar{L} = 9$ ).

We also show in this figure, for comparison purposes, the PSD MSE of the constrained and unconstrained ML estimators obtained with the LIKES and IIA algorithms. Note that SSPICE is not defined for the leftmost point since  $K$  is too small for the biased SCM to be non-singular. We observe that SIIA and SLIKES achieve an estimation performance which is almost identical to the performance of IIA or LIKES, respectively, yet with a much lower computational complexity. The advantage of using a constrained estimate is also noticed.

The influence of the compression ratio on the MSE is investigated in Figure 5.4, where SLIKES and SSPICE were omitted for simplicity. Clearly, the MSE is in all cases a decreasing function of  $\bar{N}/N$  since a larger  $\bar{N}/N$  entails a larger  $\bar{K}$ . Interestingly, small ratios  $\bar{N}/N$  can be used without affecting the performance meaningfully. On the other hand, the influence of the number of channels  $B$  in the estimation MSE is analyzed in Figure 5.5. The vector  $\alpha$  is set to  $\alpha = [1, 1, \dots, 1, 10]^T$  in all cases. As intuition predicts, the MSE increases with  $B$  since the number of parameters to be estimated becomes larger.

#### 5.4.2 Detection Performance

The interest here is to decide over the presence of the first signal, that is, whether  $\alpha_0 = 0$  or  $\alpha_0 > 0$  (see (5.3)). We use the schemes from Section 5.2 to construct detectors by substituting their respective estimates in the GLR from (5.5). Note that only the estimate obtained via LIKES results in the *GLR test*, the others being approximations. Any negative component of  $\alpha$  is set to zero prior to evaluation of (5.5), since otherwise  $\bar{\Xi}$  may not be positive definite.



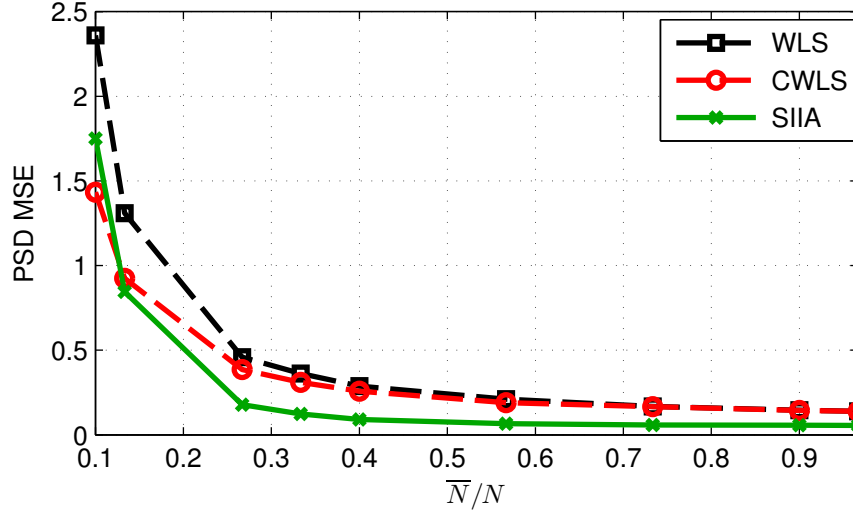


Figure 5.4: A large portion of the samples can be discarded without a meaningful performance loss ( $K = 900$ ,  $\alpha = [4, 9, 1]^T$ , dense sampler,  $N = 30$ ,  $\tilde{L} = 16$ ).

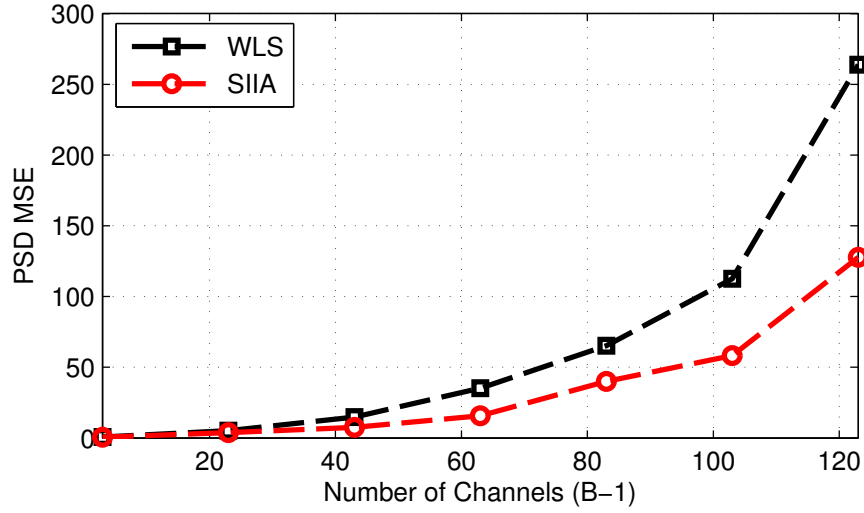


Figure 5.5: Influence of the number of channels in the estimation performance.  $\alpha_b = 1$  for  $b = 0, 1, \dots, B-2$  and  $\alpha_{B-1} = 10$  ( $K = 5120$ , dense sampler,  $N = 10$ ,  $\bar{N} = 5$ ,  $\tilde{L} = 11$ ).

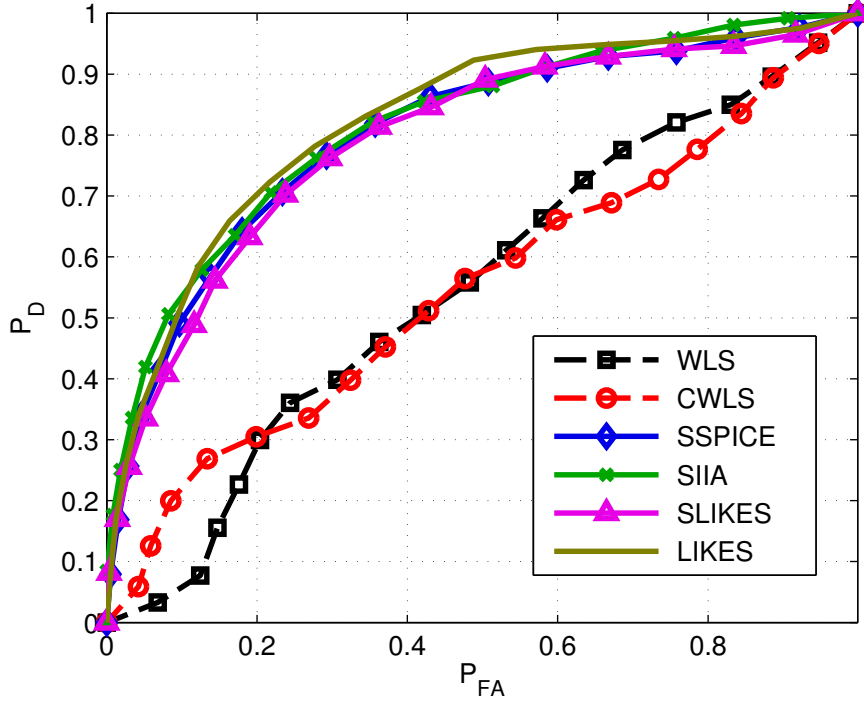


Figure 5.6: ROC comparing the algorithms of this chapter. ( $K = 300$ ,  $\alpha = [0.2, 9, 1]^T$ , sparse sampler,  $N = 10$ ,  $\tilde{N} = 5$ ,  $\tilde{L} = 5$ ).

Figure 5.6 shows the ROCs of the proposed schemes. We observe that the probability of detection of LIKES, SLIKES, SIIA and SSPICE is roughly the same. On the other hand, the LS criterion is seen not to result in good detection rules. In fact, we observe that the ROC curves corresponding to WLS and CWLS are not even concave, meaning that their performance can be improved by using randomized versions of these tests [Lehmann and Romano, 2005].

Finally, Figure 5.7 represents the probability of detection for fixed  $P_{FA} = 0.10$  *vs.* the number of channels. The LS detectors were omitted for the reasons provided in the previous paragraph. It is observed that the influence of  $B$  on the probability of detection is not as important as its influence on the MSE: only small variations are noticed. It is also seen that this influence is more important in SSPICE for larger values of  $\tilde{L}$ .

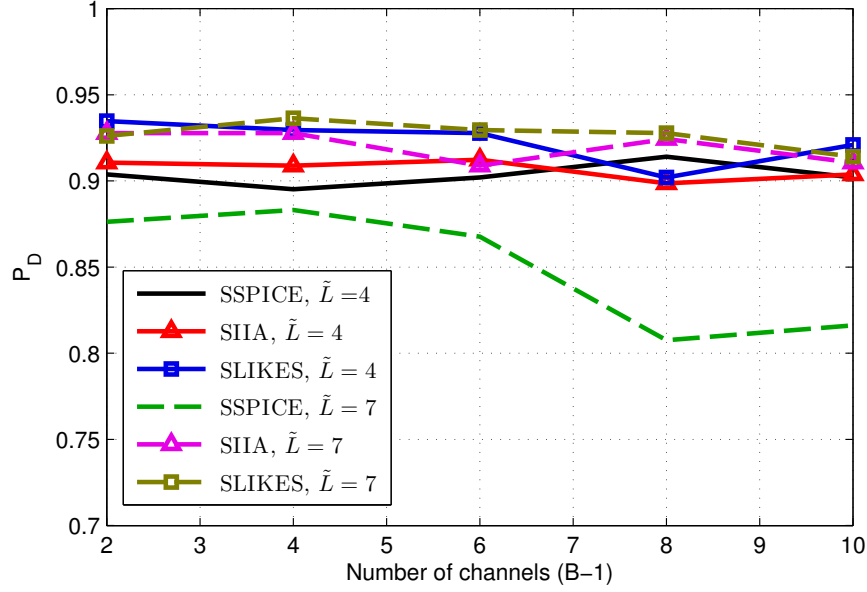


Figure 5.7: Influence of the number of channels on the detection performance.  $\alpha_0 = 0.4$ ,  $\alpha_1 = 4$ ,  $\alpha_{B-1} = 10$  and  $\alpha_b = 0$  for  $b = 2, 3, \dots, B-2$  ( $K = 300$ , sparse sampler,  $N = 10$ ,  $\bar{N} = 5$ ).

## 5.5 Conclusions

The problem of power estimation and activity detection for WSS was formulated for the case when a frequency band is observed through an C-ADC. We proposed a collection of methods that capitalize on the prior knowledge of the spectral structure of the transmitted signals. Under a Gaussian assumption, we saw that computing the ML estimate is computationally intensive, which motivated us to seek low-complexity approximations. Further schemes and approximations were also proposed for the case where the Gaussian assumption is dropped. In both cases, we relied on the usage of an averaged and cropped version of the SCM.

The proposed algorithms (SLIKES, SIHA, WLS, CWLS and SSPICE) produce consistent estimates and trade performance for complexity. Although they require much fewer computational resources than existing methods, we observed via Monte Carlo simulations that their performance is similar. Moreover, it was observed that the observations can be strongly compressed without a meaningful performance degradation.

The work presented in this chapter was published on the *IEEE Transactions on Signal Processing* [Romero and Leus, 2013b] and presented in part in the *2013 IEEE International Conference on Acoustics, Speech and Signal Processing (ICASSP 2013)* [Romero et al., 2013].

## 5.A Proof of Theorem 5.1

Let us define  $\bar{\mathbf{Y}} \triangleq [\bar{\mathbf{y}}[0], \bar{\mathbf{y}}[1], \dots, \bar{\mathbf{y}}[L-1]]$  and  $\tilde{\mathbf{Y}} \triangleq [\bar{\mathbf{Y}}, \mathbf{0}_{\tilde{N} \times \tilde{L}-1}]$ . Since the columns of  $\bar{\mathbf{Y}}$  are drawn from a continuous distribution, they are linearly independent with probability one and, consequently,  $\text{rank}\{\bar{\mathbf{Y}}\} = \min\{L, \tilde{N}\}$ . Let us also consider the group of  $(L + \tilde{L} - 1) \times (L + \tilde{L} - 1)$  circular rotation matrices  $\mathbf{R}_l$ , where  $\mathbf{R}_l$  is defined as the  $l$ -th circular shift of the columns of the identity matrix to the left. Except for their dimensions, the  $\mathbf{R}_l$  are defined here as in Section 5.1.3. Note that  $\mathbf{R}_{-l} = \mathbf{R}_l^H$  and  $\mathbf{R}_l \mathbf{R}_{l'} = \mathbf{R}_{l+l'}$ .

With this notation, it is possible to rewrite  $\hat{\mathbf{S}}[l]$  more conveniently as  $\hat{\mathbf{S}}[l] = c_l \tilde{\mathbf{Y}} \mathbf{R}_l \tilde{\mathbf{Y}}^H$ , with  $c_l = 1/M_l$ . It follows that  $\hat{\mathbf{S}} = \tilde{\mathbf{Y}}_d \mathbf{U} \tilde{\mathbf{Y}}_d^H$ , where  $\tilde{\mathbf{Y}}_d = \mathbf{I}_{\tilde{L}} \otimes \tilde{\mathbf{Y}}$  and

$$\mathbf{U} = \begin{bmatrix} c_0 \mathbf{R}_0 & c_1 \mathbf{R}_{-1} & \dots & c_{\tilde{L}-1} \mathbf{R}_{-\tilde{L}+1} \\ c_1 \mathbf{R}_1 & c_0 \mathbf{R}_0 & \dots & c_{\tilde{L}-2} \mathbf{R}_{-\tilde{L}+2} \\ \vdots & \vdots & \ddots & \vdots \\ c_{\tilde{L}-1} \mathbf{R}_{\tilde{L}-1} & c_{\tilde{L}-2} \mathbf{R}_{\tilde{L}-2} & \dots & c_0 \mathbf{R}_0 \end{bmatrix}. \quad (5.31)$$

This matrix can also be written as  $\mathbf{U} = \bar{\mathbf{R}}_d (\mathbf{U}_0 \otimes \mathbf{I}_{L+\tilde{L}-1}) \bar{\mathbf{R}}_d^H$ , where  $\bar{\mathbf{R}}_d = \text{diag}\{\mathbf{R}_0, \mathbf{R}_1, \dots, \mathbf{R}_{\tilde{L}-1}\}$  is a block diagonal matrix with the blocks  $\mathbf{R}_l$  on its diagonal and

$$\mathbf{U}_0 \triangleq \begin{bmatrix} c_0 & c_1 & \dots & c_{\tilde{L}-1} \\ c_1 & c_0 & \dots & c_{\tilde{L}-2} \\ \vdots & \vdots & \ddots & \vdots \\ c_{\tilde{L}-1} & c_{\tilde{L}-2} & \dots & c_0 \end{bmatrix}. \quad (5.32)$$

In the biased case, where  $c_l = c_0 \forall l$ , we can go a step further by factoring

$$\mathbf{U}_0 \otimes \mathbf{I}_{L+\tilde{L}-1} = c_0 (\mathbf{1}_{\tilde{L}} \otimes \mathbf{I}_{L+\tilde{L}-1}) (\mathbf{1}_{\tilde{L}} \otimes \mathbf{I}_{L+\tilde{L}-1})^H, \quad (5.33)$$

which means that  $\hat{\mathbf{S}}$  can be written as  $\hat{\mathbf{S}} = c_0 \mathbf{A}_{\hat{\mathbf{S}}} \mathbf{A}_{\hat{\mathbf{S}}}^H$  for  $\mathbf{A}_{\hat{\mathbf{S}}} \triangleq \tilde{\mathbf{Y}}_d \bar{\mathbf{R}}_d (\mathbf{1}_{\tilde{L}} \otimes \mathbf{I}_{L+\tilde{L}-1})$ . Noting that  $c_0 > 0$  concludes the proof of the first part.

The same factorization also shows that [Bernstein, 2009, Ch. 2]

$$\begin{aligned} \text{rank}\{\hat{\mathbf{S}}\} &= \text{rank}\{c_0 \mathbf{A}_{\hat{\mathbf{S}}} \mathbf{A}_{\hat{\mathbf{S}}}^H\} \\ &= \text{rank}\{\mathbf{A}_{\hat{\mathbf{S}}}\}. \end{aligned}$$

Since  $\mathbf{A}_{\hat{\mathbf{S}}}$  has the special form of

$$\mathbf{A}_{\hat{\mathbf{S}}} = \tilde{\mathbf{Y}}_d \bar{\mathbf{R}}_d (\mathbf{1}_{\tilde{L}} \otimes \mathbf{I}_{L+\tilde{L}-1}) = \begin{bmatrix} \tilde{\mathbf{Y}} \mathbf{R}_0 \\ \tilde{\mathbf{Y}} \mathbf{R}_1 \\ \vdots \\ \tilde{\mathbf{Y}} \mathbf{R}_{\tilde{L}-1} \end{bmatrix},$$

it is possible to compute the rank by counting the number of linearly independent columns. If  $L \leq \bar{N}\tilde{L}$ , where  $\bar{N}\tilde{L}$  is the number of rows, we obtain  $L$  columns from the non-null columns of  $\tilde{\mathbf{Y}} \mathbf{R}_0$  and one extra column for each  $\tilde{\mathbf{Y}} \mathbf{R}_l$  with  $l = 1, 2, \dots, \tilde{L} - 1$ . Therefore there are  $\min(L + \tilde{L} - 1, \bar{N}\tilde{L})$  independent columns. If  $L > \bar{N}\tilde{L}$ , the number of independent columns is also  $\bar{N}\tilde{L}$ . Consequently, we have established that  $\text{rank}\{\hat{\mathbf{S}}\} = \min(L + \tilde{L} - 1, \bar{N}\tilde{L})$ , which concludes the proof of the second part.

Proving the third part is slightly more involved since the factorization of the biased estimate does not apply to its unbiased counterpart. We start by considering the case  $L \leq \bar{N}$  and then move to the case  $L > \bar{N}$ . Since all entries of  $\tilde{\mathbf{Y}}$  are different from zero with probability one, there exists an  $\bar{N} \times \bar{N}$  invertible matrix of elementary row operations  $\mathbf{F}$  such that

$$\mathbf{F} \tilde{\mathbf{Y}} = \begin{bmatrix} \mathbf{I}_L \\ \mathbf{0} \end{bmatrix}$$

or, alternatively,  $\mathbf{F} \tilde{\mathbf{Y}} = \mathbf{E}$ , with

$$\mathbf{E} = \begin{bmatrix} \mathbf{I}_L & \mathbf{0} \\ \mathbf{0} & \mathbf{0} \end{bmatrix}. \quad (5.34)$$

Clearly, the block diagonal matrix  $\mathbf{F}_d = \mathbf{I}_{\tilde{L}} \otimes \mathbf{F}$  is also invertible and, consequently,

$$\text{rank}\{\hat{\mathbf{S}}\} = \text{rank}\{\mathbf{F}_d \hat{\mathbf{S}} \mathbf{F}_d^H\} \quad (5.35a)$$

$$= \text{rank}\{\mathbf{E}_d \bar{\mathbf{R}}_d (\mathbf{U}_0 \otimes \mathbf{I}_{L+\tilde{L}-1}) \bar{\mathbf{R}}_d^H \mathbf{E}_d^H\} \quad (5.35b)$$

$$= \text{rank}\{\mathbf{E}_d \bar{\mathbf{R}}_d (\mathbf{U}_0 \otimes \mathbf{I}_{L+\tilde{L}-1}) \bar{\mathbf{R}}_d^H\} \quad (5.35c)$$

$$= \text{rank}\{\mathbf{E}_d \bar{\mathbf{R}}_d (\mathbf{U}_0 \otimes \mathbf{I}_{L+\tilde{L}-1})\} \quad (5.35d)$$

where  $\mathbf{E}_d = \mathbf{I}_{\tilde{L}} \otimes \mathbf{E}$ . The third equality is shown in Appendix 5.B, whereas the fourth is a consequence of the fact that  $\bar{\mathbf{R}}_d$  is invertible. In order to prove the third part of the theorem, we note that  $\text{rank}\{\mathbf{U}_0\} = \tilde{L}$  in the unbiased case [Bernstein, 2009, Ch. 2], which means that

$\mathbf{U}_0 \otimes \mathbf{I}_{L+\tilde{L}-1}$  is invertible. Therefore,

$$\text{rank}\{\hat{\mathbf{S}}\} = \text{rank}\{\mathbf{E}_d \bar{\mathbf{R}}_d\} = \tilde{L} \text{rank}\{\mathbf{E}\} = \tilde{L} \cdot L$$

This concludes the proof for the case  $L \leq \bar{N}$ . In particular, for  $L = \bar{N}$  we have that  $\hat{\mathbf{S}}$  is full rank with probability one. Thus, for  $L > \bar{N}$ , it is easy to see that  $\hat{\mathbf{S}}$  will also be full rank with probability one, since the resulting matrix is obtained by adding further random contributions to the averaged SCM that corresponds to the  $\bar{N}$  first vectors  $\bar{\mathbf{y}}[l]$ .

## 5.B Proof of Expression (5.35c)

The purpose of this section is to show that

$$\text{rank}\{\mathbf{E}_d \mathbf{U} \mathbf{E}_d^H\} = \text{rank}\{\mathbf{E}_d \mathbf{U}\}. \quad (5.36)$$

Although in Appendix 5.A we made use of this expression *from left to right*, here we will proceed from right to left by noting that left-multiplying  $\mathbf{U}$  by  $\mathbf{E}_d$  amounts to a row selection where we take the first  $L$  rows of every block of  $\tilde{L} + L - 1$  rows. The rows that are not selected are set to zero but, as far as the rank is concerned, this is equivalent to removing those rows. Right multiplying by  $\mathbf{E}_d^H$  performs the analogous operation with the columns. Although the rank of  $\mathbf{E}_d \mathbf{U}$  can be less than or equal to the rank of  $\mathbf{U}$ , we will see that once we have left-multiplied by  $\mathbf{E}_d$ , the right multiplication by  $\mathbf{E}_d^H$  entails no further rank reduction.

In other words, we must show that the columns of  $\mathbf{E}_d \mathbf{U}$  that  $\mathbf{E}_d^H$  sets to zero in  $\mathbf{E}_d \mathbf{U} \mathbf{E}_d^H$  are linearly dependent on the columns that are not set to zero. To do so, we must examine the structure of  $\mathbf{U}$ . From (5.31) we observe that  $\mathbf{U}$  is a sparse matrix since the blocks  $c_l \mathbf{R}_l$  have exactly one non-null element in each row and column. As we will see, to establish (5.36) it suffices to analyze the position of the non-null elements of  $\mathbf{U}$ . To simplify the explanation, let us define  $\bar{\mathbf{U}}$  as a matrix which is zero where  $\mathbf{U}$  is zero and one where  $\mathbf{U}$  is different from zero.

Let  $\mathbf{u}_k$ ,  $k = 0, 1, \dots, \tilde{L}(L + \tilde{L} - 1) - 1$ , denote the  $k$ -th column of  $\mathbf{U}$ . We define  $\mathcal{U}_k \subset \{0, 1, \dots, \tilde{L}(L + \tilde{L} - 1) - 1\}$  as the set containing the indices of the nonzero entries of  $\mathbf{u}_k$ . It is easy to see that all the columns of  $\bar{\mathbf{U}}$  are present in the first block-column since the rest of the block-columns are just cyclic shifts of the first one. In particular we have that, for  $k = 0, 1, \dots, s - 1$ ,

$$\mathcal{U}_k = \mathcal{U}_{s+(k+1)_s} = \mathcal{U}_{2s+(k+2)_s} = \dots = \mathcal{U}_{(\tilde{L}-1)s+(k+\tilde{L}-1)_s} \quad (5.37)$$

where  $s = L + \tilde{L} - 1$  and  $(\cdot)_s$  means remainder of integer division by  $s$ . Clearly, these sets have

$\tilde{L}$  elements:

$$\begin{aligned}\mathcal{U}_k &= \{k, s + (k + 1)_s, 2s + (k + 2)_s, \dots, (\tilde{L} - 1)s + (k + \tilde{L} - 1)_s\} \\ &= \{ns + (k + n)_s, n = 0, 1, \dots, \tilde{L} - 1\}\end{aligned}\quad (5.38)$$

for  $k = 0, 1, \dots, s - 1$ . Note that because  $\bar{\mathbf{U}}$  is symmetric, the elements in  $\mathcal{U}_k$  are the same as those in the subscripts of (5.37).

Let  $\tilde{\mathbf{u}}_k$ ,  $k = 0, 1, \dots, \tilde{L}(L + \tilde{L} - 1) - 1$ , denote the  $k$ -th column of  $\mathbf{E}_d \mathbf{U}$ . As discussed above, the left multiplication by this matrix amounts to setting to zero the rows of  $\mathbf{U}$  whose indices are not in (see (5.34))

$$\mathcal{C} = \{n(L + \tilde{L} - 1) + k : n = 0, 1, \dots, \tilde{L} - 1; k = 0, 1, \dots, L - 1\}.$$

In other words, only the rows with indices in  $\mathcal{C}$  are preserved. Thus, if the set  $\tilde{\mathcal{U}}_k$  contains the indices of the non-null entries of  $\tilde{\mathbf{u}}_k$ , it is clear that  $\tilde{\mathcal{U}}_k = \mathcal{U}_k \cap \mathcal{C}$  and also that

$$\tilde{\mathcal{U}}_k = \tilde{\mathcal{U}}_{s+(k+1)_s} = \tilde{\mathcal{U}}_{2s+(k+2)_s} = \dots = \tilde{\mathcal{U}}_{(\tilde{L}-1)s+(k+\tilde{L}-1)_s}, \quad (5.39)$$

which follows from (5.37). This expression allows us to arrange the columns of  $\mathbf{E}_d \mathbf{U}$  in  $s$  equivalence classes. We say that the column  $\tilde{\mathbf{u}}_q$  is in the  $k$ -th class if  $q$  is in

$$\begin{aligned}\mathcal{B}_k &= \{k, s + (k + 1)_s, 2s + (k + 2)_s, \dots, (\tilde{L} - 1)s + (k + \tilde{L} - 1)_s\} \\ &= \{ns + (k + n)_s, n = 0, 1, \dots, \tilde{L} - 1\}\end{aligned}\quad (5.40)$$

Note that  $\tilde{\mathcal{U}}_q \cap \tilde{\mathcal{U}}_{q'} = \emptyset$  if  $q$  and  $q'$  belong to different classes. Also, a collection of  $|\tilde{\mathcal{U}}_k|$  or fewer columns of class  $k$  is necessarily independent, since the coefficients of the non-null entries of  $\tilde{\mathbf{u}}_k$  are taken from  $\mathbf{U}_0$ . Conversely, a collection of more than  $|\tilde{\mathcal{U}}_k|$  elements of class  $k$  is necessarily a dependent set of vectors.

With these observations in mind it is clear that the right-multiplication of  $\mathbf{E}_d \mathbf{U}$  by  $\mathbf{E}_d^H$  is not going to change the rank provided that this column selection respects at least  $|\tilde{\mathcal{U}}_k|$  columns from class  $k$ , for all  $k$ . The number of columns surviving in class  $k$  is clearly  $|\mathcal{B}_k \cap \mathcal{C}|$ . But, from (5.38) and (5.40) it follows that  $\mathcal{B}_k = \mathcal{U}_k$ , which in turn means that  $|\mathcal{B}_k \cap \mathcal{C}| = |\mathcal{U}_k \cap \mathcal{C}| = |\tilde{\mathcal{U}}_k|$ .





## Chapter 6

# Sampler Design for Compressive Covariance Sampling

This chapter is concerned with the design of linear compression systems for CCS. The model from Section 1.1.2 is adopted, where the covariance matrix  $\Xi$  of the uncompressed observations  $\mathbf{y}$  is linearly parameterized in terms of a basis  $\mathcal{B}$  of HT matrices. The goal is to design a compression matrix  $\Phi$  such that the compression operation, represented as  $\bar{\mathbf{y}} = \Phi\mathbf{y}$ , preserves all the second-order statistical information of interest. To formalize this notion, we put forth abstract criteria, irrespective of any algorithm, that establishes which samplers are *admissible*. The design of both sparse and dense samplers, operating in either a periodic or non-periodic fashion, is addressed for several common linear parameterizations, with special attention to those maximizing the compression ratio.

This chapter is structured as follows. Section 6.1 sets the theoretical background, where the notions of maximum compression ratio and covariance sampler are introduced. Section 6.2 develops some tools for the design of covariance samplers, which are applied in Sections 6.3 and 6.4 to develop universal and non-universal covariance samplers, respectively. Asymptotic compression ratios are discussed in Section 6.5. Finally, Sections 6.6 and 6.7 respectively provide some remarks and conclusions.

### 6.1 Theoretical Framework

The definition of *maximum* compression ratio requires to first specify which samplers we are willing to accept. As mentioned above, we are interested in those samplers preserving all relevant second-order statistical information, i.e., those samplers that allow to recover the second-order statistics of  $\mathbf{y}$  from those of  $\bar{\mathbf{y}}$ . In order to formalize this notion, we start by associating the

compression matrix  $\Phi \in \mathbb{C}^{\bar{K} \times K}$  with a linear map that relates the covariance matrices of  $\mathbf{y}$  and  $\bar{\mathbf{y}}$ . This function is defined as

$$\begin{array}{ccc} \text{span}_{\mathbb{R}} \mathcal{B} & \xrightarrow{\phi} & \text{span}_{\mathbb{R}} \bar{\mathcal{B}} \\ \Xi & \longrightarrow & \phi(\Xi) = \Phi \Xi \Phi^H, \end{array} \quad (6.1)$$

where  $\mathcal{B}$  is a linearly independent set of  $B$  HT matrices and  $\text{span}_{\mathbb{R}} \mathcal{B}$  is referred to as the *covariance subspace*.<sup>1</sup> We next specify which sampling matrices are *admissible*:

DEFINITION 6.1. *A matrix  $\Phi$  defines a  $\mathcal{B}$ -covariance sampler, or simply a covariance sampler when there is no ambiguity, if the associated function  $\phi$ , defined in (6.1), is invertible.*

The *maximum compression ratio* is the largest value of  $\rho \triangleq K/\bar{K}$  for which a covariance sampler  $\Phi \in \mathbb{C}^{\bar{K} \times K}$  can be found. Above this value, it is not possible to consistently estimate the second-order statistics of  $\mathbf{y}$ , even if an arbitrarily large number of realizations of  $\bar{\mathbf{y}}$  are observed, since the statistical identifiability of  $\Xi$  is lost [Lehmann and Casella, 1998]. For convenience, throughout the chapter we regard  $K$  as given and attempt to minimize  $\bar{K}$ .

One may argue that the requirement in Definition 6.1 is too strong since it suffices to require  $\phi$  to be invertible only for those matrices in the covariance subspace that are positive semidefinite. More generally, the prior information may constrain  $\Xi$  to be in a certain non-linear set<sup>2</sup>  $\mathcal{A}$  such as the set of positive semidefinite matrices, the set of covariance matrices of autoregressive processes with a given order, the non-linear sets in [Ottersten et al., 1998], etc. In those cases, we may reformulate Definition 6.1 to require  $\phi$  to be invertible only in  $\mathcal{A} \cap \text{span}_{\mathbb{R}} \mathcal{B}$ . However, this relaxation is unnecessary, as shown by the following lemma:

LEMMA 6.1. *Let  $\phi$  be the function defined in (6.1), where  $\mathcal{B}$  is a linearly independent set of  $B$  HT matrices, let  $\mathcal{A}$  be a set of matrices satisfying that  $\dim_{\mathbb{R}}[\mathcal{A} \cap \text{span}_{\mathbb{R}} \mathcal{B}] = B$  and let  $\phi|_{\mathcal{A}}$  be the restriction of  $\phi$  to  $\mathcal{A} \cap \text{span}_{\mathbb{R}} \mathcal{B}$ , defined as:*

$$\begin{array}{ccc} \mathcal{A} \cap \text{span}_{\mathbb{R}} \mathcal{B} & \xrightarrow{\phi|_{\mathcal{A}}} & \phi(\mathcal{A} \cap \text{span}_{\mathbb{R}} \mathcal{B}) \\ \Xi & \longrightarrow & \phi|_{\mathcal{A}}(\Xi) = \phi(\Xi). \end{array} \quad (6.2)$$

*Then,  $\phi$  is invertible if and only if  $\phi|_{\mathcal{A}}$  is invertible.*

*Proof.* See Appendix 6.A. □

<sup>1</sup>For mathematical convenience,  $\phi$  is not only defined for positive semidefinite matrices.

<sup>2</sup>We say that a set  $\mathcal{A}$  is linear if  $\alpha_0 \mathbf{a}_0 + \alpha_1 \mathbf{a}_1 \in \mathcal{A}$  for any elements  $\mathbf{a}_0, \mathbf{a}_1 \in \mathcal{A}$  and scalars  $\alpha_0, \alpha_1$ . A non-linear set is a set which does not satisfy this condition.

Therefore, the non-linear information captured by  $\mathcal{A}$  is irrelevant from the linear compression perspective whenever  $\dim_{\mathbb{R}}[\mathcal{A} \cap \text{span}_{\mathbb{R}} \mathcal{B}] = B$ . If this condition is not satisfied, one must choose a different basis  $\mathcal{B}'$  such that  $\mathcal{A} \cap \text{span}_{\mathbb{R}} \mathcal{B}' = \mathcal{A} \cap \text{span}_{\mathbb{R}} \mathcal{B}$  and  $\dim_{\mathbb{R}}[\mathcal{A} \cap \text{span}_{\mathbb{R}} \mathcal{B}'] = |\mathcal{B}'|$ , which is always possible. This establishes the generality of Definition 6.1 and enables us to work with covariance subspaces without further concerns. In particular, if  $\mathcal{A}$  is the cone of positive semidefinite matrices, then  $\mathcal{B}$  satisfies  $\dim_{\mathbb{R}}[\mathcal{A} \cap \text{span}_{\mathbb{R}} \mathcal{B}] = B$  in most cases of interest:

LEMMA 6.2. *Let  $\mathcal{A}$  be the set of positive semidefinite matrices. Then  $\dim_{\mathbb{R}}[\mathcal{A} \cap \text{span}_{\mathbb{R}} \mathcal{B}] = B$  if  $\mathcal{B}$  satisfies at least one of the following conditions:*

1.  $\Xi \geq \mathbf{0}$  for all  $\Xi \in \mathcal{B}$
2.  $\exists \Xi \in \text{span}_{\mathbb{R}} \mathcal{B}$  such that  $\Xi > \mathbf{0}$

*Proof.* 1) means that  $\mathcal{B} \subset [\mathcal{A} \cap \text{span}_{\mathbb{R}} \mathcal{B}]$ . Then  $\dim_{\mathbb{R}}[\mathcal{A} \cap \text{span}_{\mathbb{R}} \mathcal{B}] \geq \dim_{\mathbb{R}} \mathcal{B} = B$ . Noting that  $\dim_{\mathbb{R}}[\mathcal{A} \cap \text{span}_{\mathbb{R}} \mathcal{B}] \leq B$  for any  $\mathcal{B}$  shows that  $\dim_{\mathbb{R}}[\mathcal{A} \cap \text{span}_{\mathbb{R}} \mathcal{B}] = B$ . On the other hand, if 2) holds, we can assume without any loss of generality that  $\mathcal{B} = \{\Xi_0, \dots, \Xi_{B-1}\}$  where  $\Xi_0 = \Xi > \mathbf{0}$ . If  $\mathcal{B}' = \{\Xi_0, \Xi_1 + c\Xi_0, \dots, \Xi_{B-1} + c\Xi_0\}$ , then  $\text{span}_{\mathbb{R}} \mathcal{B} = \text{span}_{\mathbb{R}} \mathcal{B}'$  for any  $c$ . Choose  $c = |\min_b \lambda_{\min}(\Xi_b) / \lambda_{\min}(\Xi_0)|$ , with  $\lambda_{\min}$  representing the minimum eigenvalue. Then  $\mathcal{B}'$  satisfies 1), which concludes the proof.  $\square$

Lemma 6.2 establishes that positive semidefiniteness plays no role in the compression of the covariance subspaces considered in this thesis and in most practical linear parameterizations.

Clearly, a matrix  $\Phi$  may define a covariance sampler for certain sets  $\mathcal{B}$  but not for others. If a matrix  $\Phi$  is a covariance sampler for any choice of  $\mathcal{B}$ , we call it *universal*:

DEFINITION 6.2. *A sampling matrix  $\Phi \in \mathbb{C}^{\bar{K} \times K}$  defines a universal covariance sampler if it is a  $\mathcal{B}$ -covariance sampler for any linearly independent set  $\mathcal{B}$  of  $K \times K$  HT matrices.*

Knowing  $\mathcal{B}$  is always beneficial since  $\Phi$  may be tailored to obtain optimal compression ratios and estimation performance. Universal samplers are motivated by those cases where  $\mathcal{B}$ , or even  $B$ , is unknown at the time of designing the compression matrix. Other notions of universal samplers have been previously introduced in different contexts [Feng and Bresler, 1996, Mishali and Eldar, 2009, Baraniuk et al., 2008, Candès and Wakin, 2008, Yen et al., 2013].

### 6.1.1 Interpretation

Due to the definition of domain and codomain in (6.1),  $\phi$  clearly represents a surjective map. Therefore, the notion of invertibility actually means that  $\phi$  must be injective, that is, for any

set of real coefficients  $\alpha_b$  and  $\alpha'_b$ ,

$$\phi\left(\sum_b \alpha_b \Xi_b\right) = \phi\left(\sum_b \alpha'_b \Xi_b\right) \Rightarrow \alpha_b = \alpha'_b \forall b. \quad (6.3)$$

This condition is, in turn, equivalent to

$$\sum_b \alpha_b \bar{\Xi}_b = \sum_b \alpha'_b \bar{\Xi}_b \Rightarrow \alpha_b = \alpha'_b \forall b, \quad (6.4)$$

which means that  $\bar{\mathcal{B}} = \{\bar{\Xi}_0, \dots, \bar{\Xi}_{B-1}\}$  must be linearly independent. Thus, determining whether a given matrix  $\Phi$  defines a  $\mathcal{B}$ -covariance sampler amounts to checking whether  $\bar{\mathcal{B}} = \phi(\mathcal{B})$  is linearly independent or not. Alternatively, (6.4) states that no two different linear combinations of the matrices in  $\bar{\mathcal{B}}$  can result in the same  $\bar{\Xi}$ , which means that covariance samplers can also be defined as those samplers preserving the identifiability of the coefficients  $\alpha_b$ .

To the best of our knowledge, Definition 6.1 is the first attempt to formalize the design of samplers for CCS problems using abstract criteria not depending on specific algorithms. In the sequel, we will provide means of determining whether a matrix defines a covariance sampler or, in some cases, even a universal covariance sampler.

### 6.1.2 Notable Covariance Subspaces

In Section 6.2 we will provide general tools to design covariance samplers. We then particularize those results to some of the most common covariance subspaces, which are introduced next. Recall that, although the covariance subspaces contain complex-valued matrices, the scalars are real (see Section 1.1.2).

#### TOEPLITZ SUBSPACE

A matrix is Toeplitz if it is constant along its diagonals [Gray, 2006]. The set of all  $K \times K$  HT matrices, represented as  $\mathbb{T}^K$ , is a subspace of  $\mathbb{C}^{K \times K}$  over the real scalar field,<sup>3</sup> and it is the largest subspace considered in this chapter. The *standard basis* of  $\mathbb{T}^K$  is defined as the set

$$\mathcal{B}_T \triangleq \{\mathbf{I}_K\} \cup \{\mathbf{T}_1, \dots, \mathbf{T}_{K-1}\} \cup \{\tilde{\mathbf{T}}_1, \dots, \tilde{\mathbf{T}}_{K-1}\}, \quad (6.5)$$

---

<sup>3</sup>The reason is that any linear combination with real coefficients of HT matrices is also HT. This statement is false for complex coefficients.

where  $\mathbf{T}_k$  denotes the HT matrix with all zeros except for the entries on the diagonals  $+k$  and  $-k$ , which have ones, and  $\tilde{\mathbf{T}}_k$  represents the HT matrix with all zeros except for the entries on the diagonal  $+k$ , which have the imaginary unit  $j$ , and those on the diagonal  $-k$ , which have  $-j$ . More formally,

$$\mathbf{T}_k \triangleq \mathbf{J}_K^k + (\mathbf{J}_K^k)^T \quad k \geq 1 \quad (6.6)$$

$$\tilde{\mathbf{T}}_k \triangleq j\mathbf{J}_K^k - j(\mathbf{J}_K^k)^T \quad k \geq 1, \quad (6.7)$$

where  $\mathbf{J}_K$  is the first linear shift of  $\mathbf{I}_K$  to the right, i.e., the matrix whose element  $(k, k')$  is one if  $k' - k = 1$  and zero otherwise. The basis  $\mathcal{B}_T$  shows that  $\dim_{\mathbb{R}} \mathbb{T}^K = 2K - 1$ . Another important basis for this subspace, which arises in spectrum estimation problems, is the Fourier basis:

$$\mathcal{B}_F \triangleq \{\boldsymbol{\Xi}_0, \dots, \boldsymbol{\Xi}_{2K-2}\}, \quad (\boldsymbol{\Xi}_b)_{k,k'} = \frac{e^{j\frac{2\pi}{2K-1}(k-k')b}}{2K-1}. \quad (6.8)$$

## CIRCULANT SUBSPACE

In some cases, for example when the covariance matrix of  $\mathbf{y}$  is diagonal in the frequency or angular domain, which typically results from a polyphase interpretation of the C-ADC in the frequency domain [Yen et al., 2013, Ariananda et al., 2013], the matrix  $\boldsymbol{\Xi}$  is *circulant*. A circulant matrix is a matrix whose  $k$ -th row equals the  $k$ -th circular rotation of the zeroth row<sup>4</sup> to the right [Gray, 2006]. In other words, the element  $(k_0, k_1)$  equals the element  $(k'_0, k'_1)$  if  $(k_0 - k_1)_K = (k'_0 - k'_1)_K$ . In our case, the matrices in the circulant subspace must be HT and circulant simultaneously. A possible basis is

$$\mathcal{B}_C \triangleq \{\mathbf{I}_K\} \cup \{\mathbf{C}_1, \dots, \mathbf{C}_{\frac{K-1}{2}}\} \cup \{\tilde{\mathbf{C}}_1, \dots, \tilde{\mathbf{C}}_{\frac{K-1}{2}}\}, \quad (6.9)$$

for  $K$  odd and

$$\mathcal{B}_C \triangleq \{\mathbf{I}_K\} \cup \{\mathbf{C}_1, \dots, \mathbf{C}_{\frac{K}{2}-1}\} \cup \{\tilde{\mathbf{C}}_1, \dots, \tilde{\mathbf{C}}_{\frac{K}{2}-1}\} \cup \{\mathbf{T}_{\frac{K}{2}}\} \quad (6.10)$$

for  $K$  even, where

$$\mathbf{C}_b \triangleq \mathbf{T}_b + \mathbf{T}_{K-b}, \quad (6.11)$$

$$\tilde{\mathbf{C}}_b \triangleq \tilde{\mathbf{T}}_b - \tilde{\mathbf{T}}_{K-b}. \quad (6.12)$$

Clearly, the dimension of this subspace is  $K$  in both cases.

---

<sup>4</sup>Recall the conventions introduced in Section 1.4.

## BANDED SUBSPACE

Banded covariance matrices arise when the autocorrelation sequence of a stationary process vanishes for large time lags [Ariananda and Leus, 2012]. A *d-banded matrix* is a matrix where all the elements above the diagonal  $+d$  and below the diagonal  $-d$  (these diagonals noninclusive) are zero. A possible basis for the subspace of HT *d*-banded matrices is given by

$$\mathcal{B}_B^d \triangleq \{\mathbf{I}_K\} \cup \{\mathbf{T}_1, \dots, \mathbf{T}_d\} \cup \{\tilde{\mathbf{T}}_1, \dots, \tilde{\mathbf{T}}_d\}, \quad (6.13)$$

which is a subset of  $\mathcal{B}_T$ . The dimension is therefore  $2d + 1$ .

## 6.2 Design of Covariance Samplers

This section presents a collection of results that can be used to determine whether a compression matrix  $\Phi$  defines a covariance sampler or not, and to design these matrices for a given  $\mathcal{B}$ . Before delving into the derivation, let us consider the following fact from linear algebra:

LEMMA 6.3. *Let  $\mathcal{B} = \{\Xi_0, \dots, \Xi_{B-1}\}$  be a set of Hermitian matrices. If  $\mathcal{B}$  is linearly independent over the real scalar field, that is,*

$$\sum_{b=0}^{B-1} \alpha_b \Xi_b = \mathbf{0}, \quad \alpha_b \in \mathbb{R} \Rightarrow \alpha_b = 0 \quad \forall b, \quad (6.14)$$

*then it is also independent over the complex scalar field, i.e., (6.14) also holds when  $\alpha_b \in \mathbb{C}$ .*

*Proof.* It easily follows by combining expression (6.14) with the fact that  $\Xi_b = \Xi_b^H \forall b$ .  $\square$

The importance of this basic fact is that it allows us to focus on the complex extension of  $\phi$ , defined as

$$\begin{array}{ccc} \text{span}_{\mathbb{C}} \mathcal{B} & \xrightarrow{\phi_{\mathbb{C}}} & \text{span}_{\mathbb{C}} \bar{\mathcal{B}} \\ \Xi & \longrightarrow & \phi_{\mathbb{C}}(\Xi) = \Phi \Xi \Phi^H. \end{array} \quad (6.15)$$

In other words,  $\Phi$  defines a covariance sampler iff the associated  $\phi_{\mathbb{C}}$  is an invertible function. An equivalent statement is provided by the following lemma, which is the basic tool to be used in the design of covariance samplers.

LEMMA 6.4. *Let  $\ker \phi_{\mathbb{C}}$  denote the set of matrices  $\Xi \in \text{span}_{\mathbb{C}} \mathcal{B}$  satisfying  $\phi_{\mathbb{C}}(\Xi) = \mathbf{0}$ . Then, a matrix  $\Phi$  defines a covariance sampler if and only if  $\ker \phi_{\mathbb{C}} = \{\mathbf{0}\}$ .*

*Proof.* It is an immediate consequence of Definition 6.1 and Lemma 6.3.  $\square$

### 6.2.1 Design of Sparse Samplers

Designing sparse samplers involves manipulating *difference sets*, which contain all possible distances between elements of another set:

DEFINITION 6.3. *The difference set of  $\mathcal{A} \subset \mathbb{Z}$ , denoted as  $\Delta(\mathcal{A})$ , is defined as:*

$$\Delta(\mathcal{A}) = \{\delta \geq 0 : \exists a_1, a_2 \in \mathcal{A} \text{ satisfying } \delta = a_2 - a_1\}. \quad (6.16)$$

Note that the difference set considers no repetition of elements, i.e., every distance shows up at most once. The cardinality of  $\Delta(\mathcal{A})$  is upper bounded by one plus the number of unordered subsets of  $\mathcal{A}$  with two elements:

$$|\Delta(\mathcal{A})| \leq \frac{|\mathcal{A}| \cdot (|\mathcal{A}| - 1)}{2} + 1, \quad (6.17)$$

where the +1 term accounts for the fact that  $0 \in \Delta(\mathcal{A})$  for any non-empty  $\mathcal{A}$ .

Define the correlation vector  $\xi_b$  associated with the HT matrix  $\Xi_b$  as the first column of  $\Xi_b$ . The following theorem is a quick method to verify whether a sparse sampler defined by a set  $\mathcal{K}$  is a covariance sampler (see Section 1.1.2).

THEOREM 6.1. *Let  $\mathcal{B} = \{\Xi_b\}_{b=0}^{B-1}$  be a linearly independent set of HT matrices, let  $\{\xi_b\}_{b=0}^{B-1}$  be the associated set of correlation vectors, and let  $\bar{\xi}_b$  be the vector whose entries are the elements of  $\xi_b$  indexed by  $\Delta(\mathcal{K})$ . Then,  $\mathcal{K}$  defines a  $\mathcal{B}$ -covariance sampler if and only if  $\text{rank } \mathbf{C} = B$ , where*

$$\mathbf{C} = \begin{bmatrix} \bar{\xi}_0 & \bar{\xi}_1 & \cdots & \bar{\xi}_{B-1} \\ \bar{\xi}_0^* & \bar{\xi}_1^* & \cdots & \bar{\xi}_{B-1}^* \end{bmatrix}. \quad (6.18)$$

*Proof.* Observe that  $\bar{\Xi}_b$  contains at least one element from the  $\delta$ -th diagonal of  $\Xi_b$  iff  $|\delta| \in \Delta(\mathcal{K})$ . Now vectorize the matrices in  $\bar{\mathcal{B}}$  and arrange the resulting vectors as columns of a matrix. By removing repeated rows and duplicating the row corresponding to the main diagonal we obtain  $\mathbf{C}$ . Therefore, the number of linearly independent columns in  $\mathbf{C}$  equals the number of linearly independent matrices in  $\bar{\mathcal{B}}$ . The result follows from Lemma 6.4 by noting that  $\ker \phi_{\mathbf{C}} = \{\mathbf{0}\}$  iff  $\text{rank } \mathbf{C} = B$ .  $\square$

From (6.18), it is easy to conclude<sup>5</sup> that  $2|\Delta(\mathcal{K})| - 1 \geq B$  in order for  $\mathbf{C}$  to be full column

---

<sup>5</sup>Note the existence of a duplicate row in  $\mathbf{C}$ .

rank. Combining this expression with (6.17) results in the following necessary condition for  $\mathcal{K}$  to define a covariance sampler:

$$\bar{K} \cdot (\bar{K} - 1) + 1 \geq B. \quad (6.19)$$

### 6.2.2 Design of Dense Samplers

Designing sampling matrices is oftentimes involved due to the nature of the design criteria. In many cases, a simple but effective approach is to draw  $\check{\Phi}$  at random using a distribution that provides an admissible sampler with a certain probability [Candès and Wakin, 2008, Baraniuk et al., 2008]. This chapter relies on this idea to propose probabilistic methods capable of generating dense covariance samplers for CCS. Interestingly, these techniques do not require any knowledge about the structure of the covariance subspace other than its dimension. The next result establishes the minimum dimensions of a random matrix  $\check{\Phi}$  to define a covariance sampler.

**THEOREM 6.2.** *Let  $\check{\Phi} \in \mathbb{C}^{\bar{N} \times N}$ , with  $\bar{N} \leq N$ , be a random matrix with a continuous probability distribution.<sup>6</sup> Then, with probability one, the matrix  $\Phi = \mathbf{I}_L \otimes \check{\Phi}$  defines a  $\mathcal{B}$ -covariance sampler if and only if  $B \leq \bar{N}^2(2L - 1)$ , where  $B$  is the cardinality of the HT basis set  $\mathcal{B}$ .*

*Proof.* See Appendix 6.B. □

Note that the matrices in  $\text{span}_{\mathbb{R}} \bar{\mathcal{B}}$ , where  $\bar{\mathcal{B}}$  is the corresponding basis of the compressed subspace, are Hermitian and block-Toeplitz with  $\bar{N} \times \bar{N}$  blocks. It can be seen that the dimension of such a subspace is at most  $\bar{N}^2(2L - 1)$ , which is exactly the one achieved by the random design from Theorem 6.2 when  $B = \bar{N}^2(2L - 1)$  (see Section 6.1.1). Therefore, no other design can achieve a higher compression ratio.

## 6.3 Universal Covariance Samplers

After having laid the mathematical framework, we are ready to present methods that produce covariance samplers independently of which basis of HT matrices is considered. The first result of this section simplifies the task of checking whether a given matrix defines a covariance sampler for all possible bases to that of checking it just for a single basis.

**LEMMA 6.5.** *Let  $\mathcal{B}$  be a basis for  $\mathbb{T}^K$ . Then, a sampler  $\Phi$  is universal if and only if it is a  $\mathcal{B}$ -covariance sampler.*

---

<sup>6</sup>Recall that a distribution  $\mu$  is continuous if it is *absolutely continuous with respect to Lebesgue measure*, that is,  $\mu(B) = 0$  for all Borel sets of  $\mathbb{C}^{\bar{N} \times N}$  with zero Lebesgue measure [Billingsley, 1995]. This hypothesis was also considered in Theorem 5.1.



*Proof.* Clearly, if  $\Phi$  is universal, it is also a  $\mathcal{B}$ -covariance sampler. Conversely, if  $\Phi$  is a  $\mathcal{B}$ -covariance sampler, it is also a  $\mathcal{B}'$ -covariance sampler for any basis  $\mathcal{B}'$  of HT matrices since the restriction of an injective map is always injective.  $\square$

The rest of this section capitalizes on this result to find sparse and dense universal covariance samplers.

### 6.3.1 Sparse Samplers

The next necessary and sufficient condition for a sparse sampler to be universal basically states that all autocorrelation lags must be identifiable from the compressed observations.

**THEOREM 6.3.** *The set  $\mathcal{K} \subset \{0, \dots, K-1\}$  defines a universal covariance sampler if and only if  $\Delta(\mathcal{K}) = \{0, \dots, K-1\}$ .*

*Proof.* Consider the basis  $\mathcal{B}_T$  from (6.5). If  $\Delta(\mathcal{K}) = \{0, \dots, K-1\}$ , the matrix  $\mathbf{C}$  from Theorem 6.1 becomes

$$\mathbf{C} = \begin{bmatrix} \mathbf{I}_K & -j\tilde{\mathbf{I}}_K \\ \mathbf{I}_K & j\tilde{\mathbf{I}}_K \end{bmatrix}, \quad (6.20)$$

where  $\tilde{\mathbf{I}}_K$  is the submatrix of  $\mathbf{I}_K$  that results from removing the first column. Since  $\mathbf{C}$  has rank  $2K-1$ ,  $\mathcal{K}$  defines a  $\mathcal{B}_T$ -covariance sampler and, due to Lemma 6.5, it is universal.

If one or more elements of  $\{0, \dots, K-1\}$  are missing in  $\Delta(\mathcal{K})$ , at least two of the rows of  $\mathbf{C}$  are missing, meaning that  $\text{rank}[\mathbf{C}] < 2K-1$ . Then,  $\text{rank}[\mathbf{C}] = 2K-1$  iff  $\{0, \dots, K-1\} \subset \Delta(\mathcal{K})$ . From Theorem 6.1,  $\mathcal{K}$  defines a  $\mathcal{B}_T$ -covariance sampler iff  $\Delta(\mathcal{K}) = \{0, \dots, K-1\}$ . Now apply Lemma 6.5.  $\square$

This theorem provides a simple means of checking whether  $\mathcal{K}$  is universal or not. Interestingly, this is closely related to the classical problem in number theory known as the *sparse ruler problem*, or as the representation of integers by difference bases (see [Miller, 1971, Leech, 1956] and references therein). Its application to array processing dates back to the 60's [Moffet, 1968].

**DEFINITION 6.4.** *A length- $(K-1)$  (linear) sparse ruler is a set  $\mathcal{K} \subset \{0, 1, \dots, K-1\}$  satisfying  $\Delta(\mathcal{K}) = \{0, 1, \dots, K-1\}$ . It is called minimal if there exists no other length- $(K-1)$  sparse ruler with smaller cardinality.*

Intuitively, we may associate this set with a classical ruler (the physical object) with some marks erased, which is still capable of measuring all integer distances between 0 and its length

using pairs of marks. Two examples of minimal sparse rulers are shown in Figure 6.1, where red dots correspond to the marks that have not been erased. Sparse rulers exist for all  $K$ , although they are not necessarily unique. For instance, two different length-10 sparse rulers are  $\{0, 1, 2, 3, 6, 10\}$  and  $\{0, 1, 2, 5, 7, 10\}$ . The most remarkable properties of a length- $(K-1)$  sparse ruler are that the endpoints are always present, i.e.,  $\{0, K-1\} \subset \mathcal{K}$ , and that its reflection  $(K-1) - \mathcal{K} = \{(K-1) - k : k \in \mathcal{K}\}$  is also a sparse ruler. Trivially, if  $\mathcal{K}$  is minimal, then  $(K-1) - \mathcal{K}$  is also minimal. Therefore, (minimal) sparse rulers exist at least in pairs unless  $\mathcal{K} = (K-1) - \mathcal{K}$ . The cardinality  $\bar{K} = |\mathcal{K}|$  of a sparse ruler is lower bounded as

$$\bar{K} \geq \frac{1}{2} + \sqrt{2(K-1) + \frac{1}{4}}, \quad (6.21)$$

which follows directly from (6.17) and is only attained for  $K-1 = 0, 1, 3$  and 6 (see e.g. [Linebarger et al., 1993]); or as (see [Rédei and Rényi, 1949, Leech, 1956]):

$$\bar{K} \geq \sqrt{\tau(K-1)}, \quad (6.22)$$

where  $\tau = \max_{\varphi} 2(1 - \frac{\sin \varphi}{\varphi}) \approx 2.4345$ ; and, if it is minimal it is upper bounded by [Pearson et al., 1990]:

$$\bar{K} \leq \left\lceil \sqrt{3(K-1)} \right\rceil, \quad K-1 \geq 3. \quad (6.23)$$

Thus, in the non-periodic case ( $L = 1$ ), Theorem 6.3 reduces our design problem to finding a length- $(K-1)$  sparse ruler, for which design algorithms abound. A trivial example is  $\{0, \dots, K-1\}$ , which clearly represents a universal sampler since in that case  $\bar{\mathbf{y}} = \mathbf{y}$ . More sophisticated constructions were discussed in [Rédei and Rényi, 1949, Leech, 1956, Pearson et al., 1990, Wichmann, 1963, Linebarger et al., 1993, Pumphrey, 1993, Pal and Vaidyanathan, 2010]. However, if the compression ratio is to be maximized, then one should look for a *minimal* sparse ruler, which is an exhaustive-search problem. Fortunately, there exist tables for values of  $K-1$  up to the order of 100. Although higher values of this parameter demand, in principle, intensive computation, one may resort to the designs in [Pearson et al., 1990, Wichmann, 1963, Linebarger et al., 1993], which provide nearly minimal rulers despite being really simple.

On the other hand, it is not clear how to design sampling patterns in the periodic case ( $L > 1$ ) since periodicity needs to be enforced on  $\mathcal{K}$ . Before that, the next definition is required.

**DEFINITION 6.5.** *A length- $(K-1)$  periodic sparse ruler of period  $N$ , where  $N$  divides  $K$ , is a set  $\mathcal{K} \subset \{0, 1, \dots, K-1\}$  satisfying two conditions:*

1. *if  $k \in \mathcal{K}$ , then  $k + lN \in \mathcal{K}$  for all  $l \in \mathbb{Z}$  such that  $0 \leq k + lN < K$*

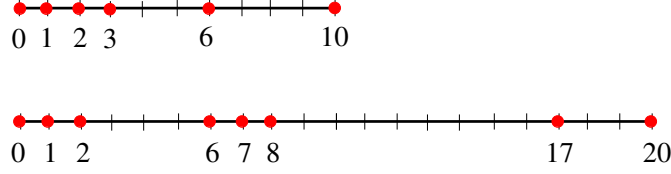


Figure 6.1: Example of a length-10 minimal sparse ruler (above) and length-20 minimal sparse ruler (below).

$$2. \Delta(\mathcal{K}) = \{0, 1, \dots, K - 1\}.$$

*It is called minimal if there exists no other periodic sparse ruler with the same length and period and smaller cardinality.*

Observe that any periodic sparse ruler is also a sparse ruler, whereas the converse need not be true. Clearly, Theorem 6.3 could be rephrased to say that  $\mathcal{K}$  is universal iff it is a length- $(NL - 1)$  periodic sparse ruler of period  $N$ . The problem of designing sparse covariance samplers thus becomes that of designing periodic sparse rulers. The next result simplifies this task by stating that a length- $(NL - 1)$  periodic sparse ruler of period  $N$  is indeed the concatenation of  $L$  length- $(N - 1)$  sparse rulers:

**THEOREM 6.4.** *A set  $\mathcal{K}$  is a periodic sparse ruler of length  $NL - 1$  and period  $N$  if and only if there exists a sparse ruler  $\mathcal{N}$  of length  $N - 1$  such that*

$$\mathcal{K} = \{n + lN : n \in \mathcal{N}, l = 0, 1, \dots, L - 1\}. \quad (6.24)$$

*Proof.* See Appendix 6.D. □

One of the consequences of Theorem 6.4 is that increasing the number of blocks in a periodic sparse sampler cannot improve the compression ratio. For example, concatenating two equal length- $(N - 1)$  minimal sparse rulers with  $\bar{N}$  elements results in a length- $(2N - 1)$  sparse ruler with  $2\bar{N}$  elements. Note, however, that the situation is different if the periodicity requirement is dropped. For instance, a minimal length-10 sparse ruler has 6 elements, whereas a length-21 minimal sparse ruler has  $8 < 6 \times 2$  elements.

As a corollary of Theorem 6.4, we conclude that a minimal periodic sparse ruler is the concatenation of minimal sparse rulers. Thus, the problem of designing optimal sparse universal covariance samplers (either periodic or non-periodic) reduces to designing a minimal length- $(N - 1)$  sparse ruler.

Table 6.1 illustrates the minimum value of  $\bar{N} = |\mathcal{N}|$  (labeled as  $\bar{N}_{\text{LSR}}$ ) for several values of  $N$ , enabling us to obtain the optimum compression ratio for block lengths  $N$  up to 60, which

$N$	5	6	7	8	9	10	11	12	13	14	15	16
$\bar{N}_{\text{CSR}}$	3	3	3	4	4	4	4	4	4	5	5	5
$\bar{N}_{\text{HLSR}}$	3	3	3	4	4	4	4	4	4	5	5	5
$\bar{N}_{\text{LSR}}$	4	4	4	5	5	5	6	6	6	6	7	7

$N$	17	18	19	20	21	22	23	24	25	26	27
$\bar{N}_{\text{CSR}}$	5	5	5	6	5	6	6	6	6	6	6
$\bar{N}_{\text{HLSR}}$	5	5	5	6	6	6	6	6	6	6	6
$\bar{N}_{\text{LSR}}$	7	7	8	8	8	8	8	8	9	9	9

$N$	28	29	30	31	32	33	34	35	36	37	38
$\bar{N}_{\text{CSR}}$	6	7	7	6	7	7	7	7	7	7	8
$\bar{N}_{\text{HLSR}}$	7	7	7	7	7	7	7	7	8	8	8
$\bar{N}_{\text{LSR}}$	9	9	9	10	10	10	10	10	10	10	11

$N$	39	40	41	42	43	44	45	46	47	48	49
$\bar{N}_{\text{CSR}}$	7	8	8	8	8	8	8	8	8	8	8
$\bar{N}_{\text{HLSR}}$	8	8	8	8	8	8	8	8	8	9	9
$\bar{N}_{\text{LSR}}$	11	11	11	11	11	11	12	12	12	12	12

$N$	50	51	52	53	54	55	56	57	58	59	60
$\bar{N}_{\text{CSR}}$	8	8	9	9	9	9	9	8	9	9	9
$\bar{N}_{\text{HLSR}}$	9	9	9	9	9	9	9	9	9	9	10
$\bar{N}_{\text{LSR}}$	12	12	13	13	13	13	13	13	13	13	14

Table 6.1: Values of  $\bar{N}$  for a length- $(N - 1)$  minimal circular sparse ruler ( $\bar{N}_{\text{CSR}}$ ), length- $\lfloor \frac{N}{2} \rfloor$  minimal linear sparse ruler ( $\bar{N}_{\text{HLSR}}$ ) and length- $(N - 1)$  minimal linear sparse ruler ( $\bar{N}_{\text{LSR}}$ ).

covers most practical cases. For higher  $N$ , one may resort to another table, to a computer program, or to the asymptotic considerations in Section 6.5. However, although there is no closed form expression for the maximum achievable compression ratio  $\rho$ , the bounds in (6.22) and (6.23) show that

$$\frac{N}{\left\lceil \sqrt{3(N-1)} \right\rceil} \leq \rho \leq \frac{N}{\sqrt{\tau(N-1)}}. \quad (6.25)$$

### 6.3.2 Dense Samplers

Deriving conditions for universality of dense samplers is simpler than for sparse samplers since most mathematical complexity has been subsumed by Theorem 6.2. Moreover, the results are also simpler and can be expressed in closed form.

**THEOREM 6.5.** *Let  $\tilde{\Phi}$  be an  $\bar{N} \times N$  random matrix satisfying the hypotheses of Theorem 6.2.*

Then,  $\Phi = \mathbf{I}_L \otimes \tilde{\Phi}$  defines a universal covariance sampler with probability 1 if and only if

$$\bar{N} \geq \sqrt{\frac{2NL - 1}{2L - 1}}. \quad (6.26)$$

*Proof.* If  $\mathcal{B}$  is a basis for  $\mathbb{T}^K$ , then  $|\mathcal{B}| = 2K - 1 = 2NL - 1$ . From Theorem 6.2,  $\Phi$  is a  $\mathcal{B}$ -covariance sampler iff  $2NL - 1 \leq \bar{N}^2(2L - 1)$ , which is equivalent to (6.26). Universality then follows from Lemma 6.5.  $\square$

Expression (6.26) can be interpreted as  $\bar{N}^2(2L - 1) \geq 2NL - 1$ , where  $2NL - 1$  is the dimension of the uncompressed subspace and  $\bar{N}^2(2L - 1)$  is the maximum dimension of a subspace of Hermitian block-Toeplitz matrices. Thus, this design provides optimal compression, which is achieved when

$$\bar{N} = \left\lceil \sqrt{\frac{2NL - 1}{2L - 1}} \right\rceil, \quad (6.27)$$

and given by

$$\rho = \frac{N}{\bar{N}} \approx \sqrt{\frac{(2L - 1)N^2}{2NL - 1}}. \quad (6.28)$$

## 6.4 Non-Universal Covariance Samplers

Universal samplers are used when no structure exists in the covariance subspace or when it is unknown. However, when prior information is available, the values that  $\Xi$  can take on are restricted, thus enabling a stronger compression. This section analyzes this effect for the covariance subspaces introduced in Section 6.1.2. Since the Toeplitz subspace has already been considered in Section 6.3, we directly proceed to analyze circulant and  $d$ -banded subspaces.

### 6.4.1 Circulant Covariance Subspace

#### SPARSE SAMPLERS

Constraining  $\Xi$  to be circulant yields considerable compression gains with respect to the Toeplitz case since the requirements on every period of  $\mathcal{K}$  can be relaxed. In particular, every period must be a *circular* sparse ruler, which is a much weaker requirement than that of being a *linear*

sparse ruler. This concept is related to the *modular* difference set defined next. Recall from Section 1.4 that  $(y)_A$  denotes the remainder of the integer division of  $y$  by  $A$ .

DEFINITION 6.6. *Let  $\mathcal{A}$  be a set of integers. The  $A$ -modular difference set of  $\mathcal{A}$ , denoted as  $\Delta_A(\mathcal{A})$ , is defined as*

$$\Delta_A(\mathcal{A}) = \{\delta \geq 0 : \exists a_1, a_2 \in \mathcal{A} \text{ satisfying } \delta = (a_2 - a_1)_A\}. \quad (6.29)$$

Clearly, for any  $\mathcal{A} \subset \{0, 1, \dots, A-1\}$ , we have that  $\Delta(\mathcal{A}) \subset \Delta_A(\mathcal{A})$ , which means that  $|\Delta_A(\mathcal{A})|$  is never less than  $|\Delta(\mathcal{A})|$ . Actually,  $\Delta_A(\mathcal{A})$  will typically be larger than  $\Delta(\mathcal{A})$  since the fact that  $\delta$  is in  $\Delta_A(\mathcal{A})$  implies that  $A - \delta$  is also in that set. For example, if  $\mathcal{A} = \{0, 1, 5\}$  and  $A = 10$ , then  $\Delta(\mathcal{A}) = \{0, 1, 4, 5\} \subset \Delta_{10}(\mathcal{A}) = \{0, 1, 4, 5, 6, 9\}$ . Finally, the cardinality of the modular difference set is upper bounded by noting that any pair of elements in a set  $\mathcal{A}$  with cardinality  $|\mathcal{A}|$  generates at most two distances in  $\Delta_A(\mathcal{A})$ :

$$|\Delta_A(\mathcal{A})| \leq |\mathcal{A}| \cdot (|\mathcal{A}| - 1) + 1. \quad (6.30)$$

Now it is possible to state the requirements to compress circulant subspaces:

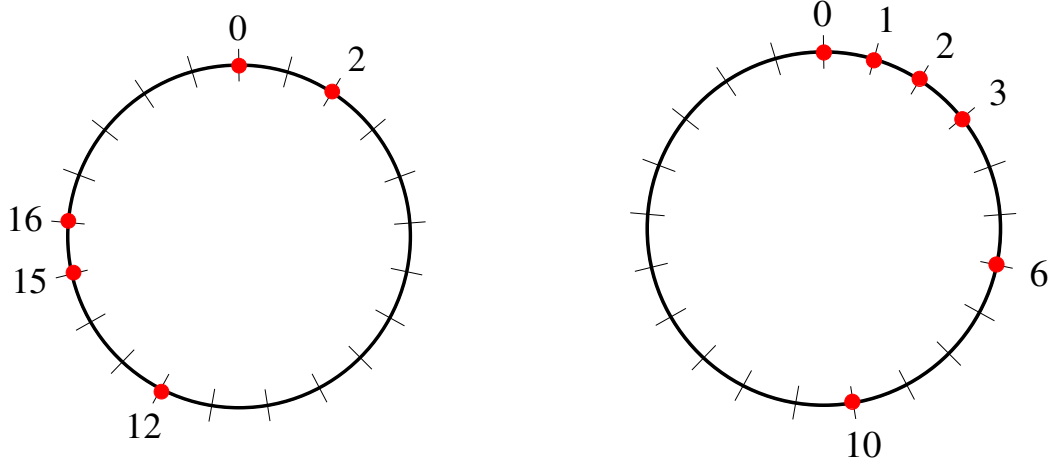
THEOREM 6.6. *Let  $\mathcal{B}_C$  be given by (6.9) or (6.10). Then, the set  $\mathcal{K} \subset \{0, \dots, K-1\}$  is a  $\mathcal{B}_C$ -covariance sampler if and only if  $\Delta_K(\mathcal{K}) = \{0, \dots, K-1\}$ .*

*Proof.* See Appendix 6.E. □

Theorem 6.6 is therefore the dual of Theorem 6.3 for circulant subspaces. However, in this case the conclusion does not lead to a *linear* sparse ruler but to a *circular* one:

DEFINITION 6.7. *A length- $(K-1)$  circular (or modular) sparse ruler is a set  $\mathcal{K} \subset \{0, \dots, K-1\}$  satisfying  $\Delta_K(\mathcal{K}) = \{0, \dots, K-1\}$ ; it is said to be minimal if no other length- $(K-1)$  circular sparse ruler exists with smaller cardinality.*

Similarly to linear sparse rulers, a geometric interpretation is possible in terms of a physical ruler. Suppose that we wrap around a conventional ruler (made of some flexible material) until the first mark and the last mark lie at unit distance, thus making a *circular ruler*. Now assume that some of the marks are erased, but that it is still possible to measure all distances between 0 and the length of the original ruler using pairs of marks. The advantage with respect to a linear ruler is that any pair of marks provides, in general, *two* distances, which are the lengths of the two circular segments that they define. Two length-20 circular sparse rulers are illustrated in



(a) Example of length-20 minimal circular sparse ruler. (b) Example of length-20 circular sparse ruler designed with a length-10 *linear* sparse ruler.

Figure 6.2: Comparison of two length-20 circular sparse rulers. The ruler on the left, with 5 elements, is minimal whereas the one on the right, with 6 elements, is not.

Figure 6.2, the one on the left being minimal. Other examples of length- $(K - 1)$  circular sparse rulers are  $\{0, \dots, K - 1\}$  and  $\{0, \dots, \lfloor \frac{K}{2} \rfloor\}$ , which are termed *trivial* circular sparse rulers.

Circular sparse rulers, also known as *difference cycles*, were analyzed by the mathematical community using finite group theory and additive number theory (see [Miller, 1971] for an overview of the main results). Among the most remarkable properties, we note that a reflection of a circular sparse ruler is also a circular sparse ruler (see Section 6.3.1) and that any circular rotation of a circular sparse ruler  $\mathcal{K}$ , defined as

$$\mathcal{K}_{(i)} = \{(k + i)_K : k \in \mathcal{K}\}, \quad i \in \mathbb{Z}, \quad (6.31)$$

is also a circular sparse ruler. Moreover, since  $\Delta(\mathcal{K}) \subset \Delta_K(\mathcal{K})$  for any  $\mathcal{K} \subset \{0, \dots, K - 1\}$ , any *linear* sparse ruler is also a *circular* sparse ruler. Hence, the cardinality of a *minimal* circular sparse ruler can never be greater than the cardinality of a *minimal* linear sparse ruler if both have the same length. It is possible to go even further by noting that any length- $\lfloor \frac{K}{2} \rfloor$  linear sparse ruler is also a length- $(K - 1)$  circular sparse ruler. For example, Figure 6.2b shows a length-20 circular sparse ruler constructed with a length-10 *linear* sparse ruler. From this observation and (6.23), we obtain

$$|\mathcal{K}| \leq \left\lceil \sqrt{3 \left\lfloor \frac{K}{2} \right\rfloor} \right\rceil \quad (6.32)$$

for any minimal circular sparse ruler. On the other hand, expression (6.30) yields

$$|\mathcal{K}| \geq \frac{1}{2} + \sqrt{K - \frac{3}{4}}. \quad (6.33)$$

A length- $(K - 1)$  circular sparse ruler can be designed in several ways. For certain values of  $K$ , minimal rulers attaining (6.33) can be obtained in closed form (see [Xia et al., 2005, Sec. III-B], also [Singer, 1938]). Other cases may require exhaustive search, which motivates sub-optimal designs. Immediate choices are length- $(K - 1)$  or length- $\lfloor \frac{K}{2} \rfloor$  minimal *linear* sparse rulers [Ariananda and Leus, 2012]. In fact, the latter provides optimal solutions for most values of  $K$  below 60 (see Table 6.1). Further alternatives include [Domínguez-Jiménez et al., 2012].

Circular sparse rulers seem to have been introduced in signal/array processing in [Romero and Leus, 2013a] and used later in [Krieger et al., 2013, Ariananda et al., 2013, Domínguez-Jiménez and González-Prelcic, 2013]. Theorem 6.6 basically states that a covariance sampler for circulant subspaces is a length- $(K - 1)$  circular sparse ruler, which gives a practical design criterion just for the non-periodic case. We now move on to introduce periodicity:

**DEFINITION 6.8.** *A length- $(K - 1)$  periodic circular sparse ruler of period  $N$ , where  $N$  divides  $K$ , is a set  $\mathcal{K} \subset \{0, 1, \dots, K - 1\}$  satisfying:*

1. *if  $k \in \mathcal{K}$ , then  $k + lN \in \mathcal{K}$  for all  $l \in \mathbb{Z}$  such that  $0 \leq k + lN < K$ ;*
2.  $\Delta_K(\mathcal{K}) = \{0, 1, \dots, K - 1\}$ .

*It is called minimal if there is no other periodic circular sparse ruler with the same length and period but smaller cardinality.*

Hence, Theorem 6.6 could be rephrased to say that  $\mathcal{K}$  is a  $\mathcal{B}_C$ -covariance sampler iff it is a length- $(NL - 1)$  periodic circular sparse ruler of period  $N$ . Although designing these rulers may seem difficult, the next result simplifies this task by stating that every period is, indeed, a circular sparse ruler.

**THEOREM 6.7.** *A set  $\mathcal{K}$  is a periodic circular sparse ruler of length  $NL - 1$  and period  $N$  if and only if there exists a circular sparse ruler  $\mathcal{N}$  of length  $N - 1$  such that*

$$\mathcal{K} = \{n + lN : n \in \mathcal{N}, l = 0, 1, \dots, L - 1\} \quad (6.34)$$

*Proof.* See Appendix 6.F. □



Table 6.1 reveals that the cardinality  $\bar{N}$  of a minimal circular sparse ruler is not monotone with  $N$ . For example, minimal length-19 circular sparse rulers have 6 elements whereas minimal length-20 circular sparse rulers have 5 elements (see [Miller, 1971] for a proof). Table 6.1 also illustrates the compression gain due to the knowledge that  $\Xi$  is circulant. For example, when  $N = 60$ , a universal sampler has a compression ratio of  $\frac{N}{\bar{N}} = \frac{60}{14} \approx 4.28$ , whereas a covariance sampler for circulant subspaces has a compression ratio of  $\frac{N}{\bar{N}} = \frac{60}{9} \approx 6.67$ .

Although maximum compression ratios cannot be expressed in closed form, simple bounds follow from (6.32) and (6.33):

$$\frac{N}{\left\lceil \sqrt{3 \lfloor \frac{N}{2} \rfloor} \right\rceil} \leq \rho \leq \frac{2N}{1 + \sqrt{4N - 3}}. \quad (6.35)$$

## DENSE SAMPLERS

Similarly to universal sampling, designing dense samplers is much easier than designing sparse samplers. The following corollary of Theorem 6.2 follows by noting that any basis for the circulant subspace has  $K = NL$  elements.

**COROLLARY 6.1.** *Let  $\check{\Phi}$  be an  $\bar{N} \times N$  random matrix satisfying the hypotheses of Theorem 6.2 and let  $\mathcal{B}_C$  be given by (6.9) or (6.10). Then, with probability one, the matrix  $\Phi = \mathbf{I}_L \otimes \check{\Phi}$  defines a  $\mathcal{B}_C$ -covariance sampler if and only if*

$$\bar{N} \geq \sqrt{\frac{NL}{2L - 1}}. \quad (6.36)$$

The optimum compression ratio is, therefore,

$$\rho = \frac{N}{\bar{N}} \approx \sqrt{\frac{(2L - 1)N}{L}}. \quad (6.37)$$

For large  $L$ , this represents an approximate gain of  $\sqrt{2}$  with respect to the universal case.

### 6.4.2 Banded Covariance Subspace

## SPARSE SAMPLERS

The prior knowledge that  $\Xi$  is  $d$ -banded may also provide compression gains. In particular, we will see that, for sparse samplers,  $d$ -banded subspaces with  $N \leq d \leq N(L - 1)$  are compressed in the same way as circulant subspaces.

THEOREM 6.8. Let  $\mathcal{B}_B^d$  be given by (6.13) with  $N \leq d \leq N(L-1)$ . Then, the set

$$\mathcal{K} = \{n + lN, n \in \mathcal{N}, l = 0, 1, \dots, L-1\}, \quad (6.38)$$

where  $\mathcal{N} \subset \{0, \dots, N-1\}$ , defines a  $\mathcal{B}_B^d$ -covariance sampler if and only if  $\mathcal{N}$  is a length- $(N-1)$  circular sparse ruler.

*Proof.* See Appendix 6.G. □

Observe that the condition  $d \leq N(L-1)$  is a mild assumption since we are only requiring that the last  $N-1$  lags of the associated autocorrelation sequence be zero.<sup>7</sup> Note as well that other cases rather than  $N \leq d \leq N(L-1)$  may be considered, resulting in different conclusions. For example, in the non-periodic case ( $L=1$ ) it can be shown from Theorem 6.1 that the only requirement on  $\mathcal{K}$  to define an  $\mathcal{B}_B^d$ -covariance sampler is that  $\Delta(\mathcal{K}) = \{0, \dots, d\}$ .

From Theorem 6.8 and Theorem 6.7, it follows that  $\mathcal{K}$  must be a length- $(NL-1)$  periodic circular sparse ruler of period  $N$ , which means that samplers for  $d$ -banded subspaces mimic those for circulant subspaces. Thus, one should apply the design and compression ratio considerations from Section 6.4.1. Interestingly, note that the latter does not depend on  $d$  provided that this parameter remains within the aforementioned limits.

## DENSE SAMPLERS

From Theorem 6.2 and noting that  $d$ -banded subspaces have dimension  $2d+1$  we obtain:

COROLLARY 6.2. Let  $\check{\Phi}$  be an  $\bar{N} \times N$  random matrix satisfying the hypotheses of Theorem 6.2 and let  $\mathcal{B}_B^d$  be given by (6.13). Then, with probability one, the matrix  $\Phi = \mathbf{I}_L \otimes \check{\Phi}$  defines a  $\mathcal{B}_B^d$ -covariance sampler if and only if

$$\bar{N} \geq \sqrt{\frac{2d+1}{2L-1}}. \quad (6.39)$$

According to this result, the maximum compression ratio is:

$$\rho = \frac{N}{\bar{N}} \approx \sqrt{\frac{(2L-1)N^2}{2d+1}}, \quad (6.40)$$

which clearly improves the ratio in (6.28) since  $d \leq NL-1$ .

---

<sup>7</sup>Strictly speaking, we only need the lags  $NL-N+1$  through  $NL-1$  to be zero since the lags greater than  $NL-1$  are not relevant in the model.

## 6.5 Asymptotic Regime

We next provide the optimal compression ratios for universal dense samplers and bound the optimal ratios for universal sparse samplers as  $\bar{N}$  and  $N$  become larger.

- **Dense Samplers:** The maximum compression ratio  $\rho_{\text{DS}}$  of universal dense samplers is given by (6.28). Asymptotically in  $N$ , we have that  $\rho_{\text{DS}} \rightarrow \sqrt{\frac{2L-1}{2L}}N$ , which becomes  $\rho_{\text{DS}} \rightarrow \sqrt{\frac{\bar{N}}{2}}$  in the non-periodic case and  $\rho_{\text{DS}} \rightarrow \sqrt{\bar{N}}$  if the number of periods  $L$  also becomes large. Alternatively, we observe that  $\bar{N} \rightarrow \sqrt{\frac{2L}{2L-1}}N$  as  $N$  becomes large, which means that  $\bar{N} \rightarrow \sqrt{2\bar{N}}$  in the non-periodic case and  $\bar{N} \rightarrow \sqrt{\bar{N}}$  as  $L \rightarrow \infty$ .
- **Sparse Samplers:** In [Leech, 1956, Pearson et al., 1990] it is established that the quotient  $\bar{N}^2/N$  asymptotically converges to a constant  $c$ , which is between<sup>8</sup>  $\tau \approx 2.434$  and 3, with  $\bar{N}$  and  $N - 1$  respectively denoting the cardinality and length of a minimal linear sparse ruler. Therefore, the asymptotic optimal compression ratio is given by

$$\rho_{\text{SS}} \rightarrow \sqrt{\frac{\bar{N}}{c}}. \quad (6.41)$$

In terms of  $\bar{N}$ , this means that  $\bar{N} \rightarrow \sqrt{c\bar{N}}$ . Interestingly, if we use nested arrays [Pumphrey, 1993, Pal and Vaidyanathan, 2010], the maximum achievable compression we can obtain for suitable choices of the parameters is  $\rho_{\text{NA}} \rightarrow \sqrt{\frac{\bar{N}}{4}}$ , which is therefore suboptimal. However, they present the advantage of having a simple design. The scheme in [Wichmann, 1963, Pearson et al., 1990] allows the simple construction of sparse rulers satisfying  $\bar{N}^2/N < 3$ , which entail compression ratios greater than  $\sqrt{\frac{\bar{N}}{3}}$  even for finite  $\bar{N}$  and  $N$ .

To sum up, dense samplers provide better asymptotic compression ratios than sparse samplers. The compression loss between both approaches is quantified by the constant  $c$ , and hence between 36% and 42% compression may be lost for large  $L$  if we use sparse sampling instead of dense sampling. Similar observations arise for non-universal samplers by using the expressions in Section 6.4.

Interestingly, these expressions show that the compression ratio can be made arbitrarily large just by increasing the number of observations. This conclusion agrees with [Masry, 1978].

---

<sup>8</sup>As an informal guess, consider the length-90 minimal sparse ruler, which has 16 elements. A simple approximation yields  $c \approx 16^2/91 \approx 2.8132$ .

## 6.6 Discussion

The compression ratio was defined such that it is independent of the number of realizations of  $\bar{\mathbf{y}}$ : note that each one is compressed using that ratio. In case of an arbitrarily large number of realizations, the maximum compression ratio separates consistency from inconsistency in the estimation. However, the notion of consistency is not truly meaningful in case of just one realization. For those cases, the values presented here provide simple guidelines to select suitable compression ratios and a guess of the quality of the estimation, in the sense that a good performance is expected when the actual compression ratio is much lower than the maximum one and *vice versa*.

## 6.7 Conclusions

We have formalized the problem of sampler design for CCS under the notion of covariance sampler, which are those preserving the second-order statistics. Based on a linear compression model and a linear covariance parameterization, we found optimal covariance samplers for a number of important cases, including Toeplitz, circulant, and banded covariance subspaces, both operating in a periodic or non-periodic fashion.

Two compression architectures were considered, namely sparse and dense samplers. For Toeplitz subspaces, the design of optimal sparse samplers is related to the minimal *linear* sparse ruler problem, which, despite requiring exhaustive search, can be approximately solved using simple methods. For circulant and banded subspaces, optimal sparse samplers deal with *circular* sparse rulers, which enable stronger compression ratios than their linear counterpart. On the other hand, a much simpler technique was presented to design dense samplers: a compression matrix drawn using a continuous distribution was seen to be a covariance sampler with probability one if its dimensions are properly set. As opposed to the presented sparse designs, which are optimal *only* within the family of sparse samplers, the random designs proposed here result in samplers which are optimal in general, that is, no other covariance sampler (either dense or sparse) can do better.

The work in this chapter was published on the *IEEE Transactions on Information Theory* [Romero et al., 2015d] and presented in part in the *2013* and *2014 Information Theory and Applications Workshop (ITA 2013 and ITA 2014)* [Romero and Leus, 2013a].

## 6.A Proof of Lemma 6.1

Clearly, if  $\phi$  is invertible so is  $\phi|_{\mathcal{A}}$ . In order to prove the converse statement, it suffices to show that  $\phi$  is injective if  $\phi|_{\mathcal{A}}$  is injective. This is a simple consequence of the definition of the codomains for both functions. Therefore, we need to prove that, given any two vectors  $\mathbf{c} = [c_0, \dots, c_{B-1}]^T$  and  $\mathbf{d} = [d_0, \dots, d_{B-1}]^T$  in  $\mathbb{R}^B$ , the matrices

$$\Xi_{\mathbf{c}} = \sum_b c_b \Xi_b \quad \text{and} \quad \Xi_{\mathbf{d}} = \sum_b d_b \Xi_b \quad (6.42)$$

must satisfy that

$$\phi(\Xi_{\mathbf{c}}) = \phi(\Xi_{\mathbf{d}}) \Rightarrow \Xi_{\mathbf{c}} = \Xi_{\mathbf{d}} \quad (6.43)$$

or, equivalently, that

$$\phi(\Xi_{\mathbf{c}}) = \phi(\Xi_{\mathbf{d}}) \Rightarrow \mathbf{c} = \mathbf{d}, \quad (6.44)$$

since  $\mathcal{B}$  is linearly independent. To do so, let us consider  $B$  linearly independent vectors  $\alpha_0, \dots, \alpha_{B-1}$ , where  $\alpha_i = [\alpha_{i,0} \dots \alpha_{i,B-1}]^T$ , such that the  $B$  matrices

$$\Xi_{\alpha_i} = \sum_b \alpha_{i,b} \Xi_b, \quad i = 0, \dots, B-1 \quad (6.45)$$

are in  $\mathcal{A}$ . This operation is possible since  $\dim_{\mathbb{R}}[\mathcal{A} \cap \text{span}_{\mathbb{R}} \mathcal{B}] = B$ . Moreover, since  $\phi|_{\mathcal{A}}$  is injective and  $\{\Xi_{\alpha_i}\}_{i=0}^{B-1}$  is a linearly independent set of matrices, it follows that the matrices

$$\bar{\Xi}_{\alpha_i} = \phi|_{\mathcal{A}}(\Xi_{\alpha_i}) = \phi(\Xi_{\alpha_i}) = \sum_b \alpha_{i,b} \bar{\Xi}_b \quad (6.46)$$

also form an independent set of matrices. On the other hand, since the  $B$  vectors  $\alpha_i$  constitute a basis for  $\mathbb{R}^B$ , it is possible to write  $\mathbf{c}$  and  $\mathbf{d}$  as:

$$\mathbf{c} = \sum_i \tilde{c}_i \alpha_i \quad \text{and} \quad \mathbf{d} = \sum_i \tilde{d}_i \alpha_i, \quad (6.47)$$

for some  $\tilde{c}_i, \tilde{d}_i \in \mathbb{R}$ , which in turn means that

$$\Xi_{\mathbf{c}} = \sum_i \tilde{c}_i \Xi_{\alpha_i} \quad \text{and} \quad \Xi_{\mathbf{d}} = \sum_i \tilde{d}_i \Xi_{\alpha_i} \quad (6.48)$$

or

$$\phi(\Xi_c) = \sum_i \tilde{c}_i \bar{\Xi}_{\alpha_i} \quad \text{and} \quad \phi(\Xi_d) = \sum_i \tilde{d}_i \bar{\Xi}_{\alpha_i}. \quad (6.49)$$

Noting that the matrices  $\bar{\Xi}_{\alpha_i}$  are linearly independent leads to the statement

$$\phi(\Xi_c) = \phi(\Xi_d) \quad \Rightarrow \quad \tilde{c}_i = \tilde{d}_i \quad \forall i, \quad (6.50)$$

which is equivalent to (6.44), thus concluding the proof.

## 6.B Proof of Theorem 6.2

In order to show Theorem 6.2, we will compute the dimension of  $\ker \phi_{\mathbb{C}}$  and derive the conditions under which  $\dim \ker \phi_{\mathbb{C}} = 0$ , which, in virtue of Lemma 6.4, are the conditions determining whether  $\Phi$  defines a covariance sampler. The computation of  $\ker \phi_{\mathbb{C}}$  is accomplished in several steps. First, we find  $\ker \tilde{\phi}_{\mathbb{C}}$ , where  $\tilde{\phi}_{\mathbb{C}}$  is defined as the extension of  $\phi_{\mathbb{C}}$  to  $\mathbb{C}^{K \times K}$ :

$$\begin{array}{ccc} \mathbb{C}^{NL \times NL} & \xrightarrow{\tilde{\phi}_{\mathbb{C}}} & \mathbb{C}^{\bar{N}L \times \bar{N}L} \\ \Xi & \longrightarrow & \bar{\Xi} = \Phi \Xi \Phi^H. \end{array} \quad (6.51)$$

We then compute  $\dim \ker \phi_{\mathbb{C}}$  by noting that

$$\ker \phi_{\mathbb{C}} = \text{span}_{\mathbb{C}} \mathcal{B} \cap \left( \mathbb{P}^{NL} \cap \left( \mathbb{B}^{N,L} \cap \ker \tilde{\phi}_{\mathbb{C}} \right) \right), \quad (6.52)$$

where  $\mathbb{P}^{NL}$  represents the set of (not necessarily Hermitian)  $NL \times NL$  Toeplitz matrices and  $\mathbb{B}^{N,L}$  represents the set of  $NL \times NL$  matrices with Toeplitz  $N \times N$  blocks. The matrices in  $\mathbb{B}^{N,L}$  can thus be written as

$$\begin{bmatrix} \mathbf{A}_{0,0} & , \cdots , & \mathbf{A}_{0,L-1} \\ \vdots & & \vdots \\ \mathbf{A}_{L-1,0} & , \cdots , & \mathbf{A}_{L-1,L-1} \end{bmatrix} \quad (6.53)$$

where the blocks  $\mathbf{A}_{l,l'} \in \mathbb{C}^{N \times N}$  are Toeplitz. Expression (6.52) follows from the fact that  $\ker \phi_{\mathbb{C}} = \text{span}_{\mathbb{C}} \mathcal{B} \cap \ker \tilde{\phi}_{\mathbb{C}}$  and

$$\text{span}_{\mathbb{C}} \mathcal{B} \subset \mathbb{P}^{NL} \subset \mathbb{B}^{N,L}. \quad (6.54)$$

On the other hand, the fact that the probability measure is absolutely continuous with respect to Lebesgue measure means that the probability that any row (or column) of  $\tilde{\Phi}$  is in a *given* subspace of dimension less than  $N$  (resp.  $\bar{N}$ ) is zero. Another consequence is that  $\text{rank } \tilde{\Phi} = \bar{N} \leq N$  with probability one and, as a result, the (right) null space of  $\tilde{\Phi}$  has dimension  $N - \bar{N}$ . Let us denote by  $\mathbf{V}$  an  $N \times (N - \bar{N})$  matrix whose columns span this null space. For the same argument, it is clear that the probability that the columns of  $\mathbf{V}$  are contained in a given subspace of dimension less than  $N$  is zero.

We start by computing a basis for  $\ker \tilde{\phi}_{\mathbb{C}}$  in terms of  $\mathbf{V}$ .

LEMMA 6.6. *Let  $\mathbf{E}_{l,l'} \in \mathbb{C}^{L \times L}$  be the matrix with all entries set to zero but the  $(l, l')$ -th entry, which is one, and let  $\mathbf{e}_n$  denote the  $n$ -th column of the identity matrix  $\mathbf{I}_N$ . Let also  $\tilde{\phi}_{\mathbb{C}}$  be defined as in (6.51), and let the columns of  $\mathbf{V} = [\mathbf{v}_0, \dots, \mathbf{v}_{N-\bar{N}-1}] \in \mathbb{C}^{N \times (N-\bar{N})}$  form a basis for the null space of  $\tilde{\Phi}$ . Then, a basis for  $\ker \tilde{\phi}_{\mathbb{C}}$  is given by*

$$\mathcal{W} = \bigcup_{l=0}^{L-1} \bigcup_{l'=0}^{L-1} \mathcal{W}_{l,l'}, \quad (6.55)$$

where

$$\begin{aligned} \mathcal{W}_{l,l'} = & \left\{ \mathbf{E}_{l,l'} \otimes \mathbf{e}_n \otimes \mathbf{v}_m^H, n = 0, 1, \dots, N-1, m = 0, 1, \dots, N-\bar{N}-1 \right\} \\ & \cup \left\{ \mathbf{E}_{l,l'} \otimes \mathbf{e}_n^H \otimes \mathbf{v}_m, n = 0, 1, \dots, \bar{N}-1, m = 0, 1, \dots, N-\bar{N}-1 \right\}. \end{aligned} \quad (6.56)$$

*Proof.* See Appendix 6.C. □

Now let us evaluate the intersection  $\mathbb{B}^{N,L} \cap \ker \tilde{\phi}_{\mathbb{C}}$ , which means that we must look for the matrices in  $\ker \tilde{\phi}_{\mathbb{C}}$  whose  $N \times N$  blocks have a Toeplitz structure. For the sake of simplicity, let us proceed on a block-by-block basis by separately considering the subspaces generated by each  $\mathcal{W}_{l,l'}$ . Clearly, only the  $(l, l')$ -th block of size  $N \times N$  can be nonzero in the matrices of  $\text{span}_{\mathbb{C}} \mathcal{W}_{l,l'}$ . This block is in the subspace spanned by the following basis:

$$\begin{aligned} & \{ \mathbf{e}_n \otimes \mathbf{v}_m^H, n = 0, 1, \dots, N-1, m = 0, 1, \dots, N-\bar{N}-1 \} \\ & \cup \{ \mathbf{e}_n^H \otimes \mathbf{v}_m, n = 0, 1, \dots, \bar{N}-1, m = 0, 1, \dots, N-\bar{N}-1 \}. \end{aligned} \quad (6.57)$$

Therefore, all the blocks in this subspace can be written as

$$\sum_n \sum_m \alpha_{n,m} (\mathbf{e}_n \otimes \mathbf{v}_m^H) + \sum_n \sum_m \alpha'_{n,m} (\mathbf{e}_n^H \otimes \mathbf{v}_m) \quad (6.58)$$

for some  $\alpha_{n,m} \in \mathbb{C}$  and  $\alpha'_{n,m} \in \mathbb{C}$ . The blocks with Toeplitz structure must necessarily satisfy

$$\sum_{n=-N+1}^{N-1} \beta_n \mathbf{P}_n = \sum_{n=0}^{N-1} \sum_{m=0}^{N-\bar{N}-1} \alpha_{n,m} (\mathbf{e}_n \otimes \mathbf{v}_m^H) + \sum_{n=0}^{\bar{N}-1} \sum_{m=0}^{N-\bar{N}-1} \alpha'_{n,m} (\mathbf{e}_n^H \otimes \mathbf{v}_m) \quad (6.59)$$

for some  $\beta_n \in \mathbb{C}$ , where  $\mathbf{P}_n$  equals  $\mathbf{J}_N^n$  for  $n \geq 0$  and  $(\mathbf{J}_N^{-n})^T$  for  $n < 0$ , with  $\mathbf{J}_N$  defined in Section 6.1.2.

Expression (6.59) represents a system of linear equations in  $\alpha_{n,m}$ ,  $\alpha'_{n,m}$ , and  $\beta_n$ , with  $N^2 - \bar{N}^2 + 2N - 1$  complex unknowns and  $N^2$  equations. On the other hand, since  $\tilde{\Phi}$ , and consequently  $\mathbf{V}$ , follows a continuous distribution, there are  $\min(N^2, N^2 - \bar{N}^2 + 2N - 1)$  independent matrices in (6.59). Consequently, if  $N^2 \geq N^2 - \bar{N}^2 + 2N - 1$  the only solution is  $\beta_n = 0 \forall n$ , and  $\mathbb{B}^{N,L} \cap \ker \tilde{\phi}_{\mathbb{C}} = \{\mathbf{0}\}$ , which in turn means that  $\ker \phi_{\mathbb{C}} = \{\mathbf{0}\}$ . Therefore, a sufficient condition for  $\Phi$  to define a covariance sampler (see Lemma 6.4) is

$$\bar{N}^2 \geq 2N - 1. \quad (6.60)$$

Conversely, if  $N^2 < N^2 - \bar{N}^2 + 2N - 1$  the subspace of solutions has dimension  $N^2 - \bar{N}^2 + 2N - 1 - N^2 = 2N - \bar{N}^2 - 1$ . Therefore, the blocks of the matrices in  $\mathbb{B}^{N,L} \cap \ker \tilde{\phi}_{\mathbb{C}}$  can be written as a linear combination of  $2N - \bar{N}^2 - 1$  Toeplitz matrices  $\bar{\mathbf{P}}_k$ . By considering all blocks, it follows that  $\mathbb{B}^{N,L} \cap \ker \tilde{\phi}_{\mathbb{C}}$  is generated by the following basis:

$$\left\{ \mathbf{E}_{l,l'} \otimes \bar{\mathbf{P}}_k, \quad l, l' = 0, 1, \dots, L-1; \quad k = 0, 1, \dots, 2N - \bar{N}^2 - 2 \right\}. \quad (6.61)$$

Thus, any matrix in  $\mathbb{B}^{N,L} \cap \ker \tilde{\phi}_{\mathbb{C}}$  can be written as

$$\Xi = \sum_{l,l',k} c_{l,l',k} \mathbf{E}_{l,l'} \otimes \bar{\mathbf{P}}_k. \quad (6.62)$$

Now we compute the dimension of  $\mathbb{P}^{NL} \cap (\mathbb{B}^{N,L} \cap \ker \tilde{\phi}_{\mathbb{C}})$ . First note that  $\dim(\mathbb{B}^{N,L} \cap \ker \tilde{\phi}_{\mathbb{C}}) = L^2(2N - \bar{N}^2 - 1)$ . In order for  $\Xi \in \mathbb{B}^{N,L} \cap \ker \tilde{\phi}_{\mathbb{C}}$  to be Toeplitz, we require that  $c_{l,l',k}$  only depend on the difference  $l - l'$ , which reduces the dimension of this subspace to  $2N - \bar{N}^2 - 1$  times the number of block diagonals, i.e.,  $(2N - \bar{N}^2 - 1)(2L - 1)$ . Moreover, since any two adjacent block diagonals share  $N - 1$  diagonals, this imposes  $(2L - 2)(N - 1)$  additional equations and thus

$$\dim\left(\mathbb{P}^{NL} \cap \left(\mathbb{B}^{N,L} \cap \ker \tilde{\phi}_{\mathbb{C}}\right)\right) = (2N - \bar{N}^2 - 1)(2L - 1) - (2L - 2)(N - 1).$$



At this point, note that  $\mathbb{P}^{NL}$  is the smallest subspace containing both  $\mathbb{P}^{NL} \cap \mathbb{B}^{N,L} \cap \ker \tilde{\phi}_{\mathbb{C}}$  and  $\text{span}_{\mathbb{C}} \mathcal{B}$ . Since  $\tilde{\Phi}$  was generated according to a continuous distribution, then with probability one these two subspaces will not overlap — except for the zero matrix — unless the sum of their dimensions exceeds the dimension of the parent subspace, which is  $2NL - 1$ . Invoking Lemma 6.4 we find that  $\Phi$  defines a covariance sampler if and only if

$$(2N - \bar{N}^2 - 1)(2L - 1) - (2L - 2)(N - 1) + B \leq 2NL - 1$$

or, equivalently

$$B \leq \bar{N}^2(2L - 1). \quad (6.63)$$

It remains only to show that one only needs to look at (6.63) in order to assess whether a matrix  $\Phi$  defines a covariance sampler, the condition in (6.60) being completely irrelevant. This follows from the fact that (6.60) implies (6.63). Indeed, if we multiply both sides of (6.60) by  $(2L - 1)$ , we obtain

$$\bar{N}^2(2L - 1) \geq (2N - 1)(2L - 1) \quad (6.64a)$$

$$= (2NL - 1) + 2(N - 1)(L - 1) \quad (6.64b)$$

$$\geq (2NL - 1) \geq B \quad (6.64c)$$

where the second inequality follows from the fact that  $(N - 1)(L - 1) \geq 0$  and the third one is a consequence of the linear independence of  $\mathcal{B}$ . Therefore, (6.60) implies (6.63), and  $\Phi$  defines a covariance sampler if and only if (6.63) holds.

## 6.C Proof of Lemma 6.6

Computing  $\ker \tilde{\phi}_{\mathbb{C}}$  amounts to finding a basis for the subspace of matrices  $\Xi$  in  $\mathbb{C}^{NL \times NL}$  satisfying  $\Phi \Xi \Phi^H = \mathbf{0}$ . Vectorizing this expression produces  $(\Phi^* \otimes \Phi) \xi = \mathbf{0}$ , where  $\xi = \text{vec } \Xi$  (see e.g. [Bernstein, 2009]). Thus,  $\ker \tilde{\phi}_{\mathbb{C}}$  is given, up to inverse vectorization, by the null space of the  $(\bar{N}L)^2 \times (NL)^2$  matrix  $\Phi^* \otimes \Phi$ .

Since the columns of  $V$  constitute a basis for the null space of  $\tilde{\Phi}$  and since  $\Phi = I_L \otimes \tilde{\Phi}$ , the columns of  $\bar{V} = I_L \otimes V$  constitute a basis for the null-space of  $\Phi$ . It can be shown that  $\ker \tilde{\phi}_{\mathbb{C}}$  is composed of matrices of the form  $\Xi = \bar{V}C^H + D\bar{V}^H$ , where  $C$  and  $D$  are arbitrary matrices of the appropriate dimensions. It follows that the null space of  $\Phi^* \otimes \Phi$  is spanned by

the columns of the matrix

$$\bar{\mathbf{W}} = [\mathbf{I}_{NL} \otimes \bar{\mathbf{V}}, \quad \bar{\mathbf{V}}^* \otimes \mathbf{I}_{NL}]. \quad (6.65)$$

By the properties of the Kronecker product [Bernstein, 2009], the fact that  $\check{\Phi}$  has maximum rank implies that  $\Phi^* \otimes \Phi$  has maximum rank too, which means that its null space has dimension  $(N^2 - \bar{N}^2)L^2$ . However, since  $\bar{\mathbf{V}}$  is  $NL \times (N - \bar{N})L$ , it is clear that  $\bar{\mathbf{W}}$  has  $2(N - \bar{N})NL^2$  columns, which is greater than  $(N^2 - \bar{N}^2)L^2$ . Thus, in order to obtain a basis for the null space of  $\Phi^* \otimes \Phi$  we should remove dependent columns from  $\bar{\mathbf{W}}$ . This procedure is carried out by the following lemma:

LEMMA 6.7. *Let  $\mathbf{V} \in \mathbb{C}^{N \times (N - \bar{N})}$ , with  $\bar{N} \leq N$ , be a matrix whose columns generate the null space of  $\check{\Phi} \in \mathbb{C}^{\bar{N} \times N}$ , which follows a continuous distribution, and let  $\bar{\mathbf{V}} = \mathbf{I}_L \otimes \mathbf{V}$ . Then, the columns of  $\bar{\mathbf{W}}$ , defined by (6.65), span the same subspace as the columns of  $\bar{\bar{\mathbf{W}}}$ , which is defined as*

$$\bar{\bar{\mathbf{W}}} = [\mathbf{I}_{NL} \otimes \bar{\mathbf{V}}, \quad \bar{\mathbf{V}}^* \otimes \mathbf{I}_L \otimes \mathbf{F}_{N, \bar{N}}], \quad (6.66)$$

where  $\mathbf{F}_{N, \bar{N}} = [\mathbf{I}_{\bar{N}}, \quad \mathbf{0}_{\bar{N}, N - \bar{N}}]^T$ .

*Proof.* The procedure we follow in this proof is to remove linearly dependent columns from  $\bar{\mathbf{W}}$ . Since the case  $L > 1$  is quite tedious, here we only show this result for the case  $L = 1$ . The proof for the former case follows the same lines and it is easily extrapolated, but it requires overloading the notation. For  $L = 1$  we have that

$$\bar{\mathbf{W}} = [\mathbf{I}_N \otimes \mathbf{V}, \quad \mathbf{V}^* \otimes \mathbf{I}_N]. \quad (6.67)$$

Now scale the last  $N(N - \bar{N})$  columns of  $\bar{\mathbf{W}}$  to obtain

$$\bar{\mathbf{W}}' = [\mathbf{I}_N \otimes \mathbf{V}, \quad \mathbf{G} \otimes \mathbf{I}_N], \quad (6.68)$$

where  $\mathbf{G}$  is the result of scaling the columns of  $\mathbf{V}^*$  such that the first row contains only ones<sup>9</sup>:

$$\mathbf{G} = \begin{bmatrix} 1 & 1 & \dots & 1 \\ g_{1,0} & g_{1,1} & \dots & g_{1,N-\bar{N}-1} \\ \vdots & \vdots & \ddots & \vdots \\ g_{N-1,0} & g_{N-1,1} & \dots & g_{N-1,N-\bar{N}-1} \end{bmatrix} \quad (6.69)$$

---

<sup>9</sup>This is always possible whenever the elements of the first row of  $\mathbf{V}$  are all different from zero. However, it is possible with probability one to choose  $\mathbf{V}$  such that it generates the null space of  $\check{\Phi}$  and satisfies this condition.

Now consider a submatrix of  $\bar{\mathbf{W}}'$  obtained by retaining the first  $N(N - \bar{N})$  columns and the columns with indices  $N(N - \bar{N}) + Ni, \dots, N(N - \bar{N}) + N(i + 1) - 1$ , i.e.,

$$\bar{\mathbf{W}}'_i = \begin{bmatrix} \mathbf{V} & \mathbf{0} & \dots & \mathbf{0} & \mathbf{I}_N \\ \mathbf{0} & \mathbf{V} & \dots & \mathbf{0} & g_{1,i}\mathbf{I}_N \\ & & \ddots & & \\ \mathbf{0} & \mathbf{0} & \dots & \mathbf{V} & g_{N-1,i}\mathbf{I}_N \end{bmatrix}, \quad (6.70)$$

where  $i = 0, \dots, N - \bar{N} - 1$ . Scaling the diagonal blocks on the left yields:

$$\bar{\mathbf{W}}''_i = \begin{bmatrix} \mathbf{V} & \mathbf{0} & \dots & \mathbf{0} & \mathbf{I}_N \\ \mathbf{0} & g_{1,i}\mathbf{V} & \dots & \mathbf{0} & g_{1,i}\mathbf{I}_N \\ & & \ddots & & \\ \mathbf{0} & \mathbf{0} & \dots & g_{N-1,i}\mathbf{V} & g_{N-1,i}\mathbf{I}_N \end{bmatrix}. \quad (6.71)$$

Now, since  $\check{\Phi}$  follows a continuous distribution, the last  $N - \bar{N}$  columns of  $[\mathbf{V}, \mathbf{I}_N]$  can be written as linear combinations of the first  $N$  columns, which means that the last  $N - \bar{N}$  columns of  $\bar{\mathbf{W}}'_i$  are linearly dependent of the others. Repeating this operation for  $i = 0, \dots, N - \bar{N} - 1$  and removing from  $\bar{\mathbf{W}}$  the columns declared as dependent at each  $i$  gives

$$\bar{\bar{\mathbf{W}}} = [\mathbf{I}_N \otimes \mathbf{V}, \quad \mathbf{V}^* \otimes \mathbf{F}_{N,\bar{N}}], \quad (6.72)$$

which clearly spans the same subspace as  $\bar{\mathbf{W}}$ . For  $L \geq 1$  we obtain (6.66).  $\square$

Note that, indeed, the matrix defined in (6.66) has  $(N^2 - \bar{N}^2)L^2$  columns, which means that they constitute a basis for the null space of  $\Phi^* \otimes \Phi$ . Upon considering the inverse vectorization of the columns of  $\bar{\bar{\mathbf{W}}}$ , we obtain the sought basis in matrix form:

$$\begin{aligned} \mathcal{W} = & \left\{ \mathbf{E}_{l,l'} \otimes \mathbf{e}_m \otimes \mathbf{v}_m^H, \quad l, l' = 0, 1, \dots, L - 1, \quad m = 0, 1, \dots, N - 1, \quad m = 0, 1, \dots, N - \bar{N} - 1 \right\} \\ & \cup \left\{ \mathbf{E}_{l,l'} \otimes \mathbf{e}_m^H \otimes \mathbf{v}_m, \quad l, l' = 0, 1, \dots, L - 1, \quad m = 0, 1, \dots, \bar{N} - 1, \quad m = 0, 1, \dots, N - \bar{N} - 1 \right\}. \end{aligned}$$

## 6.D Proof of Theorem 6.4

Clearly, if  $\mathcal{N}$  is a length- $(N - 1)$  sparse ruler, then (6.24) defines a periodic sparse ruler. To show the converse statement, assume that  $\mathcal{K}$  is a periodic sparse ruler and take  $\mathcal{N} = \mathcal{K} \cap \{0, \dots, N - 1\}$ . Then,  $\{0, \dots, NL - 1\} \subset \Delta(\mathcal{K})$  and, in particular,  $\{N(L - 1), \dots, NL - 1\} \subset \Delta(\mathcal{K})$ , meaning

that

$$\forall \delta \in \{N(L-1), \dots, NL-1\}, \exists q, q' \in \mathcal{K} \text{ s.t. } q' - q = \delta.$$

Due to the periodicity of  $\mathcal{K}$ , any  $k \in \mathcal{K}$  can be uniquely decomposed as  $k = n_k + l_k N$ , where  $n_k \in \mathcal{N}$  and  $l_k \in \{0, \dots, L-1\}$ . Denote as  $n_q$ ,  $n_{q'}$ ,  $l_q$  and  $l_{q'}$  the corresponding coefficients of the decomposition of  $q$  and  $q'$ . Therefore, the condition above becomes

$$\begin{aligned} \forall \delta \in \{N(L-1), \dots, NL-1\}, \exists n_q, n_{q'} \in \mathcal{N} \\ \text{and } l_q, l_{q'} \in \{0, \dots, L-1\} \text{ s.t. } n_{q'} - n_q + (l_{q'} - l_q)N = \delta. \end{aligned} \quad (6.73)$$

Since  $n_{q'} - n_q \leq N-1$  and  $\delta \geq N(L-1)$ , it is clear that  $l_{q'} - l_q$  must equal  $L-1$  in order for the condition  $n_{q'} - n_q + (l_{q'} - l_q)N = \delta$  to hold. Then, after subtracting  $N(L-1)$ , the following equivalent expression arises:

$$\forall \delta \in \{0, \dots, N-1\}, \exists n_q, n_{q'} \in \mathcal{N} \text{ s.t. } n_{q'} - n_q = \delta.$$

Hence,  $\mathcal{N}$  is a sparse ruler.

## 6.E Proof of Theorem 6.6

Assume that  $K$  is odd. The proof for  $K$  even follows similar lines. If  $\Delta(\mathcal{K}) = \{0, \dots, K-1\}$ , then the matrix from Theorem 6.1 is given by:

$$\mathbf{C} = \begin{bmatrix} 1 & \mathbf{0}_{\tilde{K}}^T & \mathbf{0}_{\tilde{K}}^T \\ \mathbf{0}_{\tilde{K}} & \mathbf{I}_{\tilde{K}} & -j\mathbf{I}_{\tilde{K}} \\ \mathbf{0}_{\tilde{K}} & \mathbf{V}_{\tilde{K}} & j\mathbf{V}_{\tilde{K}} \\ 1 & \mathbf{0}_{\tilde{K}}^T & \mathbf{0}_{\tilde{K}}^T \\ \mathbf{0}_{\tilde{K}} & \mathbf{I}_{\tilde{K}} & j\mathbf{I}_{\tilde{K}} \\ \mathbf{0}_{\tilde{K}} & \mathbf{V}_{\tilde{K}} & -j\mathbf{V}_{\tilde{K}} \end{bmatrix} \quad (6.74)$$

where  $\tilde{K} = \frac{K-1}{2}$ ,  $\mathbf{0}_{\tilde{K}}$  is an  $\tilde{K} \times 1$  vector with all zeros and  $\mathbf{V}_{\tilde{K}}$  is an  $\tilde{K} \times \tilde{K}$  Hankel matrix with ones on the antidiagonal and zeros elsewhere, i.e., its  $(i, j)$ -th element equals 1 if  $i + j = \tilde{K} - 1$  and 0 otherwise. Since all the columns are linearly independent,  $\text{rank}(\mathbf{C}) = K$  and, according to Theorem 6.1,  $\mathcal{K}$  is a  $\mathcal{B}_C$ -covariance sampler.

Now consider removing elements from  $\Delta(\mathcal{K})$ . It can readily be seen that  $\mathbf{C}$  is not full rank iff there is some  $\delta \in \{0, \dots, K-1\}$  such that  $\delta \notin \Delta(\mathcal{K})$  and  $K - \delta \notin \Delta(\mathcal{K})$ . Equivalently, we

can say that  $\mathcal{C}$  is full rank iff  $\Delta_K(\mathcal{K}) = \{0, \dots, K-1\}$ .

## 6.F Proof of Theorem 6.7

Let us start by showing that if  $\mathcal{N}$  is a circular sparse ruler, then  $\mathcal{K}$  is a periodic circular sparse ruler or, in other words, if  $\Delta_N(\mathcal{N}) = \{0, \dots, N-1\}$ , then  $\Delta_{NL}(\mathcal{K}) = \{0, \dots, NL-1\}$ . Consider any  $\delta \in \{0, \dots, N-1\}$ . Since  $\delta \in \Delta_N(\mathcal{N})$ , at least one of the following two conditions will hold:

$$\text{C1: } \exists n_1, n_2 \in \mathcal{N}, n_2 \geq n_1 \text{ such that } (n_2 - n_1)_N = n_2 - n_1 = \delta, \quad (6.75)$$

$$\text{C2: } \exists n_1, n_2 \in \mathcal{N}, n_2 < n_1 \text{ such that } (n_2 - n_1)_N = N + n_2 - n_1 = \delta.$$

In both cases, all the elements of the form  $\delta + lN$ , with  $l = 0, \dots, L-1$ , are in  $\Delta_{NL}(\mathcal{K})$ :

- C1: consider  $k_2 = n_2 + lN$  and  $k_1 = n_1$  for any  $l = 0, \dots, L-1$ . Since  $k_1, k_2 \in \mathcal{K}$ , it follows that  $(k_2 - k_1)_{NL} = n_2 + lN - n_1 = \delta + lN \in \Delta_{NL}(\mathcal{K})$ .
- C2: first make  $k_1 = n_1$  and  $k_2 = n_2 + N + lN$  with  $l = 0, \dots, L-2$ . Since  $k_1, k_2 \in \mathcal{K}$ , then  $(k_2 - k_1)_{NL} = n_2 + N + lN - n_1 = \delta + lN \in \Delta_{NL}(\mathcal{K})$ . It remains only to show that  $\delta + lN \in \Delta_{NL}(\mathcal{K})$  when  $l = L-1$ . To this end, consider  $k_1 = n_1$  and  $k_2 = n_2$ , which results in  $(k_2 - k_1)_{NL} = NL + n_2 - n_1 = N(L-1) + N + n_2 - n_1 = N(L-1) + \delta \in \Delta_{NL}(\mathcal{K})$ .

To sum up, we have shown that  $\delta + lN \in \Delta_{NL}(\mathcal{K})$  for any  $\delta = 0, \dots, N-1$  and  $l = 0, \dots, L-1$ , which establishes that  $\mathcal{K}$  is a circular sparse ruler.

For the converse theorem, suppose that  $\mathcal{K}$  is a circular sparse ruler, i.e.,  $\Delta_{NL}(\mathcal{K}) = \{0, \dots, NL-1\}$ . In particular, all modular distances of the form  $\delta = \{0, \dots, N-1\}$  are present in  $\Delta_{NL}(\mathcal{K})$ , which means that one or both of the following two conditions will be satisfied:

$$\text{C1': } \exists k_1, k_2 \in \mathcal{K}, k_2 \geq k_1 \text{ such that } (k_2 - k_1)_{NL} = k_2 - k_1 = \delta, \quad (6.76)$$

$$\text{C2': } \exists k_1, k_2 \in \mathcal{K}, k_2 < k_1 \text{ such that } (k_2 - k_1)_{NL} = NL + k_2 - k_1 = \delta. \quad (6.77)$$

But, if  $\mathcal{N} = \mathcal{K} \cap \{0, \dots, N-1\}$ , then  $\delta \in \Delta_N(\mathcal{N})$  in both cases:

- C1': clearly, we can assume without any loss of generality that  $k_1 \in \mathcal{N}$ . According to whether  $k_2$  is also in  $\mathcal{N}$  or not, we distinguish two scenarios:
  - $k_2 \in \mathcal{N}$ : in this case, it is clear that  $(k_2 - k_1)_N = k_2 - k_1 = \delta \in \Delta_N(\mathcal{N})$ .
  - $k_2 \notin \mathcal{N}$ : since  $0 \leq \delta < N$ , it follows that  $k_2$  can be written as  $k_2 = n + N$  for some  $n \in \mathcal{N}$  with  $n < k_1$ . Therefore,  $(n - k_1)_N = N + n - k_1 = k_2 - k_1 = \delta \in \Delta_N(\mathcal{N})$ .

- C2': since  $0 \leq \delta < N$ , it can be seen that  $N(L-1) < k_1 - k_2 \leq NL$ , which in turn requires  $k_2 \in \mathcal{N}$  and  $k_1 = n + N(L-1)$  for some  $n \in \mathcal{N}$  with  $n > k_2$ . Now consider the circular distance between  $n$  and  $k_2$ :

$$(k_2 - n)_N = N + k_2 - n = N + k_2 - [k_1 - N(L-1)] = k_2 - k_1 + NL = \delta \in \Delta_N(\mathcal{N}).$$

Therefore, we have shown that  $\delta \in \Delta_N(\mathcal{N})$  for all  $\delta = 0, \dots, N-1$ , which means that  $\mathcal{N}$  is a circular sparse ruler.

## 6.G Proof of Theorem 6.8

If we form the matrix  $\mathbf{C}$  in Theorem 6.1 using the matrices from (6.13), we conclude that  $\mathcal{K}$  defines a covariance sampler iff  $\{0, \dots, d\} \subset \Delta(\mathcal{K})$ . The latter condition is equivalent to:

$$\begin{aligned} \forall \delta \in \{0, \dots, d\}, \exists n_1, n_2 \in \mathcal{N} \text{ and } l_1, l_2 \in \{0, \dots, L-1\} \\ \text{such that } n_2 - n_1 + (l_2 - l_1)N = \delta. \end{aligned} \quad (6.78)$$

We next show that, if  $\mathcal{N}$  is a circular sparse ruler, then  $\delta \in \Delta(\mathcal{K})$  for all  $\delta \in \{0, \dots, N(L-1)\}$ , which in turn implies (6.78). Consider two cases:

- Case  $0 \leq \delta < N(L-1)$ : It suffices to write  $\delta$  as  $\delta = n_\delta + l_\delta N$ , with  $n_\delta \in \{0, \dots, N-1\}$  and  $l_\delta \in \{0, \dots, L-2\}$ . Since  $n_\delta \in \Delta_N(\mathcal{N})$ , then  $n_\delta$  can be represented either as  $n_{\delta,2} - n_{\delta,1}$  or as  $N + n_{\delta,2} - n_{\delta,1}$ , with  $n_{\delta,1}, n_{\delta,2} \in \mathcal{N}$ . In the former case just make  $n_2 = n_{\delta,2}$ ,  $n_1 = n_{\delta,1}$ ,  $l_2 = l_\delta$  and  $l_1 = 0$ . In the latter case make  $n_2 = n_{\delta,2}$ ,  $n_1 = n_{\delta,1}$ ,  $l_2 = l_\delta + 1$  and  $l_1 = 0$ .
- Case  $\delta = N(L-1)$ : this is trivial since  $N(L-1) \in \Delta(\mathcal{K})$  for any non-empty choice of  $\mathcal{N}$ .

Now, in order to prove the converse theorem, we show that if  $\{0, \dots, N-1\} \subset \Delta(\mathcal{K})$ , then  $\{0, \dots, N-1\} \subset \Delta_N(\mathcal{N})$ . Choose  $\delta \in \{0, \dots, N-1\}$ . Since  $\delta \in \Delta(\mathcal{K})$ , it is clear that there exist some  $n_1, n_2 \in \mathcal{N}$  and  $l_1, l_2 \in \{0, \dots, L-1\}$  such that  $n_2 - n_1 + (l_2 - l_1)N = \delta$ . In particular,  $(l_2 - l_1)$  can be either 0 or 1. Therefore, for any  $\delta \in \{0, \dots, N-1\}$ , there exists  $n_1, n_2 \in \mathcal{N}$  such that either  $n_2 - n_1 = \delta$  or  $N + n_2 - n_1 = \delta$ . Noting that this condition is equivalent to the condition  $\{0, \dots, N-1\} \subset \Delta_N(\mathcal{N})$  concludes the proof.

## Part III

# Cartography Learning in Multiple Channels





## Chapter 7

# Learning Power Spectrum Maps from Compressed Measurements

This chapter presents a novel family of spectrum cartography techniques to estimate PSD maps from the observations gathered by a collection of inexpensive sensors reporting strongly compressed measurements to a fusion center (FC) — each sensor acquires the frequency band of interest using a C-ADC, estimates the power of the output sequence using sample statistics, and transmits a quantized version of the resulting estimate to the FC. The cartography model from Section 1.1.1, where the second-order statistics of the signal of interest are linearly parametrized in terms of space-dependent coordinates, enables us to reformulate the estimation problem as a vector-field regression task.

After stating the problem in Section 7.1, two cartography techniques that perform nonparametric and semiparametric regression in *reproducing kernel Hilbert spaces* (RKHSs) of vector-valued functions are proposed in Section 7.2. Noting that the resulting optimization problems mimic those arising in support vector machines (SVMs) entails numerous benefits in terms of implementation issues and theoretical understanding. These schemes are extended in Section 7.3 to allow for multiple measurements per sensor, to accommodate non-uniform quantization, and to enforce nonnegativity constraints. Section 7.4 then provides an online algorithm for nonparametric regression based on stochastic gradient descent in RKHSs, and Section 7.5 discusses implementation issues. The performance of the proposed techniques is evaluated via Monte Carlo simulations in Section 7.6 and, finally, conclusions are drawn in Section 7.7.

## 7.1 Problem Formulation

We adopt the cartography model from Section 1.1.1, which extends the wideband model — already used in Chapter 5 — to incorporate spatial dependence. Within this framework, recall that the PSD at frequency  $f$  and location  $\mathbf{z}$  can be expressed as

$$\Xi(\mathbf{z}; f) = \sum_{b=0}^{B-1} \alpha_b(\mathbf{z}) \Xi_b(f). \quad (7.1)$$

Since the (linearly independent) *basis functions*  $\Xi_b(f)$  are known *a priori*, estimating  $\Xi(\mathbf{z}; f)$  is tantamount to estimating the  $\alpha_b(\mathbf{z})$ , which will be seen as  $B$  functions of the spatial coordinate  $\mathbf{z}$ . Because the  $\Xi_b(f)$  are normalized such that  $\int_{-\infty}^{\infty} \Xi_b(f) df = 1$ , the coordinate  $\alpha_b(\mathbf{z})$  represents the power of the signal received from the  $b$ -th transmitter at point  $\mathbf{z}$ .

Suppose that a collection of  $Z$  sensors is deployed across the area of interest at positions  $\mathcal{Z} \triangleq \{\mathbf{z}_0, \dots, \mathbf{z}_{Z-1}\}$ . For concreteness, we assume that the spectrum sensor located at  $\mathbf{z}$  acquires the received signal using a C-ADC. Alternative schemes include the one described in Appendix 7.A, which is based on the pseudo-random filters from [Mehanna and Sidiropoulos, 2013]. The compressed observations obtained by this sensor are given by

$$\bar{\mathbf{y}}(\mathbf{z}) = \Phi(\mathbf{z}) \mathbf{y}(\mathbf{z}), \quad \mathbf{z} \in \mathcal{Z}, \quad (7.2)$$

where (see Section 1.1.2)  $\Phi(\mathbf{z}) = \mathbf{I}_L \otimes \check{\Phi}(\mathbf{z})$  is the compression matrix of the sensor  $\mathbf{z}$  and  $\mathbf{y}(\mathbf{z})$  is a vector containing  $K$  Nyquist samples of the received signal. Using the coordinates from (7.1), the covariance matrix of  $\mathbf{y}(\mathbf{z})$  can be written as

$$\Xi(\mathbf{z}) = \sum_{b=0}^{B-1} \alpha_b(\mathbf{z}) \Xi_b. \quad (7.3)$$

On the other hand, the power of the compressed observations is

$$\bar{\eta}^2(\mathbf{z}) \triangleq \frac{1}{K} \mathbb{E} \{ \bar{\mathbf{y}}^T(\mathbf{z}) \bar{\mathbf{y}}(\mathbf{z}) \} = \frac{1}{K} \text{Tr} (\Phi(\mathbf{z}) \Xi(\mathbf{z}) \Phi^T(\mathbf{z})). \quad (7.4)$$

Substituting (7.3) in (7.4) yields

$$\bar{\eta}^2(\mathbf{z}) = \beta^T(\mathbf{z}) \alpha(\mathbf{z}), \quad (7.5)$$

where the entries of  $\beta(\mathbf{z}) \triangleq [\beta_0(\mathbf{z}), \dots, \beta_{B-1}(\mathbf{z})]^T$  are given by  $\beta_b(\mathbf{z}) \triangleq \bar{K}^{-1} \text{Tr} (\Phi(\mathbf{z}) \Xi_b \Phi^T(\mathbf{z}))$ . As will become clear later, it is desirable that  $\text{rank}_{\mathbb{R}} \{\beta(\mathbf{z})\}_{\mathbf{z} \in \mathcal{Z}} = B$ , otherwise the components

of  $\alpha(\mathbf{z})$  will not be identifiable in general.

The sensor at position  $\mathbf{z}$  estimates  $\bar{\eta}^2(\mathbf{z})$  using sample statistics, for instance, by computing  $\hat{\eta}^2(\mathbf{z}) = \frac{1}{K} \|\bar{\mathbf{y}}^T(\mathbf{z})\|^2$ . Afterwards, the estimate  $\hat{\eta}^2(\mathbf{z})$  is uniformly quantized according to the map

$$\mathcal{Q}(\hat{\eta}^2) \triangleq \lfloor \hat{\eta}^2 / (2\epsilon) \rfloor \in \mathbb{Z}, \quad (7.6)$$

where  $2\epsilon$  is the quantization step. The result  $q(\mathbf{z}) \triangleq \mathcal{Q}(\hat{\eta}^2(\mathbf{z}))$  is sent to the FC through a control channel. Depending on the quality of the estimate, it may be possible that either  $\mathcal{Q}(\bar{\eta}^2(\mathbf{z})) = \mathcal{Q}(\hat{\eta}^2(\mathbf{z}))$  or  $\mathcal{Q}(\bar{\eta}^2(\mathbf{z})) \neq \mathcal{Q}(\hat{\eta}^2(\mathbf{z}))$ . The latter case will be termed a *measurement error*.

The problem considered in this chapter is that of estimating the vector-valued spatial field  $\alpha : \mathbb{R}^d \rightarrow \mathbb{R}^B$  based on the knowledge of the vectors  $\{\beta(\mathbf{z})\}_{\mathbf{z} \in \mathcal{Z}}$ , the quantized observations  $\{q(\mathbf{z})\}_{\mathbf{z} \in \mathcal{Z}}$ , and the set  $\mathcal{Z} = \{\mathbf{z}_0, \dots, \mathbf{z}_{Z-1}\} \subset \mathbb{R}^d$ . As opposed to  $q(\mathbf{z})$ , the vectors  $\beta(\mathbf{z})$  and the positions  $\mathbf{z}$  may not need to be communicated since the FC may know them *a priori*. For simplicity, we start by considering the setting where each sensor reports a single measurement to the FC. More general scenarios will be discussed in Sections 7.3.1 and 7.4.

## 7.2 Cartography Learning

Suppose that no measurement errors have occurred. Upon receiving  $q(\mathbf{z})$ , the FC learns that  $\alpha$  satisfies

$$2\epsilon q(\mathbf{z}) \leq \beta^T(\mathbf{z})\alpha(\mathbf{z}) < 2\epsilon(q(\mathbf{z}) + 1). \quad (7.7)$$

The problem becomes that of choosing a member of the family of functions on  $\mathbb{R}^d$  satisfying (7.7) for all  $\mathbf{z} \in \mathcal{Z}$ . A standard approach is to constrain this search to a function space  $\mathcal{F}$  determined by the prior information and seek the smoothest member which is consistent with (7.7). If  $J$  is a continuous real (non-necessarily linear) functional defined on  $\mathcal{F}$  which takes small values for smooth arguments, this problem can be formally stated as<sup>1</sup>

$$\begin{aligned} & \underset{\alpha \in \mathcal{F}}{\text{minimize}} && J(\alpha) \\ & \text{s.t.} && 2\epsilon q(\mathbf{z}) \leq \beta^T(\mathbf{z})\alpha(\mathbf{z}) \leq 2\epsilon(q(\mathbf{z}) + 1), \quad \mathbf{z} \in \mathcal{Z}. \end{aligned} \quad (7.8)$$

---

<sup>1</sup>Note that the second inequality need not be strict since  $J$  is continuous.

For notational convenience, we define  $\tilde{q}(\mathbf{z}) \triangleq (2q(\mathbf{z}) + 1)\epsilon$  and rewrite (7.8) as

$$\begin{aligned} & \underset{\boldsymbol{\alpha} \in \mathcal{F}}{\text{minimize}} && J(\boldsymbol{\alpha}) \\ & \text{s.t.} && |\tilde{q}(\mathbf{z}) - \boldsymbol{\beta}^T(\mathbf{z})\boldsymbol{\alpha}(\mathbf{z})| \leq \epsilon, \quad \forall \mathbf{z} \in \mathcal{Z}. \end{aligned} \quad (7.9)$$

In the presence of measurement errors, the value of some of the  $\tilde{q}(\mathbf{z})$  has been incorrectly determined, and the true  $\boldsymbol{\alpha}$  does not satisfy  $|\tilde{q}(\mathbf{z}) - \boldsymbol{\beta}^T(\mathbf{z})\boldsymbol{\alpha}(\mathbf{z})| \leq \epsilon$  at those positions. For this reason, the feasible set of (7.9) need not contain the true  $\boldsymbol{\alpha}$ , and one must rely on prior information to provide a reasonable estimate. To do so, it is customary to rely on the *regularization* inductive principle, where the goal is to minimize an empirical risk functional penalized by a smoothness-enforcing term (see e.g. [Schölkopf and Smola, 2001, Cherkassky and Mulier, 2007]):

$$\underset{\boldsymbol{\alpha} \in \mathcal{F}}{\text{minimize}} \quad R_{\text{emp}}(\boldsymbol{\alpha}; \{(\mathbf{z}, \boldsymbol{\beta}(\mathbf{z}), \tilde{q}(\mathbf{z}))\}_{\mathbf{z} \in \mathcal{Z}}) + \lambda J(\boldsymbol{\alpha}). \quad (7.10)$$

The empirical risk  $R_{\text{emp}}$  measures how much  $\boldsymbol{\alpha}$  deviates from the observations  $\{(\mathbf{z}, \boldsymbol{\beta}(\mathbf{z}), \tilde{q}(\mathbf{z}))\}_{\mathbf{z} \in \mathcal{Z}}$  and it is defined below. The regularization constant  $\lambda > 0$  is adjusted to attain the desired trade-off between smoothness and reliance on the observations: in general, a small  $\lambda$  results in estimates with low smoothness but good fit, whereas a large  $\lambda$  produces smooth estimates with a poor fit. The dilemma embodied in the choice of  $\lambda$  is consequently that of trusting the prior information *vs.* trusting the data. A modern approach to address this decision is by means of *complexity control* techniques that minimize generalization risks [Schölkopf and Smola, 2001, Cherkassky and Mulier, 2007], among which the most popular example is, perhaps, *cross-validation*.

For reasons that will become clear, we choose  $R_{\text{emp}}$  to penalize deviations from (7.7) in a linear fashion. In terms of the so-called  $\epsilon$ -insensitive function, defined as  $u_\epsilon(x) \triangleq \max(0, |x| - \epsilon)$  [Cherkassky and Mulier, 2007, Smola and Schölkopf, 2004], this criterion reads as:

$$R_{\text{emp}}(\boldsymbol{\alpha}; \{(\mathbf{z}, \boldsymbol{\beta}(\mathbf{z}), \tilde{q}(\mathbf{z}))\}_{\mathbf{z} \in \mathcal{Z}}) \triangleq \frac{1}{Z} \sum_{\mathbf{z} \in \mathcal{Z}} u_\epsilon(\tilde{q}(\mathbf{z}) - \boldsymbol{\beta}^T(\mathbf{z})\boldsymbol{\alpha}(\mathbf{z})). \quad (7.11)$$

Because the empirical risk defined in (7.11) can be regarded as a convex surrogate of the number of measurement errors in the same way as the  $\ell_1$ -norm replaces the  $\ell_0$ -norm as a regularizer in sparse regression [Cherkassky and Mulier, 2007, Sec. 9.3], it follows that  $R_{\text{emp}}$  captures the *sparsity* present in the measurement errors.

In the rest of this section, we propose two batch estimation methods based on solving (7.10) for different choices of the function space  $\mathcal{F}$  and penalty  $J$ . While both of them are parametric along the frequency dimension, they differ as to how they model the variations across space.

The PSD map estimate can then be recovered by substituting the resulting  $\alpha$  in (7.1).

### 7.2.1 Nonparametric Regression

A powerful nonparametric regression approach can be obtained by endowing  $\mathcal{F}$  with the structure of an RKHS [Berlinet and Thomas-Agnan, 2004] and setting  $J$  to a non-decreasing function of the norm induced by the associated inner product. If  $J(\alpha) = \|\alpha\|_{\mathcal{F}}^2 = \langle \alpha, \alpha \rangle$ , where  $\langle \cdot, \cdot \rangle$  denotes the inner product on  $\mathcal{F}$ , then the problem becomes:

$$\underset{\alpha \in \mathcal{F}}{\text{minimize}} \quad \frac{1}{Z} \sum_{z \in \mathcal{Z}} u_{\epsilon}(\tilde{q}(z) - \beta^T(z)\alpha(z)) + \lambda \|\alpha\|_{\mathcal{F}}^2. \quad (7.12)$$

Due to the nature of  $\alpha$ , in our case  $\mathcal{F}$  must be an RKHS of vector-valued functions from  $\mathbb{R}^d \rightarrow \mathbb{R}^B$  [Micchelli and Pontil, 2005, Carmeli et al., 2010]. To specify this RKHS, we use a *reproducing kernel*, which is a function  $\mathbf{K} : \mathbb{R}^d \times \mathbb{R}^d \rightarrow \mathbb{R}^{B \times B}$  that satisfies certain conditions [Micchelli and Pontil, 2005]. Simple constructions for  $\mathbf{K}$  can be found using kernels for scalar RKHSs. For instance, a diagonal kernel is a function of the form  $\mathbf{K}(z, z') = \text{diag}\{k_0(z, z'), \dots, k_{B-1}(z, z')\}$ ,  $z, z' \in \mathbb{R}^d$ , where the  $k_i$  are valid scalar kernels. An example of those, used in our experiments in Section 7.6, is the Gaussian kernel

$$k_b(z', z) = \exp \left\{ -\frac{\|z' - z\|^2}{\sigma_b^2} \right\}, \quad (7.13)$$

where  $\sigma_b^2$  is a parameter controlling the *width* of  $k_b$  and translates into the variability that we expect of the scalar field  $\alpha_b$ . Because they result in *translation and unitary invariant* kernels [Schölkopf and Smola, 2001, Sec. 2.3], radial basis functions, such as the one in (7.13), are especially interesting in spectrum cartography applications where the propagation takes place in a uniform and isotropic medium.

Among the most remarkable properties of reproducing kernels, we have that  $\mathbf{K}(z', z) = \mathbf{K}(z, z')^T$  and that  $\mathbf{K}(z, z)$  is positive semidefinite. The *kernel matrix* is the block matrix given by (recall the notation introduced in Section 1.4):

$$\tilde{\mathbf{K}} \triangleq \sum_{i,j=0}^{Z-1} (\mathbf{e}_{Z,i} \mathbf{e}_{Z,j}^T) \otimes \mathbf{K}(z_i, z_j) \in \mathbb{R}^{BZ \times BZ} \quad (7.14)$$

and can be shown to be positive semidefinite [Micchelli and Pontil, 2005, eq. (2.4)].

The problem (7.12) is infinite-dimensional in nature but, exploiting the theory of RKHSs, a solution can be found solving a finite-dimensional optimization program. Let us form the vector

$\tilde{\mathbf{q}} \triangleq [\tilde{q}(\mathbf{z}_0), \dots, \tilde{q}(\mathbf{z}_{Z-1})]^T$  and the matrices  $\tilde{\mathbf{B}} \triangleq [\beta(\mathbf{z}_0), \dots, \beta(\mathbf{z}_{Z-1})]$  and  $\mathbf{B} \triangleq \mathbf{I}_Z \odot \tilde{\mathbf{B}}$ . Then, we have the following:

PROPOSITION 7.1. *Let  $\mathbf{c}(\mathbf{z}_i) \in \mathbb{R}^B$ ,  $i = 0, \dots, Z-1$ , and let  $\mathbf{c} = [\mathbf{c}^T(\mathbf{z}_0), \dots, \mathbf{c}^T(\mathbf{z}_{Z-1})]^T \in \mathbb{R}^{BZ}$  be a solution to<sup>2</sup>*

$$\begin{aligned} & \underset{\mathbf{c}, \boldsymbol{\zeta}, \boldsymbol{\zeta}^*}{\text{minimize}} && \mathbf{1}_Z^T (\boldsymbol{\zeta} + \boldsymbol{\zeta}^*) + \lambda Z \mathbf{c}^T \tilde{\mathbf{K}} \mathbf{c} \\ & \text{s.t.} && \boldsymbol{\zeta} \geq \tilde{\mathbf{q}} - \mathbf{B}^T \tilde{\mathbf{K}} \mathbf{c} - \epsilon \mathbf{1}_Z \\ & && \boldsymbol{\zeta}^* \geq -\tilde{\mathbf{q}} + \mathbf{B}^T \tilde{\mathbf{K}} \mathbf{c} - \epsilon \mathbf{1}_Z \\ & && \boldsymbol{\zeta}, \boldsymbol{\zeta}^* \geq \mathbf{0}_Z, \end{aligned} \tag{7.15}$$

Then, the function defined by

$$\boldsymbol{\alpha}(\mathbf{z}) = \sum_{i=0}^{Z-1} \tilde{\mathbf{K}}(\mathbf{z}, \mathbf{z}_i) \mathbf{c}(\mathbf{z}_i) \tag{7.16}$$

is a solution to (7.12).

*Proof.* See Appendix 7.B. □

The quadratic problem (7.15) is convex. Applying the change of variables  $\tilde{\mathbf{c}} = \tilde{\mathbf{K}}^{1/2} \mathbf{c}$ , where  $\tilde{\mathbf{K}}^{1/2}$  represents a symmetric square root of  $\tilde{\mathbf{K}}$ , it can be seen that (7.15) is a standard SVM problem without offset term. This connection between nonparametric regression and SVMs entails numerous benefits both in terms of implementation and theoretical understanding [Micchelli and Pontil, 2005, Wang et al., 2001, Smola et al., 1998]. In particular, the resulting expansion (7.16) is expected to be sparse in the sense that many of the  $\mathbf{c}(\mathbf{z}_i)$  are zero, which yields sparse representations for the estimated PSD maps. On the other hand, it is known that (7.15) can be solved more efficiently in the dual domain, where it becomes

$$\begin{aligned} & \underset{\boldsymbol{\alpha}, \boldsymbol{\alpha}^*}{\text{minimize}} && \frac{1}{4Z\lambda} (\boldsymbol{\alpha} - \boldsymbol{\alpha}^*)^T \tilde{\mathbf{K}} (\boldsymbol{\alpha} - \boldsymbol{\alpha}^*) \\ & && - (\tilde{\mathbf{q}} - \epsilon \mathbf{1}_Z)^T \boldsymbol{\alpha} + (\tilde{\mathbf{q}} + \epsilon \mathbf{1}_Z)^T \boldsymbol{\alpha}^* \\ & \text{s.t.} && \mathbf{0}_Z \leq \boldsymbol{\alpha} \leq \mathbf{1}_Z, \mathbf{0}_Z \leq \boldsymbol{\alpha}^* \leq \mathbf{1}_Z, \end{aligned} \tag{7.17}$$

with

$$\tilde{\mathbf{K}} \triangleq \mathbf{B}^T \tilde{\mathbf{K}} \mathbf{B}. \tag{7.18}$$

---

<sup>2</sup>Throughout the chapter,  $\boldsymbol{\zeta}$  and  $\boldsymbol{\zeta}^*$  denote different variables. The superscript  $*$ , which does not represent complex conjugate (these vectors are real), is adopted here since it is standard practice in SVM theory.

The primal variables solving (7.15) can be recovered from the dual solution  $(\boldsymbol{\alpha}, \boldsymbol{\alpha}^*)$  using

$$\mathbf{c} = \frac{1}{2\lambda Z} \mathbf{B}(\boldsymbol{\alpha} - \boldsymbol{\alpha}^*) \quad (7.19a)$$

$$\boldsymbol{\zeta} = \max(\mathbf{0}_Z, \tilde{\mathbf{q}} - \mathbf{B}^T \tilde{\mathbf{K}} \mathbf{c} - \epsilon \mathbf{1}_Z) \quad (7.19b)$$

$$\boldsymbol{\zeta}^* = \max(\mathbf{0}_Z, -\tilde{\mathbf{q}} + \mathbf{B}^T \tilde{\mathbf{K}} \mathbf{c} - \epsilon \mathbf{1}_Z). \quad (7.19c)$$

### 7.2.2 Semiparametric Regression

One of the major strengths of SVMs and the regression scheme from Section 7.2.1 is their non-parametric nature, which, for instance, confers them properties as universal approximators [Micchelli, 1984]. *Parametric* methods, on the other hand, have a limited flexibility but can easily accommodate many forms of prior information. Halfway between both approaches are *semi-parametric* techniques, which combine the advantages of both parametric and nonparametric methods [Smola et al., 1999, Schölkopf and Smola, 2001].

In semiparametric regression, we decompose the hypothesis into a nonparametric and a parametric component as

$$\boldsymbol{\alpha} = \boldsymbol{\alpha}_{\text{np}} + \boldsymbol{\alpha}_{\text{par}}. \quad (7.20)$$

As in Section 7.2.1, the nonparametric component  $\boldsymbol{\alpha}_{\text{np}}$  is a function in an RKHS  $\mathcal{F}'$ . The parametric component  $\boldsymbol{\alpha}_{\text{par}}$ , on the other hand, is a function of the form

$$\boldsymbol{\alpha}_{\text{par}}(\mathbf{z}) = \sum_{b=0}^{B'-1} \boldsymbol{\Psi}_b(\mathbf{z}) \mathbf{d}_b, \quad (7.21)$$

where  $\{\boldsymbol{\Psi}_b(\mathbf{z})\}_{b=0}^{B'-1}$  is a collection of basis functions  $\boldsymbol{\Psi}_b : \mathbb{R}^d \rightarrow \mathbb{R}^{B \times B}$  and  $\mathbf{d}_b \in \mathbb{R}^B$ . In spectrum cartography, for instance, we may be aware of the location of some transmitters and the path loss exponent. One can therefore define the basis functions

$$\boldsymbol{\Psi}_b(\mathbf{z}) = f_b(\|\mathbf{z} - \mathbf{z}'_b\|) \mathbf{e}_{B,b} \mathbf{e}_{B,b}^T, \quad (7.22)$$

where  $f_b$  models attenuation as a function of distance and  $\mathbf{z}'_b \in \mathbb{R}^d$  is the location of the  $b$ -th transmitter. This example showcases a further advantage of semiparametric models: they facilitate *understanding* the data [Smola et al., 1999]. In particular, the estimated  $\mathbf{d}_b$  contains information about the power transmitted by the  $b$ -th source.

After having introduced the nonparametric scheme from Section 7.2.1, one may think that a possible approach to estimate  $\boldsymbol{\alpha}$  is to fit the data with the parametric component and then fit the

residuals with the nonparametric component. This approach is called *backfitting* and is known to provide good estimates only in very restricted situations [Smola et al., 1999, Schölkopf and Smola, 2001]. Indeed, a good approximation performance can only be obtained if we simultaneously fit both components, as described next.

Let  $\mathcal{F}$  denote the space of functions of the form (7.20), where  $\alpha_{\text{np}} \in \mathcal{F}'$  and  $\alpha_{\text{par}}$  is of the form (7.21). The problem of semiparametric regression is [Smola et al., 1999, Schölkopf and Smola, 2001]:

$$\underset{\alpha \in \mathcal{F}}{\text{minimize}} \quad \frac{1}{Z} \sum_{z \in \mathcal{Z}} u_{\epsilon}(\tilde{q}(z) - \beta^T(z)\alpha(z)) + \lambda \|\alpha_{\text{np}}\|_{\mathcal{F}'}^2, \quad (7.23)$$

where  $\|\cdot\|_{\mathcal{F}'}$  is the norm induced by the inner product of  $\mathcal{F}'$ . Observe that the parametric component  $\alpha_{\text{par}}$  is not regularized.

Since the problem (7.23) is again infinite-dimensional, the theory of RKHSs is required to work out a solution. Let  $\mathbf{K}$  be the reproducing kernel of  $\mathcal{F}'$  and let the basis functions  $\{\Psi_b(z)\}_{b=0}^{B'-1}$  be given. Let us also define the block matrix

$$\tilde{\Psi} \triangleq \sum_{i=0}^{Z-1} \sum_{b=0}^{B'-1} (\mathbf{e}_{Z,i} \mathbf{e}_{B',b}^T) \otimes \Psi_b(z_i) \in \mathbb{R}^{BZ \times BB'} \quad (7.24)$$

and assume that  $\tilde{\Psi}$  is full rank.

**PROPOSITION 7.2.** *Let  $\mathbf{c}(z_i), \mathbf{d}_b \in \mathbb{R}^B$ , and let  $\mathbf{c} = [\mathbf{c}^T(z_0), \dots, \mathbf{c}^T(z_{Z-1})]^T \in \mathbb{R}^{BZ}$  and  $\mathbf{d} = [\mathbf{d}_0^T, \dots, \mathbf{d}_{B'-1}^T]^T \in \mathbb{R}^{BB'}$  be a solution to*

$$\begin{aligned} & \underset{\mathbf{c}, \mathbf{d}, \zeta, \zeta^*}{\text{minimize}} \quad \mathbf{1}_Z^T (\zeta + \zeta^*) + \lambda Z \mathbf{c}^T \tilde{\mathbf{K}} \mathbf{c} \\ & \text{s.t.} \quad \zeta \geq \tilde{\mathbf{q}} - \mathbf{B}^T \tilde{\mathbf{K}} \mathbf{c} - \mathbf{B}^T \tilde{\Psi} \mathbf{d} - \epsilon \mathbf{1}_Z \\ & \quad \zeta^* \geq -\tilde{\mathbf{q}} + \mathbf{B}^T \tilde{\mathbf{K}} \mathbf{c} + \mathbf{B}^T \tilde{\Psi} \mathbf{d} - \epsilon \mathbf{1}_Z \\ & \quad \zeta, \zeta^* \geq \mathbf{0}_Z. \end{aligned} \quad (7.25)$$

Then, the function  $\alpha$ , defined by

$$\alpha(z) = \sum_{i=0}^{Z-1} \mathbf{K}(z, z_i) \mathbf{c}(z_i) + \sum_{b=0}^{B'-1} \Psi_b(z) \mathbf{d}_b, \quad (7.26)$$

is a solution to (7.23)

*Proof.* See Appendix 7.C. □



The problem (7.25) is the generalization of a semiparametric SVM [Smola et al., 1999] to the regression of vector-valued functions. The dual problem is

$$\begin{aligned}
& \underset{\boldsymbol{\alpha}, \boldsymbol{\alpha}^*}{\text{minimize}} && \frac{1}{4Z\lambda} (\boldsymbol{\alpha} - \boldsymbol{\alpha}^*)^T \bar{\mathbf{K}} (\boldsymbol{\alpha} - \boldsymbol{\alpha}^*) \\
& && - (\tilde{\mathbf{q}} - \epsilon \mathbf{1}_Z)^T \boldsymbol{\alpha} + (\tilde{\mathbf{q}} + \epsilon \mathbf{1}_Z)^T \boldsymbol{\alpha}^* \\
& \text{s.t.} && \tilde{\boldsymbol{\Psi}}^T \mathbf{B} (\boldsymbol{\alpha} - \boldsymbol{\alpha}^*) = \mathbf{0} \\
& && \mathbf{0}_Z \leq \boldsymbol{\alpha} \leq \mathbf{1}_Z, \mathbf{0}_Z \leq \boldsymbol{\alpha}^* \leq \mathbf{1}_Z,
\end{aligned} \tag{7.27}$$

which, except for the equality constraint, is identical to (7.17).

The primal variable  $\mathbf{c}$  solving (7.25) can be computed from the solution  $(\boldsymbol{\alpha}, \boldsymbol{\alpha}^*)$  of (7.27) using the Karush-Kuhn-Tucker (KKT) conditions [Boyd and Vandenberghe, 2004], resulting in (7.19a). The primal variable  $\mathbf{d}$  can also be obtained from these conditions, but the resulting expressions are prone to numerical problems. A more convenient alternative follows by observing that the *bidual* (i.e., the dual of the dual) of (7.25) is again (7.25). This means that the primal variables are actually the Lagrange multipliers of (7.27). In particular,  $\mathbf{d}$  can be obtained as the multipliers associated with the equality constraint in (7.27). Note that these multipliers are often available without additional computational costs, for instance if one uses interior-point methods (see Section 7.5). Finally, the variables  $\boldsymbol{\zeta}$  and  $\boldsymbol{\zeta}^*$  can be recovered as

$$\boldsymbol{\zeta} = \max(\mathbf{0}_Z, \tilde{\mathbf{q}} - \mathbf{B}^T \tilde{\mathbf{K}} \mathbf{c} - \mathbf{B}^T \tilde{\boldsymbol{\Psi}} \mathbf{d} - \epsilon \mathbf{1}_Z) \tag{7.28a}$$

$$\boldsymbol{\zeta}^* = \max(\mathbf{0}_Z, -\tilde{\mathbf{q}} + \mathbf{B}^T \tilde{\mathbf{K}} \mathbf{c} + \mathbf{B}^T \tilde{\boldsymbol{\Psi}} \mathbf{d} - \epsilon \mathbf{1}_Z). \tag{7.28b}$$

## CONDITIONALLY POSITIVE DEFINITE KERNELS

From (7.19a) and the equality constraint in (7.27), we observe that the optimum  $\mathbf{c}$  is in the null space of  $\tilde{\boldsymbol{\Psi}}^T$ , that is, it satisfies  $\tilde{\boldsymbol{\Psi}}^T \mathbf{c} = \mathbf{0}$ . Therefore, (7.25) is equivalent to

$$\begin{aligned}
& \underset{\mathbf{c}, \boldsymbol{\zeta}, \boldsymbol{\zeta}^*}{\text{minimize}} && \mathbf{1}_Z^T (\boldsymbol{\zeta} + \boldsymbol{\zeta}^*) + \lambda Z \mathbf{c}^T \tilde{\mathbf{K}} \mathbf{c} \\
& \text{s.t.} && \boldsymbol{\zeta} \geq \tilde{\mathbf{q}} - \mathbf{B}^T \tilde{\mathbf{K}} \mathbf{c} - \mathbf{B}^T \tilde{\boldsymbol{\Psi}} \mathbf{d} - \epsilon \mathbf{1}_Z \\
& && \boldsymbol{\zeta}^* \geq -\tilde{\mathbf{q}} + \mathbf{B}^T \tilde{\mathbf{K}} \mathbf{c} + \mathbf{B}^T \tilde{\boldsymbol{\Psi}} \mathbf{d} - \epsilon \mathbf{1}_Z \\
& && \boldsymbol{\zeta}, \boldsymbol{\zeta}^* \geq \mathbf{0}_Z, \quad \tilde{\boldsymbol{\Psi}}^T \mathbf{c} = \mathbf{0}.
\end{aligned} \tag{7.29}$$

The equality constraint allows us to handle conditionally positive definite (CPD) kernels (see e.g. [Schölkopf and Smola, 2001, Sec. 2.4]), which are defined next by generalizing the definition for scalar kernels to the vector case:

DEFINITION 7.1. A reproducing kernel  $\mathbf{K} : \mathbb{R}^d \times \mathbb{R}^d \rightarrow \mathbb{R}^B$  is CPD with respect to  $\{\Psi_b(\mathbf{z})\}_{b=0}^{B'-1}$  if, for every finite  $\mathcal{Z} \subset \mathbb{R}^d$ , satisfies  $\mathbf{c}^T \tilde{\mathbf{K}} \mathbf{c} \geq 0$  for all  $\mathbf{c}$  such that  $\tilde{\Psi}^T \mathbf{c} = \mathbf{0}$ , where  $\tilde{\mathbf{K}}$  and  $\tilde{\Psi}$  were respectively defined in (7.14) and (7.24).

We now generalize our semiparametric method to allow regression with CPD kernels — note that any conventional positive definite kernel is also CPD. Among other advantages, this enables us to accommodate *thin-plate splines* (TPS) regression, which was successfully applied to cartography problems in [Bazerque et al., 2011]. See below for more details.

In view of Definition 7.1, a CPD kernel can be used in (7.29) without further modifications [Smola et al., 1999]. The problem is still convex since the objective is convex in the feasible set. However, this form is particularly prone to numerical problems<sup>3</sup> since  $\tilde{\mathbf{K}}$  is not positive semidefinite. For this reason, one may apply the change of variable  $\mathbf{c} = \mathbf{P}_{\tilde{\Psi}}^\perp \tilde{\mathbf{c}}$ , where  $\mathbf{P}_{\tilde{\Psi}}^\perp \in \mathbb{R}^{BZ \times BZ}$  is the orthogonal projector onto the null space of  $\tilde{\Psi}^T$ :

$$\begin{aligned} \underset{\tilde{\mathbf{c}}, d, \zeta, \zeta^*}{\text{minimize}} \quad & \mathbf{1}_Z^T (\zeta + \zeta^*) + \lambda Z \tilde{\mathbf{c}}^T \mathbf{P}_{\tilde{\Psi}}^\perp \tilde{\mathbf{K}} \mathbf{P}_{\tilde{\Psi}}^\perp \tilde{\mathbf{c}} \\ \text{s.t.} \quad & \zeta \geq \tilde{\mathbf{q}} - \mathbf{B}^T \tilde{\mathbf{K}} \mathbf{P}_{\tilde{\Psi}}^\perp \tilde{\mathbf{c}} - \mathbf{B}^T \tilde{\Psi} d - \epsilon \mathbf{1}_Z \\ & \zeta^* \geq -\tilde{\mathbf{q}} + \mathbf{B}^T \tilde{\mathbf{K}} \mathbf{P}_{\tilde{\Psi}}^\perp \tilde{\mathbf{c}} + \mathbf{B}^T \tilde{\Psi} d - \epsilon \mathbf{1}_Z \\ & \zeta, \zeta^* \geq \mathbf{0}_Z. \end{aligned} \tag{7.30}$$

Now it is clear that  $\mathbf{P}_{\tilde{\Psi}}^\perp \tilde{\mathbf{K}} \mathbf{P}_{\tilde{\Psi}}^\perp$  is positive semidefinite. The projector  $\mathbf{P}_{\tilde{\Psi}}^\perp$  can be computed as

$$\mathbf{P}_{\tilde{\Psi}}^\perp = \mathbf{I}_{BZ} - \tilde{\Psi} (\tilde{\Psi}^T \tilde{\Psi})^{-1} \tilde{\Psi}^T. \tag{7.31}$$

A similar argument carries over to the dual problem (7.27). From (7.18), (7.19a) and (7.27), we find that if  $\mathbf{K}$  is CPD, then  $(\alpha - \alpha^*)^T \bar{\mathbf{K}} (\alpha - \alpha^*) \geq 0$  for feasible  $\alpha, \alpha^*$ . Hence, the objective is again convex but prone to numerical errors. Since in the feasible set

$$\mathbf{B}(\alpha - \alpha^*) = \mathbf{P}_{\tilde{\Psi}}^\perp \mathbf{B}(\alpha - \alpha^*), \tag{7.32}$$

---

<sup>3</sup>In fact, it will not be accepted by most convex/quadratic solvers.

the problem (7.27) is equivalent to

$$\begin{aligned}
& \underset{\alpha, \alpha^*}{\text{minimize}} && \frac{1}{4Z\lambda} (\alpha - \alpha^*)^T \bar{\mathbf{K}}_{\Psi} (\alpha - \alpha^*) \\
& && - (\tilde{\mathbf{q}} - \epsilon \mathbf{1}_Z)^T \alpha + (\tilde{\mathbf{q}} + \epsilon \mathbf{1}_Z)^T \alpha^* \\
& \text{s.t.} && \tilde{\Psi}^T \mathbf{B} (\alpha - \alpha^*) = \mathbf{0} \\
& && \mathbf{0}_Z \leq \alpha \leq \mathbf{1}_Z, \mathbf{0}_Z \leq \alpha^* \leq \mathbf{1}_Z,
\end{aligned} \tag{7.33}$$

where  $\bar{\mathbf{K}}$  has been replaced with the positive semidefinite matrix

$$\bar{\mathbf{K}}_{\Psi} \triangleq \mathbf{B}^T \mathbf{P}_{\tilde{\Psi}}^{\perp} \tilde{\mathbf{K}} \mathbf{P}_{\tilde{\Psi}}^{\perp} \mathbf{B}. \tag{7.34}$$

For efficiency, one is interested in solving (7.33) and recovering the optimal  $\mathbf{d}$  and  $\tilde{\mathbf{c}}$  in (7.30) from that solution. This operation was simple when we computed the primal solution of (7.25), since the bidual of (7.25) was again (7.25). However, due to the substitution of  $\bar{\mathbf{K}}$  by  $\bar{\mathbf{K}}_{\Psi}$ , (7.30) is no longer the *dual* of (7.33) and, correspondingly,  $\mathbf{d}$  and  $\tilde{\mathbf{c}}$  cannot be obtained directly as the Lagrange multipliers of (7.33). Instead, a more careful procedure is required. As shown in Appendix 7.D,  $\mathbf{c}$  can be obtained using (7.19a), whereas  $\mathbf{d}$  has to be computed as

$$\mathbf{d} = \boldsymbol{\nu} - (\tilde{\Psi}^T \tilde{\Psi})^{-1} \tilde{\Psi}^T \bar{\mathbf{K}} \mathbf{c}, \tag{7.35}$$

with  $\boldsymbol{\nu}$  the multiplier associated with the equality constraint in (7.33).

## THIN-PLATE SPLINES

TPS regression can be obtained as a particularization of the above scheme. As opposed to the Gaussian kernels from (7.13), where one has to adjust  $\sigma_i^2$  based on prior information, TPS do not require parameter tuning. The name of this approach comes from scalar TPS interpolation, where the interpolant mimics the shape of a *thin metal plate* in  $\mathbb{R}^{d+1}$  anchored to the data points, which is known to minimize the *bending energy* [Bookstein, 1989].

To generalize TPS to the vector case ( $B > 1$ ), we may choose (see [Wahba, 1990, eq. (2.4.9)]; also [Bazerque et al., 2011])  $\Psi_0(\mathbf{z}) = \mathbf{I}_B$ ,  $\Psi_1(\mathbf{z}) = z_0 \mathbf{I}_B$ , ...,  $\Psi_d(\mathbf{z}) = z_{d-1} \mathbf{I}_B$ , where  $\mathbf{z} \triangleq [z_0, \dots, z_{d-1}]^T$ , and

$$\mathbf{K}(\mathbf{z}, \mathbf{z}') = \varrho(\|\mathbf{z} - \mathbf{z}'\|_2^2) \mathbf{I}_B, \tag{7.36}$$

where

$$\varrho(z) \triangleq \begin{cases} z^{2s-d} \log(z) & \text{if } d \text{ is even} \\ z^{2s-d} & \text{otherwise} \end{cases} \quad (7.37)$$

for  $s$  a positive integer parameter, typically set to  $s = 2$ . The kernel in (7.36) is CPD, as shown in [Wahba, 1990, p. 32] for the scalar case.

The norm in the RKHS  $\mathcal{F}'$  defined by (7.36) (semi-norm when defined on  $\mathcal{F}$ ) can be computed as [Wahba, 1990, Bazerque et al., 2011]

$$\|\alpha\|_{\mathcal{F}}^2 = \|\alpha_{\text{par}}\|_{\mathcal{F}'}^2 = \sum_{b=0}^{B-1} \int_{\mathbb{R}^d} \|\nabla^2 \alpha_b(\mathbf{z}')\|_F^2 d\mathbf{z}', \quad (7.38)$$

where  $\|\cdot\|_F$  denotes Frobenius norm and  $\nabla^2$  denotes Hessian. This expression is indeed the sum of the bending energy of the  $B$  components of  $\alpha$ . Observe that the parametric part of  $\alpha$  is in the null space of this semi-norm since the second-order derivatives of  $\Psi_b(\mathbf{z})$  vanish for all  $b$ .

### 7.3 Extensions

This section presents several extensions of the proposed schemes that either improve their practical applicability or exploit the prior information more efficiently.

#### 7.3.1 Extension to Multiple Measurements per Sensor

In a practical scenario, it is reasonable that the sensors report more than one measurement to the FC. A sensor can obtain multiple measurements by separately estimating the power of different output branches of the C-ADC, that is, considering the sequences  $\{\bar{y}[\bar{k} + lN]\}_l$  for different values of  $\bar{k} \in \{0, \dots, \bar{K} - 1\}$ ; or by modifying their compression matrix  $\check{\Phi}(\mathbf{z})$  for each observation. To improve the accuracy of the estimate, the resulting vectors  $\beta(\mathbf{z})$  at each sensor should be different from one measurement to another and, if possible, linearly independent.

Suppose that each sensor reports  $M$  measurements to the fusion center — the case where each sensor reports a different number of measurements can be addressed with straightforward modifications. The setting from the previous sections can be immediately extended by regarding the different measurements generated by each sensor as produced by  $M$  different sensors that occupy the same physical position. To this end, we construct  $\tilde{\mathbf{K}} \in \mathbb{R}^{BZM \times BZM}$ ,  $\tilde{\Psi} \in \mathbb{R}^{BZM \times BB'}$ ,  $\mathbf{B} \in \mathbb{R}^{BZM \times ZM}$  and  $\tilde{\mathbf{q}} \in \mathbb{R}^{ZM}$  by considering every location  $M$  times. However, this approach is

highly inefficient as can be noted from the fact that every row or column of  $\tilde{\mathbf{K}}$  is present at least  $M$  times. Even if the kernel is strictly positive definite [Schölkopf and Smola, 2001, Sec. 2.2], the resulting  $\tilde{\mathbf{K}}$  is rank deficient, meaning that no unique solution of (7.15) exists. As described next, more convenient alternatives arise if the whole derivation takes into account multiple measurements from the very beginning.

## NONPARAMETRIC REGRESSION

Introducing multiple measurements in the criterion (7.12) produces

$$\underset{\boldsymbol{\alpha} \in \mathcal{F}}{\text{minimize}} \quad \frac{1}{ZM} \sum_{\mathbf{z} \in \mathcal{Z}} \sum_{m=0}^{M-1} u_{\epsilon}(\tilde{q}_m(\mathbf{z}) - \boldsymbol{\beta}_m(\mathbf{z})^T \boldsymbol{\alpha}(\mathbf{z})) + \lambda \|\boldsymbol{\alpha}\|_{\mathcal{F}}^2, \quad (7.39)$$

where  $\tilde{q}_m(\mathbf{z})$  and  $\boldsymbol{\beta}_m(\mathbf{z})$  correspond to the  $m$ -th measurement reported by the sensor located at  $\mathbf{z}$ . By arranging the observations in the vector  $\tilde{\mathbf{q}} \triangleq [\tilde{q}_0(\mathbf{z}_0), \tilde{q}_1(\mathbf{z}_0), \dots, \tilde{q}_{M-1}(\mathbf{z}_{Z-1})]^T$  and the matrix  $\tilde{\mathbf{B}} \triangleq [\boldsymbol{\beta}_0(\mathbf{z}_0), \boldsymbol{\beta}_1(\mathbf{z}_0), \dots, \boldsymbol{\beta}_{M-1}(\mathbf{z}_{Z-1})]$  and following the same procedure as in Appendix 7.B, we find that the optimum  $\boldsymbol{\alpha}$  satisfies (7.16) when  $\mathbf{c}$  is a solution to

$$\begin{aligned} & \underset{\mathbf{c}, \boldsymbol{\zeta}, \boldsymbol{\zeta}^*}{\text{minimize}} \quad \mathbf{1}_{ZM}^T (\boldsymbol{\zeta} + \boldsymbol{\zeta}^*) + \lambda ZM \mathbf{c}^T \tilde{\mathbf{K}} \mathbf{c} \\ & \text{s.t.} \quad \boldsymbol{\zeta} \geq \tilde{\mathbf{q}} - \mathbf{B}^T \tilde{\mathbf{K}} \mathbf{c} - \epsilon \mathbf{1}_{ZM} \\ & \quad \boldsymbol{\zeta}^* \geq -\tilde{\mathbf{q}} + \mathbf{B}^T \tilde{\mathbf{K}} \mathbf{c} - \epsilon \mathbf{1}_{ZM} \\ & \quad \boldsymbol{\zeta}, \boldsymbol{\zeta}^* \geq \mathbf{0}_{ZM}, \end{aligned} \quad (7.40)$$

with  $\tilde{\mathbf{K}} \in \mathbb{R}^{BZ \times BZ}$  given by (7.14), and

$$\mathbf{B} = (\mathbf{I}_Z \otimes \mathbf{1}_M^T) \odot \check{\mathbf{B}} \in \mathbb{R}^{BZ \times ZM}. \quad (7.41)$$

Observe that all these expressions boil down to those in Section 7.2.1 when  $M = 1$ . The optimization variable  $\mathbf{c}$  has dimension  $BZ$ , rather than  $BZM$  in the trivial approach described at the beginning of Section 7.3.1. Moreover,  $\tilde{\mathbf{K}}$  can be kept of size  $BZ \times BZ$  rather than  $BZM \times BZM$ , which accelerates the computation of  $\tilde{\mathbf{K}}$  and the evaluation of  $\boldsymbol{\alpha}$  (see (7.16)).

The dual of (7.40) is

$$\begin{aligned} & \underset{\boldsymbol{\alpha}, \boldsymbol{\alpha}^*}{\text{minimize}} \quad \frac{1}{4ZM\lambda} (\boldsymbol{\alpha} - \boldsymbol{\alpha}^*)^T \mathbf{B}^T \tilde{\mathbf{K}} \mathbf{B} (\boldsymbol{\alpha} - \boldsymbol{\alpha}^*) \\ & \quad - (\tilde{\mathbf{q}} - \epsilon \mathbf{1}_{ZM})^T \boldsymbol{\alpha} + (\tilde{\mathbf{q}} + \epsilon \mathbf{1}_{ZM})^T \boldsymbol{\alpha}^* \\ & \text{s.t.} \quad \mathbf{0}_{ZM} \leq \boldsymbol{\alpha} \leq \mathbf{1}_{ZM}, \mathbf{0}_{ZM} \leq \boldsymbol{\alpha}^* \leq \mathbf{1}_{ZM} \end{aligned} \quad (7.42)$$

and the primal variable  $\mathbf{c}$  has to be recovered using

$$\mathbf{c} = \frac{1}{2\lambda ZM} \mathbf{B}(\boldsymbol{\alpha} - \boldsymbol{\alpha}^*). \quad (7.43)$$

## SEMIPARAMETRIC REGRESSION

With semiparametric regression, the extension follows the same guidelines as described for nonparametric regression. In the multiple-measurement setting, (7.23) becomes

$$\underset{\boldsymbol{\alpha} \in \mathcal{F}}{\text{minimize}} \quad \frac{1}{ZM} \sum_{\mathbf{z} \in \mathcal{Z}} \sum_{m=0}^{M-1} u_{\epsilon}(\tilde{q}_m(\mathbf{z}) - \boldsymbol{\beta}_m(\mathbf{z})^T \boldsymbol{\alpha}(\mathbf{z})) + \lambda \|\boldsymbol{\alpha}_{\text{par}}\|_{\mathcal{F}'}^2. \quad (7.44)$$

We now reproduce how the expressions used for CPD kernels in Section 7.2.2 generalize to the case  $M > 1$ . To recover the ones used for positive definite kernels in Section 7.2.2, it suffices to set  $\mathbf{P}_{\tilde{\Psi}}^{\perp} = \mathbf{I}_{BZ}$ . By defining  $\tilde{\mathbf{q}} \in \mathbb{R}^{ZM}$ ,  $\mathbf{B} \in \mathbb{R}^{BZ \times ZM}$  and  $\tilde{\mathbf{K}} \in \mathbb{R}^{BZ \times BZ}$  as we did in this section for nonparametric regression, the problem (7.30) becomes

$$\begin{aligned} & \underset{\tilde{\mathbf{c}}, \mathbf{d}, \boldsymbol{\zeta}, \boldsymbol{\zeta}^*}{\text{minimize}} \quad \mathbf{1}_{ZM}^T (\boldsymbol{\zeta} + \boldsymbol{\zeta}^*) + \lambda ZM \tilde{\mathbf{c}}^T \mathbf{P}_{\tilde{\Psi}}^{\perp} \tilde{\mathbf{K}} \mathbf{P}_{\tilde{\Psi}}^{\perp} \tilde{\mathbf{c}} \\ & \text{s.t.} \quad \boldsymbol{\zeta} \geq \tilde{\mathbf{q}} - \mathbf{B}^T \tilde{\mathbf{K}} \mathbf{P}_{\tilde{\Psi}}^{\perp} \tilde{\mathbf{c}} - \mathbf{B}^T \tilde{\Psi} \mathbf{d} - \epsilon \mathbf{1}_{ZM} \\ & \quad \boldsymbol{\zeta}^* \geq -\tilde{\mathbf{q}} + \mathbf{B}^T \tilde{\mathbf{K}} \mathbf{P}_{\tilde{\Psi}}^{\perp} \tilde{\mathbf{c}} + \mathbf{B}^T \tilde{\Psi} \mathbf{d} - \epsilon \mathbf{1}_{ZM} \\ & \quad \boldsymbol{\zeta}, \boldsymbol{\zeta}^* \geq \mathbf{0}_{ZM}, \end{aligned} \quad (7.45)$$

where  $\tilde{\Psi}$  is given by (7.24). On the other hand, the dual problem (7.33) becomes

$$\begin{aligned} & \underset{\boldsymbol{\alpha}, \boldsymbol{\alpha}^*}{\text{minimize}} \quad \frac{1}{4ZM\lambda} (\boldsymbol{\alpha} - \boldsymbol{\alpha}^*)^T \bar{\mathbf{K}}_{\Psi} (\boldsymbol{\alpha} - \boldsymbol{\alpha}^*) \\ & \quad - (\tilde{\mathbf{q}} - \epsilon \mathbf{1}_{ZM})^T \boldsymbol{\alpha} + (\tilde{\mathbf{q}} + \epsilon \mathbf{1}_{ZM})^T \boldsymbol{\alpha}^* \\ & \text{s.t.} \quad \tilde{\Psi}^T \mathbf{B}(\boldsymbol{\alpha} - \boldsymbol{\alpha}^*) = \mathbf{0} \\ & \quad \mathbf{0}_{ZM} \leq \boldsymbol{\alpha} \leq \mathbf{1}_{ZM}, \mathbf{0}_{ZM} \leq \boldsymbol{\alpha}^* \leq \mathbf{1}_{ZM}, \end{aligned} \quad (7.46)$$

where  $\bar{\mathbf{K}}_{\Psi} \triangleq \mathbf{B}^T \mathbf{P}_{\tilde{\Psi}}^{\perp} \tilde{\mathbf{K}} \mathbf{P}_{\tilde{\Psi}}^{\perp} \mathbf{B}$ . The primal variables can be recovered using (7.43) and (7.35). Again, important computational savings result from this approach, either when  $\boldsymbol{\alpha}$  is estimated or evaluated.

### 7.3.2 Non-uniform Quantization

Until now, we have used uniform quantization, but when the probability distribution of  $\hat{\eta}^2(\mathbf{z})$  is not uniform, better alternatives exist. In particular, we may define a certain number  $\Delta$  of quantization regions with boundaries  $0 = \delta_0 < \delta_1 < \dots < \delta_\Delta$  and quantize  $\hat{\eta}^2(\mathbf{z})$  to  $q(\mathbf{z}) = \mathcal{Q}(\hat{\eta}^2(\mathbf{z}))$  if  $\delta_{q(\mathbf{z})} \leq \hat{\eta}^2(\mathbf{z}) < \delta_{q(\mathbf{z})+1}$ . Expressions (7.39) and (7.44) remain valid if  $\epsilon$  and  $\tilde{q}(\mathbf{z})$  are respectively replaced with

$$\epsilon(q(\mathbf{z})) = \frac{\delta_{q(\mathbf{z})+1} - \delta_{q(\mathbf{z})}}{2} \quad \text{and} \quad \tilde{q}(\mathbf{z}) = \frac{\delta_{q(\mathbf{z})+1} + \delta_{q(\mathbf{z})}}{2}. \quad (7.47)$$

All other expressions in the previous sections can be easily generalized to the case of non-uniform quantization just by replacing the vector  $\epsilon \mathbf{1}_{ZM}$  with  $\epsilon = [\epsilon(q_0(\mathbf{z}_0)), \epsilon(q_1(\mathbf{z}_0)), \dots, \epsilon(q_{M-1}(\mathbf{z}_{Z-1}))]^T$ .

### 7.3.3 Enforcing Non-negativity

The schemes described in the previous sections do not exploit the fact that the  $\alpha_b$  represent power and, consequently, they are nonnegative. Although it is not straightforward to enforce nonnegativity in the whole domain of  $\boldsymbol{\alpha}$ , several approaches can be used to enforce this property on a discrete set of points. A simple trick is to introduce *virtual sensors* — notion similar to that of *virtual examples* [Schölkopf et al., 1996] — by enlarging the set  $\mathcal{Z}$  with those locations where we wish to enforce nonnegativity. If  $\mathbf{z}$  is one of such locations, we may assume that a virtual sensor at  $\mathbf{z}$  reports the following  $B$  measurements:

$$\tilde{q}_m(\mathbf{z}) = \frac{\delta_0 + \delta_\Delta}{2}, \quad \epsilon_{\mathbf{z},m} = \frac{\delta_\Delta - \delta_0}{2}, \quad \beta_m(\mathbf{z}) = \mathbf{e}_{B,m}, \quad m = 0, \dots, B-1. \quad (7.48)$$

The problem with this approach is that it allows negative values even at those points where a virtual sensor has been placed. The reason is that virtual sensors are treated like any other physical sensor, even though their measurements are error-free. If one is not willing to tolerate these violations of nonnegativity, a different approach needs to be adopted. For example, one may introduce the constraint  $\tilde{\mathbf{K}} \mathbf{P}_{\tilde{\Psi}}^\perp \tilde{\mathbf{c}} + \tilde{\Psi} \mathbf{d} \geq \mathbf{0}_{BZ}$  in (7.40) or (7.45) to enforce the nonnegativity of the  $\alpha_b$  at the locations of the physical sensors.

## 7.4 Online Implementation

The schemes described in the previous sections are batch algorithms: all observations have to be collected before the learning stage starts. Since their complexity is superlinear in the number of observations, obtaining PSD maps using those methods may become prohibitive. Therefore, it is of interest to develop *online* approaches, where each observation is processed at the time when it is received to update the estimate of  $\alpha$ . This enables implementations with linear complexity and allows us to track changes in the field of interest.

Although online schemes can be trivially found by using batch algorithms with sliding windows [Sebald and Bucklew, 2000], fully online algorithms are preferable [Diethe and Girolami, 2013]. An elegant approach to solve regression problems in an RKHS hinges on stochastic gradient descent in the function space, as applied in [Kivinen et al., 2004] to propose the *NORMA* algorithm. For regression in RKHSs of vector-valued functions, a modification called *ONORMA* has been proposed in [Audiffren and Kadri, 2013]. This algorithm can be applied to solve (7.12) by defining the *instantaneous regularized error* as

$$R_{\text{inst}}(\alpha, \beta, \mathbf{z}, \tilde{q}) \triangleq u_\epsilon(\tilde{q} - \beta^T \alpha(\mathbf{z})) + \lambda \|\alpha\|_{\mathcal{F}}^2. \quad (7.49)$$

Observe that the objective in (7.12) follows from averaging  $R_{\text{inst}}$  for all observations.

Suppose that, at time  $t = 1, 2, \dots$ , an observation is received from the sensor located at position  $\mathbf{z}_t$ . Multiple observations per sensor are possible with straightforward modifications. The update rule for the stochastic gradient descent algorithm is

$$\alpha^{(t+1)} = \alpha^{(t)} - \kappa_t \nabla_{\alpha} R_{\text{inst}}(\alpha^{(t)}, \beta(\mathbf{z}_t), \mathbf{z}_t, \tilde{q}(\mathbf{z}_t)), \quad (7.50)$$

where, in this context, the step size  $\kappa_t > 0$  is called *learning rate*.<sup>4</sup> Using [Audiffren and Kadri, 2013, Eq. (2)], we find that

$$\nabla_{\alpha} R_{\text{inst}}(\alpha, \beta, \mathbf{z}, \tilde{q}) = k_{\mathbf{z}} \partial_{\mathbf{z}} u_\epsilon(\tilde{q} - \beta^T \alpha) |_{\mathbf{z}=\alpha} + 2\lambda \alpha \quad (7.51a)$$

$$= -u'_\epsilon(\tilde{q} - \beta^T \alpha) \cdot k_{\mathbf{z}} \beta + 2\lambda \alpha, \quad (7.51b)$$

where  $k_{\mathbf{z}}$  is the kernel operator of  $\mathcal{F}$  (see Appendix 7.B),  $\partial_{\mathbf{z}}$  represents a sub-gradient with respect to  $\mathbf{z}$  and  $u'_\epsilon$  is a sub-derivative of  $u_\epsilon$ ; for example

$$u'_\epsilon(x) = \frac{\text{sign}\{x - \epsilon\} + \text{sign}\{x + \epsilon\}}{2}. \quad (7.52)$$

---

<sup>4</sup>All the expressions in this section can be readily rewritten for the case where  $\kappa_t$  is replaced by a matrix, which provides more flexibility to set the learning rates for different components of  $\alpha$ .



Substituting (7.51b) in (7.50) yields

$$\boldsymbol{\alpha}^{(t+1)} = (1 - 2\kappa_t\lambda)\boldsymbol{\alpha}^{(t)} + \kappa_t u'_\epsilon(\tilde{q}(\mathbf{z}_t) - \boldsymbol{\beta}^T(\mathbf{z}_t)\boldsymbol{\alpha}^{(t)}(\mathbf{z}_t)) \cdot k_{\mathbf{z}_t}\boldsymbol{\beta}(\mathbf{z}_t) \quad (7.53)$$

Applying the representer theorem [Micchelli and Pontil, 2005, Th. 5] up to time  $t - 1$  leads to the following representation:

$$\boldsymbol{\alpha}^{(t)} = \sum_{i=1}^{t-1} k_{\mathbf{z}_i} \mathbf{c}^{(t)}(\mathbf{z}_i) \quad (7.54)$$

for some vectors  $\mathbf{c}^{(t)}(\mathbf{z}_i) \in \mathbb{R}^B$ ,  $i = 1, \dots, t - 1$ . If different observations come from different sensors, the operators  $k_{\mathbf{z}_i}$ ,  $i = 1, \dots, t + 1$ , are linearly independent, which means that the vectors of coefficients must be updated as

$$\mathbf{c}^{(t+1)}(\mathbf{z}_i) = (1 - 2\kappa_t\lambda)\mathbf{c}^{(t)}(\mathbf{z}_i), \quad i = 1, \dots, t - 1 \quad (7.55a)$$

$$\mathbf{c}^{(t+1)}(\mathbf{z}_t) = \kappa_t u'_\epsilon(\tilde{q}(\mathbf{z}_t) - \boldsymbol{\beta}^T(\mathbf{z}_t)\boldsymbol{\alpha}^{(t)}(\mathbf{z}_t)) \cdot \boldsymbol{\beta}(\mathbf{z}_t). \quad (7.55b)$$

As an initialization, one can set  $\boldsymbol{\alpha}^{(1)} = 0$ .

Due to the decomposition in (7.54), the number of parameters increases linearly with the number of observations. However, from (7.55a) we observe that the coefficients  $\mathbf{c}(\mathbf{z}_i)$ ,  $i = 1, \dots, t - 1$  are shrunk by a factor of  $(1 - 2\kappa_t\lambda)$  at each iteration provided that  $2\kappa_t\lambda < 1$ , which we assume. For this reason, it is common to truncate this sequence at some point [Kivinen et al., 2004, Audiffren and Kadri, 2013], thus maintaining the following hypothesis:

$$\boldsymbol{\alpha}^{(t)} = \sum_{i=\max(1, t-\tau)}^{t-1} k_{\mathbf{z}_i} \mathbf{c}^{(t)}(\mathbf{z}_i) \quad (7.56)$$

for some  $\tau > 1$ . However, in the application at hand, it makes more sense to maintain one term per sensor since their number remains constant. Thus, the hypothesis in (7.54) can be replaced with

$$\boldsymbol{\alpha}^{(t)} = \sum_{\mathbf{z} \in \mathcal{Z}} k_{\mathbf{z}} \mathbf{c}^{(t)}(\mathbf{z}) \quad (7.57)$$

and, every time an observation  $(\tilde{q}(\mathbf{z}_{\text{new}}), \boldsymbol{\beta}(\mathbf{z}_{\text{new}}))$  is received from the sensor at location  $\mathbf{z}_{\text{new}} \in$

$\mathcal{Z}$ , the update from (7.53) becomes

$$\begin{aligned} \mathbf{c}^{(t+1)}(\mathbf{z}) &= (1 - 2\kappa_t\lambda)\mathbf{c}^{(t)}(\mathbf{z}), \quad \mathbf{z} \in \mathcal{Z}, \mathbf{z} \neq \mathbf{z}_{\text{new}} \\ \mathbf{c}^{(t+1)}(\mathbf{z}_{\text{new}}) &= (1 - 2\kappa_t\lambda)\mathbf{c}^{(t)}(\mathbf{z}_{\text{new}}) + \kappa_t u'_\epsilon(\tilde{q}(\mathbf{z}_{\text{new}}) - \boldsymbol{\beta}^T(\mathbf{z}_{\text{new}})\boldsymbol{\alpha}^{(t)}(\mathbf{z}_{\text{new}})) \cdot \boldsymbol{\beta}(\mathbf{z}_{\text{new}}). \end{aligned} \quad (7.58)$$

The convergence of this algorithm is characterized by the next result, which extends [Audiffren and Kadri, 2013, Thm. 1] to our setting.

**THEOREM 7.1.** *If  $\lambda_{\max}(\mathbf{K}(\mathbf{z}, \mathbf{z})) < U < \infty$  for all  $\mathbf{z}$ ,  $\|\boldsymbol{\beta}(\mathbf{z}_t)\|_2 \leq V$  for all  $t$ , and  $\kappa_t \triangleq \kappa t^{-1/2}$  with  $\kappa\lambda < 1$ , then the sequence  $\{\boldsymbol{\alpha}^{(t)}\}_t$  satisfies*

$$\begin{aligned} \frac{1}{T} \sum_{t=1}^T R_{\text{inst}}(\boldsymbol{\alpha}^{(t)}, \boldsymbol{\beta}(\mathbf{z}_t), \mathbf{z}_t, \tilde{q}_{\mathbf{z}_t}) &\leq \\ \inf_{\boldsymbol{\alpha} \in \mathcal{F}} \left[ \frac{1}{T} \sum_{t=1}^T R_{\text{inst}}(\boldsymbol{\alpha}, \boldsymbol{\beta}(\mathbf{z}_t), \mathbf{z}_t, \tilde{q}_{\mathbf{z}_t}) \right] &+ \frac{e_1}{\sqrt{T}} + \frac{e_2}{T} \end{aligned} \quad (7.59)$$

where  $e_2 = U^2 V^2 / (8\lambda^2 \kappa)$  and  $e_1 = 4(U^2 V^2 \kappa + e_2)$ .

*Proof.* The proof of [Audiffren and Kadri, 2013, Thm. 1] generalizes the proof of [Kivinen et al., 2004, Thm. 4] to the vector-valued case. To prove Theorem 7.1, one can follow the same approach with two small differences. First, the proof in [Audiffren and Kadri, 2013] involves a gradient, rather than a *subgradient*, in (7.50). It can be seen that this subtlety requires no modification since the vector version of the argument used to establish [Kivinen et al., 2004, eq. (49)] holds for both gradients and subgradients, and this is the only part of the proof that requires the properties of gradients/subgradients.

Secondly, in the proof in [Audiffren and Kadri, 2013], the fitting term of the instantaneous regularized error (in our case the first term of (7.49)) seen as a function of the vector  $\boldsymbol{\alpha}(\mathbf{z})$ , say  $f(\mathbf{v}) = u_\epsilon(\tilde{q} - \boldsymbol{\beta}^T \mathbf{v})$ , is not dependent on  $t$ . In our case, this dependence exists through  $\boldsymbol{\beta}(\mathbf{z}_t)$  and  $\tilde{q}_{\mathbf{z}_t}$ . However, it can be seen that the proof of [Audiffren and Kadri, 2013] can easily accommodate this situation provided that the functions share a common Lipschitz constant. That is, for  $f_t(\mathbf{v}) = u_\epsilon(\tilde{q}_{\mathbf{z}_t} - \boldsymbol{\beta}(\mathbf{z}_t)^T \mathbf{v})$ , there must exist a  $c$  such that

$$|f_t(\mathbf{v}_1) - f_t(\mathbf{v}_2)| \leq c \|\mathbf{v}_1 - \mathbf{v}_2\|_2 \quad (7.60)$$

for all  $\mathbf{v}_1, \mathbf{v}_2 \in \mathbb{R}^B$  and  $t = 1, \dots, T$ . In our case, it can be noted that

$$\begin{aligned} |f_t(\mathbf{v}_1) - f_t(\mathbf{v}_2)| &= |u_\epsilon(\tilde{\mathbf{q}}_{\mathbf{z}_t} - \boldsymbol{\beta}(\mathbf{z}_t)^T \mathbf{v}_1) - u_\epsilon(\tilde{\mathbf{q}}_{\mathbf{z}_t} - \boldsymbol{\beta}(\mathbf{z}_t)^T \mathbf{v}_2)| \\ &= |\boldsymbol{\beta}(\mathbf{z}_t)^T (\mathbf{v}_2 - \mathbf{v}_1)| \leq \|\boldsymbol{\beta}(\mathbf{z}_t)\|_2 \|\mathbf{v}_1 - \mathbf{v}_2\|_2 \end{aligned} \quad (7.61)$$

where the second equality is due to the fact that  $u_\epsilon(z)$  is a Lipschitz function of  $z$  with constant 1. Thus, (7.60) holds for any  $c \geq \max_{1 \leq t \leq T} \|\boldsymbol{\beta}(\mathbf{z}_t)\|_2$ .  $\square$

In summary, the averaged instantaneous error from the online algorithm converges to the to the regularized empirical error of the batch solution.

## 7.5 Implementation Issues

This section describes some considerations to take into account when solving the optimization problems presented in this chapter by numerical methods.

First, standard algorithms to solve problems of the form (7.17) include *sequential minimal optimization* (SMO), an algorithm proposed in [Platt, 1999] for SVMs. In the case at hand, a simplification is possible due to the absence of bias term [Kecman et al., 2003]. However, for moderate problem sizes ( $BZ < 5000$  for the primal or  $MZ < 5000$  for the dual), interior-point methods are regarded as the most reliable [Schölkopf and Smola, 2001, Ch. 10]. They also come with the advantage of providing the Lagrange multipliers, useful for recovering the primal variables. Other problems discussed in this chapter, including (7.40), (7.45), and (7.46), can also be reliably solved using interior-point methods.

Second, as in any quadratic program, special caution must be taken to ensure that the matrix in the quadratic term does not have negative eigenvalues. This situation, which is caused by finite-precision arithmetic effects, is possible even when a strictly positive definite kernel is used. In those cases, one may replace the matrix  $\tilde{\mathbf{K}}$  with  $\tilde{\mathbf{K}} - c\mathbf{I}_{BZ}$ , where  $c = \min(0, \lambda_{\min}(\tilde{\mathbf{K}}))$ .

Third, if we are not interested in modeling dependencies among the components  $\alpha_b(\mathbf{z})$ ,  $b = 0, \dots, B-1$ , it is possible to use a diagonal kernel  $\mathbf{K}$  and diagonal basis functions  $\boldsymbol{\Psi}_b$ . If, moreover, all these components are modeled in the same way, as in TPS, both the kernel and the basis functions are of the form

$$\mathbf{K}(\mathbf{z}, \mathbf{z}') = K(\mathbf{z}, \mathbf{z}')\mathbf{I}_B \quad (7.62a)$$

$$\boldsymbol{\Psi}_b(\mathbf{z}) = \Psi_b(\mathbf{z})\mathbf{I}_B, \quad b = 0, \dots, B'-1 \quad (7.62b)$$

for certain scalar functions  $K$  and  $\Psi_b$ . This structure yields considerable simplifications in the

computation of the matrices involved in the optimization problems of this chapter, as explained in Appendix 7.E.

## 7.6 Simulation Results

We now illustrate the performance of the proposed techniques via Monte Carlo simulation. To this end, the propagation model that we adopt is the standard inverse polynomial law given by

$$\alpha_b(\mathbf{z}) = \frac{\delta A_b}{\delta + \|\mathbf{z} - \mathbf{z}_b\|^c}, \quad b = 0, \dots, B-2, \quad (7.63)$$

where  $\delta = 10^{-3}$  is a small constant to ensure that the denominator does not vanish,  $c = 3$  is the pathloss exponent and the parameters  $A_b$  and  $\mathbf{z}_b$  respectively represent transmit-power and source location. The noise power is set to  $\alpha_{B-1}(\mathbf{z}) = 0.75$  across the whole region.

The  $Z$  sensors, which are deployed uniformly at random, report  $M$  measurements to the FC. These measurements are generated as  $q_m(\mathbf{z}) = \mathcal{Q}(|\hat{\eta}_m^2(\mathbf{z}) + \varrho_m(\mathbf{z})|) = \mathcal{Q}(|\boldsymbol{\beta}_m^T(\mathbf{z})\boldsymbol{\alpha}(\mathbf{z}) + \varrho_m(\mathbf{z})|)$ , where  $\varrho_m(\mathbf{z}) \sim \mathcal{N}(0, \sigma_\varrho^2)$  is measurement noise that models errors in the estimation of  $\hat{\eta}_m^2(\mathbf{z})$ , for example due to finite observation windows. The estimates are quantized to  $n$  bits using two different schemes. Under *uniform quantization* (UQ), we determine the range of  $\hat{\eta}_m^2(\mathbf{z})$  using Monte Carlo simulation and set the boundaries  $\delta_0 < \delta_1 < \dots < \delta_\Delta$  of the quantization regions, where  $\Delta = 2^n$ , in such a way that  $\delta_{i+1} - \delta_i$  is constant for all  $i$  and the probability of clipping  $\mathbb{P}\{\hat{\eta}_m^2(\mathbf{z}) > \delta_\Delta\}$  is approximately  $10^{-3}$ . Under *constant-probability quantization* (CPQ), these boundaries are chosen so that  $\mathbb{P}\{\delta_j \leq \hat{\eta}_m^2(\mathbf{z}) < \delta_{j+1}\} \approx \mathbb{P}\{\delta_l \leq \hat{\eta}_m^2(\mathbf{z}) < \delta_{l+1}\}$ ,  $\forall j, l$ .

We will analyze nonparametric methods using the diagonal Gaussian kernel (GK) from (7.13) and semiparametric methods using TPS. Note that, in all cases, the relevant spectral information about the compressed signal is captured by the entries of the vector  $\boldsymbol{\beta}_m(\mathbf{z})$ . For the sake of generality, we do not specify this structure; instead, we generate the components of the vectors  $\boldsymbol{\beta}_m(\mathbf{z})$  as independent uniform random variables over the interval  $[0, 1]$  for all  $\mathbf{z}$  and  $m$ .

The first experiment is a simple example of cartography estimation in the two-dimensional region  $[0, 1] \times [0, 1] \subset \mathbb{R}^2$  where the band of interest contains the contributions of  $B-1 = 3$  independent sources with radiation parameters given by  $A_1 = 0.9$ ,  $A_2 = 0.8$ ,  $A_3 = 0.7$ ,  $\mathbf{z}_1 = (0.2, 0.8)$ ,  $\mathbf{z}_2 = (0.4, 0.5)$  and  $\mathbf{z}_3 = (0.8, 0.9)$ . Figure 7.1 shows the true and estimated fields for a particular realization of sensor locations  $\mathcal{Z}$ , marked with white crosses, and vectors  $\boldsymbol{\beta}_m(\mathbf{z})$ . GK regression is implemented with  $\sigma_b^2 = 0.1$  for  $b = 1, 2, 3$  and  $\sigma_4^2$  a very large constant, enforcing nonnegativity with  $B$  virtual measurements per sensor. Each sensor transmits 6 measurements quantized to 8 bits using CPQ, and  $\sigma_\varrho^2$  is set such that 15% of the measurements contain some

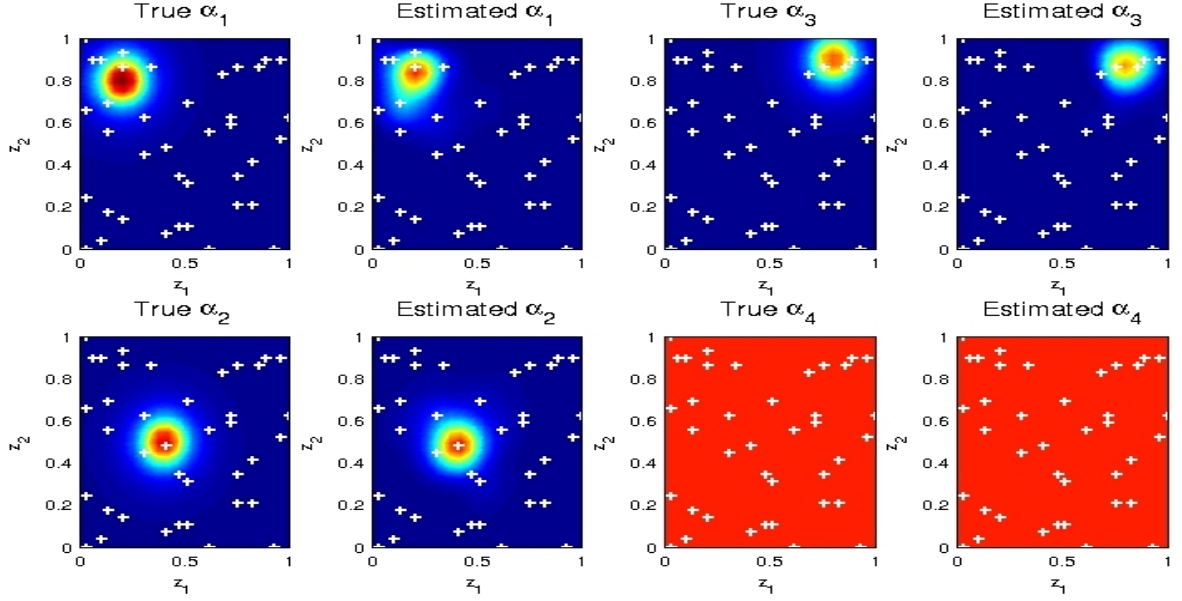


Figure 7.1: Comparison of the true and estimated maps for  $Z = 40$  sensors,  $M = 6$  measurements per sensor, 8 bits/measurement,  $\lambda = 10^{-7}$ , constant probability quantization and nonnegativity enforcement.

error. Although each sensor transmits only 6 bytes, it is observed that the reconstructed PSD maps match well the true ones for all the three sources and background noise.

The rest of experiments illustrate the influence of specific parameters/algorithms on the estimation performance, measured by the normalized mean squared error:

$$\text{NMSE} \triangleq \frac{\mathbb{E} \{ \|\alpha(\mathbf{z}) - \hat{\alpha}(\mathbf{z})\|_2^2 \}}{\mathbb{E} \{ \|\alpha(\mathbf{z})\|_2^2 \}}. \quad (7.64)$$

The expectation is taken with respect to  $\mathbf{z}$ , which is uniformly distributed on the spatial region of interest. After every estimate  $\hat{\alpha}(\mathbf{z})$  is obtained, the NMSE is approximated using the Monte Carlo method. The result of this operation may also be averaged over multiple realizations of the sensor locations and vectors  $\beta_m(\mathbf{z})$ . The region of interest is set to the unidimensional interval  $[0, 1] \subset \mathbb{R}^1$ , where  $B - 1 = 4$  sources radiate with parameters  $\mathbf{z}_1 = 0.1$ ,  $\mathbf{z}_2 = 0.2$ ,  $\mathbf{z}_3 = 0.4$ ,  $\mathbf{z}_4 = 0.8$ ,  $A_1 = 0.8$ ,  $A_2 = 0.9$ ,  $A_3 = 0.8$  and  $A_4 = 0.7$ .

To analyze the effects of compression, Figure 7.2 represents the NMSE, averaged over multiple realizations, as a function of  $Z$  for several numbers of bits/sample using both GK and TPS regression. To capture solely compression effects, we apply uniform quantization with no measurement errors. It is seen that the proposed estimators are consistent with  $Z$  in all cases. Although it is observed that TPS generally outperforms GK-based regression, this need not be

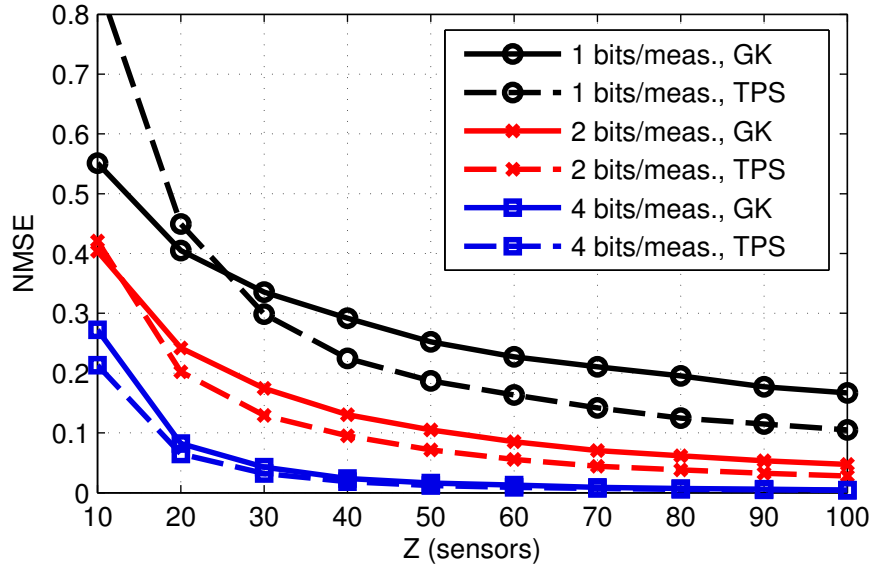


Figure 7.2: Effects of compression ( $B = 5$ ,  $M = 5$  measurements per sensor, uniform quantization,  $\sigma_\theta^2 = 0$ ,  $\lambda = 10^{-6}$ , nonnegativity not enforced).

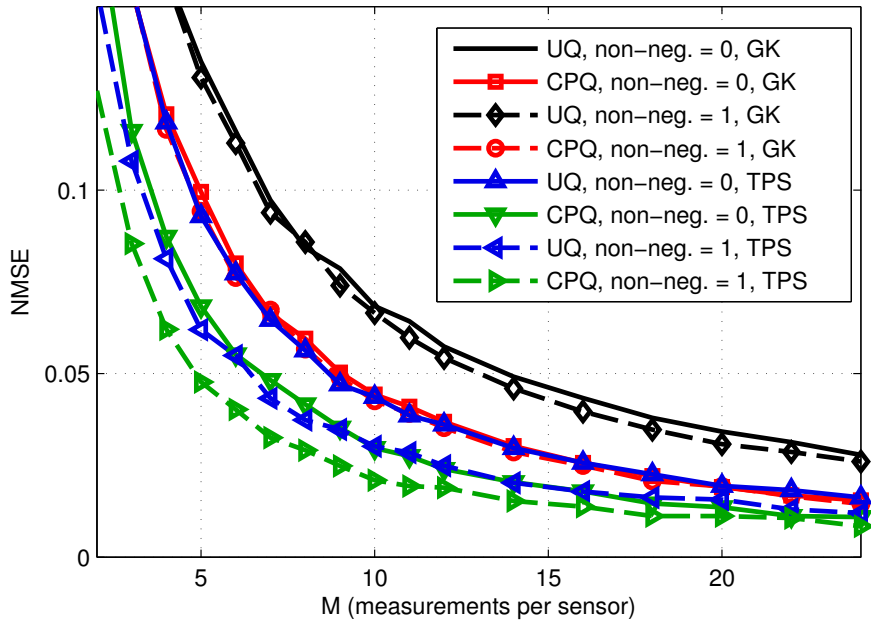


Figure 7.3: Influence of the extensions discussed in Section 7.3 on the estimation performance ( $B = 5$ ,  $Z = 40$ , 2 bits/measurement,  $\sigma_\theta^2 = 0$ ,  $\lambda = 10^{-6}$ ).

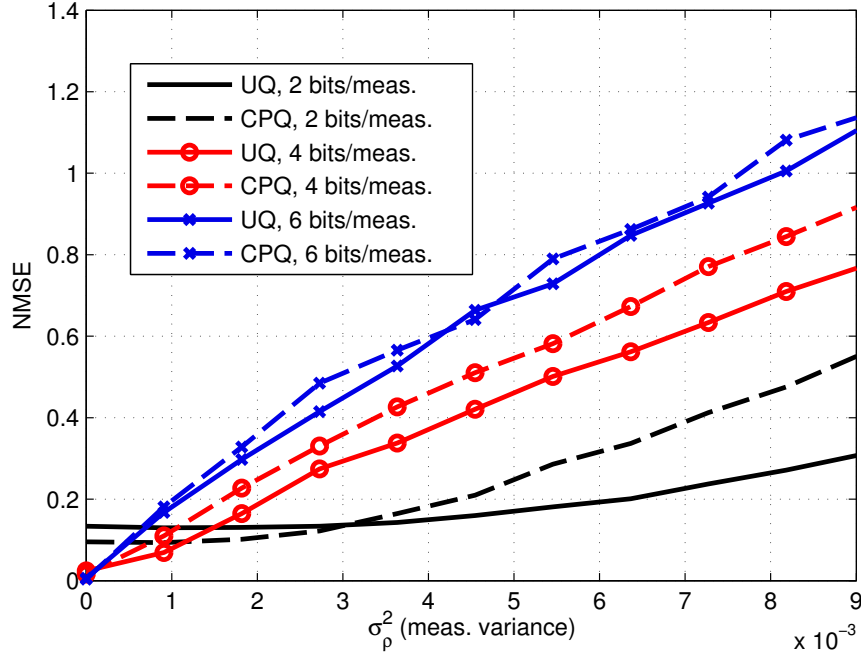


Figure 7.4: Influence of the measurement noise ( $B = 5$ ,  $Z = 40$ ,  $M = 5$ , Gaussian kernel,  $\lambda = 10^{-6}$ , nonnegativity not enforced).

the case in other scenarios with other nonparametric and semiparametric methods since their relative performance depends on the fields to be estimated as well as on the specific choice of the kernels and basis functions.

The extensions introduced in Section 7.3 are compared in Figure 7.3, which represents the NMSE vs.  $M$  for several settings. It can be noted that the estimates are not consistent in  $M$ , which is a consequence of the fact that the number of sensors is fixed — the field can only be accurately estimated in a finite set of points. It is also observed that TPS is much more sensitive than GK to the enforcement of nonnegativity via virtual measurements and that CPQ leads to better results than UQ. However, it can be seen this last observation ceases to hold when the measurement variance  $\sigma_\rho^2$  is sufficiently large, as shown in Figure 7.4, which suggests that other quantization schemes must be investigated. Figure 7.4 further shows that the impact of  $\sigma_\rho^2$  is heavier for larger  $\Delta$ . As predicted by intuition, a finer quantization demands a higher accuracy in the estimates  $\hat{\eta}_m^2(\mathbf{z})$ , which in turn requires longer observation windows.

Figure 7.5 compares the batch methods from Sections 7.2 and 7.3 with the online algorithm from Section 7.4. At every time slot, each sensor reports one measurement and the FC updates its estimate. To do so, the batch methods are executed with all the data received up to that time slot. On the top panel, it is observed the influence of the step size  $\kappa_t$  on the evolution of the

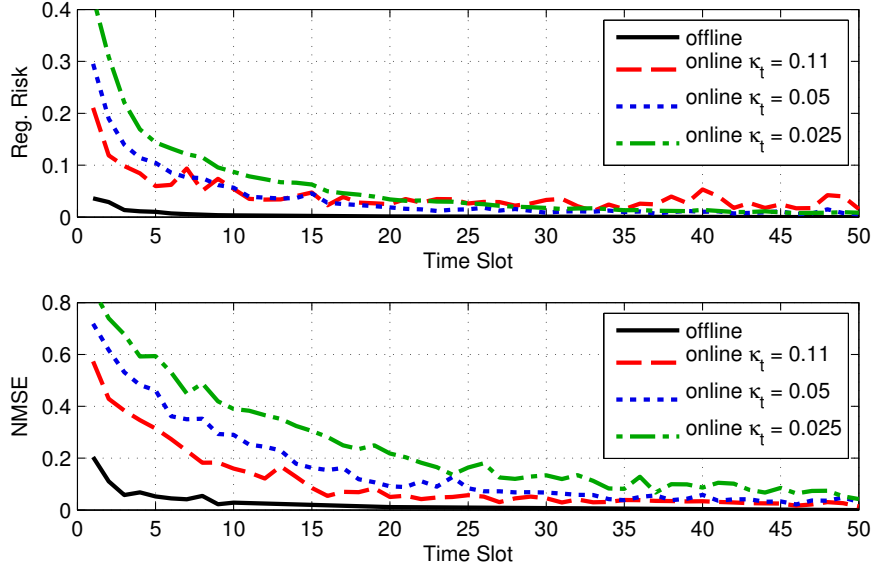


Figure 7.5: Comparison batch *vs.* online ( $B = 5$  components,  $Z = 30$  sensors, 4 bits/measurement, uniform quantization,  $\sigma_\rho^2 = 0$ , Gaussian kernel,  $\lambda = 10^{-6}$ , nonnegativity not enforced).

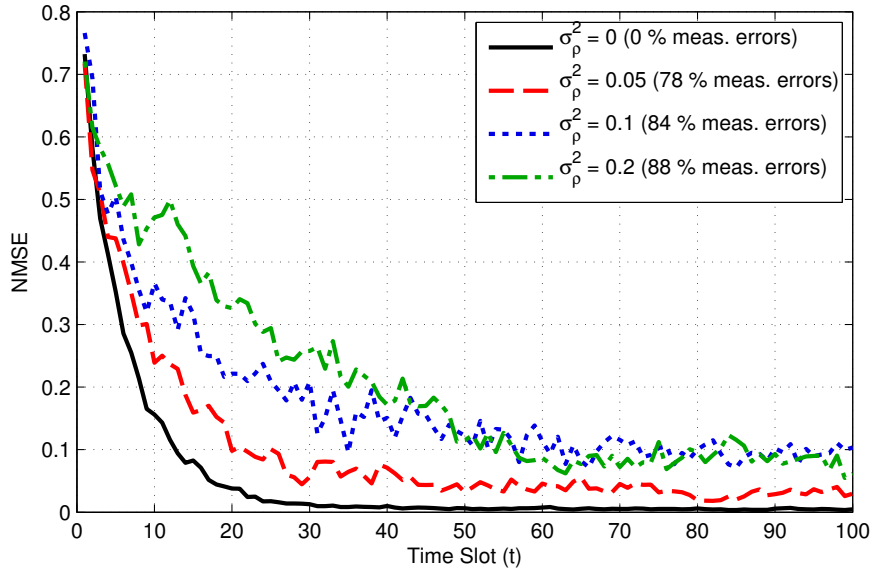


Figure 7.6: Influence of the measurement errors in the convergence of the online algorithm ( $B = 5$  components,  $Z = 30$  sensors, 4 bits/measurement, uniform quantization, Gaussian kernel,  $\lambda = 10^{-6}$ , nonnegativity not enforced,  $\kappa_t = 0.05$ ).



regularized risk, which is evaluated at each point using the whole set of observations, including past and future. As usual, a larger  $\kappa_t$  results in a faster convergence but a larger residual error in the steady state. However, it is seen on the bottom panel that the NMSE is less sensitive to this effect.

Finally, Figure 7.6 represents the evolution of the normalized mean-square error for several values of  $\sigma_\epsilon^2$ . It is observed that a larger  $\sigma_\epsilon^2$  results in a slower convergence and a larger residual error. However, even for large  $\sigma_\epsilon^2$  (e.g. for  $\sigma_\epsilon^2 = 0.2$ , 88 % of the measurements contain an error), the algorithm is capable of converging.

## 7.7 Conclusions

From a spectrum cartography perspective, we have proposed a family of methods for nonparametric/semiparametric estimation of spatial vector fields observed by a collection of sensors which linearly compress and quantize their measurements. Based on the regularization inductive principle, the problem is formulated within the framework of regression of vector-valued functions in RKHSs and can be cast as an SVM problem. The resulting estimates inherit the properties of SVMs, such as the sparsity of their expansion coefficients.

Existing techniques for semiparametric regression were generalized to accommodate regression of vector-valued functions with CPD kernels, TPS representing a particular case. The proposed batch methods were extended to allow multiple measurements per sensor, non-uniform quantization, and non-negative enforcement. An alternative online implementation was also proposed based on stochastic gradient descent in the RKHS.

The work in this chapter has been submitted to *IEEE Transactions on Signal Processing* [Romero et al., 2015b] and was presented in part in the *40th IEEE International Conference on Acoustics, Speech and Signal Processing (ICASSP 2015)* [Romero et al., 2015c] and the *49th Annual Conference on Information Systems and Science (CISS 2015)* [Romero et al., 2015a].

## 7.A Acquisition with Pseudo-Random Filters

This appendix describes how the acquisition architecture from [Mehanna and Sidiropoulos, 2013], based on pseudo-random filters, can be used in place of the one proposed in Section 7.1, based on C-ADCs. To simplify the exposition, our notation assumes analog processing, but the operations described here may also be implemented digitally.

Suppose that a sensor located at position  $\mathbf{z}$  passes  $y(\mathbf{z}; t)$  through a linear and time-invariant

filter with impulse response  $\phi(\mathbf{z}; t)$ . The filtered signal has power

$$\bar{\eta}^2(\mathbf{z}) \triangleq \mathbb{E} \{ |\phi(\mathbf{z}; t) \star y(\mathbf{z}; t)|^2 \} = \int_{-\infty}^{\infty} |\Phi(\mathbf{z}; f)|^2 \Xi(\mathbf{z}; f) df, \quad (7.65)$$

where  $\Phi(\mathbf{z}; f)$  is the Fourier transform of  $\phi(\mathbf{z}; t)$ . From (7.1), it follows that

$$\bar{\eta}^2(\mathbf{z}) = \sum_{b=0}^{B-1} \alpha_b(\mathbf{z}) \int_{-\infty}^{\infty} |\Phi(\mathbf{z}; f)|^2 \Xi_b(f) df. \quad (7.66)$$

By defining  $\beta_b(\mathbf{z}) \triangleq \int_{-\infty}^{\infty} |\Phi(\mathbf{z}; f)|^2 \Xi_b(f) df$  and forming the vector  $\boldsymbol{\beta}(\mathbf{z}) \triangleq [\beta_0(\mathbf{z}), \dots, \beta_{B-1}(\mathbf{z})]^T$ , expression (7.66) reduces to (7.5).

The sensor at  $\mathbf{z}$  estimates  $\bar{\eta}^2(\mathbf{z})$  using either digital or analog processing, and sends a quantized version of the estimate to the FC, as described in Section 7.1. The filters  $\phi(\mathbf{z}; t)$  can be generated using pseudo-random sequences, where multiple measurements can be obtained by initializing the random generator with different seeds (see Section 7.3.1).

## 7.B Proof of Proposition 7.1

In any vector-valued RKHS  $\mathcal{F}$ , for every point  $\mathbf{z} \in \mathbb{R}^d$  there exists a linear operator  $k_{\mathbf{z}} : \mathbb{R}^B \rightarrow \mathcal{F}$  satisfying

$$\boldsymbol{\beta}^T \boldsymbol{\alpha}(\mathbf{z}) = \langle \boldsymbol{\alpha}, k_{\mathbf{z}} \boldsymbol{\beta} \rangle \quad (7.67)$$

for all  $\boldsymbol{\beta} \in \mathbb{R}^B$  [Micchelli and Pontil, 2005]. It can be thought of as a matrix of scalar operators:

$$k_{\mathbf{z}} = \begin{bmatrix} k_{\mathbf{z}}^{(0,0)} & \dots & k_{\mathbf{z}}^{(0,B-1)} \\ \vdots & \ddots & \vdots \\ k_{\mathbf{z}}^{(B-1,0)} & \dots & k_{\mathbf{z}}^{(B-1,B-1)} \end{bmatrix}. \quad (7.68)$$

The reproducing kernel is the result of evaluating  $k_{\mathbf{z}}$ , seen as a function on  $\mathbb{R}^d$ , at a given  $\mathbf{z}' \in \mathbb{R}^d$ ; that is,  $\mathbf{K}(\mathbf{z}', \mathbf{z}) \triangleq k_{\mathbf{z}}(\mathbf{z}') \in \mathbb{R}^{B \times B}$ . Since the evaluation is linear in an RKHS,  $(k_{\mathbf{z}}(\mathbf{z}'))\boldsymbol{\beta}_2 = (k_{\mathbf{z}}\boldsymbol{\beta}_2)(\mathbf{z}')$  and, consequently:

$$\boldsymbol{\beta}_1^T \mathbf{K}(\mathbf{z}', \mathbf{z}) \boldsymbol{\beta}_2 = \boldsymbol{\beta}_1^T (k_{\mathbf{z}}\boldsymbol{\beta}_2)(\mathbf{z}') = \langle k_{\mathbf{z}}\boldsymbol{\beta}_2, k_{\mathbf{z}'}\boldsymbol{\beta}_1 \rangle. \quad (7.69)$$

In virtue of the representer theorem [Micchelli and Pontil, 2005, Th. 5], for  $\lambda > 0$ , the

solution of the problem (7.12) has the form

$$\boldsymbol{\alpha} = \sum_{\mathbf{z} \in \mathcal{Z}} k_{\mathbf{z}} \mathbf{c}(\mathbf{z}) \quad (7.70)$$

for some vectors  $\{\mathbf{c}(\mathbf{z})\}_{\mathbf{z} \in \mathcal{Z}} \subset \mathbb{R}^B$ . Then, we can rewrite (7.12) in terms of the coefficient vectors  $\mathbf{c}(\mathbf{z})$  by noting that

$$\boldsymbol{\beta}^T \boldsymbol{\alpha}(\mathbf{z}) = \sum_{\mathbf{z}' \in \mathcal{Z}} \langle k_{\mathbf{z}'} \mathbf{c}(\mathbf{z}'), k_{\mathbf{z}} \boldsymbol{\beta} \rangle = \sum_{\mathbf{z}' \in \mathcal{Z}} \boldsymbol{\beta}^T \mathbf{K}(\mathbf{z}, \mathbf{z}') \mathbf{c}(\mathbf{z}'), \quad (7.71)$$

where the first equality follows from the linearity of the inner product and the second one is a consequence of (7.69); and

$$\|\boldsymbol{\alpha}\|_{\mathcal{F}}^2 = \langle \boldsymbol{\alpha}, \boldsymbol{\alpha} \rangle = \sum_{\mathbf{z}, \mathbf{z}' \in \mathcal{Z}} \langle k_{\mathbf{z}} \mathbf{c}(\mathbf{z}), k_{\mathbf{z}'} \mathbf{c}(\mathbf{z}') \rangle \quad (7.72a)$$

$$= \sum_{\mathbf{z}, \mathbf{z}' \in \mathcal{Z}} \mathbf{c}^T(\mathbf{z}') \mathbf{K}(\mathbf{z}', \mathbf{z}) \mathbf{c}(\mathbf{z}), \quad (7.72b)$$

which follows from (7.69). Equivalently, we may write  $\|\boldsymbol{\alpha}\|_{\mathcal{F}}^2 = \mathbf{c}^T \tilde{\mathbf{K}} \mathbf{c}$  and  $\boldsymbol{\beta}^T(\mathbf{z}_i) \boldsymbol{\alpha}(\mathbf{z}_i) = \boldsymbol{\beta}_i^T \tilde{\mathbf{K}} \mathbf{c}$ , where  $\tilde{\mathbf{K}}$  is defined in (7.14),  $\mathbf{c} = [\mathbf{c}^T(\mathbf{z}_0), \dots, \mathbf{c}^T(\mathbf{z}_{Z-1})]^T \in \mathbb{R}^{BZ}$ , and  $\boldsymbol{\beta}_i \triangleq \mathbf{e}_{Z,i} \otimes \boldsymbol{\beta}(\mathbf{z}_i)$ . Therefore, (7.12) becomes

$$\underset{\mathbf{c} \in \mathbb{R}^{BZ}}{\text{minimize}} \quad \frac{1}{Z} \sum_{i=0}^{Z-1} u_{\epsilon}(\tilde{q}(\mathbf{z}_i) - \boldsymbol{\beta}_i^T \tilde{\mathbf{K}} \mathbf{c}) + \lambda \mathbf{c}^T \tilde{\mathbf{K}} \mathbf{c}. \quad (7.73)$$

By noting that  $\epsilon \geq 0$  implies that  $u_{\epsilon}(z) = \max(0, z - \epsilon) + \max(0, -z - \epsilon)$ , the problem (7.73) is equivalent to

$$\underset{\mathbf{c} \in \mathbb{R}^{BZ}}{\text{minimize}} \quad \frac{1}{Z} \sum_{i=0}^{Z-1} [\max(0, \tilde{q}(\mathbf{z}_i) - \boldsymbol{\beta}_i^T \tilde{\mathbf{K}} \mathbf{c} - \epsilon) + \max(0, -\tilde{q}(\mathbf{z}_i) + \boldsymbol{\beta}_i^T \tilde{\mathbf{K}} \mathbf{c} - \epsilon)] + \lambda \mathbf{c}^T \tilde{\mathbf{K}} \mathbf{c}, \quad (7.74)$$

which, after scaling the objective and introducing the slack variables  $\zeta_{z_i}$  and  $\zeta_{z_i}^*$ , reads as

$$\begin{aligned}
& \underset{\mathbf{c} \in \mathbb{R}^{BZ}, \zeta_{z_i}, \zeta_{z_i}^*}{\text{minimize}} && \sum_{i=0}^{Z-1} [\zeta_{z_i} + \zeta_{z_i}^*] + \lambda Z \mathbf{c}^T \tilde{\mathbf{K}} \mathbf{c} \\
& \text{s.t.} && \zeta_{z_i} \geq \tilde{q}(\mathbf{z}_i) - \beta_i^T \tilde{\mathbf{K}} \mathbf{c} - \epsilon \quad i = 0, \dots, Z-1, \\
& && \zeta_{z_i}^* \geq -\tilde{q}(\mathbf{z}_i) + \beta_i^T \tilde{\mathbf{K}} \mathbf{c} - \epsilon \quad i = 0, \dots, Z-1, \\
& && \zeta_{z_i}, \zeta_{z_i}^* \geq 0, \quad i = 0, \dots, Z-1.
\end{aligned} \tag{7.75}$$

Finally, by defining  $\boldsymbol{\zeta} \triangleq [\zeta_{z_0}, \dots, \zeta_{z_{Z-1}}]^T$ ,  $\boldsymbol{\zeta}^* \triangleq [\zeta_{z_0}^*, \dots, \zeta_{z_{Z-1}}^*]^T$  and  $\mathbf{B} = [\beta_0, \beta_1, \dots, \beta_{Z-1}] = \mathbf{I}_Z \odot \check{\mathbf{B}}$ , we obtain (7.15).

## 7.C Proof of Proposition 7.2

Let  $\psi_b : \mathbb{R}^B \rightarrow \mathcal{F}$ ,  $b = 0, \dots, B'-1$ , be an operator with value  $\Psi_b(\mathbf{z})$  at point  $\mathbf{z}$  when seen as an element of  $\mathcal{F}$ . Then,  $\boldsymbol{\alpha}_{\text{par}}$  can be written as

$$\boldsymbol{\alpha}_{\text{par}} = \sum_{b=0}^{B'-1} \psi_b \mathbf{d}_b. \tag{7.76}$$

Using [Argyriou and Dinuzzo, 2014, Th. 3.1] to extend the semiparametric representer theorem [Schölkopf and Smola, 2001, Th. 4.3] to the vector case, we find that the solution of (7.23) can be written as

$$\boldsymbol{\alpha} = \sum_{\mathbf{z} \in \mathcal{Z}} k_{\mathbf{z}} \mathbf{c}(\mathbf{z}) + \sum_{b=0}^{B'-1} \psi_b \mathbf{d}_b, \tag{7.77}$$

where  $k_{\mathbf{z}}$  is the kernel operator of  $\mathcal{F}'$  (see Appendix 7.B). Substituting (7.77) in (7.23) and following the same steps as in Appendix 7.B yields

$$\underset{\mathbf{c}, \mathbf{d}}{\text{minimize}} \quad \frac{1}{Z} \sum_{i=0}^{Z-1} u_{\epsilon}(\tilde{q}(\mathbf{z}_i) - \beta_i^T (\tilde{\mathbf{K}} \mathbf{c} + \tilde{\Psi} \mathbf{d})) + \lambda \mathbf{c}^T \tilde{\mathbf{K}} \mathbf{c}, \tag{7.78}$$

where  $\beta_i \triangleq \mathbf{e}_{Z,i} \otimes \beta(\mathbf{z}_i)$ . After scaling and introducing the slack variables  $\zeta_{\mathbf{z}_i}$  and  $\zeta_{\mathbf{z}_i}^*$ , the problem (7.78) becomes

$$\begin{aligned}
& \underset{\mathbf{c}, \mathbf{d}, \zeta_{\mathbf{z}_i}, \zeta_{\mathbf{z}_i}^*}{\text{minimize}} && \sum_{i=0}^{Z-1} [\zeta_{\mathbf{z}_i} + \zeta_{\mathbf{z}_i}^*] + \lambda Z \mathbf{c}^T \tilde{\mathbf{K}} \mathbf{c} \\
& \text{s.t.} && \zeta_{\mathbf{z}_i} \geq \tilde{q}(\mathbf{z}_i) - \beta_i^T (\tilde{\mathbf{K}} \mathbf{c} + \tilde{\Psi} \mathbf{d}) - \epsilon, \quad i = 0, \dots, Z-1, \\
& && \zeta_{\mathbf{z}_i}^* \geq -\tilde{q}(\mathbf{z}_i) + \beta_i^T (\tilde{\mathbf{K}} \mathbf{c} + \tilde{\Psi} \mathbf{d}) - \epsilon, \quad i = 0, \dots, Z-1, \\
& && \zeta_{\mathbf{z}_i}, \zeta_{\mathbf{z}_i}^* \geq 0, \quad i = 0, \dots, Z-1,
\end{aligned} \tag{7.79}$$

or, in vector form, (7.25).

## 7.D Derivation of (7.35)

This appendix describes how to obtain the optimal  $\tilde{\mathbf{c}}$  and  $\mathbf{d}$  in (7.30) from the optimal solution of (7.33). If (7.30) were the dual of (7.33), then these variables could be recovered as the Lagrange multipliers of (7.33). However, this is not the case since (7.33) is not the *true* dual of (7.30), although both are trivially related. In particular, the *true* dual of (7.30) is

$$\begin{aligned}
& \underset{\tilde{\mathbf{c}}, \boldsymbol{\alpha}, \boldsymbol{\alpha}^*}{\text{minimize}} && \lambda Z \tilde{\mathbf{c}}^T \mathbf{P}_{\tilde{\Psi}}^\perp \tilde{\mathbf{K}} \mathbf{P}_{\tilde{\Psi}}^\perp \tilde{\mathbf{c}} - (\tilde{\mathbf{q}} - \epsilon \mathbf{1}_Z)^T \boldsymbol{\alpha} + (\tilde{\mathbf{q}} + \epsilon \mathbf{1}_Z)^T \boldsymbol{\alpha}^* \\
& \text{s.t.} && 2\lambda Z \mathbf{P}_{\tilde{\Psi}}^\perp \tilde{\mathbf{K}} \mathbf{P}_{\tilde{\Psi}}^\perp \tilde{\mathbf{c}} + \mathbf{P}_{\tilde{\Psi}}^\perp \tilde{\mathbf{K}} \mathbf{B}(\boldsymbol{\alpha} - \boldsymbol{\alpha}^*) = \mathbf{0}_{BZ}, \\
& && \tilde{\Psi}^T \mathbf{B}(\boldsymbol{\alpha} - \boldsymbol{\alpha}^*) = \mathbf{0}_{BB'}, \\
& && \boldsymbol{\alpha} - \mathbf{1}_Z \leq \mathbf{0}_Z, \quad -\boldsymbol{\alpha} \leq \mathbf{0}_Z, \\
& && \boldsymbol{\alpha}^* - \mathbf{1}_Z \leq \mathbf{0}_Z, \quad -\boldsymbol{\alpha}^* \leq \mathbf{0}_Z.
\end{aligned} \tag{7.80}$$

The fact that  $\tilde{\mathbf{c}}$  shows up both in (7.30) and in (7.80) is a consequence of the fact that  $\mathbf{P}_{\tilde{\Psi}}^\perp \tilde{\mathbf{K}} \mathbf{P}_{\tilde{\Psi}}^\perp$  is not invertible. Since the dual of (7.80) is again (7.30), both  $\tilde{\mathbf{c}}$  and  $\mathbf{d}$  can be immediately recovered from the solution of (7.80):  $\mathbf{d}$  is the Lagrange multiplier associated with the first equality constraint, whereas  $\tilde{\mathbf{c}}$  is directly the one solving (7.80).

Observe that, due to the second equality constraint,  $\mathbf{B}(\boldsymbol{\alpha} - \boldsymbol{\alpha}^*) = \mathbf{P}_{\tilde{\Psi}}^\perp \mathbf{B}(\boldsymbol{\alpha} - \boldsymbol{\alpha}^*)$  in the feasible set, meaning that the first equality constraint can be rewritten as

$$2\lambda Z \mathbf{P}_{\tilde{\Psi}}^\perp \tilde{\mathbf{K}} \mathbf{P}_{\tilde{\Psi}}^\perp \tilde{\mathbf{c}} + \mathbf{P}_{\tilde{\Psi}}^\perp \tilde{\mathbf{K}} \mathbf{P}_{\tilde{\Psi}}^\perp \mathbf{B}(\boldsymbol{\alpha} - \boldsymbol{\alpha}^*) = \mathbf{0}_{BZ}. \tag{7.81}$$

This equation is solved for  $\tilde{\mathbf{c}}$  when

$$\tilde{\mathbf{c}} = \frac{1}{2\lambda Z} \mathbf{B}(\boldsymbol{\alpha} - \boldsymbol{\alpha}^*) + \mathcal{N}(\mathbf{P}_{\tilde{\Psi}}^\perp \tilde{\mathbf{K}} \mathbf{P}_{\tilde{\Psi}}^\perp), \quad (7.82)$$

where the notation  $\mathcal{N}(\mathbf{A})$  is used to represent any vector in the null space of  $\mathbf{A}$ . Since the component in  $\mathcal{N}(\mathbf{P}_{\tilde{\Psi}}^\perp \tilde{\mathbf{K}} \mathbf{P}_{\tilde{\Psi}}^\perp)$  does not affect the problem, without any loss of generality we can take it to be the zero vector. Substituting (7.82) in (7.80) produces (7.33).

Although we have arrived at an equivalent problem, due to the transformations introduced, the Lagrange multipliers of (7.80) are not the same as those of (7.33). Fortunately, the latter can be easily recovered from the former. Let us associate the multipliers  $\boldsymbol{\mu}_1, \boldsymbol{\mu}_2, \boldsymbol{\nu}_1, \boldsymbol{\nu}_2, \boldsymbol{\nu}_3$  and  $\boldsymbol{\nu}_4$  to the constraints in (7.80); and associate the multipliers  $\boldsymbol{\mu}'_2, \boldsymbol{\nu}'_1, \boldsymbol{\nu}'_2, \boldsymbol{\nu}'_3$  and  $\boldsymbol{\nu}'_4$  to the constraints in (7.33), following the same order as they have been listed here. By stating the KKT conditions of (7.33) and (7.80), it can be seen that if  $\boldsymbol{\alpha}$  and  $\boldsymbol{\alpha}^*$  solve (7.33) with multipliers  $\boldsymbol{\mu}'_2, \boldsymbol{\nu}'_1, \boldsymbol{\nu}'_2, \boldsymbol{\nu}'_3$  and  $\boldsymbol{\nu}'_4$ , then the following values satisfy the KKT conditions of (7.80):

$$\tilde{\mathbf{c}} = \frac{1}{2\lambda Z} \mathbf{B}(\boldsymbol{\alpha} - \boldsymbol{\alpha}^*), \quad \boldsymbol{\mu}_1 = -\tilde{\mathbf{c}}, \quad (7.83a)$$

$$\boldsymbol{\mu}_2 = \boldsymbol{\mu}'_2 - (\tilde{\Psi}^T \tilde{\Psi})^{-1} \tilde{\Psi}^T \tilde{\mathbf{K}} \tilde{\mathbf{c}}, \quad (7.83b)$$

$$\boldsymbol{\nu}_1 = \boldsymbol{\nu}'_1, \quad \boldsymbol{\nu}_2 = \boldsymbol{\nu}'_2, \quad \boldsymbol{\nu}_3 = \boldsymbol{\nu}'_3, \quad \boldsymbol{\nu}_4 = \boldsymbol{\nu}'_4. \quad (7.83c)$$

Due to the second constraint in (7.80), it is clear that  $\tilde{\mathbf{c}} = \mathbf{P}_{\tilde{\Psi}}^\perp \tilde{\mathbf{c}}$ , which means that  $\mathbf{c} = \tilde{\mathbf{c}}$ . Finally, from (7.83b) and noting that  $\mathbf{d} = \boldsymbol{\mu}_2$ , expression (7.35) arises.

## 7.E Efficient Matrix Computation for Decoupled Models

As explained at the end of Section 7.5, when  $\mathbf{K}(\mathbf{z}, \mathbf{z}')$  and  $\Psi_b(\mathbf{z})$  are of the form (7.62), considerable simplifications are possible. Note that, in this case,  $\tilde{\mathbf{K}}$  can be written as

$$\tilde{\mathbf{K}} = \tilde{\mathbf{K}}_0 \otimes \mathbf{I}_B, \quad (7.84)$$

where  $\tilde{\mathbf{K}}_0 \in \mathbb{R}^{Z \times Z}$  is a matrix whose  $(i, j)$  entry equals  $K(\mathbf{z}_i, \mathbf{z}_j)$ . Correspondingly, the matrix  $\tilde{\Psi}$  can be written as

$$\tilde{\Psi} = \tilde{\Psi}_0 \otimes \mathbf{I}_B, \quad (7.85)$$

where  $\tilde{\Psi}_0 \in \mathbb{R}^{Z \times B'}$  is a matrix whose  $(i, b)$  element equals  $\Psi_b(\mathbf{z}_i)$ . Using (7.84) and (7.85), the computation of the matrices involved in the optimization problems of the previous sections can be efficiently obtained as described next.

From (7.41) and (7.84)

$$\begin{aligned}
\mathbf{B}^T \tilde{\mathbf{K}} &= [(\mathbf{I}_Z \otimes \mathbf{1}_M^T) \odot \check{\mathbf{B}}]^T (\tilde{\mathbf{K}}_0 \otimes \mathbf{I}_B) \\
&= \mathbf{\Gamma}^T [(\mathbf{I}_Z \otimes \mathbf{1}_M) \otimes \check{\mathbf{B}}^T] (\tilde{\mathbf{K}}_0 \otimes \mathbf{I}_B) \\
&= \mathbf{\Gamma}^T [(\mathbf{I}_Z \otimes \mathbf{1}_M) \tilde{\mathbf{K}}_0 \otimes \check{\mathbf{B}}^T] \\
&= \mathbf{\Gamma}^T [(\tilde{\mathbf{K}}_0 \otimes \mathbf{1}_M) \otimes \check{\mathbf{B}}^T] \\
&= [(\tilde{\mathbf{K}}_0 \otimes \mathbf{1}_M^T) \odot \check{\mathbf{B}}]^T,
\end{aligned} \tag{7.86}$$

where  $\mathbf{\Gamma}$  is a selection matrix containing ones and zeros arranged such that  $\mathbf{A} \odot \mathbf{B} = (\mathbf{A} \otimes \mathbf{B})\mathbf{\Gamma}$ . Likewise, from (7.41) and (7.85) we find that

$$\mathbf{B}^T \tilde{\Psi} = [(\tilde{\Psi}_0^T \otimes \mathbf{1}_M^T) \odot \check{\mathbf{B}}]^T. \tag{7.87}$$

Using the properties of the Kronecker product,  $\mathbf{P}_{\tilde{\Psi}}^\perp$  can be written as

$$\mathbf{P}_{\tilde{\Psi}}^\perp = \mathbf{I}_{BZ} - (\tilde{\Psi}_0(\tilde{\Psi}_0^T \tilde{\Psi}_0)^{-1} \tilde{\Psi}_0^T) \otimes \mathbf{I}_B \tag{7.88a}$$

$$= (\mathbf{I}_Z - \tilde{\Psi}_0(\tilde{\Psi}_0^T \tilde{\Psi}_0)^{-1} \tilde{\Psi}_0^T) \otimes \mathbf{I}_B \tag{7.88b}$$

$$= \mathbf{P}_{\tilde{\Psi}_0}^\perp \otimes \mathbf{I}_B, \tag{7.88c}$$

where  $\mathbf{P}_{\tilde{\Psi}_0}^\perp = \mathbf{I}_Z - \tilde{\Psi}_0(\tilde{\Psi}_0^T \tilde{\Psi}_0)^{-1} \tilde{\Psi}_0^T$ . This expression reduces the inversion of a  $BB' \times BB'$  matrix, as required from (7.31), to the inversion of a  $B' \times B'$  matrix.

From (7.34), we find that  $\tilde{\mathbf{K}}_\Psi$  can be computed as

$$\begin{aligned}
\tilde{\mathbf{K}}_\Psi &= \mathbf{B}^T (\mathbf{P}_{\tilde{\Psi}_0}^\perp \otimes \mathbf{I}_B) (\tilde{\mathbf{K}}_0 \otimes \mathbf{I}_B) (\mathbf{P}_{\tilde{\Psi}_0}^\perp \otimes \mathbf{I}_B) \mathbf{B} \\
&= \mathbf{B}^T (\mathbf{P}_{\tilde{\Psi}_0}^\perp \tilde{\mathbf{K}}_0 \mathbf{P}_{\tilde{\Psi}_0}^\perp \otimes \mathbf{I}_B) \mathbf{B} \\
&= ((\mathbf{I}_Z \otimes \mathbf{1}_M^T) \odot \check{\mathbf{B}})^T (\mathbf{P}_{\tilde{\Psi}_0}^\perp \tilde{\mathbf{K}}_0 \mathbf{P}_{\tilde{\Psi}_0}^\perp \otimes \mathbf{I}_B) ((\mathbf{I}_Z \otimes \mathbf{1}_M^T) \odot \check{\mathbf{B}}) \\
&= \mathbf{\Gamma}^T ((\mathbf{I}_Z \otimes \mathbf{1}_M^T) \otimes \check{\mathbf{B}})^T (\mathbf{P}_{\tilde{\Psi}_0}^\perp \tilde{\mathbf{K}}_0 \mathbf{P}_{\tilde{\Psi}_0}^\perp \otimes \mathbf{I}_B) ((\mathbf{I}_Z \otimes \mathbf{1}_M^T) \otimes \check{\mathbf{B}}) \mathbf{\Gamma} \\
&= \mathbf{\Gamma}^T [(\mathbf{I}_Z \otimes \mathbf{1}_M) \mathbf{P}_{\tilde{\Psi}_0}^\perp \tilde{\mathbf{K}}_0 \mathbf{P}_{\tilde{\Psi}_0}^\perp (\mathbf{I}_Z \otimes \mathbf{1}_M^T) \otimes \check{\mathbf{B}}^T \check{\mathbf{B}}] \mathbf{\Gamma} \\
&= (\mathbf{I}_Z \otimes \mathbf{1}_M) \mathbf{P}_{\tilde{\Psi}_0}^\perp \tilde{\mathbf{K}}_0 \mathbf{P}_{\tilde{\Psi}_0}^\perp (\mathbf{I}_Z \otimes \mathbf{1}_M^T) \odot \check{\mathbf{B}}^T \check{\mathbf{B}} \\
&= (\mathbf{P}_{\tilde{\Psi}_0}^\perp \tilde{\mathbf{K}}_0 \mathbf{P}_{\tilde{\Psi}_0}^\perp \otimes \mathbf{1}_M \mathbf{1}_M^T) \odot \check{\mathbf{B}}^T \check{\mathbf{B}}.
\end{aligned} \tag{7.89}$$

Finally,  $\mathbf{d}$  from (7.35) can be obtained as:

$$\mathbf{d} = \boldsymbol{\nu} - [(\tilde{\Psi}_0^T \tilde{\Psi}_0)^{-1} \tilde{\Psi}_0^T \tilde{\mathbf{K}}_0 \otimes \mathbf{I}_B] \mathbf{c}. \tag{7.90}$$





## Chapter 8

# Conclusions and Future Work

### 8.1 Conclusions

In the end, all the problems addressed in this thesis have a common theme: how to efficiently exploit our knowledge about the structure of certain signals in order to detect their presence or to estimate their power in a noisy environment. How detailed this knowledge is will decisively impact our ability to achieve our goal. In each case, a model that provides a partial statistical characterization of the observations serves as a starting point for the development of functions of the data, either detectors or estimators, that return the information we are looking for. Our methods range from those exploiting spatial structure, such as the rank-1 channel assumption, to those exploiting amplitude information, such as the CM property or the Gaussian assumption, and those exploiting spectral information, such as bandlimitedness or second-order statistics.

We moved a step towards expanding the state of the art in settings that we found of special practical relevance. For instance, in no case did we assume that the noise power or the channel between the primary user and the spectrum sensor were known. Our interest centered mainly on spectrum sensing for wireless microphone signals in television bands, spectrum sensing in time-varying channels, and spectrum sensing for waveforms of known spectral characteristics. The information that our methods are capable of inferring ranges from binary data regarding whether a certain primary user is operating in a given band, to detailed descriptions on how the power radiated by the primary source spreads across space. It may be used by secondary users to carefully plan their transmission strategies, for instance by selecting one band or another, by setting its radiation pattern, or by adjusting its rate or power.

The main tools required were taken from detection theory, estimation theory, and statistical learning. In the first chapters, we made extensive use of the *generalized likelihood ratio* as a tool to leverage the partial knowledge of the signal structure. Although the performance

obtained with this widely used approach is satisfactory in general, it is not necessarily optimal, and this fact prompted us to consider alternative approaches such as the search for (locally) optimal detectors within a family satisfying certain invariances. In this context, we addressed a fundamental question in *multivariate analysis of variance* regarding the existence of *locally most powerful invariant* tests for homogeneity of covariance problems (see the Appendix).

We have also considered the introduction of compression in the acquisition stage, which allowed us to estimate the occupancy state of wide frequency bands at a low hardware cost and power consumption. In this context, we addressed the problem of power estimation and activity detection of multiple wide-sense stationary processes immersed in noise of unknown variance. But this setting also lends itself to an in-depth treatment on how to *compress* the second-order statistics of this class of processes. We faced this fundamental problem, where we found optimum structures capable of maximizing the compression ratio while preserving all relevant second-order information. The applicability of our results extends well beyond spectrum sensing applications.

Finally, we delved into the problem of spectrum cartography, where contemporary tools of regression theory and statistical learning were applied to develop nonparametric and semiparametric schemes that learn power spectrum maps from the observations reported to the fusion center by a collection of inexpensive sensors. It was observed that a relatively small amount of highly compressed measurements suffices to reconstruct accurate representations of how the radiated power in different frequency channels spreads across a certain spatial region.

## 8.2 Open Lines and Future Work

Although the last few years have witnessed a great progress in spectrum sensing methods, there still remains a long way ahead to achieve fully intelligent exploitation of all prior information. For example most existing techniques rely on *frequentist* or *Bayesian* approaches, which may be useful in order to achieve good performance in terms of mean-squared error, probability of false alarm, probability of detection, etc; but can hardly accommodate past experience. On the other hand, contemporary machine learning tools may allow a rapid adaptation to changing conditions, but are difficult to analyze and manipulate in terms of the aforementioned performance metrics. It is envisioned that bridging this gap will be of critical importance for the upcoming DSA systems.

Broadly speaking, we can say that the vast majority of existing spectrum sensing methods do not exploit the fact that the spectrum sensor repeatedly observes the channel — in practice, such a sensor must typically provide a decision after each observation window (see e.g. [IEEE,

2011]). Instead, these methods implicitly assume that a single window is provided and a single decision needs to be made. Thus, numerous benefits may arise from exploiting past experience via learning, quite along the philosophy of *cognitive radio*. Note that, in particular, *online* learning methods would be highly desirable.

Another manifestation of this issue can be found when dealing with deleterious signal contributions. In particular, note that the interference inflicted by a distant primary or secondary user may be temporally or spatially correlated. Similarly, a machine operating in the vicinity of that sensor may introduce correlated noise. Learning the spatial and spectral features of these disturbances may assist decisively in improving detection/estimation performance. But exploiting this information requires devising models capable of capturing the (possibly time-fluctuating) nature of these processes and inference methods capable of exploiting the learned structure.

Approaching these somewhat *Utopian* goals will require extensive research in this area. Meanwhile, a number of more specific research directions that are related to the topics covered in this thesis are briefly summarized next.

### 8.2.1 Spectrum Sensing in a Single Channel

- In the context of detecting WM signals, we assumed that the noise process was spatially and temporally white. However, in accordance with what was explained above, it would be convenient to generalize our methods to accommodate correlated noise.
- Furthermore, the proposed schemes assume the presence of at most one WM waveform in the band of interest. However, it is not uncommon in practice that multiple WMs operate simultaneously in the same frequency band. Efficient methods that cope with the presence of multiple WM waveforms are yet to be devised.
- Regarding the detection of primary signals in time-varying channels, our schemes could be extended to accommodate further forms of signal structure other than the CM property or the Gaussian distribution. Allowing for colored noise would also be of interest.
- As pointed out in Section 4.3.3, multiantenna detection in rapidly-changing channels was left as an open line. A possible approach is the application of tests for homogeneity of covariance.

### 8.2.2 Spectrum Sensing in Multiple Channels

- Although we developed a number of computationally efficient techniques to estimate the power received from each of the primary users that operate in a wide frequency band, activity detection in such setting constitutes a future line of research. In particular, the only detector we discussed relies on a GLR test and is not CFAR due to the (possible) presence of more than one primary user in the band of interest. However, this is not a limitation of just our detection scheme — the power of other primary users may affect the probability of detection/false alarm of potentially any detector. Circumventing this drawback is therefore of clear interest, otherwise setting the test threshold may be troublesome. To do so, one of the first steps should be to investigate how the detection performance requirements must be specified: one can no longer ask a detector to guarantee a certain probability of detection under any circumstance; instead, one must first provide the conditions under which those requirements must be fulfilled.
- It would be of great interest to extend our techniques in order to accommodate sensors with multiple antennas and/or temporal channel variations.
- As for sampler design for CCS, most existing schemes rely either on specific algorithms or on identifiability criteria (see Chapter 6), but further design criteria are yet to be explored. For instance, it seems natural to seek sampler designs minimizing the Cramér-Rao bound for unbiased estimation of the parameters of interest [Romero and López-Valcarce, 2014a]. Devising deterministic designs that maximize the compression ratio under some minimal performance constraints would be particularly relevant. Moreover, further sampling schemes such as *gridless* or continuous irregular sampling have to be investigated from a CCS perspective.
- Future research may also consider non-linear covariance parameterizations as well as non-linear compression. This includes, for instance, exploiting information about the rank of the covariance matrix or the knowledge that the signal of interest is *auto-regressive* of order  $p$ .
- CCS may be applied in other contexts such as big data analytics due to its ability to meaningfully reduce the dimension of the data set. Both inference and compression methods need to be revisited to accommodate the special needs imposed by big data records. In particular, online, adaptive and distributed implementations for existing estimation methods are yet to be devised.

### 8.2.3 Spectrum Cartography in Multiple Channels

- When presenting our cartography scheme from Chapter 7, we only considered a limited number of choices for the *reproducing kernel Hilbert space*. Future research may take advantage of this degree of freedom in order to capture the propagation information via kernel selection.
- Another interesting line is that of designing the compression matrices and the quantizers that sensors implement. In this sense, vector quantization techniques, where multiple measurements are simultaneously quantized, may be useful.
- It may be worth delving deeper into the connections between the proposed regression techniques and *support vector machines*. They may provide some insight into how to choose the regularization parameter  $\lambda$  without resorting to cross-validation [Cherkassky and Mulier, 2007].
- Our regression scheme from Chapter 7 considered sensors with an extremely simple architecture. However, similar approaches carry over to settings where the sensors apply the procedures described in earlier chapters. For instance, each sensor may report to the fusion center a compressed and quantized version of the ML estimates from Chapters 2 to 5. This may allow to obtain cartography methods capable of constructing PSD maps for wireless microphones or in presence of time-varying channels. In the latter case, it would be interesting to jointly exploit the observed time dynamics of the channels and the observed motion of the sources.
- Rather than reporting just a quantized version of a power estimate, sensors may quantize multiple lags of the autocorrelation and send the result to the fusion center. How to recover PSD maps from that information is yet to be investigated.



# Appendix: On the Existence of Locally Optimal Invariant Tests for Homogeneity of Covariance Matrices

Given a set of samples drawn from several multivariate Gaussian distributions, the problem is to decide whether the associated covariance matrices are all identical or not. Although many hypothesis tests have been proposed in the past, a complete analysis focusing on those tests that preserve the problem invariances has not been provided yet. In particular, whether locally optimal tests exist within this family for the important case of *close hypotheses* has remained as an open problem.

In this appendix, the conditions under which locally optimal invariant tests exist are derived and, in those cases where they do, expressions for their statistics are presented in closed form. Wijsman's theorem is applied to derive the likelihood ratio of the maximal invariant statistic. It then follows that a locally optimal invariant test exists only in those cases where this ratio determines locally a family of equivalent tests for all values of the parameters of the model. The related *scale problem* is also considered, where the covariance matrices of different populations are known to be scaled versions of each other. It is shown in this case that a locally optimal invariant test always exists.

## A.1 Introduction

The assumption that a set of Gaussian populations have the same covariance matrix is central in a wide variety of classical problems in statistics and signal processing, such as discriminant analysis [Anderson, 2003, Muirhead, 2005], multiple-output regression [Hallin and Paindaveine, 2009],  $N$ -sample location [Hallin and Paindaveine, 2009], low-rank matrix approximation [Chen, 2008], time-frequency analysis [Huillery et al., 2008], speech recognition [Kumar and Andreou,

1998] and synthetic aperture radar imaging [Amirmazlaghani et al., 2009], just to name a few. Therefore, statistical procedures must be employed in practice to decide whether this assumption holds or not. In fact, the problem of testing equality of covariance matrices has become one of the fundamental problems in multivariate analysis of variance (MANOVA) [Anderson, 2003].

A standard test for this problem relies on the GLR test [Kay, 1998], which was first derived in [Wilks, 1932]. In cases where the number of observations is not the same for all populations, this test was shown to be biased [Das Gupta, 1969] and a slight modification to obtain an unbiased test was proposed by Bartlett [Anderson, 2003]. This test has been widely analyzed over the past decades and we now know asymptotic expansions of the distributions under both hypotheses, moments, exact distributions, etc (see [Anderson, 2003, Muirhead, 2005, Hallin and Paindaveine, 2009] and references therein). Although no optimality properties are associated with the Bartlett test, it seems to be the default procedure for many statisticians and engineers up to now.

Several alternatives to the GLR test have been explored in the past, including Schott's Wald test [Schott, 2001] and Nagao tests [Nagao, 1973], which can be seen as simplifications with the same asymptotic performance. For the case where the dimension of the problem is large relative to the number of observations, several heuristic tests have been proposed in [Schott, 2007] and [Srivastava and Yanagihara, 2010]. Later, the asymptotic equivalence of several of these tests was established in [Hallin and Paindaveine, 2009], where locally and asymptotically optimal adaptive tests [Lehmann and Romano, 2005] were also proposed using Le Cam's local asymptotic normality [Le Cam, 1986].

Interestingly, all of the tests above are invariant to certain transformations that are inherent to the problem. For example, note that scaling all the observations by any non-null constant should not affect our decision regarding whether all the populations have the same covariance matrix or not. This is not coincidental and, in fact, it is typically argued that any test not satisfying a certain family of invariances associated with the problem is not<sup>1</sup> *reasonable* [Gabriel and Kay, 2002]. This fact suggests looking for those tests within the family of invariant tests which are uniformly optimal (see Section 1.1.1). In the general problem of testing equality of covariance matrices, it is known that no such a test exists [Muirhead, 2005], and researchers were traditionally forced to resort to heuristic invariant criteria [Muirhead, 2005, Sec. 8.2.8.]. Nevertheless, even when a uniformly optimal test does not exist, it may be possible to find a locally optimal test in the challenging scenario of *close hypotheses* [Ramirez et al., 2013].

The purpose of this appendix is to look at the problem of testing homogeneity of covariance matrices from an invariance perspective. Although the conditions under which uniformly optimal

---

<sup>1</sup>See also [Lehmann and Romano, 2005, Sec. 1.5] for further motivation of why we should require a test to be invariant.



invariant tests exist have already been derived, little is known about the existence of *locally* optimal invariant tests in the regime of close hypotheses. In this appendix, we determine the cases where those tests exist and obtain expressions for their statistic in closed form. Our main tool is Wijsman's Theorem [Wijsman, 1967, Gabriel and Kay, 2002], which allows direct computation of the likelihood ratio of the maximal invariant statistic [Lehmann and Romano, 2005, Scharf, 1991] by integrating the densities of the observations over a group defining the invariances of the problem. The importance of this theorem relies on the fact that it avoids the explicit evaluation of the distribution of the maximal invariant statistic, which is typically intractable.

The main contribution of this appendix is to show that, when the same number of observations is available for all populations, the *locally most powerful<sup>2</sup> invariant* (LMPI) test is given by a linear combination of two statistics. The first one is the sum of squared traces of the (appropriately normalized) sample covariance matrices of each population, whereas the second one is the sum of their squared Frobenius norms. The fact that the relative weight of these two terms depends on parameters of the model means that no LMPI test exists in the general case. Only in the case with scalar observations and in the case with two vector observations per population<sup>3</sup> does this linear combination determine a family of equivalent tests for any value of the model parameters. Every member of that family is, therefore, an LMPI test. This completely solves the existence of LMPI tests when the number of observations is the same for all populations. On the other hand, if the latter condition does not hold, an LMPI test only exists if it coincides with the *uniformly most powerful invariant* (UMPI) test, that is, in the case with two scalar populations. For completeness, it is also shown that, in the related scale problem, where all covariance matrices are known to be scaled versions of each other, an LMPI test always exists since the relative weight of both statistics does not depend on the parameters of the model.

The rest of the appendix is structured as follows: Section A.2 formulates the problem of testing equality of covariance matrices and provides a review of existing methods. We next move to discuss invariance in Section A.3, where Wijsman's theorem is applied to obtain the likelihood ratio of the maximal invariant statistic. It turns out that no UMPI test exists in general, which prompts us to adopt an approximation of close hypotheses in Section A.4 and determine those cases where a locally optimal invariant test can be found. Finally, in Section A.5 we consider the scale problem, where a locally optimal test exists, and in Section A.6 we highlight some important conclusions.

---

<sup>2</sup>Throughout the appendix, the terms *optimal* and *most powerful* would be used interchangeably.

<sup>3</sup>Or just one observation if the mean vector is known.

## A.2 Testing Equality of Covariance Matrices

We now formalize the problem of deciding whether the covariance matrices of a collection of Gaussian populations are all the same or not. It will be assumed that the same number of observations are available from all populations. The reason is that it can be shown that no locally optimal test exists for different number of observations per population except in the simple case with two scalar populations, where a UMPI test can be found. After stating the observation model, we summarize a number of existing tests for this problem, highlighting the connections among them. In order to keep the notation simple and natural, the conventions adopted in this appendix differ from those adopted in the previous chapters.

### A.2.1 Problem Formulation

Suppose that we are given a set of complex<sup>4</sup> vector-valued samples  $\{\mathbf{x}_{n,k}, n = 0, \dots, N-1, k = 0, \dots, K-1\} \subset \mathbb{C}^{M \times 1}$ , where  $\mathbf{x}_{n,k}$  represents the  $k$ -th sample drawn from the  $n$ -th population, thus having a total of  $KN$  samples. We collect the samples from the  $n$ -th population in the matrix  $\mathbf{X}_n \triangleq [\mathbf{x}_{n,0}, \mathbf{x}_{n,1}, \dots, \mathbf{x}_{n,K-1}]$  and the whole dataset in the matrix  $\mathbf{X} \triangleq [\mathbf{X}_0, \mathbf{X}_1, \dots, \mathbf{X}_{N-1}]$ .

A probability measure is defined such that the data samples are multivariate circularly symmetric Gaussian distributed, mutually independent, with mean and covariance matrix depending on the population, that is,  $\mathbf{x}_{n,k} \sim \mathcal{CN}(\boldsymbol{\mu}_n, \boldsymbol{\Xi}_n)$ . Thus,

$$\pi^M \cdot p(\mathbf{x}_{n,k}) = |\boldsymbol{\Xi}_n|^{-1} \exp \left\{ -(\mathbf{x}_{n,k} - \boldsymbol{\mu}_n)^H \boldsymbol{\Xi}_n^{-1} (\mathbf{x}_{n,k} - \boldsymbol{\mu}_n) \right\},$$

where  $p(\mathbf{x}_{n,k})$  denotes the density of  $\mathbf{x}_{n,k}$  with respect to Lebesgue measure. Due to the mutual independence between data vectors, the joint density of those drawn from the  $n$ -th population can be expressed as<sup>5</sup>

$$\begin{aligned} \pi^{MK} p(\mathbf{X}_n) &= |\boldsymbol{\Xi}_n|^{-K} \times \\ &\exp \left\{ - \sum_k (\mathbf{x}_{n,k} - \boldsymbol{\mu}_n)^H \boldsymbol{\Xi}_n^{-1} (\mathbf{x}_{n,k} - \boldsymbol{\mu}_n) \right\}. \end{aligned} \quad (\text{A.1})$$

<sup>4</sup>This appendix assumes complex data due to the signal processing perspective adopted, but a similar derivation is possible in the case of real-valued observations, with appropriate changes in some of the constants involved.

<sup>5</sup>In order not to overload the notation, throughout the appendix we will omit the sum and product limits when it is clear from the context.

An alternative expression, which will be used later, arises from application in (A.1) of the identity

$$\begin{aligned} \sum_k (\mathbf{x}_{n,k} - \boldsymbol{\mu}_n)(\mathbf{x}_{n,k} - \boldsymbol{\mu}_n)^H = \\ K(\bar{\mathbf{x}}_n - \boldsymbol{\mu}_n)(\bar{\mathbf{x}}_n - \boldsymbol{\mu}_n)^H + \sum_k (\mathbf{x}_{n,k} - \bar{\mathbf{x}}_n)(\mathbf{x}_{n,k} - \bar{\mathbf{x}}_n)^H, \end{aligned} \quad (\text{A.2})$$

where  $\bar{\mathbf{x}}_n \triangleq K^{-1} \sum_k \mathbf{x}_{n,k}$  is the sample mean of the  $n$ -th population. Thus (A.1) can be rewritten as

$$\begin{aligned} \pi^{MK} p(\mathbf{X}_n) = |\boldsymbol{\Xi}_n|^{-K} \text{etr} \left\{ -\boldsymbol{\Xi}_n^{-1} \hat{\mathbf{V}}_{\mathbf{x},n} \right\} \times \\ \text{etr} \left\{ -K \boldsymbol{\Xi}_n^{-1} (\bar{\mathbf{x}}_n - \boldsymbol{\mu}_n)(\bar{\mathbf{x}}_n - \boldsymbol{\mu}_n)^H \right\}, \end{aligned} \quad (\text{A.3})$$

where  $\hat{\mathbf{V}}_{\mathbf{x},n}$  is the *scatter matrix* of the  $n$ -th population, defined as

$$\hat{\mathbf{V}}_{\mathbf{x},n} \triangleq \sum_k (\mathbf{x}_{n,k} - \bar{\mathbf{x}}_n)(\mathbf{x}_{n,k} - \bar{\mathbf{x}}_n)^H. \quad (\text{A.4})$$

Since all populations are assumed to be mutually independent, the density of the whole data record can be readily obtained as  $p(\mathbf{X}) = \prod_n p(\mathbf{X}_n)$ .

The problem of testing equality of covariance matrices, also known as homogeneity of covariance matrices or *homoscedasticity*, can be formulated as the problem of testing the null hypothesis  $\mathcal{H}_0$ , stating that there exists  $\boldsymbol{\Xi}$  such that  $\boldsymbol{\Xi}_n = \boldsymbol{\Xi} \quad \forall n$ , against the alternative  $\mathcal{H}_1$ , which states that there exist some  $n, m$  such that  $\boldsymbol{\Xi}_n \neq \boldsymbol{\Xi}_m$ . In this framework, the covariance matrices and the mean vectors are the unknown parameters of the model. Note in particular that assuming unknown means only makes sense if  $K > 1$ , since otherwise the problem becomes ill-posed. Interestingly, it can be seen that the case with known means is equivalent to the case with unknown means if in the latter we replace the sample means by their true values in the definition of the scatter matrices and  $K$  by  $K + 1$  in the expressions below. In such case the requirement  $K > 1$  is replaced by  $K > 0$ .

At this point we find it convenient to introduce some matrix notation. First, defining  $\bar{\mathbf{X}}_n \triangleq \bar{\mathbf{x}}_n \mathbf{1}_K^H$  enables us to write  $\hat{\mathbf{V}}_{\mathbf{x},n} = (\mathbf{X}_n - \bar{\mathbf{X}}_n)(\mathbf{X}_n - \bar{\mathbf{X}}_n)^H$ . Then, upon defining  $\bar{\mathbf{X}} \triangleq [\bar{\mathbf{X}}_0, \bar{\mathbf{X}}_1, \dots, \bar{\mathbf{X}}_{N-1}]$ , the global scatter matrix, defined as

$$\hat{\mathbf{V}}_{\mathbf{x}} \triangleq \sum_n \hat{\mathbf{V}}_{\mathbf{x},n}, \quad (\text{A.5})$$

can be written as

$$\hat{\mathbf{V}}_{\mathbf{x}} = (\mathbf{X} - \bar{\mathbf{X}})(\mathbf{X} - \bar{\mathbf{X}})^H. \quad (\text{A.6})$$

### A.2.2 Existing Tests

We now review some of the tests for homogeneity of covariance matrices that can be found in the literature. All of them are derived from some standard criterion except for the Nagao test, which is heuristic. Other tests of this kind can be found for the case  $N = 2$  in [Muirhead, 2005, Sec. 8.2.8.].

### GENERALIZED LIKELIHOOD RATIO TEST

The GLR test rejects the hypothesis  $\mathcal{H}_0$  for high values of

$$\mathcal{G}(\mathbf{X}) = \frac{\sup_{\boldsymbol{\mu}_0, \dots, \boldsymbol{\mu}_{N-1}, \boldsymbol{\Xi}_0, \dots, \boldsymbol{\Xi}_{N-1}} p(\mathbf{X}; \boldsymbol{\mu}_0, \dots, \boldsymbol{\mu}_{N-1}, \boldsymbol{\Xi}_0, \dots, \boldsymbol{\Xi}_{N-1})}{\sup_{\boldsymbol{\mu}_0, \dots, \boldsymbol{\mu}_{N-1}, \boldsymbol{\Xi}} p(\mathbf{X}; \boldsymbol{\mu}_0, \dots, \boldsymbol{\mu}_{N-1}, \boldsymbol{\Xi}, \dots, \boldsymbol{\Xi})}. \quad (\text{A.7})$$

As derived by Wilks [Wilks, 1932], this test statistic can be expressed in closed-form as<sup>6,7</sup>:

$$\mathcal{G}(\mathbf{X}) \propto \frac{|\hat{\mathbf{V}}_{\mathbf{x}}|^N}{\prod_n |\hat{\mathbf{V}}_{\mathbf{x},n}|}, \quad (\text{A.8})$$

Observe that this test can only be used when  $K > M$ , since otherwise the determinants in the denominator vanish. The well-known Bartlett test [Anderson, 2003] is a modification of the GLR test that corrects the bias arising when the number of observations of different populations is not the same [Das Gupta, 1969].

### WALD TEST

The Wald test for homogeneity of covariance matrices was first derived by Schott in [Schott, 2001], and rejects the null hypothesis for high values of

$$\mathcal{T}_{\text{Wald}}(\mathbf{X}) \propto \sum_n \text{Tr} \left( \left( \hat{\mathbf{V}}_{\mathbf{x},n} \hat{\mathbf{V}}_{\mathbf{x}}^{-1} \right)^2 \right) - \frac{1}{N} \sum_n \sum_m \text{Tr} \left( \hat{\mathbf{V}}_{\mathbf{x},n} \hat{\mathbf{V}}_{\mathbf{x}}^{-1} \hat{\mathbf{V}}_{\mathbf{x},m} \hat{\mathbf{V}}_{\mathbf{x}}^{-1} \right). \quad (\text{A.9})$$

<sup>6</sup>The symbol  $\propto$  means equality up to a monotonically increasing function (see Section 1.4).

<sup>7</sup>Recall that two statistics related by a monotonically increasing function define the same test if the thresholds are set accordingly.

Asymptotically, the performance of the Wald test is the same as that of the GLR test [Kay, 1998]. Therefore, the tests defined by (A.8) and (A.9) are asymptotically equivalent, though (A.9) is easier to compute, especially for large  $N$ .

### LOCALLY ASYMPTOTICALLY OPTIMAL GAUSSIAN TEST

Using Le Cam's asymptotic theory of statistical experiments [Le Cam, 1986], Hallin and Paindaveine derived the locally asymptotically optimal (most stringent) test for homogeneity of covariances [Hallin and Paindaveine, 2009]. When the populations are Gaussian distributed, their test statistic reduces to

$$\mathcal{T}_{\text{LAOGT}}(\mathbf{X}) \propto \sum_{n < m} \text{Tr} \left( \left( \hat{\mathbf{V}}_{\mathbf{x}}^{-1} (\hat{\mathbf{V}}_{\mathbf{x},n} - \hat{\mathbf{V}}_{\mathbf{x},m}) \right)^2 \right). \quad (\text{A.10})$$

### NAGAO TEST

Several tests have been proposed based on different heuristic criteria. Perhaps the most remarkable example is due to Nagao [Nagao, 1973] and is based on the distribution of the statistic in (A.8). This test rejects  $\mathcal{H}_0$  for large values of

$$\mathcal{T}_{\text{Nagao}}(\mathbf{X}) \propto \sum_n \text{Tr} \left( \left( \hat{\mathbf{V}}_{\mathbf{x},n} \hat{\mathbf{V}}_{\mathbf{x}}^{-1} - N(K-1)^2 \mathbf{I}_M \right)^2 \right). \quad (\text{A.11})$$

It can be readily checked that, except for the GLR test and the Bartlett test, all tests above are equivalent to the test based on the Frobenius norm (Frobenius test):

$$\mathcal{T}_{\text{Frobenius}}(\mathbf{X}) = \sum_n \|\hat{\mathbf{V}}_{\mathbf{x}}^{-1/2} \hat{\mathbf{V}}_{\mathbf{x},n} \hat{\mathbf{V}}_{\mathbf{x}}^{-1/2}\|_F^2. \quad (\text{A.12})$$

Note that we do not have this equivalence whenever the number of available observations is not the same for all populations. Furthermore, as will be shown, when the LMPI test exists, it is also equivalent to (A.12). Finally, it is interesting to note that all the previous tests are equivalent in the two-population scalar problem, i.e., for  $(N = 2, M = 1)$ , and it can be shown that the resulting test is uniformly most powerful unbiased [Muirhead, 2005].

### A.3 Optimal Invariant Test

The existence of a great variety of tests for equality of covariance matrices owes to the fact that no uniformly optimal test exists, as can be easily checked by noting that the likelihood ratio does not define equivalent tests for all values of the model parameters  $\{\Xi_0, \dots, \Xi_{N-1}, \mu_0, \dots, \mu_{N-1}\}$ . A typical approach to sidestep this difficulty is to focus on the family of those tests satisfying certain invariances that are inherent to the problem. These invariances are formalized by means of groups of transformations, and must be chosen so that no test violating any of them could reasonably be accepted. We begin this section by identifying the invariances of the problem.

#### A.3.1 Problem Invariances

The problem at hand is invariant to three classes of transformations, namely,

- invertible linear transformations common to all populations,
- translations common to all vectors in a given population,
- permutations of the populations.

Moreover, although the problem is also invariant to permutations of the observations belonging to each population, it can be seen that this invariance is implicit in the distribution and, consequently, the final test statistic will be invariant to these permutations as a desirable byproduct.

In order to apply Wijsman's theorem in the next section, we need to endow these transformations with a group structure. The first two invariances can be considered simultaneously by properly defining a group of affine transformations. These transformations map  $\mathbf{x}_{n,k}$  to  $g\mathbf{x}_{n,k} = \mathbf{A}\mathbf{x}_{n,k} + \mathbf{b}_n$ , where  $\mathbf{A} \in \mathbb{C}^{M \times M}$  is an invertible matrix and  $\mathbf{b}_n \in \mathbb{C}^{M \times 1}$ . To consider this transformation while restricting ourselves to the  $n$ -th population, define  $\mathbf{B}_n \triangleq \mathbf{b}_n \mathbf{1}_K^H$  and write  $g\mathbf{X}_n = \mathbf{A}\mathbf{X}_n + \mathbf{B}_n$ . Similarly, if we consider the whole set of observations, we can write  $g\mathbf{X} = \mathbf{A}\mathbf{X} + \mathbf{B}$  by defining  $\mathbf{B} = [\mathbf{B}_0, \dots, \mathbf{B}_{N-1}]$ . Formally speaking, this group is given by the set  $\mathbb{G}_1 \triangleq \{g = (\mathbf{A}, \mathbf{B}) : \mathbf{A} \in \mathbb{A}, \mathbf{B} \in \mathbb{B}\}$  together with a composition operation, where  $\mathbb{A}$  is the set of all  $M \times M$  invertible matrices and  $\mathbb{B}$  is the set of  $M \times NK$  matrices with the block structure  $\mathbf{B} = [\mathbf{b}_0 \mathbf{1}_K^H, \mathbf{b}_1 \mathbf{1}_K^H, \dots, \mathbf{b}_{N-1} \mathbf{1}_K^H]$ .

A permutation of populations is a transformation  $\mathbf{X} \mapsto \pi(\mathbf{X}) = [\mathbf{X}_{\pi[0]}, \mathbf{X}_{\pi[1]}, \dots, \mathbf{X}_{\pi[N-1]}]$ , where  $\pi[\cdot]$  is a permutation of the first  $N$  non-negative integers. Let  $\mathbb{G}_2$  denote the set of population permutations  $\pi(\mathbf{X})$  induced by the set of all permutations  $\Pi = \{\pi[\cdot]\}$  of the first  $N$  non-negative integers. When this set is considered together with the natural composition operation  $\pi_1 \pi_2$ , it constitutes a group.

Both forms of invariance can be manipulated simultaneously by regarding  $\mathbb{G}_1$  and  $\mathbb{G}_2$  as subgroups of a larger group  $\mathbb{G} = \{g = (\mathbf{A}, \mathbf{B}, \pi) : (\mathbf{A}, \mathbf{B}) \in \mathbb{G}_1, \pi \in \mathbb{G}_2\}$  together with the operation  $(\mathbf{A}^{(1)}, \mathbf{B}^{(1)}, \pi_1)(\mathbf{A}^{(2)}, \mathbf{B}^{(2)}, \pi_2) = (\mathbf{A}^{(1)}\mathbf{A}^{(2)}, \mathbf{A}^{(1)}\pi_1(\mathbf{B}^{(2)}) + \mathbf{B}^{(1)}, \pi_1\pi_2)$ . This group acts on the data as  $g\mathbf{X} = (\mathbf{A}, \mathbf{B}, \pi)\mathbf{X} = \mathbf{A}\pi(\mathbf{X}) + \mathbf{B} = \pi(\mathbf{A}\mathbf{X}) + \mathbf{B}$ , and induces a transformation  $\bar{g}$  in the parameters of the distributions as

$$\begin{aligned} \bar{g} \{ \boldsymbol{\Xi}_0, \dots, \boldsymbol{\Xi}_{N-1}, \boldsymbol{\mu}_0, \dots, \boldsymbol{\mu}_{N-1} \} = & \{ \mathbf{A}\boldsymbol{\Xi}_{\pi[0]}\mathbf{A}^H, \dots, \\ & \mathbf{A}\boldsymbol{\Xi}_{\pi[N-1]}\mathbf{A}^H, \mathbf{A}\boldsymbol{\mu}_{\pi[0]} + \mathbf{b}_0, \dots, \mathbf{A}\boldsymbol{\mu}_{\pi[N-1]} + \mathbf{b}_{N-1} \}. \end{aligned} \quad (\text{A.13})$$

Recall that a group  $\mathbb{G}$  defines an equivalence relation  $\sim$  as follows:  $\mathbf{X} \sim \mathbf{Y}$  iff there exists some  $g \in \mathbb{G}$  such that  $g\mathbf{X} = \mathbf{Y}$ . In the context of invariant statistics, the classes of equivalence defined by this equivalence relation are called *orbits* and play a central role in Wijsman's theorem.

To simplify the ensuing derivation, it is convenient at this point to introduce the equivalent (normalized) data set  $\mathbf{Y} = g_0\mathbf{X}$ , where  $g_0 \triangleq (\mathbf{A}_0, -\mathbf{A}_0\bar{\mathbf{X}}, 1_\pi)$  for  $1_\pi$  the identity permutation and  $\mathbf{A}_0 \in \mathbb{C}^{M \times M}$  an invertible matrix satisfying

$$\hat{\mathbf{V}}_{\mathbf{y}} = \mathbf{A}_0 \hat{\mathbf{V}}_{\mathbf{x}} \mathbf{A}_0^H = \mathbf{I}_M. \quad (\text{A.14})$$

Note that the normalized data set has zero mean, i.e.  $\bar{\mathbf{Y}} = \mathbf{0}$ . This normalization does not incur any loss of information since any invariant statistic  $\mathcal{T}$  satisfies  $\mathcal{T}(\mathbf{X}) = \mathcal{T}(g\mathbf{X})$ ,  $\forall g \in \mathbb{G}$ .

### A.3.2 Maximal Invariant Statistic

It is well known [Lehmann and Romano, 2005, Scharf, 1991] that any invariant statistic is a function of the maximal invariant statistic, which is, in turn, a function of the data assigning the same value to all possible observations  $\mathbf{X}$  lying in the same orbit and different values to observations in different orbits. In other words, if  $\delta$  represents a maximal invariant statistic,

$$\delta(\mathbf{X}) = \delta(\mathbf{X}') \Leftrightarrow \exists g \in \mathbb{G} \text{ such that } \mathbf{X}' = g\mathbf{X}. \quad (\text{A.15})$$

Intuitively, a maximal invariant is a canonical transformation returning a representative for each orbit. Note as well that any injective transformation of a maximal invariant is again a maximal invariant, which means that this class of statistics are not unique.

A possible maximal invariant that we may arbitrarily choose when  $N > 2$  and  $M > 2$  is as follows: first take the sufficient statistic, given by

$$\{ \hat{\mathbf{V}}_{\mathbf{x},0}, \dots, \hat{\mathbf{V}}_{\mathbf{x},N-1}, \bar{\mathbf{x}}_0, \dots, \bar{\mathbf{x}}_{N-1} \}. \quad (\text{A.16})$$

Next normalize the data as described in Section A.3.1. Since the sample means become zero in that case, this is equivalent to consider just the sample scatter matrices  $\{\hat{\mathbf{V}}_{\mathbf{y},1}, \dots, \hat{\mathbf{V}}_{\mathbf{y},N}\}$ . It is still possible to apply a pair of transformations without violating the normalization condition in (A.14). First, we can permute the normalized sample scatter matrices in the decreasing order of their traces — this is possible with probability one —, i.e., we take the ordered set  $\{\hat{\mathbf{V}}_{\mathbf{y},n_0}, \hat{\mathbf{V}}_{\mathbf{y},n_1}, \dots, \hat{\mathbf{V}}_{\mathbf{y},n_{N-1}}\}$ , where  $n_0, n_1, \dots, n_{N-1}$  are such that  $\text{Tr}(\hat{\mathbf{V}}_{\mathbf{y},n_0}) > \text{Tr}(\hat{\mathbf{V}}_{\mathbf{y},n_1}) > \dots > \text{Tr}(\hat{\mathbf{V}}_{\mathbf{y},n_{N-1}})$ . Similarly, it is possible to multiply the observations by a unitary matrix that we can write as  $\mathbf{A}_0 = \mathbf{D}_0 \mathbf{U}_0$ , where  $\mathbf{D}_0 = \text{diag}\{e^{j\varphi_0}, \dots, e^{j\varphi_{N-1}}\}$ ,  $\mathbf{U}_0$  is a unitary matrix and  $\varphi_n \in \mathbb{R} \forall n$ . We can set  $\mathbf{U}_0$  such that  $\mathbf{U}_0 \hat{\mathbf{V}}_{\mathbf{y},n_0} \mathbf{U}_0^H$  is diagonal,  $\varphi_1, \dots, \varphi_{N-1}$  such that the first row and column of  $\mathbf{A}_0 \hat{\mathbf{V}}_{\mathbf{y},n_1} \mathbf{A}_0^H$  is formed by positive real numbers and  $\varphi_0$  such that the  $(0,1)$  and  $(1,0)$  elements of  $\mathbf{A}_0 \hat{\mathbf{V}}_{\mathbf{y},n_2} \mathbf{A}_0^H$  are also real and positive. To sum up, we have found that the following statistic is maximally invariant:

$$\{\mathbf{A}_0 \hat{\mathbf{V}}_{\mathbf{y},n_0} \mathbf{A}_0^H, \mathbf{A}_0 \hat{\mathbf{V}}_{\mathbf{y},n_1} \mathbf{A}_0^H, \dots, \mathbf{A}_0 \hat{\mathbf{V}}_{\mathbf{y},n_{N-1}} \mathbf{A}_0^H\}. \quad (\text{A.17})$$

The UMPI test exists if and only if the maximal invariant is scalar valued since the test statistic is a maximal invariant itself. In view of (A.17), we conclude that no UMPI test exists for  $N > 2$  and  $M > 2$ . In fact, it can be shown that the UMPI test will exist only in the case where  $M = 1$  and  $N = 2$ .

It is interesting to note that the problem can be parameterized in terms of the so-called *maximal invariant parameters* just by mimicking the procedure in this section with the parameters of the distribution. For convenience, however, in the next section we apply a different choice of maximal invariant parameters which still summarizes the relevant information. We define the *precision matrices*

$$\mathbf{S}_n \triangleq \mathbf{\Xi}_n^{-1}, \quad (\text{A.18})$$

the *average precision matrix*

$$\mathbf{S} \triangleq \frac{1}{N} \sum_n \mathbf{S}_n, \quad (\text{A.19})$$

and the *homogeneity matrices*

$$\mathbf{\Delta}_n \triangleq \mathbf{S}^{-1/2}(\mathbf{S}_n - \mathbf{S})\mathbf{S}^{-1/2}, \quad (\text{A.20})$$

where  $\mathbf{S}^{-1/2}$  is the Hermitian square root of  $\mathbf{S}$ ; and show, in the next section, that the maximal invariant statistic can be written solely in terms of  $\mathbf{\Delta}_n$ .



### A.3.3 Most Powerful Invariant Test

As stated above, the UMPI test, when it exists, is a function of the maximal invariant statistic. The standard approach to derive this test is to first find a maximal invariant statistic  $\mathbf{m}$  and then to compute the associated likelihood ratio, which is defined as

$$\mathcal{U}(\mathbf{m}) \triangleq \frac{p(\mathbf{m}; \boldsymbol{\mu}_0, \dots, \boldsymbol{\mu}_{N-1}, \boldsymbol{\Xi}_0, \dots, \boldsymbol{\Xi}_{N-1})}{p(\mathbf{m}; \boldsymbol{\mu}_0, \dots, \boldsymbol{\mu}_{N-1}, \boldsymbol{\Xi}, \dots, \boldsymbol{\Xi})}. \quad (\text{A.21})$$

This requires the computation of the likelihood functions associated with this statistic under both hypotheses, which is typically a highly involved task. However, in many cases, one can apply Wijsman's theorem [Wijsman, 1967] to directly compute the likelihood ratio of the maximal invariant statistic by integrating the likelihood functions under both hypotheses over the group defining the invariances with respect to an invariant group measure. Although Wijsman only proved this result for *Lie groups*, the theorem can be easily extended to accommodate finite groups [Gabriel and Kay, 2005, App. B]. In our case,  $\mathbb{G}$  is a composition of a Lie group  $\mathbb{G}_1$  and a finite group  $\mathbb{G}_2$ , but we can sidestep this difficulty by considering a measure  $\nu$  which is the product measure of the counting measure in  $\mathbb{G}_2$  and a left-invariant measure<sup>8</sup> over a  $\sigma$ -field containing  $\mathbb{G}_1$ . With this in mind, the likelihood ratio of the maximal invariant statistic can be computed as:

$$\mathcal{U}(\mathbf{m}) = \frac{\int_{\mathbb{G}} p(g\mathbf{X}; \boldsymbol{\mu}_0, \dots, \boldsymbol{\mu}_{N-1}, \boldsymbol{\Xi}_0, \dots, \boldsymbol{\Xi}_{N-1}) \Gamma_g \nu(dg)}{\int_{\mathbb{G}} p(g\mathbf{X}; \boldsymbol{\mu}_0, \dots, \boldsymbol{\mu}_{N-1}, \boldsymbol{\Xi}) \Gamma_g \nu(dg)}, \quad (\text{A.22})$$

where  $\Gamma_g$  is the Jacobian of the transformation  $g \in \mathbb{G}$ . Observe that one must be able to replace  $\mathbf{X}$  in either the numerator or the denominator of (A.22) by any other  $\mathbf{Y} = g\mathbf{X}$ ,  $g \in \mathbb{G}$ , without altering the value of the integral. This fact simplifies the application of Wijsman's Theorem to the problem at hand, which reads as follows:

**THEOREM A.1.** *The likelihood ratio of the maximal invariant statistic when applied to the normalized data is given by:*

$$\begin{aligned} \mathcal{U}(\mathbf{m}) = & \kappa \cdot \sum_{\pi} \int_{\mathbb{A}} \text{etr} \{ -\mathbf{A}^H \mathbf{A} \} \times \\ & \times \text{etr} \left\{ - \sum_n \Delta_n \mathbf{A} \hat{\mathbf{V}}_{\mathbf{y}, \pi[n]} \mathbf{A}^H \right\} |\mathbf{A}^H \mathbf{A}|^L d\mathbf{A}, \end{aligned} \quad (\text{A.23})$$

where the integral is with respect to Lebesgue measure,  $L \triangleq (K-1)N - M$  and  $\kappa$  is a constant

---

<sup>8</sup> Note that the fact that only invertible matrices are considered in  $\mathbb{G}_1$  need not be taken into account since the set of singular matrices has measure zero (see Appendix A.A).

given by

$$\kappa \triangleq \frac{\pi^{-M^2}}{N!} \frac{\prod_n |\mathbf{\Delta}_n + \mathbf{I}|^{K-1}}{E\{|\mathbf{A}^H \mathbf{A}|^L\}}. \quad (\text{A.24})$$

The expectation in the denominator of (A.24) is taken assuming that the entries of  $\mathbf{A}$  are independent standard complex Gaussian random variables.

*Proof.* See Appendix A.A. □

Since the tests defined by (A.23) for different values of the model parameters  $\mathbf{\Delta}_n$  are not equivalent, it follows that no UMPI test exists in general. The same conclusion was obtained in the past (c.f. [Muirhead, 2005]) for the case of two populations by noting that the maximal invariant statistic is vector-valued.

As a remarkable exception, when  $M = 1$  and  $N = 2$ , it can be seen that Theorem A.1 provides a statistic which is an increasing function of  $(\hat{v}_{x,0}^2 - \hat{v}_{x,1}^2)/(\hat{v}_{x,0}^2 + \hat{v}_{x,1}^2)$ , where  $\hat{v}_{x,i}^2$  represents the sample variance of the  $i$ -th population. This is a scalar maximal invariant [Muirhead, 2005] and defines a UMPI test that rejects  $\mathcal{H}_0$  for high values of this statistic. Moreover, it can also be seen that this test is equivalent to those in Section A.2.2, which shows that all those tests are UMPI whenever  $M = 1$  and  $N = 2$ .

## A.4 Locally Optimal Invariant Tests

Although the likelihood ratio of the maximal invariant statistic was seen to depend on the parameters of the model, sometimes this dependence fades out in the asymptotic regime of *close hypotheses* and, consequently, a locally optimal test can be found (see e.g. [Ramirez et al., 2013] and references therein). For the problem at hand, this assumption means that the matrices  $\mathbf{\Xi}_n$  are *close* to each other. The following sections are intended to derive this locally optimal test for the cases where it exists.

### A.4.1 Locally Most Powerful Invariant Tests

The assumption of close hypotheses means that the homogeneity matrices  $\mathbf{\Delta}_n$  are small. Performing a second-order Taylor expansion with respect to  $\mathbf{\Delta}_n$  about  $\mathbf{\Delta}_n = \mathbf{0}$  over the second

exponential in (A.23) gives

$$\begin{aligned} \text{etr} \left\{ - \sum_n \Delta_n \mathbf{A} \hat{\mathbf{V}}_{\mathbf{y}, \pi[n]} \mathbf{A}^H \right\} &\approx 1 - \sum_n \text{Tr} \left( \Delta_n \mathbf{A} \hat{\mathbf{V}}_{\mathbf{y}, \pi[n]} \mathbf{A}^H \right) \\ &\quad + \frac{1}{2} \left[ \sum_n \text{Tr} \left( \Delta_n \mathbf{A} \hat{\mathbf{V}}_{\mathbf{y}, \pi[n]} \mathbf{A}^H \right) \right]^2. \end{aligned} \quad (\text{A.25})$$

By substituting this approximation in (A.23) and using the fact that  $\sum_n \Delta_n = \mathbf{0}$ , one obtains that  $\mathcal{U}(\mathbf{m}) \approx \mathcal{U}'(\mathbf{m}) \triangleq \kappa' + \frac{\kappa}{2} \cdot \mathcal{L}(\mathbf{m})$ , where

$$\mathcal{L}(\mathbf{m}) = \int_{\mathbb{A}} \text{etr} \{ -\mathbf{A}^H \mathbf{A} \} \sum_{\pi} \left[ \sum_n \text{Tr} \left( \Delta_n \mathbf{A} \hat{\mathbf{V}}_{\mathbf{y}, \pi[n]} \mathbf{A}^H \right) \right]^2 |\mathbf{A}^H \mathbf{A}|^L d\mathbf{A}, \quad (\text{A.26})$$

$\kappa$  is given by (A.24), and  $\kappa'$  is a constant given by

$$\kappa' = \kappa \cdot \sum_{\pi} \int_{\mathbb{A}} \text{etr} \{ -\mathbf{A}^H \mathbf{A} \} |\mathbf{A}^H \mathbf{A}|^L d\mathbf{A} \quad (\text{A.27a})$$

$$= \kappa \cdot N! \cdot \pi^{M^2} \mathbb{E} \{ |\mathbf{A}^H \mathbf{A}|^L \}. \quad (\text{A.27b})$$

In the expression above and throughout the appendix, the expectations are taken by considering that the entries in  $\mathbf{A}$  are independent standard complex Gaussian random variables.

The following theorem shows that  $\mathcal{L}(\mathbf{m})$  is actually a linear combination of two statistics. First, we define the following constant matrices

$$\mathbf{M}_1 \triangleq \mathbb{E} \left\{ |\mathbf{A}^H \mathbf{A}|^L \tilde{\mathbf{A}}^T \mathbf{1}_M \mathbf{1}_M^T \tilde{\mathbf{A}} \right\} \quad (\text{A.28a})$$

$$\mathbf{M}_2 \triangleq \mathbb{E} \left\{ |\mathbf{A}^H \mathbf{A}|^L \tilde{\mathbf{A}}^T \tilde{\mathbf{A}} \right\}, \quad (\text{A.28b})$$

where  $\tilde{\mathbf{A}}$  is an  $M \times M$  matrix whose  $(i, j)$ -th entry is the squared magnitude of the  $(j, i)$ -th entry in the matrix  $\mathbf{A}$ , and the constant  $c \triangleq \frac{\pi^{M^2} N(N-2)!}{M(M-1)}$ . Then, we have the following:

**THEOREM A.2.** *Let  $\boldsymbol{\lambda}_n$  be a vector with the eigenvalues of the homogeneity matrix  $\Delta_n$  and let  $\Phi = \sum_n \boldsymbol{\lambda}_n \boldsymbol{\lambda}_n^T$ . Then, the statistic  $\mathcal{L}(\mathbf{m})$  in (A.26) is given by*

$$\mathcal{L}(\mathbf{m}) = \alpha \sum_n \|\hat{\mathbf{V}}_{\mathbf{y}, n}\|_F^2 + \beta \sum_n \text{Tr}^2 \left( \hat{\mathbf{V}}_{\mathbf{y}, n} \right) + \gamma, \quad (\text{A.29})$$

where the constants  $\alpha$ ,  $\beta$  and  $\gamma$  are defined as:

$$\gamma \triangleq -c \frac{M(M-1)}{N} \text{Tr}(\Phi \mathbf{M}_1) \quad (\text{A.30a})$$

$$\alpha \triangleq \begin{cases} \pi N(L+2)!(N-2)!\Phi & \text{if } M = 1 \\ c \cdot [-\text{Tr}(\Phi \mathbf{M}_1) + M \text{Tr}(\Phi \mathbf{M}_2)] & \text{if } M > 1. \end{cases} \quad (\text{A.30b})$$

$$\beta \triangleq \begin{cases} 0 & \text{if } M = 1 \\ c \cdot [\text{Tr}(\Phi \mathbf{M}_1) - \text{Tr}(\Phi \mathbf{M}_2)] & \text{if } M > 1. \end{cases} \quad (\text{A.30c})$$

*Proof.* See Appendix A.B. □

From (A.29), we observe that the likelihood ratio of the maximal invariant statistic in the regime of close hypotheses is a linear combination of two statistics: the sum of squared traces and the sum of squared Frobenius norms of the normalized sample scatter matrices. The constants  $\alpha$  and  $\beta$  determine the relative weight of these two statistics. However, since these constants depend on the model parameters  $\Delta_n$ , Theorem A.2 shows that the locally optimal test uses a different weight for these two statistics depending on the actual values of those parameters. Consequently, no test can be found that is uniformly optimal even in the regime of close hypotheses, i.e., no locally optimal test exists for the general vector-valued case. However, it is remarkable that in certain particular cases, which are summarized next, the tests defined by (A.29) for different values of the parameters are all equivalent, resulting in locally optimal tests. Before considering those situations, it is convenient to rewrite Theorem A.2 in terms of the original unnormalized data set.

COROLLARY A.1.

1. When  $M = 1$ , the statistic  $\mathcal{L}(\mathbf{m})$  in (A.26) is given by  $\mathcal{L}(\mathbf{m}) = \alpha \mathcal{L}'(\mathbf{m}) + \gamma$  where

$$\mathcal{L}'(\mathbf{m}) \triangleq \frac{\sum_n \hat{v}_{x,n}^2}{\hat{v}_x^2}. \quad (\text{A.31})$$

Here, we have defined  $\hat{v}_{x,n} \triangleq \sum_k (x_{n,k} - \bar{x}_n)^2$ , which is the scaled sample variance of the unnormalized scalar population  $\{x_{n,0}, \dots, x_{n,K-1}\}$ , with  $\bar{x}_n \triangleq \sum_k x_{n,k}$ , and  $\hat{v}_x \triangleq \sum_n \hat{v}_{x,n}$ , which is the scaled sample variance of all populations.

2. When  $M > 1$ , the statistic  $\mathcal{L}(\mathbf{m})$  in (A.26) is given by

$$\begin{aligned}\mathcal{L}(\mathbf{m}) &= \alpha \sum_n \|\hat{\mathbf{V}}_{\mathbf{x}}^{-1/2} \hat{\mathbf{V}}_{\mathbf{x},n} \hat{\mathbf{V}}_{\mathbf{x}}^{-1/2}\|_F^2 + \beta \sum_n \text{Tr}^2 \left( \hat{\mathbf{V}}_{\mathbf{x}}^{-1/2} \hat{\mathbf{V}}_{\mathbf{x},n} \hat{\mathbf{V}}_{\mathbf{x}}^{-1/2} \right) + \gamma \\ &= \alpha \sum_n \text{Tr} \left( (\hat{\mathbf{V}}_{\mathbf{x}}^{-1} \hat{\mathbf{V}}_{\mathbf{x},n})^2 \right) + \beta \sum_n \text{Tr}^2 \left( \hat{\mathbf{V}}_{\mathbf{x}}^{-1} \hat{\mathbf{V}}_{\mathbf{x},n} \right) + \gamma,\end{aligned}\quad (\text{A.32})$$

where  $\hat{\mathbf{V}}_{\mathbf{x}}^{-1/2}$  denotes the Hermitian square root of the inverse of  $\hat{\mathbf{V}}_{\mathbf{x}}$ .

#### A.4.2 Existence of the LMPI Test

In some cases, the dependence of the test  $\mathcal{U}'(\mathbf{m})$  on the model parameters reduces to a scaling factor and an additive constant, which means that all values of these parameters yield equivalent tests. In other words, any of these tests is locally optimal invariant. The conditions under which this effect takes place are summarized next. Note that the LMPI test, when exists, is equivalent to the Frobenius test from (A.12).

##### CASE $M = 1$

If  $M = 1$ , an LMPI test exists, which rejects  $\mathcal{H}_0$  for high values of the statistic in (A.31). Interestingly, this is the *generalized kurtosis* test statistic from Chapter 4, which was derived following a completely different approach. The name stems from the fact that this statistic is a function of the sample excess kurtosis of the observations.

##### CASE $K = 2$

In this case, it can easily be shown that the statistic  $\mathcal{L}(\mathbf{m})$  in (A.26) is given by  $\mathcal{L}(\mathbf{m}) = \frac{\alpha+\beta}{4} \mathcal{L}'(\mathbf{m}) + \gamma$ , where

$$\mathcal{L}'(\mathbf{m}) = \sum_n ((\mathbf{x}_{n,1} - \mathbf{x}_{n,2})^H \hat{\mathbf{V}}_{\mathbf{x}}^{-1} (\mathbf{x}_{n,1} - \mathbf{x}_{n,2}))^2. \quad (\text{A.33})$$

Clearly, the statistic in (A.33) defines an LMPI test.

##### CASE $K = 1$ WITH KNOWN MEAN

The case  $K = 2$  suggests that a similar test must be available for the related problem where the mean is known. Without any loss of generality, let us assume that that mean is zero:  $\boldsymbol{\mu} = \boldsymbol{\mu}_n = \mathbf{0} \forall n$ . The problem is thus not invariant to translations by a vector  $\mathbf{b}_n$ , as discussed

in Section A.3.1, but the derivation is quite similar to the one followed above. In that case, it can be shown that there exists an LMPI test and that it is given by ( $\mathbf{x}_n$  denotes  $\mathbf{x}_{n,1}$ ):

$$\mathcal{L}''(\mathbf{m}) = \sum_n (\mathbf{x}_n^H \hat{\mathbf{V}}_x^{-1} \mathbf{x}_n)^2. \quad (\text{A.34})$$

## A.5 Scale test

A classical problem related to that of testing equality of covariance matrices when  $M > 1$  is the so-called scale test (see e.g. [Hallin and Paindaveine, 2009]). In this case, we know that  $\mathbf{\Xi}_n = \xi_n \mathbf{\Xi}$  for some  $\xi_n > 0$ ,  $n = 0, \dots, N-1$ , i.e., all the covariance matrices are scaled versions of each other. Consequently, the homogeneity matrices  $\mathbf{\Delta}_n$  are scaled versions of the identity matrix  $\mathbf{I}_M$  and, therefore,  $\mathbf{\Phi}$  is a scaled version of the matrix with all ones. In this way, it can be seen that the dependence of the test statistic on the parameters of the model reduces to a scaling factor, which means that the locally optimal tests for different values of the parameters are actually equivalent. Before providing the expression for the test statistic, we evaluate the matrices  $\mathbf{M}_1$  and  $\mathbf{M}_2$  in (A.28a) and (A.28b) explicitly.

LEMMA A.1. *The matrices  $\mathbf{M}_1$  and  $\mathbf{M}_2$  defined in (A.28a) and (A.28b) can be written as  $(1/c')\mathbf{M}_i = a_i \mathbf{I}_M + b_i \mathbf{1}_M \mathbf{1}_M^T$ , where  $c'$  is a constant given in Appendix A.D and*

$$\begin{aligned} a_1 &\triangleq \frac{1}{3}\Gamma(L+3) + 2(M-1)\Gamma(L+2) \\ &\quad + (3p-4)\Gamma(L+1) - \frac{1}{3}(L+3)(L+2) \\ &\quad - (L+2)(2(M-2) + 1/3)\Gamma(L+1) \\ b_1 &\triangleq \frac{1}{3}(L+3)(L+2) + (M-2)^2\Gamma(L+1) \\ &\quad + \frac{2}{3}\Gamma(L+3) + (L+2)(2(M-2) + 1/3)\Gamma(L+1) \\ a_2 &\triangleq \Gamma(L+3) + M\Gamma(L+1) - \frac{1}{3}(L+3)(L+2) \\ b_2 &\triangleq (M-2)\Gamma(L+1) + \frac{1}{3}(L+3)(L+2), \end{aligned}$$

with  $L \triangleq (K-1)N - M$  and  $\Gamma(n) \triangleq (n-1)(n-2) \cdots 2 \cdot 1$  for  $n \in \mathbb{N}$ .

*Proof.* See Appendix A.D. □

Making use of the expressions in Theorem A.2 and Lemma A.1 we conclude the following:

THEOREM A.3. *The statistic of the LMPI test for scale of covariance matrices is given by*

$$\mathcal{U}'(\mathbf{m}) \propto \alpha' \sum_n \text{Tr} \left( (\hat{\mathbf{V}}_{\mathbf{x}}^{-1} \hat{\mathbf{V}}_{\mathbf{x},n})^2 \right) + \beta' \sum_n \text{Tr}^2 \left( \hat{\mathbf{V}}_{\mathbf{x}}^{-1} \hat{\mathbf{V}}_{\mathbf{x},n} \right),$$

where

$$\begin{aligned} \alpha' &\triangleq -a_1 - Mb_1 + Ma_2 + M^2b_2, \\ \beta' &\triangleq a_1 + Mb_1 - a_2 - Mb_2. \end{aligned} \tag{A.35}$$

## A.6 Conclusions

We have considered locally optimal tests for equality of covariance matrices within the family of tests preserving the invariances of the problem. In the case of a different number of observations per population there is no invariance to permutations and, consequently, no locally optimal invariant test exists, except for the case with  $M = 1$  and  $N = 2$ , where a UMPI test can be found. In the case where the number of observations per population is the same, a LMPI test exists only in certain particular cases, where it is equivalent to the Frobenius test. It was also shown that another case where an LMPI test can be found is the related scale problem.

### A.A Proof of Theorem A.1

We first compute the numerator in expression (A.22) — the denominator will follow next by considering the case  $\Xi_n = \Xi \forall n$ . We decide to construct  $\nu$ , which must be a left-invariant measure with respect to the transformations in  $\mathbb{G}$ , as the product measure of an invariant measure  $\nu_1$  in  $\mathbb{G}_1$ , for instance the one with density  $\delta_1(\mathbf{A}, \mathbf{B}) \triangleq |\mathbf{A}^H \mathbf{A}|^{-N-M}$ , and the counting measure  $\nu_2$  in  $\mathbb{G}_2$ . With this in mind, we apply Fubini's Theorem [Billingsley, 1995] to the numerator in (A.22), producing

$$\sum_{\pi} \int_{\mathbb{A}} \left[ \prod_n \int_{\mathbb{C}^M} p(\mathbf{A} \mathbf{Y}_{\pi[n]} + \mathbf{B}_n; \boldsymbol{\mu}_n, \Xi_n) d\mathbf{b}_n \right] |\mathbf{A}^H \mathbf{A}|^L d\mathbf{A}. \tag{A.36}$$

From (A.3), it follows that

$$\begin{aligned} p(\mathbf{A} \mathbf{Y}_{\pi[n]} + \mathbf{B}_n; \boldsymbol{\mu}_n, \Xi_n) = \\ \pi^{-MK} |\Xi_n|^{-K} \text{etr} \left\{ -\Xi_n^{-1} \mathbf{A} \hat{\mathbf{V}}_{\mathbf{y}, \pi[n]} \mathbf{A}^H \right\} \times \text{etr} \left\{ -K \Xi_n^{-1} (\mathbf{b}_n - \boldsymbol{\mu}_n)(\mathbf{b}_n - \boldsymbol{\mu}_n)^H \right\}. \end{aligned} \tag{A.37}$$

Observe that the first factor does not depend on  $\mathbf{b}_n$  whereas the second does not depend on  $\mathbf{A}$ . Therefore, the integral of (A.37) with respect to  $d\mathbf{b}_n$  becomes  $\text{etr} \left\{ -\Xi_n^{-1} \mathbf{A} \hat{\mathbf{V}}_{\mathbf{y}, \pi[n]} \mathbf{A}^H \right\}$  times a positive constant  $\kappa_{1,n}$  given by

$$\begin{aligned} \kappa_{1,n} &\triangleq \pi^{-MK} |\Xi_n|^{-K} \int_{\mathbb{C}^M} \text{etr} \left\{ -K \Xi_n^{-1} (\mathbf{b}_n - \boldsymbol{\mu}_n) (\mathbf{b}_n - \boldsymbol{\mu}_n)^H \right\} d\mathbf{b}_n \\ &= \frac{|\Xi_n|^{1-K}}{\pi^{M(K-1)} K^M} \int_{\mathbb{C}^M} \frac{\exp \left\{ -(\mathbf{b}_n - \boldsymbol{\mu}_n)^H \left( \frac{1}{K} \Xi_n \right)^{-1} (\mathbf{b}_n - \boldsymbol{\mu}_n) \right\}}{\pi^M \left| \frac{1}{K} \Xi_n \right|} d\mathbf{b}_n \\ &= \frac{|\Xi_n|^{1-K}}{\pi^{M(K-1)} K^M}, \end{aligned}$$

where the second equality follows from the fact that  $\mathbf{b}_n$  can be interpreted as a Gaussian random vector with mean  $\boldsymbol{\mu}_n$  and covariance matrix  $\frac{1}{K} \Xi_n$ . This means that (A.36), or equivalently the numerator of (A.22), equals

$$\kappa_1 \cdot \sum_{\pi} \int_{\mathbb{A}} \text{etr} \left\{ -\sum_n \Xi_n^{-1} \mathbf{A} \hat{\mathbf{V}}_{\mathbf{y}, \pi[n]} \mathbf{A}^H \right\} |\mathbf{A}^H \mathbf{A}|^L d\mathbf{A}, \quad (\text{A.38})$$

where  $\kappa_1 \triangleq \prod_n \kappa_{1,n}$ . This expression can be written in terms of the parameters  $\mathbf{S}$  and  $\boldsymbol{\Delta}_n$  defined in Section A.3.2 as

$$\kappa_1 \cdot \sum_{\pi} \int_{\mathbb{A}} \text{etr} \left\{ -\mathbf{A}^H \mathbf{S} \mathbf{A} \right\} \text{etr} \left\{ -\sum_n \mathbf{S}^{1/2} \boldsymbol{\Delta}_n \mathbf{S}^{1/2} \mathbf{A} \hat{\mathbf{V}}_{\mathbf{y}, \pi[n]} \mathbf{A}^H \right\} |\mathbf{A}^H \mathbf{A}|^L d\mathbf{A}. \quad (\text{A.39})$$

Applying the change of variable  $\mathbf{A} \leftarrow \mathbf{S}^{1/2} \mathbf{A}$  we obtain

$$\bar{\kappa}_1 \cdot \sum_{\pi} \int_{\mathbb{A}} \text{etr} \left\{ -\mathbf{A}^H \mathbf{A} \right\} \text{etr} \left\{ -\sum_n \boldsymbol{\Delta}_n \mathbf{A} \hat{\mathbf{V}}_{\mathbf{y}, \pi[n]} \mathbf{A}^H \right\} |\mathbf{A}^H \mathbf{A}|^L d\mathbf{A}, \quad (\text{A.40})$$

where

$$\bar{\kappa}_1 = |\mathbf{S}|^{-(K-1)N} \cdot \kappa_1 = \frac{\prod_n |\boldsymbol{\Delta}_n + \mathbf{I}_M|^{K-1}}{\pi^{MN(K-1)} K^{MN}}. \quad (\text{A.41})$$

The denominator follows from substituting  $\Xi_n = \Xi \forall n$ , or equivalently  $\boldsymbol{\Delta}_n = \mathbf{0} \forall n$ , in (A.40), which results in

$$\bar{\kappa}_0 \cdot \sum_{\pi} \int_{\mathbb{A}} \text{etr} \left\{ -\mathbf{A}^H \mathbf{A} \right\} |\mathbf{A}^H \mathbf{A}|^L d\mathbf{A}, \quad (\text{A.42})$$

where  $\bar{\kappa}_0 = \pi^{-MN(K-1)} K^{-MN}$ . Now identifying  $\mathbf{A}$  with a matrix of independent standard



complex Gaussian random variables and summing along all permutations of  $N$  elements, (A.42) becomes

$$\bar{\kappa}_0 \cdot N! \cdot \pi^{M^2} \cdot \mathbb{E} \{ |\mathbf{A}^H \mathbf{A}|^L \}. \quad (\text{A.43})$$

Finally, combining (A.40) and (A.43) concludes the proof.

## A.B Proof of Theorem A.2

We begin by proving the following result:

LEMMA A.2. *The test statistic  $\mathcal{L}(\mathbf{m})$  in (A.26) is given by*

$$\mathcal{L}(\mathbf{m}) = \tau_0 + \tau_1 \int_{\mathbb{A}} \text{etr} \{ -\mathbf{A}^H \mathbf{A} \} \sum_{n,k} \text{Tr}^2 \left( \mathbf{A}^H \Delta_n \mathbf{A} \hat{\mathbf{V}}_{\mathbf{y},k} \right) |\mathbf{A}^H \mathbf{A}|^L d\mathbf{A}, \quad (\text{A.44})$$

where  $\tau_1 = N(N-2)!$  and

$$\tau_0 = -(N-2)! \cdot \pi^{M^2} \cdot \text{Tr}(\Phi \mathbf{M}_1). \quad (\text{A.45})$$

*Proof.* The sum of the integral in (A.26) can also be written as

$$\begin{aligned} \sum_{\pi} \left[ \sum_n \text{Tr} \left( \Delta_n \mathbf{A} \hat{\mathbf{V}}_{\mathbf{y},\pi[n]} \mathbf{A}^H \right) \right]^2 &= \sum_{\pi} \sum_n \text{Tr}^2 \left( \Delta_n \mathbf{A} \hat{\mathbf{V}}_{\mathbf{y},\pi[n]} \mathbf{A}^H \right) \\ &\quad + \sum_{\pi} \sum_n \text{Tr} \left( \Delta_n \mathbf{A} \hat{\mathbf{V}}_{\mathbf{y},\pi[n]} \mathbf{A}^H \right) \sum_{m \neq n} \text{Tr} \left( \bar{\Delta}_m \mathbf{A} \hat{\mathbf{V}}_{\mathbf{y},\pi[m]} \mathbf{A}^H \right), \end{aligned}$$

where  $\sum_{m \neq n}$  means  $\sum_{m=0, m \neq n}^{N-1}$ . Expanding these sums over all permutations of  $N$  elements yields:

$$\begin{aligned} \sum_{\pi} \left[ \sum_n \text{Tr} \left( \Delta_n \mathbf{A} \hat{\mathbf{V}}_{\mathbf{y},\pi[n]} \mathbf{A}^H \right) \right]^2 &= (N-1)! \sum_n \sum_k \text{Tr}^2 \left( \Delta_n \mathbf{A} \hat{\mathbf{V}}_{\mathbf{y},k} \mathbf{A}^H \right) \\ &\quad + (N-2)! \sum_n \sum_k \text{Tr} \left( \Delta_n \mathbf{A} \hat{\mathbf{V}}_{\mathbf{y},k} \mathbf{A}^H \right) \sum_{m \neq n} \sum_{l \neq k} \text{Tr} \left( \bar{\Delta}_m \mathbf{A} \hat{\mathbf{V}}_{\mathbf{y},l} \mathbf{A}^H \right), \end{aligned} \quad (\text{A.46})$$

where we have made use of the following identities:

$$\begin{aligned} \sum_{\pi} f(\pi[n]) &= (N-1)! \sum_k f(k) \\ \sum_{\pi} f(\pi[n])g(\pi[m]) &= (N-2)! \sum_k \sum_{l \neq k} f(k)g(l) \quad \text{if } m \neq n, \end{aligned} \quad (\text{A.47})$$

where  $f(\cdot)$  and  $g(\cdot)$  are two arbitrary functions. Using  $\sum_n \Delta_n = \mathbf{0}$ , the second term in the right hand side of (A.46) becomes

$$\begin{aligned} & - (N-2)! \sum_n \sum_k \text{Tr} \left( \Delta_n \mathbf{A} \hat{\mathbf{V}}_{\mathbf{y},k} \mathbf{A}^H \right) \sum_{l \neq k} \text{Tr} \left( \Delta_n \mathbf{A} \hat{\mathbf{V}}_{\mathbf{y},l} \mathbf{A}^H \right) \\ &= - (N-2)! \sum_n \sum_k \text{Tr} \left( \Delta_n \mathbf{A} \hat{\mathbf{V}}_{\mathbf{y},k} \mathbf{A}^H \right) \text{Tr} \left( \Delta_n \mathbf{A} (\mathbf{I}_M - \hat{\mathbf{V}}_{\mathbf{y},k}) \mathbf{A}^H \right) \\ &= - (N-2)! \sum_n \text{Tr}^2 \left( \Delta_n \mathbf{A} \mathbf{A}^H \right) + (N-2)! \sum_n \sum_k \text{Tr}^2 \left( \Delta_n \mathbf{A} \hat{\mathbf{V}}_{\mathbf{y},k} \mathbf{A}^H \right), \end{aligned}$$

where both equalities owe to the fact that  $\sum_k \hat{\mathbf{V}}_{\mathbf{y},k} = \mathbf{I}_M$ . Substituting this expression in (A.46) gives

$$\begin{aligned} & \sum_{\pi} \left[ \sum_n \text{Tr} \left( \Delta_n \mathbf{A} \hat{\mathbf{V}}_{\mathbf{y},\pi[n]} \mathbf{A}^H \right) \right]^2 \\ &= N(N-2)! \sum_n \sum_k \text{Tr}^2 \left( \Delta_n \mathbf{A} \hat{\mathbf{V}}_{\mathbf{y},k} \mathbf{A}^H \right) - (N-2)! \sum_n \text{Tr}^2 \left( \Delta_n \mathbf{A} \mathbf{A}^H \right), \end{aligned}$$

which in combination with (A.26) yields (A.44) with  $\tau_1 = N(N-2)!$  and

$$\tau_0 = - (N-2)! \int_{\mathbb{A}} \text{etr} \{ -\mathbf{A}^H \mathbf{A} \} \sum_n \text{Tr}^2 \left( \mathbf{A}^H \Delta_n \mathbf{A} \right) |\mathbf{A}^H \mathbf{A}|^L d\mathbf{A}. \quad (\text{A.48})$$

Separating the integral along  $n$  results in

$$\tau_0 = - (N-2)! \sum_n \int_{\mathbb{A}} \text{etr} \{ -\mathbf{A}_n^H \mathbf{A}_n \} \text{Tr}^2 \left( \mathbf{A}_n^H \Delta_n \mathbf{A}_n \right) |\mathbf{A}_n^H \mathbf{A}_n|^L d\mathbf{A}_n. \quad (\text{A.49})$$

If  $\mathbf{W}_n \bar{\Lambda}_n \mathbf{W}_n^H$  is an eigenvalue decomposition of  $\Delta_n$ , applying the change of variable  $\mathbf{A}_n \leftarrow \mathbf{W}_n \mathbf{A}_n$ , equation (A.49) simplifies to

$$\tau_0 = - (N-2)! \int_{\mathbb{A}} \text{etr} \{ -\mathbf{A}^H \mathbf{A} \} \sum_n \text{Tr}^2 \left( \mathbf{A}^H \bar{\Lambda}_n \mathbf{A} \right) |\mathbf{A}^H \mathbf{A}|^L d\mathbf{A}. \quad (\text{A.50})$$

Since the vector  $\lambda_n$  contains the diagonal elements of  $\bar{\Lambda}_n$ , it is possible to rewrite  $\text{Tr}^2 \left( \mathbf{A}^H \bar{\Lambda}_n \mathbf{A} \right)$

as  $[\mathbf{1}_M^T \tilde{\mathbf{A}} \boldsymbol{\lambda}_n]^2$ . Using this identity in (A.50) yields, after some algebra,

$$\tau_0 = -(N-2)! \cdot \pi^{M^2} \mathbb{E} \left\{ |\mathbf{A}^H \mathbf{A}|^L \text{Tr} \left( \Phi \tilde{\mathbf{A}}^T \mathbf{1}_M \mathbf{1}_M^T \tilde{\mathbf{A}} \right) \right\}.$$

Interchanging the order of the trace and expectation, expression (A.45) immediately follows.  $\square$

Now, for reasons that will become clear later, we consider separately the cases  $M = 1$  and  $M > 1$  in the rest of the proof.

### A.B.1 Case $M = 1$

When  $M = 1$ , all matrices in (A.44) become scalars. For clarity, let us denote these scalars as  $a$  for  $\mathbf{A}$ ,  $\lambda_n$  for  $\bar{\mathbf{A}}_n$  and  $\hat{v}_{\mathbf{y},k}$  for  $\hat{\mathbf{V}}_{\mathbf{y},k}$ . Then, the integral in (A.44) reads as

$$\sum_{n,k} \lambda_n^2 \hat{v}_{\mathbf{y},k}^2 \int_{\mathbb{C}-\{0\}} |a|^{2L+4} \exp \{-|a|^2\} da. \quad (\text{A.51})$$

Noting that the integral in (A.51) is nothing but the  $(2L+4)$ -th order moment of a standard complex Gaussian distribution, it follows this integral equals  $\pi(L+2)!$ . Substituting this value in (A.44) results in

$$\mathcal{L}(\mathbf{m}) = \tau_0 + \tau_1 \pi(L+2)! \sum_n \lambda_n^2 \sum_k \hat{v}_{\mathbf{y},k}^2. \quad (\text{A.52})$$

Now, by taking the constants  $\alpha$ ,  $\beta$  and  $\gamma$  in the same way as in Theorem A.2, expression (A.29) comes up.

### A.B.2 Case $M > 1$

When  $M > 1$  the simplifications above do not apply, thus making the proof more involved. However, an important simplification follows by noting that  $\mathcal{L}(\mathbf{m})$  can be rewritten in terms of the eigenvalues of the scatter matrices  $\hat{\mathbf{V}}_{\mathbf{y},k}$ . The following lemma provides this expression.

**LEMMA A.3.** *The test statistic in (A.44) can be written in terms of the eigenvalues of the scatter matrices as*

$$\mathcal{L}(\mathbf{m}) = \tau_0 + \tau_1 \sum_k \boldsymbol{\sigma}_k^T \mathbf{G} \boldsymbol{\sigma}_k, \quad (\text{A.53})$$

where  $\boldsymbol{\sigma}_k$  is a vector with the eigenvalues of  $\hat{\mathbf{V}}_{\mathbf{y},k}$  and

$$\mathbf{G} = \pi^{M^2} E \left\{ |\mathbf{A}^H \mathbf{A}|^L \tilde{\mathbf{A}} \Phi \tilde{\mathbf{A}}^T \right\}. \quad (\text{A.54})$$

*Proof.* First decompose the integral in (A.44) as a sum of integrals depending on  $k$ :

$$\sum_k \int_{\mathbb{A}} \text{etr} \{ -\mathbf{A}_k^H \mathbf{A}_k \} \sum_n \text{Tr}^2 \left( \mathbf{A}_k^H \boldsymbol{\Delta}_n \mathbf{A}_k \hat{\mathbf{V}}_{\mathbf{y},k} \right) |\mathbf{A}_k^H \mathbf{A}_k|^L d\mathbf{A}_k. \quad (\text{A.55})$$

Now consider the eigenvalue decompositions  $\boldsymbol{\Delta}_n = \mathbf{W}_n \bar{\boldsymbol{\Lambda}}_n \mathbf{W}_n^H$  and  $\hat{\mathbf{V}}_{\mathbf{y},n} = \mathbf{U}_n \boldsymbol{\Sigma}_n \mathbf{U}_n^H$ , and apply the change of variable  $\mathbf{A}_k \leftarrow \mathbf{W}_n \mathbf{A}_k \mathbf{U}_n^H$  to (A.55) in order to diagonalize the terms inside the trace:

$$\sum_k \int_{\mathbb{A}} \text{etr} \{ -\mathbf{A}_k^H \mathbf{A}_k \} \sum_n \text{Tr}^2 \left( \mathbf{A}_k^H \bar{\boldsymbol{\Lambda}}_n \mathbf{A}_k \boldsymbol{\Sigma}_n \right) |\mathbf{A}_k^H \mathbf{A}_k|^L d\mathbf{A}_k.$$

Now considering all the integrals with the same variable and making  $\boldsymbol{\sigma}_k = \text{diag} \{ \boldsymbol{\Sigma}_k \}$ , expression (A.53) immediately follows with

$$\mathbf{G} = \int_{\mathbb{A}} \text{etr} \{ -\mathbf{A}^H \mathbf{A} \} \tilde{\mathbf{A}} \Phi \tilde{\mathbf{A}}^T |\mathbf{A}^H \mathbf{A}|^L d\mathbf{A}. \quad (\text{A.56})$$

Interpreting the elements of  $\mathbf{A}$  as standard Gaussian random variables results in (A.54). □

Since  $\mathbf{G}$  is an  $M \times M$  matrix, its computation requires to evaluate, in principle,  $M^2$  expectations. However, this task is considerably simplified by noting that the value of the statistic should not depend on the order of the eigenvalues in  $\boldsymbol{\sigma}_k$ . The next result will elucidate the structure of the aforementioned matrix.

**LEMMA A.4.** *Given any vector  $\mathbf{v} \in \mathbb{R}^M$  and matrix  $\mathbf{G} \in \mathbb{C}^{M \times M}$ , if the product  $\mathbf{v}^T \mathbf{G} \mathbf{v}$  is invariant to permutations of the elements of  $\mathbf{v}$ , that is, if  $\mathbf{v}^T \mathbf{G} \mathbf{v} = \mathbf{v}^T \mathbf{P}^T \mathbf{G} \mathbf{P} \mathbf{v}$  for any permutation matrix  $\mathbf{P}$ , then  $\mathbf{G}$  must be of the form  $\mathbf{G} = \bar{\gamma} \mathbf{I} + \tilde{\gamma} \mathbf{1}_M \mathbf{1}_M^T$ .*

*Proof.* See Appendix A.C. □

Application of Lemma A.4 to (A.53) results in

$$\mathcal{L}(\mathbf{m}) = \tau_0 + \tau_1 \left[ \bar{\gamma} \sum_k \|\boldsymbol{\sigma}_k\|^2 + \tilde{\gamma} \sum_k (\boldsymbol{\sigma}_k^T \mathbf{1}_M)^2 \right] \quad (\text{A.57a})$$

$$= \tau_0 + \tau_1 \left[ \bar{\gamma} \sum_k \|\hat{\mathbf{V}}_{\mathbf{y},k}\|_F^2 + \tilde{\gamma} \sum_k \text{Tr}^2(\hat{\mathbf{V}}_{\mathbf{y},k}) \right], \quad (\text{A.57b})$$

where the second equality follows from the fact that  $\|\boldsymbol{\sigma}_k\|^2 = \|\hat{\mathbf{V}}_{\mathbf{y},k}\|_F^2$  and  $\boldsymbol{\sigma}_k^T \mathbf{1}_M = \text{Tr}(\hat{\mathbf{V}}_{\mathbf{y},k})$ . Now it remains only to compute the constants  $\bar{\gamma}$  and  $\tilde{\gamma}$ . The following lemma provides  $\mathbf{G}$ , which is enough to compute  $\bar{\gamma}$  and  $\tilde{\gamma}$ :

LEMMA A.5. *The elements of the matrix  $\mathbf{G}$  defined in (A.54) when  $M > 1$  are given by*

$$g_{ii} = \frac{\pi^{M^2}}{M} \text{Tr}(\Phi \mathbf{M}_2) \quad (\text{A.58})$$

for  $i = 0, 1, \dots, M-1$ , where

$$g_{ij} = \frac{\pi^{M^2}}{M(M-1)} \text{Tr}(\Phi \mathbf{M}_1) - \frac{g_{ii}}{M-1} \quad (\text{A.59})$$

for  $i, j = 0, 1, \dots, M-1$  and  $j \neq i$ .

*Proof.* Since the elements on the diagonal are all the same, we have that  $g_{ii} = \frac{1}{M} \sum_k g_{kk} = \frac{1}{M} \text{Tr}(\mathbf{G})$ , which means that (A.58) immediately follows. Regarding the off-diagonal elements, it is clear that

$$g_{ij} = \frac{\mathbf{1}_M^T \mathbf{G} \mathbf{1}_M - \text{Tr}(\mathbf{G})}{M(M-1)} = \frac{\mathbf{1}_M^T \mathbf{G} \mathbf{1}_M}{M(M-1)} - \frac{g_{ii}}{M-1} \quad (\text{A.60})$$

when  $i \neq j$ . Substituting (A.54) in (A.60) results in (A.59).

□

Finally, taking into account that  $g_{ii} = \bar{\gamma} + \tilde{\gamma}$  and  $g_{ij} = \tilde{\gamma}$ , it is clear that

$$\bar{\gamma} = \frac{\pi^{M^2}}{M(M-1)} [-\text{Tr}(\Phi \mathbf{M}_1) + M \text{Tr}(\Phi \mathbf{M}_2)] \quad (\text{A.61a})$$

$$\tilde{\gamma} = \frac{\pi^{M^2}}{M(M-1)} [\text{Tr}(\Phi \mathbf{M}_1) - \text{Tr}(\Phi \mathbf{M}_2)]. \quad (\text{A.61b})$$

Now, if we rewrite (A.57b) as (A.29) with  $\alpha = \tau_1 \bar{\gamma}$ ,  $\beta = \tau_1 \tilde{\gamma}$  and  $\gamma = \tau_0$ , the constants in (A.30)

follow.

## A.C Proof of Lemma A.4

We first decompose

$$\mathbf{v}^T \mathbf{G} \mathbf{v} = \sum_i g_{ii} v_i^2 + \sum_i \sum_{j \neq i} g_{ij} v_i v_j, \quad (\text{A.62})$$

where  $g_{ij}$  and  $v_i$  are, respectively, the  $(i, j)$ -th and the  $i$ -th elements of  $\mathbf{G}$  and  $\mathbf{v}$ . It is easily seen that, in order for  $\mathbf{v}^T \mathbf{G} \mathbf{v}$  to be invariant, both terms in the sum are necessarily invariant. Then, one must be able to average them over the set of permutations of  $M$  elements and the result must be the same. For the first term one obtains that

$$\sum_i g_{ii} v_i^2 = \frac{1}{M!} \sum_{\pi} \sum_i g_{ii} v_{\pi[i]}^2 = \frac{1}{M} \sum_i g_{ii} \sum_k v_k^2, \quad (\text{A.63})$$

where we have applied the first expression in (A.47). Expression (A.63) means that all the elements on the diagonal of  $\mathbf{G}$  are identical. Regarding the second term in (A.62), one can write

$$\sum_i \sum_{j \neq i} g_{ij} v_i v_j = \frac{1}{M!} \sum_{\pi} \sum_i \sum_{j \neq i} g_{ij} v_{\pi[i]} v_{\pi[j]} \quad (\text{A.64a})$$

$$= \frac{1}{M(M-1)} \sum_i \sum_{j \neq i} g_{ij} \sum_k \sum_{l \neq k} v_k v_l, \quad (\text{A.64b})$$

where we have made use of the second equation in (A.47). Similarly, expression (A.64a) imposes that all the entries off the diagonal of  $\mathbf{G}$  are equal to each other, thus concluding the proof.

## A.D Proof of Lemma A.1

Since the traces  $\text{Tr}(\Phi \mathbf{M}_1)$  and  $\text{Tr}(\Phi \mathbf{M}_2)$  in Theorem A.2 must not depend on the ordering of the entries of the vectors  $\boldsymbol{\lambda}_n$ , these matrices are of the form (see Lemma A.4)

$$\mathbf{M}_i = a'_i \mathbf{I}_M + b'_i \mathbf{1}_M \mathbf{1}_M^T, \quad (\text{A.65})$$

and therefore our problem reduces to the computation of the four constants  $a'_1, b'_1, a'_2, b'_2$ . The (rather tedious) derivation of these constants is based on decomposing  $|\mathbf{A}^H \mathbf{A}|$  using the Schur

determinant formula [Horn and Johnson, 1985], and exploiting the independence among the elements of  $\mathbf{A}$ . Here, we provide the derivation of the diagonal entries in  $\mathbf{M}_1$ , that is  $a'_1 + b'_1$ . The derivation of the remaining constants follows similar guidelines.

Let us start by writing  $\mathbf{A} = [\mathbf{a}_1 \ \mathbf{A}_1]$ , where  $\mathbf{a}_1$  is the first column of  $\mathbf{A}$  and  $\mathbf{A}_1 \in \mathbb{C}^{M \times (M-1)}$  comprises the remaining columns. Applying Schur's determinant formula we can write

$$a'_1 + b'_1 = \mathbb{E} \left\{ |\mathbf{A}_1^H \mathbf{a}_1|^L \left( \mathbf{a}_1^H \mathbf{P}_{\mathbf{A}_1}^\perp \mathbf{a}_1 \right)^L \left( \sum_j |A_{j,1}|^2 \right)^2 \right\},$$

where  $\mathbf{P}_{\mathbf{A}_1}^\perp$  is the projection matrix onto the subspace orthogonal to the column span of  $\mathbf{A}_1$ , and  $A_{j,i}$  denotes the entry in the  $j$ -th row and  $i$ -th column of  $\mathbf{A}$ . Now, taking into account the independence between  $\mathbf{a}_1$  and  $\mathbf{A}_1$ , we can introduce a unitary transformation of  $\mathbf{A}$  without modifying its distribution, and such that  $\mathbf{a}_1^H \mathbf{P}_{\mathbf{A}_1}^\perp \mathbf{a}_1 = |A_{1,1}|^2$ . Thus, noting that the previous equation is valid for any value of  $i$ , we can select  $i = 1$  to obtain

$$a'_1 + b'_1 = \mathbb{E} \{ |\mathbf{A}_1^H \mathbf{a}_1|^L \} \mathbb{E} \left\{ |A_{1,1}|^{2L} \left( \sum_j |A_{j,1}|^2 \right)^2 \right\},$$

which reduces the problem to that of calculating two different expectations. For the first one, and following the previous lines, it is easy to show that

$$\begin{aligned} c' &\triangleq \mathbb{E} \{ |\mathbf{A}_1^H \mathbf{a}_1|^L \} = \mathbb{E} \left\{ |\mathbf{A}_2^H \mathbf{a}_2|^L \left( \mathbf{a}_2^H \mathbf{P}_{\mathbf{A}_2}^\perp \mathbf{a}_2 \right)^L \right\} \\ &= \mathbb{E} \{ |\mathbf{A}_2^H \mathbf{a}_2|^L \} \mathbb{E} \left\{ (|A_{1,2}|^2 + |A_{2,2}|^2)^L \right\}, \end{aligned} \quad (\text{A.66})$$

where we have defined  $\mathbf{A}_1 = [\mathbf{a}_2 \ \mathbf{A}_2]$ . Moreover, noting that  $2|A_{i,j}|^2$  is distributed as a  $\chi^2$  random variable with  $k = 2$  degrees of freedom ( $2|A_{i,j}|^2 \sim \chi_k^2$ ), and taking into account that, for  $W \sim \chi_k^2$ , the moments are  $\mathbb{E} \{ W^m \} = 2^m \frac{\Gamma(m+k/2)}{k/2}$ , we conclude that

$$c' = \mathbb{E} \{ |\mathbf{A}_1^H \mathbf{a}_1|^L \} = \mathbb{E} \{ |\mathbf{A}_2^H \mathbf{a}_2|^L \} \Gamma(L+2). \quad (\text{A.67})$$

For the second expectation, we expand the sum to obtain

$$\begin{aligned}
& \mathbb{E} \left\{ |A_{1,1}|^{2L} \left( \sum_{j=0}^{M-1} |A_{j,1}|^2 \right)^2 \right\} = \mathbb{E} \{ |A_{1,1}|^{2L+4} \} \\
& + \mathbb{E} \left\{ |A_{1,1}|^{2L} \sum_{j=1}^{M-1} |A_{j,1}|^4 \right\} + 2 \sum_{j=1}^{M-1} \mathbb{E} \{ |A_{1,1}|^{2L+2} |A_{j,1}|^2 \} \\
& + \mathbb{E} \left\{ |A_{1,1}|^{2L} \sum_{j=1}^{M-1} \sum_{\substack{k=1 \\ k \neq j}}^{M-1} |A_{j,1}|^2 |A_{k,1}|^2 \right\}. \tag{A.68}
\end{aligned}$$

Finally, taking independences into account, and applying the formula for the moments of  $\chi^2$  random variables, we obtain

$$a_1 + b_1 = \Gamma(L+3) + 2(M-1)\Gamma(L+2) + M(M-1)\Gamma(L+1). \tag{A.69}$$



# References

- Abramovich, Y. I., Gray, D. A., Gorokhov, A. Y., and Spencer, N. K. (1998). Positive-definite Toeplitz completion in DOA estimation for nonuniform linear antenna arrays. Part I: Fully augmentable arrays. *IEEE Trans. Sig. Process.*, 46(9):2458–2471.
- Abramovich, Y. I., Spencer, N. K., and Gorokhov, A. Y. (1999). Positive-definite Toeplitz completion in DOA estimation for nonuniform linear antenna arrays. Part II: Partially augmentable arrays. *IEEE Trans. Sig. Process.*, 47(6):1502–1521.
- Alamgir, M., Faulkner, M., Gao, J., and Conder, P. (2008). Signal detection for cognitive radio using multiple antennas. In *Proc. IEEE Int. Symp. Wireless Commun. Syst.*, pages 488–492.
- Alaya-Feki, A., Jemaa, S. B., Sayrac, B., Houze, P., and Moulines, E. (2008). Informed spectrum usage in cognitive radio networks: Interference cartography. In *Proc. IEEE Int. Symp. Personal, Indoor Mobile Radio Commun.*, pages 1–5.
- Amirmazlaghani, M., Amindavar, H., and Moghaddamjoo, A. (2009). Speckle suppression in SAR images using the 2-D GARCH model. *IEEE Trans. Image Process.*, 18(2):250–259.
- Anderson, T. W. (2003). *An introduction to multivariate statistical analysis*. John Wiley and Sons, 3rd edition.
- Argyriou, A. and Dinuzzo, F. (2014). A unifying view of representer theorems. In *Proc. Int. Conf. Mach. Learning*, Beijing, China.
- Ariananda, D. D. and Leus, G. (2012). Compressive wideband power spectrum estimation. *IEEE Trans. Sig. Process.*, 60(9):4775–4789.
- Ariananda, D. D., Romero, D., and Leus, G. (2013). Compressive angular and frequency periodogram reconstruction for multiband signals. In *Proc. IEEE Int. Workshop Comput. Advances Multi-Sensor Adaptive Process.*, pages 440–443, San Martin, France.

- Audiffren, J. and Kadri, H. (2013). Online learning with multiple operator-valued kernels. Preprint at <http://arXiv.org/abs/1311.0222>.
- Axell, E., Leus, G., Larsson, E. G., and Poor, H. V. (2012). Spectrum sensing for cognitive radio: State-of-the-art and recent advances. *IEEE Sig. Process. Mag.*, 29(3):101–116.
- Babu, P. and Stoica, P. (2012). Sparse spectral-line estimation for nonuniformly sampled multivariate time series: SPICE, LIKES and MSBL. In *Proc. European Sig. Process. Conf.*, pages 445–449.
- Baraniuk, R., Davenport, M., DeVore, R., and Wakin, M. (2008). A simple proof of the restricted isometry property for random matrices. *Constructive Approximation*, 28(3):253–263.
- Bartlett, M. S. (1937). Properties of sufficiency and statistical tests. *Proc. Royal Soc. London. Series A, Math. Phys. Sci.*, 160:268–282.
- Bazerque, J.-A. and Giannakis, G. B. (2010). Distributed spectrum sensing for cognitive radio networks by exploiting sparsity. *IEEE Trans. Sig. Process.*, 58(3):1847–1862.
- Bazerque, J.-A., Mateos, G., and Giannakis, G. B. (2011). Group-lasso on splines for spectrum cartography. *IEEE Trans. Sig. Process.*, 59(10):4648–4663.
- Becker, S. (2011). *Practical Compressed Sensing: Modern Data Acquisition and Signal Processing*. PhD thesis, California Institute of Technology.
- Berlinet, A. and Thomas-Agnan, C. (2004). *Reproducing Kernel Hilbert Spaces in Probability and Statistics*. Springer.
- Bernstein, D. S. (2009). *Matrix mathematics. Theory, facts, and formulas. 2nd expanded ed.* Princeton University Press.
- Besson, O., Kraut, S., and Scharf, L. L. (2006). Detection of an unknown rank-one component in white noise. *IEEE Trans. Sig. Process.*, 54(7):2835–2839.
- Billingsley, P. (1995). Probability and measure. *Jown Wiley & Sons*.
- Black, W. C. and Hodges, D. (1980). Time interleaved converter arrays. *IEEE J. Solid-State Circuits*, 15(6):1022–1029.
- Bookstein, F. L. (1989). Principal warps: Thin-plate splines and the decomposition of deformations. *IEEE Trans. Pattern Anal. Mach. Intel.*, 11(6):567–585.
- Boyd, S. and Vandenberghe, L. (2004). *Convex Optimization*. Cambridge University Press, Cambridge, UK.

- Burg, J. P., Luenberger, D. G., and Wenger, D. L. (1982). Estimation of structured covariance matrices. *Proc. IEEE*, 70(9):963–974.
- Cabric, D. (2008). Addressing feasibility of cognitive radios. *IEEE Sig. Process. Mag.*, 25(6):85–93.
- Candès, E. J. and Wakin, M. B. (2008). An introduction to compressive sampling. *IEEE Sig. Process. Mag.*, 25(2):21–30.
- Carmeli, C., De Vito, E., Toigo, A., and Umanita, V. (2010). Vector valued reproducing kernel Hilbert spaces and universality. *Analysis Appl.*, 8(1):19–61.
- Chen, H. and Gao, W. (2011). Spectrum sensing for TV white space in North America. *IEEE J. Sel. Areas Commun.*, 29(2):316–326.
- Chen, H., Gao, W., and Daut, D. (2008). Spectrum sensing for wireless microphone signals. In *Proc. IEEE Annual Commun. Society Conf. Sensor, Mesh, Ad Hoc Commun. Networks Workshops*, pages 1–5.
- Chen, L., Wang, J., and Li, S. (2007). An adaptive cooperative spectrum sensing scheme based on the optimal data fusion rule. In *Proc. Int. Symp. Wireless Commun. Syst.*, pages 582–586.
- Chen, P. (2008). Heteroscedastic low-rank matrix approximation by the Wiberg algorithm. *IEEE Trans. Sig. Process.*, 56(4):1429–1439.
- Cherkassky, V. and Mulier, F. M. (2007). *Learning From Data: Concepts, Theory, and Methods*. John Wiley & Sons.
- Cisco Systems (2015). Cisco visual networking index: Global mobile data traffic forecast update 2013–2018. White paper, Feb. 2015.
- Clanton, C., Kenkel, M., and Tang, Y. (2007). Wireless microphone signal simulation method. *IEEE 802.22-07/0124r0*.
- Couillet, R. and Debbah, M. (2011). *Random matrix methods for wireless communications*. Cambridge University Press.
- Dall’Anese, E., Kim, S.-J., and Giannakis, G. B. (2011). Channel gain map tracking via distributed kriging. *IEEE Trans. Veh. Technol.*, 60(3):1205–1211.
- Dall’Anese, E., Bazerque, J.-A., and Giannakis, G. B. (2012). Group sparse lasso for cognitive network sensing robust to model uncertainties and outliers. *Phy. Commun.*, 5(2):161–172.

- Das Gupta, S. (1969). Properties of power functions of some tests concerning dispersion matrices of multivariate normal distributions. *Annals Math. Stat.*, pages 697–701.
- Demmel, J. (1997). *Applied numerical algebra*. SIAM, Philadelphia.
- Dempster, A. P., Laird, N. M., and Rubin, D. B. (1977). Maximum likelihood from incomplete data via the EM algorithm. *J. Royal Stat. Soc.. Series B (Methodological)*, pages 1–38.
- Derakhtian, M., Tadaion, A., and Gazor, S. (2009a). Detection of a bandlimited signal with unknown parameters. In *Proc. Workshop Stat. Sig. Process.*, pages 145–148.
- Derakhtian, M., Tadaion, A., Gazor, S., and Nayebi, M. (2009b). Invariant activity detection of a constant magnitude signal with unknown parameters in white Gaussian noise. *IET Commun.*, 3(8):1420–1431.
- Diethe, T. and Girolami, M. (2013). Online learning with (multiple) kernels: A review. *Neural Comput.*, 25(3):567–625.
- Domínguez-Jiménez, M. E., González-Prelcic, N., Vázquez-Vilar, G., and López-Valcarce, R. (2012). Design of universal multicoset sampling patterns for compressed sensing of multiband sparse signals. In *Proc. IEEE Int. Conf. Acoust., Speech, Sig. Process.*, pages 3337–3340.
- Domínguez-Jiménez, M. E. and González-Prelcic, N. (2013). A class of circular sparse rulers for compressive power spectrum estimation. In *Proc. European Sig. Process. Conf.*
- Donoho, D. L. (2006). Compressed sensing. *IEEE Trans. Inf. Theory*, 52(4):1289–1306.
- ElRamly, S., Newagy, F., Yousry, H., and Elezabi, A. (2011). Novel modified energy detection spectrum sensing technique for FM wireless microphone signals. In *Proc. IEEE Int. Conf. Commun. Softw. Netw.*, pages 59–63.
- Erpek, T., Mchenry, M., and Stirling, A. (2011). Dynamic spectrum access operational parameters with wireless microphones. *IEEE Commun. Mag.*, 49(3):38–45.
- Federal Communications Commission (2002). Spectrum policy task force. *ET Docket No. 02-135*.
- Federal Communications Commission (2008). FCC 08-260. *Unlicensed Operation in the TV Broadcast Bands*.
- Federal Communications Commission (2010). FCC 10-174. *Unlicensed Operation in the TV Broadcast Bands*.

- Federal Communications Commission (2011). FCC 11-131. *Unlicensed Operation in the TV Broadcast Bands*.
- Federal Communications Commission (2012). Frequency assignment for low power auxiliary stations. *47 CFR Chapter I, Subchapter C, Part 74, Subpart H, point 74.802*.
- Feng, P. and Bresler, Y. (1996). Spectrum-blind minimum-rate sampling and reconstruction of multiband signals. In *Proc. IEEE Int. Conf. Acoust., Speech, Sig. Process.*, volume 3, pages 1688–1691 vol. 3.
- Fuhrmann, D. (1991). Application of Toeplitz covariance estimation to adaptive beamforming and detection. *IEEE Trans. Sig. Process.*, 39(10):2194–2198.
- Gabriel, J. and Kay, S. (2002). Use of Wijsman’s theorem for the ratio of maximal invariant densities in signal detection applications. In *Proc. Asilomar Conf. Sig., Syst., Comput.*, volume 1, pages 756–762 vol.1.
- Gabriel, J. and Kay, S. (2005). On the relationship between the GLRT and UMPI tests for the detection of signals with unknown parameters. *IEEE Trans. Sig. Process.*, 53(11):4194–4203.
- Gautier, M., Laugeois, M., and Nogu  t, D. (2010). Teager-Kaiser energy detector for narrow-band wireless microphone spectrum sensing. In *Proc. Cognitive Radio Oriented Wireless Netw. Commun.*, pages 1–5.
- Gholam, F., V  a, J., and Santamaria, I. (2011). Beamforming design for simplified analog antenna combining architectures. *IEEE Trans. Veh. Technol.*, 60(5):2373–2378.
- Giannakis, G. B. and Tepedelenlio  lu, C. (1998). Basis expansion models and diversity techniques for blind identification and equalization of time-varying channels. *Proc. IEEE*, 86(10):1969–1986.
- Glaser, R. (1976). The ratio of the geometric mean to the arithmetic mean for a random sample from a gamma distribution. *J. American Stat. Assoc.*, pages 480–487.
- Goldsmith, A. (2005). *Wireless communications*. Cambridge University Press.
- Golub, G. H. and Van Loan, C. F. (1996). *Matrix computations*, volume 3. Johns Hopkins University Press.
- Gorman, J. D. and Hero, A. O. (1990). Lower bounds for parametric estimation with constraints. *IEEE Trans. Inf. Theory*, 36(6):1285–1301.
- Gray, R. M. (2006). *Toeplitz and circulant matrices: A review*. Now Pub.

- Hallin, M. and Paindaveine, D. (2009). Optimal tests for homogeneity of covariance, scale, and shape. *J. Multivariate Analysis*, 100(3):422–444.
- Hassan, M. and Nasr, O. (2011). Adaptive spectrum sensing of wireless microphones with noise uncertainty. In *Proc. IEEE Int. Symp. Personal Indoor Mobile Radio Commun.*, pages 445–450.
- Herley, C. and Wong, P. W. (1999). Minimum rate sampling and reconstruction of signals with arbitrary frequency support. *IEEE Trans. Inf. Theory*, 45(5):1555–1564.
- Hijazi, H. and Ros, L. (2009). Polynomial estimation of time-varying multipath gains with intercarrier interference mitigation in OFDM systems. *IEEE Trans. Veh. Technol.*, 58(1):140–151.
- Hlawatsch, F. and Matz, G., editors (2011). *Wireless communications over rapidly time-varying channels*. Academic Press, Oxford, UK.
- Hocter, R. T. and Kassam, S. A. (1990). The unifying role of the coarray in aperture synthesis for coherent and incoherent imaging. *Proc. IEEE*, 78(4):735–752.
- Horn, R. A. and Johnson, C. R. (1985). *Matrix Analysis*. Cambridge University Press, Cambridge, UK.
- Huang, D.-H., Wu, S.-H., Wu, W.-R., and Wang, P.-H. (2015). Cooperative radio source positioning and power map reconstruction: A sparse Bayesian learning approach. *IEEE Trans. Veh. Technol.* to appear.
- Huillery, J., Millioz, F., and Martin, N. (2008). On the description of spectrogram probabilities with a chi-squared law. *IEEE Trans. Sig. Process.*, 56(6):2249–2258.
- IEEE (2011). IEEE 802.22 standard: Cognitive wireless RAN medium access control (MAC) and physical layer (PHY) specifications: policies and procedures for operation in the TV bands.
- Jayawickrama, B. A., Dutkiewicz, E., Oppermann, I., Fang, G., and Ding, J. (2013). Improved performance of spectrum cartography based on compressive sensing in cognitive radio networks. In *Proc. Int. Conf. Commun. (ICC)*, pages 5657–5661.
- Johnston, J. D. (1988). Transform coding of audio signals using perceptual noise criteria. *IEEE J. Sel. Areas Commun.*, 6(2):314–323.
- Kay, S. M. (1993). *Fundamentals of Statistical Signal Processing, Vol. I: Estimation Theory*. Prentice-Hall.

- Kay, S. M. (1998). *Fundamentals of Statistical Signal Processing, Vol. II: Detection Theory*. Prentice-Hall.
- Kecman, V., Vogt, M., and Huang, T. M. (2003). On the equality of kernel AdaTron and sequential minimal optimization in classification and regression tasks and alike algorithms for kernel machines. In *Proc. European Symp. Artificial Neural Netw.*, pages 215–222.
- Kim, S.-J., Dall’Anese, E., and Giannakis, G. B. (2011a). Cooperative spectrum sensing for cognitive radios using kriged Kalman filtering. *IEEE J. Sel. Topics Sig. Process.*, 5(1):24–36.
- Kim, S.-J. and Giannakis, G. B. (2013). Cognitive radio spectrum prediction using dictionary learning. In *Proc. IEEE Global Commun. Conf.*, Atlanta, GA.
- Kim, S.-J., Jain, N., Giannakis, G., and Forero, P. (2011b). Joint link learning and cognitive radio sensing. In *Proc. Asilomar Conf. Sig., Syst., Comput.*, Pacific Grove, CA.
- Kivinen, J., Smola, A. J., and Williamson, R. C. (2004). Online learning with kernels. *IEEE Trans. Sig. Process.*, 52(8):2165–2176.
- Kolmogorov, A. N. and Fomin, S. V. (1970). *Introductory Real Analysis Rev. English Ed.* Dover Publications.
- Krieger, J. D., Kochman, Y., and Wornell, G. W. (2013). Design and analysis of multi-coset arrays. In *Proc. IEEE Int. Conf. Acoust., Speech, Sig. Process.*
- Kumar, N. and Andreou, A. G. (1998). Heteroscedastic discriminant analysis and reduced rank HMMs for improved speech recognition. *Speech Commun.*, 26(4):283–297.
- Laska, J. N., Kirolos, S., Duarte, M. F., Ragheb, T. S., Baraniuk, R. G., and Massoud, Y. (2007). Theory and implementation of an analog-to-information converter using random demodulation. In *Proc. IEEE Int. Symp. Circuits Syst.*, pages 1959–1962.
- Le Cam, L. M. (1986). *Asymptotic methods in statistical theory*. Springer-Verlag New York, Inc.
- Leech, J. (1956). On the representation of 1, 2,..., n by differences. *J. London Math. Society*, 31(2):160–169.
- Lehmann, E. L. and Casella, G. (1998). *Theory of point estimation*. Springer.
- Lehmann, E. L. and Romano, J. P. (2005). *Testing statistical hypotheses*. Springer.
- Leus, G. (2004). On the estimation of rapidly time varying channels. In *Proc. European Sig. Process. Conf.*, pages 2227–2230.

- Lexa, M., Davies, M. E., Thompson, J. S., and Nikolic, J. (2011). Compressive power spectral density estimation. In *Proc. IEEE Int. Conf. Acoust., Speech, Sig. Process.*, pages 3884–3887.
- Lin, Y. P. and Vaidyanathan, P. P. (1998). Periodically nonuniform sampling of bandpass signals. *IEEE Trans. Circuits Syst. II: Analog Digit. Sig. Process.*, 45(3):340–351.
- Linebarger, D. A., Sudborough, I. H., and Tollis, I. G. (1993). Difference bases and sparse sensor arrays. *IEEE Trans. Inf. Theory*, 39(2):716–721.
- Ma, X. and Giannakis, G. B. (2002). Space-time coding for doubly selective channels. In *Proc. IEEE Int. Symp. Circuits Syst.*, volume 3, pages 647–650.
- Marage, J.-P. and Mori, Y. (2010). *Sonar and underwater acoustics*. Wiley-ISTE.
- Masry, E. (1978). Poisson sampling and spectral estimation of continuous-time processes. *IEEE Trans. Inf. Theory*, 24(2):173–183.
- Mehanna, O. (2014). Frugal sensing and estimation over wireless networks. *PhD thesis, University of Minnesota, MN*.
- Mehanna, O. and Sidiropoulos, N. (2013). Frugal sensing: Wideband power spectrum sensing from few bits. *IEEE Trans. Sig. Process.*, 61(10):2693–2703.
- Micchelli, C. A. (1984). *Interpolation of Scattered Data: Distance Matrices and Conditionally Positive Definite Functions*. Springer.
- Micchelli, C. A. and Pontil, M. (2005). On learning vector-valued functions. *Neural Comput.*, 17(1):177–204.
- Miller, J. C. P. (1971). Difference bases: Three problems in additive number theory. *Comput. Number Theory*, pages 299–322.
- Mishali, M. and Eldar, Y. C. (2009). Blind multiband signal reconstruction: Compressed sensing for analog signals. *IEEE Trans. Sig. Process.*, 57(3):993–1009.
- Mishali, M. and Eldar, Y. C. (2010). From theory to practice: Sub-Nyquist sampling of sparse wideband analog signals. *IEEE J. Sel. Topics Sig. Process.*, 4(2):375–391.
- Mishali, M. and Eldar, Y. C. (2011). Sub-Nyquist sampling: bridging theory and practice. *IEEE Sig. Process. Mag.*, 28(6):98–124.
- Mitola III, J. and Maguire Jr, G. Q. (1999). Cognitive radio: making software radios more personal. *IEEE Pers. Commun.*, 6(4):13–18.



- Moffet, A. (1968). Minimum-redundancy linear arrays. *IEEE Trans. Antennas Propag.*, 16(2):172–175.
- Muirhead, R. J. (2005). *Aspects of multivariate statistical theory*. John Wiley & Sons Inc.
- Nagao, H. (1973). On some test criteria for covariance matrix. *Annals Stat.*, pages 700–709.
- Nishimori, K., Di Taranto, R., Yomo, H., Popovski, P., Takatori, Y., Prasad, R., and Kubota, S. (2007). Spatial opportunity for cognitive radio systems with heterogeneous path loss conditions. In *Proc. IEEE Veh. Technol. Conf.*, pages 2631–2635.
- Ollila, E., Eriksson, J., and Koivunen, V. (2011). Complex elliptically symmetric random variables-generation, characterization, and circularity tests. *IEEE Trans. Sig. Process.*, 59(1):58–69.
- Ottersten, B., Stoica, P., and Roy, R. (1998). Covariance matching estimation techniques for array signal processing applications. *Digit. Sig. Process.*, 8(3):185–210.
- Pal, P. and Vaidyanathan, P. P. (2010). Nested arrays: A novel approach to array processing with enhanced degrees of freedom. *IEEE Trans. Sig. Process.*, 58(8):4167–4181.
- Pal, P. and Vaidyanathan, P. P. (2011). Coprime sampling and the MUSIC algorithm. In *IEEE Digit. Sig. Process. Workshop*, pages 289–294.
- Pal, P. and Vaidyanathan, P. P. (2012). Nested arrays in two dimensions. Part I: Geometrical considerations. *IEEE Trans. Sig. Process.*, 60(9):4694–4705.
- Papoulis, A. (1977). *Signal Analysis*. McGraw-Hill, New York.
- Papoulis, A. and Pillai, S. U. (2002). *Probability, Random Variables and Stochastic Processes*. McGraw Hill Higher Education.
- Pearson, D., Pillai, S. U., and Lee, Y. (1990). An algorithm for near-optimal placement of sensor elements. *IEEE Trans. Inf. Theory*, 36(6):1280–1284.
- Pillai, S. U., Bar-Ness, Y., and Haber, F. (1985). A new approach to array geometry for improved spatial spectrum estimation. *Proc. IEEE*, 73(10):1522–1524.
- Pillai, S. U. and Haber, F. (1987). Statistical analysis of a high resolution spatial spectrum estimator utilizing an augmented covariance matrix. *IEEE Trans. Acoust., Speech, Sig. Process.*, 35(11):1517–1523.
- Platt, J. C. (1999). Fast training of support vector machines using sequential minimal optimization. In *Advances in Kernel Methods*, pages 185–208. MIT Press, Cambridge, MA.

- Pumphrey, H. C. (1993). Design of sparse arrays in one, two, and three dimensions. *J. Acoust. Society America*, 93:1620.
- Quan, Z., Cui, S., Poor, H., and Sayed, A. (2008). Collaborative wideband sensing for cognitive radios. *IEEE Sig. Process. Mag.*, 25(6):60–73.
- Quan, Z., Cui, S., Sayed, A. H., and Poor, H. V. (2009). Optimal multiband joint detection for spectrum sensing in cognitive radio networks. *IEEE Trans. Sig. Process.*, 57(3):1128–1140.
- Ramírez, D., Vázquez-Vilar, G., López-Valcarce, R., Vía, J., and Santamaría, I. (2011). Detection of rank-P signals in cognitive radio networks with uncalibrated multiple antennas. *IEEE Trans. Sig. Process.*, 59(8):3764–3774.
- Ramirez, D., Vía, J., Santamaria, I., and Scharf, L. L. (2013). Locally most powerful invariant tests for correlation and sphericity of Gaussian vectors. *IEEE Trans. Inf. Theory*, 59(4):2128–2141.
- Rédei, L. and Rényi, A. (1949). On the representation of the numbers  $1, 2, \dots, n$  by means of differences (Russian). *Matematicheskii sbornik*, 66(3):385–389.
- Romero, D., Kim, S.-J., and Giannakis, G. B. (2015a). Online spectrum cartography via quantized measurements. In *Proc. Conf. Inf. Sci. Syst.*, Baltimore, MD.
- Romero, D., Kim, S.-J., Giannakis, G. B., and López-Valcarce, R. (2015b). Learning spectrum maps from quantized observations. *IEEE Trans. Sig. Process.* (Submitted Mar.).
- Romero, D., Kim, S.-J., López-Valcarce, R., and Giannakis, G. B. (2015c). Spectrum cartography using quantized observations. In *Proc. IEEE Int. Conf. Acoust., Speech, Sig. Process.*, Brisbane, Australia.
- Romero, D. and Leus, G. (2013a). Compressive covariance sampling. In *Proc. Inf. Theory Appl. Workshop*, pages 1–8, San Diego, CA.
- Romero, D. and Leus, G. (2013b). Wideband spectrum sensing from compressed measurements using spectral prior information. *IEEE Trans. Sig. Process.*, 61(24):6232–6246.
- Romero, D. and López-Valcarce, R. (2011a). Bandlimited or constant envelope? exploiting waveform properties in wireless microphone detection. In *Proc. IEEE Int. Workshop Comput. Advances Multi-Sensor Adaptive Process.*, pages 321–324, San Juan, Puerto Rico.
- Romero, D. and López-Valcarce, R. (2011b). Multiantenna detection of constant-envelope signals in noise of unknown variance. In *Proc. IEEE Int. Workshop Sig. Process. Advances Wireless Commun.*, pages 446–450, San Francisco, CA.

- Romero, D. and López-Valcarce, R. (2012). Detection of unknown constant magnitude signals in time-varying channels. In *Proc. Cognitive Inf. Process.*, Baiona, Spain.
- Romero, D. and López-Valcarce, R. (2013). Spectrum sensing in time-varying channels using multiple antennas. In *Proc. IEEE Int. Workshop Sig. Process. Advances Wireless Commun.*, pages 135–139, Darmstadt, Germany.
- Romero, D. and López-Valcarce, R. (2014a). Nearly-optimal compression matrices for signal power estimation. In *Proc. IEEE Int. Workshop Sig. Process. Advances Wireless Commun.*, pages 434–438, Toronto, Canada.
- Romero, D. and López-Valcarce, R. (2014b). Spectrum sensing for wireless microphone signals using multiple antennas. *IEEE Trans. Veh. Technol.*, 63(9):4395–4407.
- Romero, D., López-Valcarce, R., and Leus, G. (2012a). Generalized matched filter detector for fast fading channels. In *Proc. IEEE Int. Conf. Acoust., Speech, Sig. Process.*, pages 3165–3168, Kyoto, Japan.
- Romero, D., López-Valcarce, R., and Leus, G. (2013). Compressive wideband spectrum sensing with spectral prior information. In *Proc. IEEE Int. Conf. Acoust., Speech, Sig. Process.*, pages 4469–4473, Vancouver, Canada.
- Romero, D., López-Valcarce, R., and Leus, G. (2015d). Compression limits for random vectors with linearly parameterized second-order statistics. *IEEE Trans. Inf. Theory*, 61(3):1410–1425.
- Romero, D., Vía, J., López-Valcarce, R., and Santamaria, I. (2012b). Detection of Gaussian signals in unknown time-varying channels. In *Proc. Workshop Stat. Sig. Process.*, pages 916–919, Ann Arbor, MI.
- Sala-Álvarez, J., Vázquez-Vilar, G., and López-Valcarce, R. (2012). Multiantenna GLR detection of rank-one signals with known power spectrum in white noise with unknown spatial correlation. *IEEE Trans. Sig. Process.*, 60(6):3065–3078.
- Scharf, L. L. (1991). *Statistical signal processing: detection, estimation, and time series analysis*, volume 1. Addison-Wesley.
- Schölkopf, B., Burges, C., and Vapnik, V. (1996). Incorporating invariances in support vector learning machines. In *Proc. Int. Conf. Artificial Neural Netw.*, pages 47–52, Bochum, Germany. Springer.
- Schölkopf, B. and Smola, A. J. (2001). *Learning With Kernels: Support Vector Machines, Regularization, Optimization, and Beyond*. MIT Press.

- Schott, J. (2007). A test for the equality of covariance matrices when the dimension is large relative to the sample sizes. *Comput. Statistics & Data Analysis*, 51(12):6535–6542.
- Schott, J. R. (2001). Some tests for the equality of covariance matrices. *J. Stat. Planning Inference*, 94(1):25–36.
- Sebald, D. J. and Bucklew, J. A. (2000). Support vector machine techniques for nonlinear equalization. *IEEE Trans. Sig. Process.*, 48(11):3217–3226.
- Senol, H., Cirpan, H. A., and Panayirci, E. (2005). A low-complexity KL expansion-based channel estimator for OFDM systems. *EURASIP J. Wireless Commun. Netw.*, 2005(2):163–174.
- Shared Spectrum Company (2010). General survey of radio frequency bands – 30 MHz to 3 GHz. Technical report.
- Singer, J. (1938). A theorem in finite projective geometry and some applications to number theory. *Trans. American Math. Soc.*, 43(3):377–385.
- Smola, A. J., Frieß, T. T., and Schölkopf, B. (1999). Semiparametric support vector and linear programming machines. In Kearns, M. J., Solla, S. A., and Cohn, D., editors, *Advances in Neural Information Processing Systems*, volume 11, pages 585–591. MIT Press, Cambridge, MA.
- Smola, A. J. and Schölkopf, B. (2004). A tutorial on support vector regression. *Stat. Comput.*, 14(3):199–222.
- Smola, A. J., Schölkopf, B., and Müller, K.-R. (1998). The connection between regularization operators and support vector kernels. *Neural Netw.*, 11(4):637–649.
- Srivastava, M. and Yanagihara, H. (2010). Testing the equality of several covariance matrices with fewer observations than the dimension. *J. Multivariate Analysis*, 101(6):1319–1329.
- Stoica, P. and Babu, P. (2011). Maximum-likelihood nonparametric estimation of smooth spectra from irregularly sampled data. *IEEE Trans. Sig. Process.*, 59(12):5746–5758.
- Stoica, P. and Babu, P. (2012). SPICE and LIKES: Two hyperparameter-free methods for sparse-parameter estimation. *Signal Process.*, 92(7):1580–1590.
- Stoica, P., Babu, P., and Li, J. (2011a). New method of sparse parameter estimation in separable models and its use for spectral analysis of irregularly sampled data. *IEEE Trans. Sig. Process.*, 59(1):35–47.

- Stoica, P., Babu, P., and Li, J. (2011b). A sparse covariance-based method for direction of arrival estimation. In *Proc. IEEE Int. Conf. Acoust., Speech, Sig. Process.*, pages 2844–2847.
- Stoica, P., Babu, P., and Li, J. (2011c). SPICE: A sparse covariance-based estimation method for array processing. *IEEE Trans. Sig. Process.*, 59(2):629–638.
- Stoica, P. and Moses, R. L. (2005). *Spectral analysis of signals*. Pearson/Prentice Hall.
- Sun, H., Nallanathan, A., Wang, C.-X., and Chen, Y. (2013). Wideband spectrum sensing for cognitive radio networks: a survey. *IEEE Wireless Commun.*, 20(2):74–81.
- Taherpour, A., Gazor, S., and Nasiri-Kenari, M. (2008). Wideband spectrum sensing in unknown white Gaussian noise. *IET Commun.*, 2(6):763–771.
- Taherpour, A., Nasiri-Kenari, M., and Gazor, S. (2010). Multiple antenna spectrum sensing in cognitive radios. *IEEE Trans. Wireless Commun.*, 9(2):814–823.
- Tandra, R. and Sahai, A. (2008). SNR walls for signal detection. *IEEE J. Sel. Topics Sig. Process.*, 2(1):4–17.
- Tropp, J. A., Laska, J. N., Duarte, M. F., Romberg, J. K., and Baraniuk, R. G. (2010). Beyond Nyquist: Efficient sampling of sparse bandlimited signals. *IEEE Trans. Inf. Theory*, 56(1):520–544.
- Tsatsanis, M. K. and Giannakis, G. B. (1996a). Modelling and equalization of rapidly fading channels. *Int. J. Adaptive Control Signal Process.*, 10(2-3):159–176.
- Tsatsanis, M. K. and Giannakis, G. B. (1996b). Modelling and equalization of rapidly fading channels. *Int. J. Adaptive Control Signal Process.*, 10(2-3):159–176.
- Vaidyanathan, P. P. (2003). *Multirate systems and filter banks*. Pearson Education Taiwan.
- Vázquez-Vilar, G. and López-Valcarce, R. (2011). Spectrum sensing exploiting guard bands and weak channels. *IEEE Trans. Sig. Process.*, 59(12):6045–6057.
- Vázquez-Vilar, G., López-Valcarce, R., and Pandharipande, A. (2011a). Detection diversity of multiantenna spectrum sensors. In *Proc. IEEE Int. Conf. Acoust., Speech, Sig. Process.*, pages 2936–2939.
- Vázquez-Vilar, G., López-Valcarce, R., and Sala, J. (2011b). Multiantenna spectrum sensing exploiting spectral a priori information. *IEEE Trans. Wireless Commun.*, 10(12):4345–4355.

- Venkataramani, R. and Bresler, Y. (2000). Perfect reconstruction formulas and bounds on aliasing error in sub-Nyquist nonuniform sampling of multiband signals. *IEEE Trans. Inf. Theory*, 46(6):2173–2183.
- Venkateswaran, V. and van der Veen, A. J. (2010). Analog beamforming in MIMO communications with phase shift networks and online channel estimation. *IEEE Trans. Sig. Process.*, 58(8):4131–4143.
- Wahba, G. (1990). *Spline Models for Observational Data*, volume 59 of *CBMS-NSF Regional Conference Series in Applied Mathematics*. SIAM.
- Wakin, M., Becker, S., Nakamura, E., Grant, M., Sovero, E., Ching, D., Juhwan, Y., Romberg, J., Emami-Neyestanak, A., and Candès, E. (2012). A nonuniform sampler for wideband spectrally-sparse environments. *Emerging Select. Topics Circuits Syst., IEEE J. on*, 2(3):516–529.
- Wang, P., Fang, J., Han, N., and Li, H. (2010). Multiantenna-assisted spectrum sensing for cognitive radio. *IEEE Trans. Veh. Technol.*, 59(4):1791–1800.
- Wang, S., Zhu, W., and Liang, Z.-P. (2001). Shape deformation: SVM regression and application to medical image segmentation. In *Proc. Int. Conf. Comput. Vis.*, volume 2, pages 209–216.
- Wang, Y. and Leus, G. (2010). Space-time compressive sampling array. In *Proc. of IEEE Sensor Array Multichannel Sig. Process. Workshop*, pages 33–36.
- Wang, Y., Leus, G., and Pandharipande, A. (2009). Direction estimation using compressive sampling array processing. In *Proc. Workshop Stat. Sig. Process.*, pages 626–629.
- Wichmann, B. (1963). A note on restricted difference bases. *J. London Math. Society*, s1-s38(1):465–466.
- Wijsman, R. (1967). Cross-sections of orbits and their application to densities of maximal invariants. In *Proc. Fifth Berkeley Symp. Math. Statist. Prob*, volume 1, pages 389–400.
- Wild, P. (1987). Difference basis systems. *Discrete mathematics*, 63(1):81–90.
- Wilks, S. S. (1932). Certain generalizations in the analysis of variance. *Biometrika*, pages 471–494.
- Xia, P., Zhou, S., and Giannakis, G. B. (2005). Achieving the Welch bound with difference sets. *IEEE Trans. Inf. Theory*, 51(5):1900–1907.

- Xu, S., Shang, Y., and Wang, H. (2008). Application of SVD to sense wireless microphone signals in a wideband cognitive radio network. In *Proc. Int. Conf. Sig. Process. Commun. Syst.*, pages 1–7.
- Yen, C. P., Tsai, Y., and Wang, X. (2013). Wideband spectrum sensing based on sub-Nyquist sampling. *IEEE Trans. Sig. Process.*, 61(12):3028–3040.
- Yoo, J., Becker, S., Monge, M., Loh, M., Candes, E., and Emami-Neyestanak, A. (2012). Design and implementation of a fully integrated compressed-sensing signal acquisition system. In *Proc. IEEE Int. Conf. Acoust., Speech, Sig. Process.*, pages 5325–5328.
- Yucek, T. and Arslan, H. (2009). A survey of spectrum sensing algorithms for cognitive radio applications. *IEEE Commun. Surveys Tutorials*, 11(1):116–130.
- Zanella, A., Chiani, M., and Win, M. Z. (2009). On the marginal distribution of the eigenvalues of Wishart matrices. *IEEE Trans. Commun.*, 57(4):1050–1060.
- Zemen, T. and Mecklenbrauker, C. F. (2005). Time-variant channel estimation using discrete prolate spheroidal sequences. *IEEE Trans. Sig. Process.*, 53(9):3597–3607.
- Zeng, Y. and Liang, Y. C. (2009a). Eigenvalue-based spectrum sensing algorithms for cognitive radio. *IEEE Trans. Commun.*, 57(6):1784–1793.
- Zeng, Y. and Liang, Y. C. (2009b). Spectrum-sensing algorithms for cognitive radio based on statistical covariances. *IEEE Trans. Veh. Technol.*, 58(4):1804–1815.
- Zhao, Q. and Sadler, B. M. (2007). A survey of dynamic spectrum access. *IEEE Sig. Process. Mag.*, 24(3):79–89.

